The dynamics of the South Pacific split jet in austral winter



Matthew Patterson
Oriel College
University of Oxford

A thesis submitted for the degree of
Doctor of Philosophy

July 2020

To my wife, Abigail, for her love and friendship

Also to my parents, Colin and Judith, for their loving support

Soli Deo gloria.

Acknowledgements

I would particularly like to thank my two supervisors, Tim Woollings and Tom Bracegirdle, who have guided my research and learning over the last few years. Tim's extensive knowledge and understanding of mid-latitude dynamics has been invaluable and I am immensely grateful for his time and enthusiasm in helping me to develop my ideas. Tom's knowledge of southern hemisphere atmospheric circulation was also instrumental in this work and I very much appreciated being hosted by him at the British Antarctic Survey for three months as part of my PhD.

Doing a PhD has the potential to be a lonely endeavour, so I am grateful for the friendship and good humour of my office mates, Hugh Baker and Ronald Li. I have also benefited from the wisdom and ideas of colleagues in the Atmospheric Dynamics research group, including Chris O'Reilly, Cheikh Mbengue, Marie Drouard, Peter Watson and Tess Parker. On the technical side, I thank Neil Lewis for his help in setting up the *Isca* model, which was used for computer experiments in this thesis. I also owe my gratitude to the Natural Environment Research Council and the British Antarctic Survey for funding my work. Finally, thanks must go to Lesley Gray and Amanda Maycock for reading my thesis and for the stimulating discussion during my viva.

Abstract

The wintertime atmospheric circulation in the southern hemisphere is characterised by a zonally asymmetric, spiral-like pattern. This includes a strong jet over the Indian Ocean region, which bifurcates downstream into subtropical and polar front branches, known collectively as the South Pacific split jet. The location of the split jet, over Australia and New Zealand, means that this system exerts a considerable influence on the climate of these countries, while the jets also affect the climate of East Antarctica and southern South America.

In this thesis I investigate three major themes concerning the split jet. Firstly, I examine the surface boundary conditions which give rise to the observed split jet structure via a set of idealised, atmosphere-only model experiments. A particularly novel finding is that the presence of Antarctic orography plays a key role in shaping the split jet structure. Flattening Antarctica results in a weakened Indian Ocean jet and the destruction of the polar front branch of the split jet.

Secondly, I study the low frequency variability of the split jet, with a focus on the eddy-driven, polar front jet. I find that much of this variability can be captured by the Southern Annular Mode, while the presence of high latitude atmospheric blocking is closely correlated with equatorward jet shifts.

Finally, I evaluate the split jet and atmospheric blocking in CMIP5 models, before examining changes to the jet structure under the RCP8.5 climate change scenario. I find that circulation in the split jet region undergoes substantial changes in comparison to other regions, with zonal wind strengthening between the jets, causing the split jet to become less distinct. Following this, I demonstrate that these changes can largely be explained by considering the stationary wave response to changes in the subtropical Pacific.

List of acronyms

AGCM	Atmosphere-only General Circulation Model
AMIP	Atmospheric Model Intercomparison Project
CMIP	Coupled Model Intercomparison Project
DJF	December, January, February
EMFC	Eddy momentum flux convergence
ENSO	El Niño Southern Oscillation
EOF	Empirical Orthogonal Function
GCM	General Circulation Model
HLB	High-latitude blocking
IPCC	Intergovernmental Panel on Climate Change
JJA	June, July, August
MAM	March, April, May
NAO	North Atlantic Oscillation
NH	Northern hemisphere
OLR	Outgoing longwave radiation
PSA	Pacific South America
PV	Potential vorticity
RCP	Representative concentration pathway
RWS	Rossby wave source
SAM	Southern Annular Mode
SLP	Sea level pressure
SH	Southern hemisphere
SON	September, October, November
SST	Sea surface temperature
U850	850hPa zonal wind
WKB	Wentzel–Kramers–Brillouin
Z500	500hPa geopotential height

Contents

1 Introduction **1**

1.1 South Pacific split jet 2

1.2 Motivation 3

1.3 Thesis aims and outline 6

2 Background **9**

2.1 The general circulation of the atmosphere 9

2.1.1 The Hadley cell 11

2.1.2 Jet stream dynamics 14

2.1.2.1 Potential vorticity and eddy-driven jets 14

2.1.2.2 Jet variability 16

2.1.3 Atmospheric blocking and wave-breaking 21

2.2 Southern hemisphere circulation 24

2.2.1 Mean state 24

2.2.2 Causes of zonal asymmetries 25

2.2.3 Patterns of variability 27

2.2.4 Coupling with the stratosphere 32

2.2.5 Response to climate change 33

3 Data and methods **37**

3.1 Reanalysis data 37

3.2 Idealised modelling 38

3.2.1 General principles 38
3.2.2 Barotropic modelling 39
3.3 Coupled Model Intercomparison Project 42
3.4 Diagnostics and indices 47
3.4.1 Jet latitude and speed indices 47
3.4.2 Southern Annular Mode (SAM) index 48
3.4.3 Eliassen-Palm (EP) flux 48
3.4.4 E vectors 49
3.4.5 Wave activity flux 50
3.4.6 Wave-breaking / blocking index 51

4 The structure of the southern hemisphere mean state 54
4.1 Introduction 55
4.2 Data and methodology 58
4.3 Comparison of the control run with ERA-Interim reanalysis 62
4.4 Tropical SST asymmetries and stationary Rossby waves 66
4.5 Effects of removing Antarctic orography 70
4.6 A barotropic model of orographic effects on transient eddies 78
4.6.1 Barotropic model results 80
4.7 Discussion and conclusions 86

5 Low frequency eddy-driven jet variability 90
5.1 Introduction 91
5.2 Data and methods 96
5.2.1 Reanalysis data 96
5.2.2 SAM 96
5.2.3 Jet indices 96
5.2.4 Blocking index 96

5.3 Seasonality of jet indices 97
5.4 Split jet - SAM covariability 101
5.5 Blocking and high latitude wave-breaking 103
5.6 Dynamical regimes 106
5.7 Influence of the Indian Ocean sector 111
5.8 Discussion and conclusions 114

6 Split jet and atmospheric blocking representation in CMIP5 117
6.1 Introduction 117
6.2 Data and methods 121
6.2.1 Data 121
6.2.2 Methods 121
6.3 Mean state representation 123
6.4 Blocking representation 126
6.5 Discussion and conclusions 131

7 Split jet and atmospheric blocking response to forcing 133
7.1 Introduction 133
7.2 Data and methods 136
7.3 Circulation response to forcing 137
7.4 Blocking changes 141
7.5 Changes in the Australia-New Zealand sector 144
7.6 Discussion and conclusions 147

8 Modelling the SH winter response to forcing 149
8.1 Introduction 149
8.2 Data and methods 152
8.2.1 Model data 152
8.2.2 Indices 153

8.2.3 Barotropic vorticity equation 153
8.3 Results 156
8.4 Discussion and conclusions 168

9 Conclusions **172**
9.1 Key findings 172
9.2 Implications and future work 175
9.2.1 Role of Antarctic orography in shaping the mean-state 175
9.2.2 Low frequency variability 177
9.2.3 Climate model biases and responses 178
9.3 Final remarks 180

A List of CMIP5 models **181**

Bibliography **183**

Chapter 1

Introduction

The structure of Earth's atmospheric circulation and the variability of large scale features such as jet streams determines the weather that humans experience at the surface. The contrasting properties of land and sea, zonal variations in sea surface temperatures and the existence of topography give rise to the rich and varied structure of the time-mean flow, while transient atmospheric waves and turbulence constantly perturb it. Over the last hundred years, meteorologists and climate scientists have made remarkable advances in understanding atmospheric circulation and predicting variations on a range of timescales (e.g. Benjamin et al., 2018). Today's society depends on the short-term weather forecasts of the Met Office and other organisations, while seasonal forecasting provides important information for the energy, transport and water sectors, amongst others. Meanwhile, projections of atmospheric circulation change under climate change have become increasingly important as governments seek to mitigate and adapt to the effects of increased greenhouse gas concentrations in Earth's atmosphere. In each of these cases, a good scientific understanding of the circulation and accurate representation of the atmospheric flow in computer models is paramount for making good predictions.

1.1 South Pacific split jet

In this thesis, my focus is on the southern hemisphere (SH) atmospheric circulation and in particular on the South Pacific. The South Pacific covers a vast area, extending nearly 15,000km at its widest between Papua New Guinea and Ecuador at the Equator and spanning the tropical waters surrounding Samoa to the frigid southern Ocean. More specifically, I investigate the extratropical circulation during austral winter (often defined as June, July and August; JJA). Consequently, the various circulation features I will discuss determine the weather and climate of regions as diverse as Australia and New Zealand, South America and Antarctica.

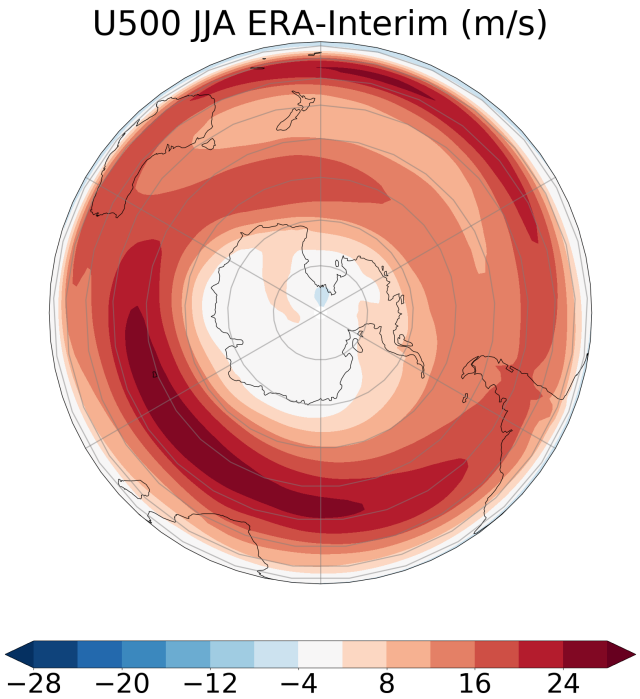


Figure 1.1: Time-mean 500hPa zonal wind for austral winter (JJA), calculated using ERA-Interim reanalysis data (1979-2015).

A fascinating aspect of the wintertime SH atmospheric circulation is that it exhibits considerable zonal asymmetry. This can be seen in figure 1.1 which shows the time-mean 500hPa zonal wind for winter, calculated using ERA-Interim reanalysis data (Dee et al., 2011). The circulation consists of a spiral jet stream, which begins

as a subtropical jet across Australia and the South Pacific, strengthening and moving poleward over the Indian Ocean before culminating in a polar front jet south of New Zealand. The existence of the wintertime 'split jet' pattern of subtropical and polar front jets straddling New Zealand, has been well documented (e.g. van Loon et al., 1972; Karoly and Vincent, 1998; Bals-Elsholz et al., 2001) and stands in marked contrast to the summertime circulation which is largely zonally symmetric. I now outline a number of motivations for my study of the South Pacific split jet.

1.2 Motivation

- The distinct seasonality of the mean flow is of practical interest for the predictability of weather and climate. This is because seasonal differences in circulation have important impacts on South Pacific storm tracks by altering the waveguides which carry cyclones (Ambrizzi et al., 1995; Hoskins and Hodges, 2005), thus affecting regional weather including rainfall over New Zealand (Kidston et al., 2009) and the occurrence of extreme frost events over southern South America (Müller and Berri, 2007; Müller and Ambrizzi, 2007). Moreover, the seasonal variations of the background state have been shown to modify teleconnections between various regions (e.g. Jin and Kirtman, 2009; Li et al., 2015; McIntosh and Hendon, 2018). An example of this which has received considerable attention in recent years is tropical forcing of trends in the West Antarctic region (Ding et al., 2011; Schneider et al., 2012; Simpkins et al., 2014; Yiu and Maycock, 2019). The mean wind patterns are also important in setting the distribution of sea-ice (Sen Gupta and England, 2006), ocean circulation (Ciasto and Thompson, 2008), mixed layer depth (Hall and Visbeck, 2002; Sallée et al., 2010) and ocean carbon uptake (Lovenduski and Gruber, 2005; Lovenduski et al., 2007; Le Quéré et al., 2007). As a consequence, SH mid-latitude circulation has either a direct or indirect impact on many aspects of the climate

system.

- The boundary conditions which give rise to the asymmetric wintertime mean state are of interest in terms of climate model development. Whilst the split jet pattern is a key feature of the observed circulation, many comprehensive general circulation models (GCMs) fail to capture this structure (Arakelian and Codron, 2012; Bracegirdle et al., 2013). Hence, understanding the drivers of the asymmetry is important in developing strategies to alleviate these biases. Several authors have attempted to understand the various boundary conditions which contribute to the wintertime asymmetry and have found that tropical sea surface temperatures (SSTs) play a major role (e.g. Inatsu and Hoskins, 2004; Nakamura and Shimpo, 2004; Williams et al., 2007; Ogawa et al., 2016), while tropical SST biases have been linked to extratropical circulation biases (Lachlan-Cope et al., 2007).

- The split jet system, consisting of a largely thermally direct, subtropical jet and a poleward, eddy-driven jet, is interesting as a case study in jet stream dynamics. These jets are maintained by distinct mechanisms and several idealised studies have examined the interaction between these jet types more generally (e.g. Lee and Kim, 2003; Son and Lee, 2005; Eichelberger and Hartmann, 2007; Barnes and Hartmann, 2011; O'Rourke and Vallis, 2013, 2016). For instance, Lee and Kim (2003) found that the strength of the subtropical jet and its proximity to the eddy-driven jet tends to weaken the latter and restrict the extent of its variation in latitude. These studies necessarily simplify the real-world picture, and hence analysis of observational data provides fertile ground for testing such ideas. Whilst at various times the subtropical and eddy-driven jets may split in other regions, for example in the North Atlantic, nowhere is the splitting as clear and unambiguous as in the South Pacific. In effect the South Pacific is

another region of 'jet stream state space' which may be explored.

- Another theoretical angle on the split jet could be provided by the study of dynamical regimes, which has been discussed extensively in the literature (see Hannachi et al., 2017, for a comprehensive review), though largely with a northern hemisphere (NH) focus (e.g. Woollings et al., 2010a). However, Ogawa et al. (2016) recently argued from model and observational evidence that the equatorward and poleward phases of the South Pacific jet could be regarded as separate dynamical regimes, one in which the jet is influenced by SST gradients and another in which internal atmospheric variability dominates. Further study of this idea is warranted as a regime view may bring enhanced intra-seasonal predictability (Colucci et al., 1992; Molteni et al., 2006), a helpful perspective on system responses to forcing (Palmer, 1999; Corti et al., 1999; Hsu and Zwiers, 2001) and a tool for climate model evaluation (Dawson et al., 2012; Dawson and Palmer, 2015).

- Finally, anthropogenic climate change is expected to alter the atmospheric circulation in various ways including expansion of the Hadley circulation and a poleward jet shift, both of which are clearest in the SH (Grise et al., 2019). Circulation changes are likely to have a significant impact on society by affecting precipitation and the occurrence of extreme weather events, depending on the region. On the other hand, the exact magnitude and mechanisms behind these projected changes remain a topic of current research. Studies have shown that the wintertime circulation response to greenhouse gas forcing is zonally asymmetric, in contrast to austral summer (Simpson et al., 2014; Grose et al., 2017). This raises questions about the mechanisms at play and a better understanding of these mechanisms may help to better constrain the magnitude and pattern of these changes.

1.3 Thesis aims and outline

The aims of this thesis are:

1. To establish the boundary conditions responsible for the wintertime South Pacific split jet structure.

2. To characterise and seek to explain the variability of the split jet from weekly to inter-annual timescales.

3. To characterise the ability of current climate models to represent the observed split jet structure.

4. To investigate the response of the split jet system to external forcing.

Following the introductory and background chapters, this thesis is divided into three main sections. These examine: I) the boundary conditions contributing to the split jet mean state (chapter 4), II) low frequency variability of the split jet (chapter 5) and III) the split jet in models (chapters 6, 7 and 8). The chapters are laid out as follows:

- In chapter 2, I outline the theory underlying the general circulation in Earth's atmosphere, jet streams and jet variability. Following this, I discuss the observed SH circulation with a particular focus on the wintertime circulation and modes of variability. I also summarise projected changes in SH circulation as a result of anthropogenic induced changes to the climate system.

- In chapter 3, I give details of the data sources used in this thesis, including reanalysis, comprehensive climate model output and idealised models. I then describe the various diagnostics and indices which I employ.

- In chapter 4, I investigate the structure of the SH wintertime mean state and split jet using the idealised model, *Isca*, with a focus on the various boundary conditions which contribute to the observed structure. As a result of findings in the first part of this chapter, I utilize a barotropic model with random stirring imposed and fluid depth varying with latitude. This provides a simple analogy for the role of Antarctic orography in shaping the flow in mid-latitudes. This work is under review in *Journal of Climate*.

- In chapter 5, I document the low frequency variability of the South Pacific split jet, particularly focusing on the eddy-driven jet. I investigate connections between the jet, the Southern Annular Mode (SAM) and high latitude Rossby wave-breaking. Following this, I examine the hypothesis that eddy-driven jet variability in this region can be explained using the framework of dynamical regimes.

- In chapter 6, I study the representation of SH jet streams and atmospheric blocking in the Coupled Model Inter-comparison Project phase 5 (CMIP5). Much of the work in this chapter has been published in Patterson et al. (2019) in *Geophysical Research Letters*.

- In chapter 7, I characterise the response of the SH jet and atmospheric blocking to anthropogenic forcing in CMIP5. I also pay particular attention to the asymmetry of the response. Much of the work in this chapter has been published in Patterson et al. (2019) in *Geophysical Research Letters*.

- In chapter 8, I model the wintertime SH stationary wave response to climate change using a barotropic model, forced with Rossby wave source changes in the tropics and subtropics. I also examine the spread in SH extratropical circulation changes in CMIP5 using linear regression techniques.

- Finally, I give conclusions in chapter 9, summarise the key findings of this thesis and discuss the implications of these findings, providing some suggestions for future work.

Chapter 2

Background

I now begin by reviewing key literature regarding atmospheric circulation, with a particular focus on jet stream dynamics and circulation in the southern hemisphere (SH). Starting with a brief discussion of the general circulation, I introduce the Hadley cell and the various mechanisms which drive jet streams. Following this, I assess some theoretical and observational studies examining the variability of jets and then review key features of the SH circulation. Finally I consider the body of literature on jet responses to forcing, again focusing on the SH.

2.1 The general circulation of the atmosphere

The general circulation of air in the atmosphere can be considered to be driven by energy imbalances between the equator and the poles and constrained by angular momentum conservation, depicted in figure 2.1. The Earth receives energy from the Sun in the form of shortwave radiation which is absorbed and re-emitted from the Earth's surface and atmosphere as outgoing longwave radiation (OLR). Given that the Earth is approximately spherical, tropical regions tend to receive a higher flux of incoming solar radiation than polar regions. However observations show that the tropics receives more incoming shortwave than it emits as OLR, while the poles emit more OLR than they receive as shortwave radiation. This implies that there is a net transport of energy from the equator to the poles via fluid motion (Vallis, 2017).

18th century meteorologist, George Hadley, suggested that this transport could be achieved by overturning cells reaching from the tropics to the poles (Hadley, 1735). In reality, the conservation of angular momentum prevents such planetary-scale motions from being stable, as air parcels moved from the equator to the mid-latitudes would achieve wind speeds of $200 - 500 ms^{-1}$, well in excess of observations. However, this idea formed the basis of what is now known as the Hadley circulation, a zonal-mean meridional overturning circulation which terminates in the subtropics, transporting energy polewards. I will shortly discuss some modern theories of the Hadley cell. Additionally, much of the energy transport in the tropics and subtropics is performed by ocean circulations (Trenberth and Caron, 2001).

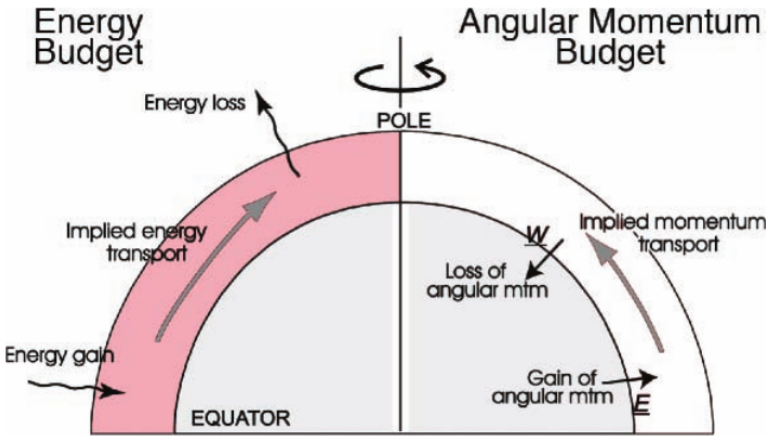


Figure 2.1: Schematic showing how the energy and angular momentum budgets constrain the Earth's atmospheric circulation. Figure reproduced from Marshall and Plumb (2008).

The remaining poleward energy transport is achieved through the motion of both transient and stationary eddies. An eddy is defined here as being any departure from zonal asymmetry and thus encompasses a wide range of phenomena of differing temporal and spatial scales. Stationary eddies are time-averaged circulations which originate from the presence of orography, land-sea contrasts and zonal variations in SSTs. Transient eddies, on the other hand, are time varying flow anomalies including extratropical cyclones and anticyclones. As has already been mentioned in referring

to the Hadley cell, angular momentum conservation constrains the overall circulation of the atmosphere. The Hadley cell transports westerly (that is, eastward) angular momentum polewards at upper levels, with the lower level return flow towards the equator. This upper level momentum transport results in a strong westerly jet at upper levels at the edge of the Hadley cell, known as the subtropical jet (Schneider, 1977; Held and Hou, 1980). The return flow at the surface transports easterly (westward) momentum equatorwards, but this is weakened by surface friction, effectively increasing the westerly momentum budget. This excess angular momentum must be dissipated somewhere. Consequently, eddies not only transport energy, but also angular momentum polewards, leading to westerly flow in the extratropics (Marshall and Plumb, 2008). Finally, westerly momentum is dissipated at the surface below the mid-latitude westerlies, ensuring that the total angular momentum remains fixed as is shown schematically on the right hand side of figure 2.1. The process by which the westerly flow is concentrated into eddy-driven jets is explained in section 2.1.2.

2.1.1 The Hadley cell

Early theories of the Hadley cell assumed a zonally symmetric overturning cell. An influential model is that of Held and Hou (1980), essentially a two-layer model with an angular momentum conserving upper layer and frictionally dominated return flow. Newtonian cooling relaxes the model to some equilibrium temperature state and net heating is required to be zero. The Held and Hou (1980) model slightly underestimates the latitudinal extent of the Hadley cell on Earth, but underestimates the Hadley strength, by an order of magnitude. The assumptions of energy and angular momentum conservation within the Hadley cell itself, have since been shown not to apply (Walker and Schneider, 2006), while non-axisymmetric features are required to explain the magnitude of the Hadley cell's strength (Schneider, 2006). Indeed, the recent study of Davis and Birner (2019) demonstrated the importance of eddy effects

on the Hadley cell. Using an idealised GCM, they showed that in the absence of eddies, the Hadley cell is confined to the upper troposphere, with virtually no poleward momentum flux and only weak poleward heat fluxes. Consequently, modern theories of the Hadley cell relax the assumptions of axisymmetry and energy and angular momentum conservation within the Hadley cell itself.

In the upper troposphere, the dominant zonal mean zonal momentum balance is between meridional angular momentum advection and eddy flux divergence (Held, 2000; Walker and Schneider, 2006). That is,

$$(f + \overline{\zeta})\overline{v} = f(1 - Ro)\overline{v} \approx S, \tag{2.1}$$

where f is the Coriolis parameter, $\overline{\zeta}$ is the zonal mean relative vorticity, v is the zonal mean meridional wind, $Ro = -\overline{\zeta}/f$ is the local Rossby number and S is the eddy momentum flux divergence. Thus, Ro effectively parameterises the relative importance of angular momentum conservation and eddy momentum flux convergence within the Hadley cell (Schneider and Bordoni, 2008; Bordoni and Schneider, 2008; Kang and Lu, 2012). This parameter also helps to explain the considerable seasonal variations in the strength and latitude of the Hadley cell, depicted in figure 2.2. It can be seen that the rising branch of the Hadley cell is found in the summer hemisphere, coincident with the location of maximum solar heating, with a larger Hadley cell extending into the winter hemisphere and a smaller branch in the summer hemisphere. In the winter hemisphere, the Hadley cell approaches the angular momentum conserving limit in which $Ro \to 1$, whereas the summer cell has transitioned to the eddy dominated limit of $Ro \to 0$ with the fast interseasonal transition between these two regimes mediated by eddy-mean flow feedbacks (Schneider and Bordoni, 2008; Bordoni and Schneider, 2010). In general, eddies act to slightly weaken the winter Hadley cell and substantially strengthen the summer Hadley cell (Schneider, 2006). In spite of the action of eddies, the Hadley cell is strongest in the winter hemisphere,

hence winter is associated with a strong subtropical jet. Conversely, the Hadley cell is weaker during summer leading to a weak subtropical jet which is often indistinguishable from the eddy-driven jet.

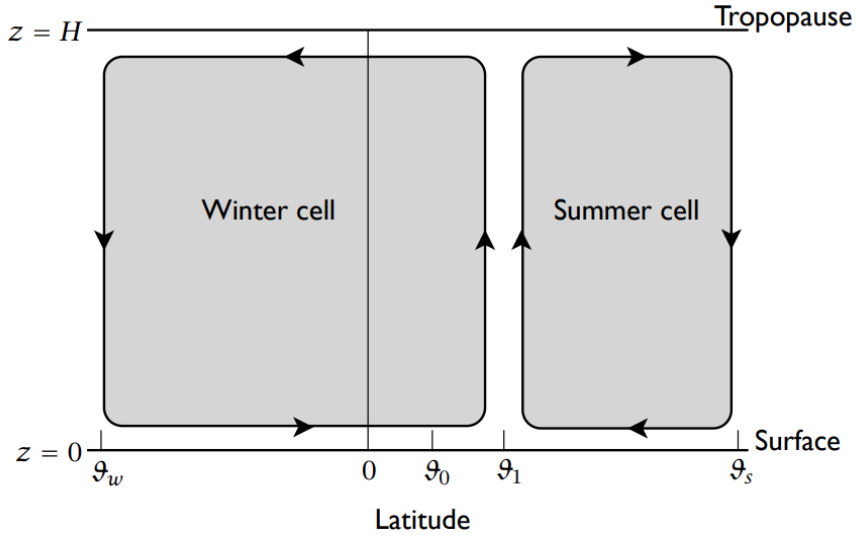


Figure 2.2: Schematic showing seasonal variations in Hadley cell extent. Ascent occurs in the summer hemisphere giving a broad winter cell and narrow summer cell. Figure reproduced from Vallis (2017).

The Hadley cell terminus is likely set by baroclinic instability (Held, 2000; Lu et al., 2007), the process in which available potential energy, generated through differential solar heating, is converted to eddy kinetic energy (Charney, 1947; Eady, 1949). In the Eady model, baroclinic instability is proportional to the vertical windshear divided by the static stability (Eady, 1949). Hence, the strong upper level winds and frictionally damped return flow imposed by the Hadley cell can give rise to significant baroclinic instability, making the Hadley cell unstable beyond a given latitude. Generally, baroclinic eddies are centred poleward of the Hadley cell, but tilted troughs trail down into the subtropics to extract energy and momentum (Vallis, 2017).

On interannual timescales, Hadley cell strength and extent is strongly influenced by Pacific SST variability via El Niño Southern Oscillation (ENSO). During El Niño, the Hadley cell contracts and strengthens, enhancing the subtropical jet strength and

weakening the eddy-driven jet in mid-latitudes (Lu et al., 2008; Tandon et al., 2013). The opposite occurs during a La Niña event. Whilst the Hadley cell is by definition a zonal mean phenomenon, heating in the tropics is far from zonally symmetric and hence the associated meridional overturning circulation varies as a function of longitude. Therefore, the variability of different 'local Hadley cells' may have differing impacts on the local surface climate. Schwendike et al. (2014) developed a method for partitioning the tropical overturning circulation into local meridional and zonal cells, thus allowing the definition of local Hadley cells. This method was later used by Nguyen et al. (2018) to study regional variations in the Hadley circulation in the SH, with them finding that variability of the zonal mean Hadley cell extent is dominated by the Asia-Pacific sector Hadley cell, particularly in spring and summer.

2.1.2 Jet stream dynamics

2.1.2.1 Potential vorticity and eddy-driven jets

Jets arise in a range of geophysical settings under conditions of rotation and stratification including ocean currents like the Agulhas and the Gulf Stream, banded structures on planets like Jupiter and of course Earth's atmospheric jet streams. Key to understanding such structures is the concept of potential vorticity, which can be defined in a number of ways. The Ertel-Rossby potential vorticity is defined as

$$P = \frac{1}{\rho}\zeta \cdot \nabla\theta, \tag{2.2}$$

in which ρ is the density of the fluid parcel, ζ is the absolute vorticity and θ, the potential temperature. Under frictionless, adiabatic motion, P is materially conserved. In addition, when combined with suitable boundary conditions, the invertibility principle means that the balanced components of flow fields, such as temperature or zonal and meridional winds, can be calculated from P at any given time (Hoskins and James, 2013).

The conditions of rotation and stratification in the Earth's atmosphere result in a flow which is largely two dimensional in nature. It is well known that in this situation the energy cascade occurs from small to large length scales. The background potential vorticity varies with latitude on a sphere, known as the β effect, which acts as a restoring force for the propagation of Rossby waves (Rossby, 1939). These waves organise the turbulent flow at scales above the Rhines scale, defined as

$$L_R = \sqrt{\frac{U}{\beta}}, \tag{2.3}$$

where U is the mean flow speed and β is the planetary vorticity gradient (Rhines, 1975). The meridional propagation of these waves fluxes momentum back towards their source region (Held, 1975; Vallis, 2017). A feedback loop is created whereby the process of Rossby wave-breaking effectively mixes potential vorticity, further enhancing wave-breaking in these regions. Consequently, an interface is created between wave-breaking regions, in which the potential vorticity gradient becomes self-sharpening (McIntyre, 1982; Dritschel and McIntyre, 2008). This sharp potential vorticity gradient is the eddy-driven jet, maintained by the organisation of turbulence into Rossby waves, which propagate away from the jet.

I have so far neglected to mention the source of energy at small scales, which is later dissipated at larger scales by breaking Rossby waves. This is provided by the process of baroclinic instability (Rhines, 1994). A region with a strong upper level jet and a lower level flow weakened by surface friction is highly baroclinic and hence eddies are primarily generated in the vicinity of the eddy-driven jet. A schematic of jet self-reinforcement can be seen in figure 2.3 with a jet forming in the baroclinically stirred region and Rossby waves propagating away meridionally, reinforcing the jet as they do so. Eddies generated in baroclinic regions act to reduce the baroclinicity by transporting westerly momentum towards the surface and simultaneously transporting heat polewards, reducing the temperature gradient at the surface. The

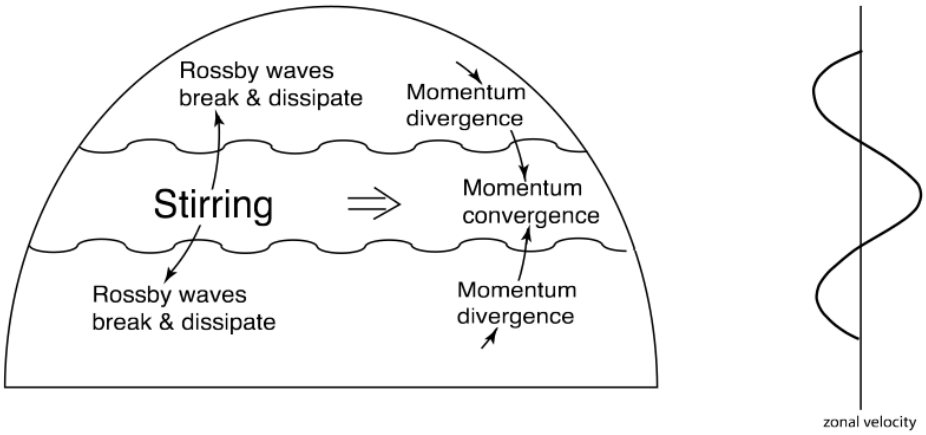


Figure 2.3: Schematic of the mechanism driving the mid-latitude westerly jet. Rossby waves form in the baroclinically stirred region, propagate meridionally and flux momentum back towards their source region, strengthening the jet. Figure reproduced from Vallis (2017).

baroclinicity is then restored, following baroclinic eddy growth, via differential heat flux from the ocean (Nakamura et al., 2004; Sampe et al., 2010; Hotta and Nakamura, 2011) and diabatic processes (Hoskins and Valdes, 1990; Papritz and Spengler, 2015), though there is some debate concerning the relative importance of each. It is clear from this discussion that storm tracks, regions in which transient, baroclinic eddies typically form and are carried by winds, are intimately linked with eddy-driven jet streams and vice-versa. For a detailed review of storm track dynamics, see Chang et al. (2002).

2.1.2.2 Jet variability

Much of the literature on eddy-driven jet variability has centred around the concept of 'annular modes' (e.g. Thompson and Wallace, 2001; Arblaster and Meehl, 2006; Gillett et al., 2006; Gillett and Fyfe, 2013; Lim et al., 2016). Annular modes broadly speaking describe a zonally symmetric movement of atmospheric mass between the mid-latitudes and the polar cap. By geostrophic balance this translates to variations in the strength and latitude of the jet with a generally stronger and more poleward

jet in the positive phase and a weaker, more equatorward jet in the negative phase. However, the mapping between annular mode and jet properties is not necessarily linear as the annular mode combines information about jet latitude, speed and width (Swart et al., 2015) and the relative importance of these is regionally and seasonally dependent (Codron, 2007; Barnes and Hartmann, 2010b). Different jet properties may also respond to a given forcing in different ways (McGraw and Barnes, 2016; Baker et al., 2017) and so in this section I will consider both jet latitude and speed separately and return to annular modes when discussing the SH circulation.

As outlined in the previous section, a key aspect of jet variability, is the interaction between waves and the mean flow. The presence of an eddy-mean flow feedback allows jets to persist at a given latitude for ten days or longer (Lorenz and Hartmann, 2001, 2003). This can be explained by noting that the eddy-driven jet is co-located with the region of maximum baroclinicity and consequently the primary source of wave activity. Baroclinic waves propagate meridionally away from their source region, converging momentum into the jet core, thus maintaining the jet against friction. Shifts in the jet will coincide with shifts in the eddy generation region and hence the jet is maintained at its new position (Hartmann, 2007). However, the strength or existence of such a baroclinic feedback depends on factors such as the background vorticity gradient and hence the nature of eddy-driven jet variability varies by location and season.

Barnes and Hartmann (2011) studied the dynamics of eddy driven jet variability with respect to jet latitude in a simplified barotropic framework. They found that the jet tends to persist for longer at lower latitudes, in line with previous studies of more complex models and reanalysis data (Barnes et al., 2010; Barnes and Hartmann, 2010c,d; Kidston et al., 2012). They again explained these results in terms of the propagation and breaking of Rossby waves. At low latitudes, the jet is reinforced at its current latitude by wave propagation away from the jet on both sides and hence it is relatively persistent, however as the jet moves further polewards, wave propagation

to higher latitudes is limited by the weak planetary vorticity gradient. This means that a high latitude jet is less strongly reinforced at its current latitude and the primary mode of variability changes from latitudinal 'shifting' to 'pulsing', that is, variations in jet strength. Woollings et al. (2017) found that stronger jets tend to vary less in latitude, showing that this result is robust in a hierarchy of models and in observational data.

Another factor which can alter eddy-driven jet variability is the presence of a thermally direct subtropical jet. Observed jets often exhibit a mixture of thermal and eddy driving, though the conceptual distinction remains useful (Li and Wettstein, 2012). As the location of the mean Hadley cell edge varies little during a given season, the subtropical jet is also relatively fixed in latitude. On the other hand, the eddy-driven jet varies considerably. Several idealised studies have investigated the effect of subtropical jets on eddy-driven jets. Lee and Kim (2003) used an idealised primitive equation model and found that in the presence of a strong subtropical jet, the region of maximum baroclinicity coincides with the subtropical jet and the two merge into a single jet. Using the same model, Son and Lee (2005) explored a two dimensional parameter space involving the rates of tropical heating and high latitude cooling. These parameters control the extent of thermal driving and width of the mid-latitude baroclinic zone respectively. They concluded that for a double jet to form, the thermal driving must be sufficiently weak and the baroclinic zone sufficiently wide. However, this study neglected the zonal asymmetry of the real Earth system so other regional factors such as stationary waves may alter the interplay between the eddy-driven and subtropical jets.

Eichelberger and Hartmann (2007) compared the behaviour of the eddy-driven jet of the North Atlantic, which is relatively separated from a weak subtropical jet, with that of the North Pacific which has a strong subtropical jet. Over the North Atlantic the primary mode of variability was found to be a shifting of the jet between latitudes,

whereas in the North Pacific case the jet remained close to the subtropical jet, varying its strength or 'pulsing'. They argued, in line with results of Lorenz and Hartmann (2001, 2003), that persistence of an eddy-driven jet at a given latitude occurs as a result of a positive feedback between transient eddies and the mean flow. The presence of a strong subtropical jet acts as a waveguide, preventing waves from propagating meridionally away from the jet and hence weakening this feedback (Nakamura and Sampe, 2002; Nakamura and Shimpo, 2004; Barnes and Hartmann, 2011).

A multitude of studies have considered the possibility of preferred states or 'dynamical regimes' in the atmosphere (see the review of Hannachi et al., 2017). Dynamical regimes represent atmospheric flow patterns which are both persistent and regularly revisited (e.g. Mo and Ghil, 1987). The regime paradigm has the potential to improve medium-term weather and climate prediction (Colucci et al., 1992; Palmer, 1999; Hsu and Zwiers, 2001; Robertson et al., 2015) and has also been used as a framework for climate model evaluation (Dawson et al., 2012; Dawson and Palmer, 2015). However, the statistical significance of some dynamical regimes studies has been called into question (Stephenson et al., 2004; Christiansen, 2005, 2007). Furthermore, the multiplicative noise paradigm of Sura et al. (2005) suggests that it may be possible to observe apparently regime-like behaviour in a linear system. More specifically, multiplicative noise is the idea that a dynamical system with a state-dependent stochastic term can give rise to non-Gaussian or even multi-modal statistics for a system which would be Gaussian in the absence of such a term. The existence of dynamical regimes therefore remains a topic of current research. Woollings et al. (2010a) argued that there are three preferred jet latitude regimes in the North Atlantic region. Their figure is reproduced in figure 2.4 in which the jet latitude index (see section 3.4.1) is plotted for northern winter using ERA-40 reanalysis data (Uppala et al., 2005). The preferred jet latitudes are clearly shown by the three distinct peaks in figure 2.4. Their figure 16f also shows a weak bimodality to the South Pacific jet, which is reproduced in the

study of Ogawa et al. (2016) using reanalysis data. At present, the underlying cause of such preferred states has not been fully explained. North Atlantic regime states have been better studied and it has been shown that the three preferred latitudes are closely associated with different frequencies of Rossby wave-breaking in different regions (Woollings et al., 2010a). Indeed, the interannual variability of the North Atlantic Oscillation (NAO, Wallace and Gutzler, 1981) is well correlated with the frequency of high latitude wave-breaking (Woollings et al., 2008). For instance, the northern jet state is associated with enhanced wave-breaking in the European region and the southern state with a pattern known as 'Greenland blocking'. In each case the occurrence of wave-breaking may act as a catalyst for future wave-breaking events, providing a potential feedback mechanism maintaining the jet at its current position. However, it is unclear whether wave-breaking and shifts in jet latitude should be viewed as causing one another or as part of the same phenomenon (Woollings et al., 2008). The findings of Woollings et al. (2010a) and Ogawa et al. (2016) with regard to the South Pacific merit further study and will be investigated in chapter 5.

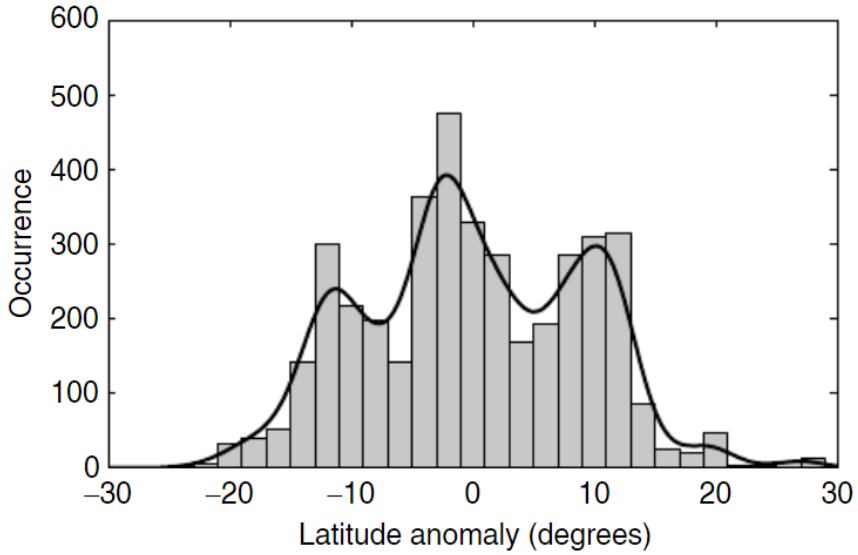


Figure 2.4: Jet latitude distribution for the North Atlantic during northern winter (DJF), calculated using ERA-40 reanalysis data. Figure reproduced from Woollings et al. (2010a)

In addition to internal tropospheric variability, eddy-driven jets are subject to interactions with external factors. For instance, diabatic heating has been shown to influence the mean strength and latitude of the jet (Held and Suarez, 1994; Baker et al., 2017), variability of the jet (Woollings et al., 2016), as well as smaller scale features such as cyclones and anticyclones (Reed et al., 1992; Pfahl et al., 2015). SSTs affect jet variability through modulation of near surface baroclinicity (e.g. Nakamura and Shimpo, 2004; Sampe et al., 2010; Novak et al., 2015; O'Reilly et al., 2017), generation of Rossby waves (e.g. Jin and Hoskins, 1995) and through modification of the subtropical jet (Seager et al., 2005; Lu et al., 2008). Coupling with the stratosphere also plays a role in eddy-driven jet variability via sudden stratospheric warmings (Baldwin and Dunkerton, 2001; Polvani and Kushner, 2002; Gerber et al., 2009; Domeisen et al., 2013; Kidston et al., 2015; Maycock et al., 2020) and the seasonal breakdown of the polar vortex (Black and McDaniel, 2007; Byrne and Shepherd, 2018). Finally, external forcing such as changes in ozone levels (e.g. Arblaster and Meehl, 2006; Thompson et al., 2011; Eyring et al., 2013) and greenhouse gas concentrations (e.g. Wu et al., 2012; Grise and Polvani, 2014b; Ceppi et al., 2018) have a profound effect on the mean state and variability of the jet by altering the temperature structure of the atmosphere.

2.1.3 Atmospheric blocking and wave-breaking

I have already discussed the topic of Rossby wave-breaking in the context of the variability of eddy-driven jets. Atmospheric blocking is a phenomenon closely related to wave-breaking (Masato et al., 2012) and is a process in which the jet stream becomes blocked or diverted by a region of high pressure, arresting the usual eastward progression of mid-latitude cyclones (Rex, 1950). This can be seen in figure 2.5, in which a poleward high pressure anomaly is diverting a cyclone towards south-east Australia. This plot uses data from the NCEP-NCAR reanalysis dataset (Kalnay et al., 1996).

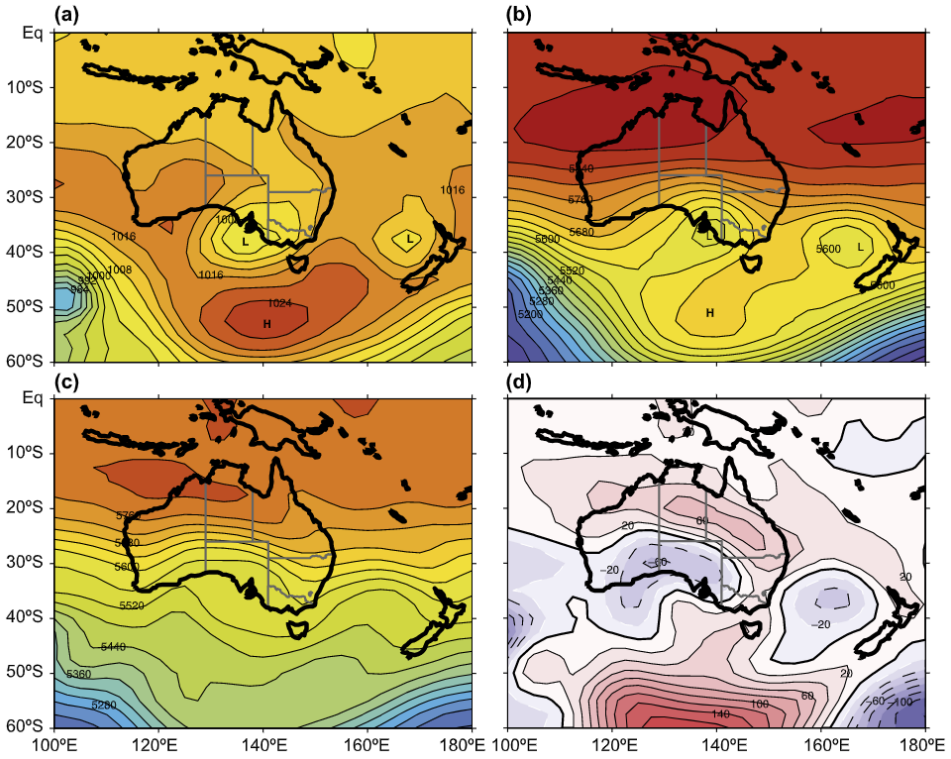


Figure 2.5: An example of atmospheric blocking in the south-east Australia region. The figure shows a blocking event at 12.00 on 27th April 2007 using the NCEP-NCAR dataset with the panels depicting a) Mean Sea Level Pressure b) 500hPa geopotential height, c) 1000-500hPa thickness and d) 1000-500hPa thickness anomaly. In each case red indicates high values and blue, low values of the given variable. Figure reproduced from Pook et al. (2013)

Although there is disagreement concerning the exact definition of blocking (Woollings et al., 2018), a key characteristic is that the block must be persistent, typically on timescales of around one week. The persistence of blocking patterns has significant implications for society as these patterns often are associated with extreme weather (e.g. Sillmann et al., 2011; Perkins-Kirkpatrick et al., 2016; Gibson et al., 2017).

A full theoretical description of the onset, maintenance and decay of blocking systems is currently lacking, though important progress has been made in this area. Typically, a region of low potential vorticity air is displaced poleward, creating a large-scale ridge (see figure 2.5b) which builds rapidly. Linear stationary wave theories such as those of Egger (1978) and Reinhold and Pierrehumbert (1982) have

been successful in predicting the primary regions of blocking as a result of forcing by SSTs (Hoskins and Karoly, 1981), land-sea contrast (Tung and Lindzen, 1979) and orography (Grose and Hoskins, 1979). In order to explain the inherent non-linearities of blocking development and decay, studies have invoked resonant interactions of the background flow with Rossby waves (Charney and DeVore, 1979) and interactions between waves of different scales (Austin, 1980). Others consider blocking to be better represented as a more local disturbance, for instance in modon (e.g. McWilliams, 1980) or soliton (e.g. Malguzzi and Malanotte-Rizzoli, 1984) theory. In reality, blocking involves a range of length scales from the synoptic to planetary (Nakamura et al., 1997; Burkhardt and Lupo, 2005), with many studies suggesting that eddy feedbacks are required to maintain the larger scale blocking structure (e.g. Shutts, 1983; Mullen, 1987; Luo, 2005; Yamazaki and Itoh, 2013). Recent studies have also suggested that diabatic processes such as latent heating may play a significant role in the development of blocking patterns (e.g. Tilly et al., 2008; Pfahl et al., 2015; Steinfeld and Pfahl, 2019).

Simulation of atmospheric blocking has also proven difficult as many General Circulation Models (GCMs) underestimate the frequency of blocking in key regions (D'Andrea et al., 1998; Woollings et al., 2018). Various suggestions for reducing this bias have been tested including increasing horizontal resolution (Berckmans et al., 2013; Schiemann et al., 2017), increasing vertical resolution (Anstey et al., 2013) and eliminating mean state biases (Scaife et al., 2010, 2011), and while all of these bring relative improvements, blocking underestimation remains a problem (Davini and D'Andrea, 2016). Consequently, there is currently fairly low confidence in any projected blocking changes with climate change (Woollings et al., 2018). However, most research on blocking in climate models has focused on the Euro-Atlantic sector and so in chapter 6 I will investigate the ability of an ensemble of GCMs to capture SH blocking.

2.2 Southern hemisphere circulation

Having outlined some general features of mid-latitude atmospheric circulation, I now focus on the mean SH circulation, describe some of the mechanisms which are responsible for shaping it and give an account of the primary modes of atmospheric variability.

2.2.1 Mean state

The boundary conditions provided by the Earth's surface are notably different in the SH compared with the NH. In the latter case, the presence of the Rocky mountains and two distinct continental landmasses punctuated by oceans, results in strong stationary waves, particularly during NH winter (Brayshaw et al., 2009, 2011). In contrast, the SH mid-latitudes contain a circumpolar band of ocean and orographic features such as the Southern African Plateau and Andes mountain range are less efficient at exciting stationary waves (Inatsu and Hoskins, 2004; Nigam and DeWeaver, 2015). Antarctic orography, which is made up of ice over 3km deep in places, has a relatively minor effect on stationary waves (Quintanar and Mechoso, 1995), though it has been shown to alter the variability of the circulation at high latitudes (Lachlan-Cope et al., 2001). The effect of Antarctic orography on transient eddies and hence the mean flow will form a major part of chapter 4. During austral summer (December, January, February; DJF) and autumn (March, April, May; MAM), tropospheric circulation is largely zonally symmetric apart from a stronger storm track in the Indian Ocean region (figure 2.6). This local deviation is caused by substantial meridional SST gradients between the Agulhas current, which brings relatively warm water south from the subtropics, and the cold Southern Ocean (Walker, 1990). However, during spring (September, October, November; SON) and winter (June, July, August; JJA), in particular, a significant zonal asymmetry arises, with the jet bifurcating into a subtropical jet and polar front jet at Australian longitudes (figure 2.6). This pattern

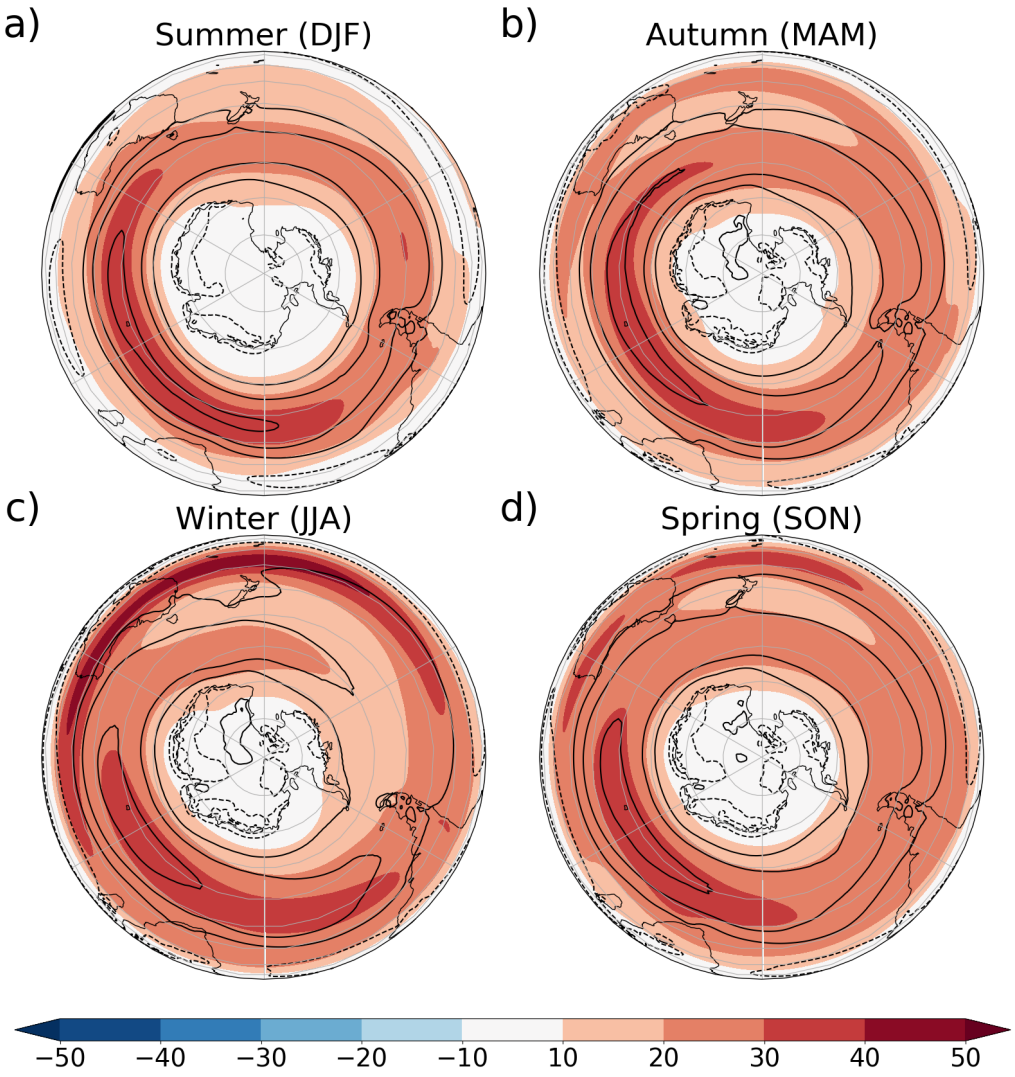


Figure 2.6: Seasonality of SH circulation. Time-mean zonal wind on the 850hPa (contours) and 300hPa levels (colours) are shown for a) austral summer (DJF), b) autumn (MAM), c) winter (JJA) and d) spring (SON), all calculated using ERA-Interim renanalysis data (1979-2015). The contour interval is $5ms^{-1}$ for 850hPa wind and $10ms^{-1}$ for the 300hPa wind.

is known as the South Pacific split jet and has been well documented (van Loon et al., 1972; Karoly and Vincent, 1998; Bals-Elsholz et al., 2001; Inatsu and Hoskins, 2006).

2.2.2 Causes of zonal asymmetries

A number of studies have attempted to understand the formation of wintertime zonal asymmetries in the SH. Inatsu and Hoskins (2004) performed a set of atmosphere-

only general circulation model (AGCM) experiments, in which they removed various aspects of the surface boundary conditions which may contribute to the structure of the SH winter storm tracks. In particular, they removed orography from Southern Africa and South America and set SSTs to the zonal mean in the tropics and mid-latitudes separately. They concluded that zonal asymmetries in tropical SSTs were responsible for most of the large-scale structure in mid-latitudes. They suggested that convection related to the Asian monsoon triggers a stationary Rossby wave as a result of divergent outflow from the Indian Ocean region. This wave propagates south-east, arcing back equatorwards over the South Pacific creating the split in the flow there. However, their analysis did not rule out the possibility that changes to background state winds could have altered stationary wave propagation. On the other hand, removing the Southern African Plateau and Andes mountain range did not have a significant impact on the split jet structure in their experiments. However, locally, the Andes mountains are associated with frequent genesis and lysis of mid-latitude cyclones (Hoskins and Hodges, 2005).

A distinct, but complementary perspective on the split jet centres around the strengthening of the subtropical jet in late spring (Nakamura and Shimpo, 2004; Williams et al., 2007). The subtropical jet, which is strongest between Western Australia and the central South Pacific, is driven by angular momentum transport via the Hadley cell and acts as a strong wave-guide for mid-latitude eddies, suppressing the eddy-mean flow feedback of the poleward eddy-driven jet (Nakamura and Shimpo, 2004). That is, upper level eddies forming upstream over the Indian Ocean become trapped by the subtropical jet and are separated in latitude from the region of maximum baroclinicity at the surface (Nakamura and Sampe, 2002). The upper level eddies are unable to interact with the surface baroclinic zone, suppressing wave activity and hence reducing the number of meridionally propagating eddies which provide the momentum source for the eddy-driven jet. However, sufficient eddy activity persists

at high latitudes to maintain a weak polar jet and hence a split jet is observed. The subtropical jet itself is localised in the SH because strong convective heating over the West Pacific Warm Pool and Indian Ocean drives a strong local Hadley cell (Nguyen et al., 2018), which results in significant poleward angular momentum transport from that region.

On the other hand, Ogawa et al. (2016) emphasised the importance of the mid-latitude SST front location in maintaining the split jet. The SST front determines the region of maximum baroclinicity and thus is the source region of transient eddies which provide the momentum driving the eddy-driven jet. They argued that a split jet forms over the South Pacific because there is sufficient separation in latitude between the mid-latitude SST front (approx. 55S) and the subtropical jet for a poleward eddy-driven jet to form. This contrasts with the Indian Ocean as the SST front formed by the Agulhas current is located further equatorwards (approx. 40S) and there is no splitting of the atmospheric flow. The causes of zonal asymmetries in the SH extratropical circulation will be further explored in chapter 4.

2.2.3 Patterns of variability

I have already introduced the concept of annular modes in my discussion of eddy-driven jet variability. The Southern Annular Mode (SAM) is the dominant mode of atmospheric variability on time scales of ten days or greater, consisting of a largely zonally symmetric vacillation in the SH jet (Hartmann and Lo, 1998; Limpasuvan and Hartmann, 1999; Thompson and Wallace, 2000). The SAM is typically defined as the principal component time series associated with the first empirical orthogonal function (EOF) of sea level pressure (SLP) or geopotential height south of 20S (e.g. Thompson and Wallace, 2000), or the difference in SLP between stations at 40S and 65S (e.g. Marshall, 2003). Its structure varies between seasons (figure 2.7) with a significant non-annular, wave 3 component in winter, while it is more zonally symmetric in

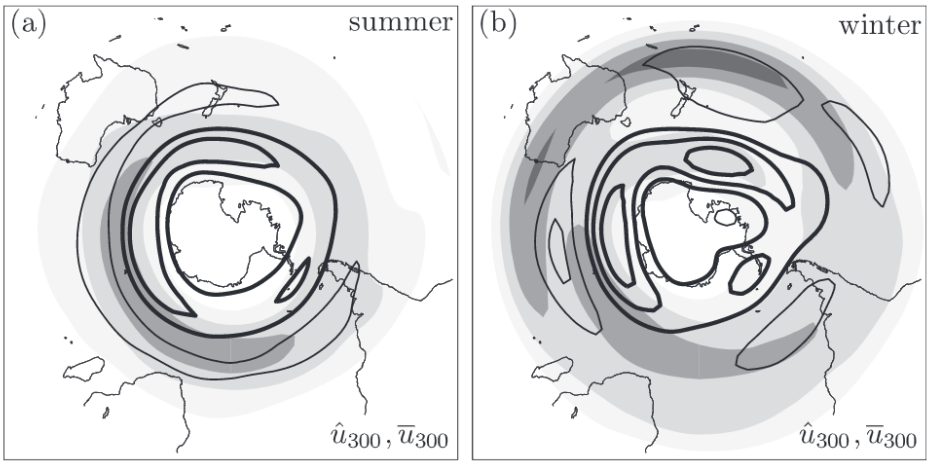


Figure 2.7: Seasonal variations in the SAM pattern. Time-mean 300hPa zonal wind (shading) and regressions of monthly 300hPa zonal wind onto the SAM index (contours) are shown for a) summer (DJF) and b) winter (JJA). The contours are drawn every $1.75ms^{-1}$ with the zero contour omitted and shading is in intervals of $10ms^{-1}$. The SAM index is defined as the leading EOF of monthly-mean sea level pressure data. Data is from the ERA-40 reanalysis dataset. Figure reproduced from Barnes and Hartmann (2010b).

summer (Codron, 2007; Kidston et al., 2009; Barnes and Hartmann, 2010b). Within the winter season there is also regional variation in the nature of jet variability. The wintertime eddy-driven jet in the Indian Ocean region is characterised by a latitudinal shifting, like in summer, however the wintertime South Pacific eddy-driven jet exhibits a pulsing (Codron, 2007). It has been suggested that this finding is a result of the low wind speeds in the South Pacific region (Barnes and Hartmann, 2010b). Codron (2007) also described the variability of the eddy-driven jet in this region as a 'see-saw' in which the jet oscillates between high and low latitudes and is rarely located in-between.

Persistence of the SAM in a given state is enhanced by the presence of a feedback process between transient eddies and the mean state (Lorenz and Hartmann, 2001), as alluded to in section 2.1.2.2. The SAM tends to persist for longer in a given state during summer (Barnes and Hartmann, 2010b; Gerber et al., 2010), which may be a result of the relative symmetry of the flow, in contrast to winter. It also shows

a significant coupling with El Niño Southern Oscillation during this season (Fogt and Bromwich, 2006; Lim et al., 2013). On the other hand Byrne and Shepherd (2018) questioned both of these results on the basis that the final breakdown of the stratospheric polar vortex occurs during late spring or early summer and ostensibly has an organising effect on tropospheric anomalies. They argued that this introduces a nonstationarity to the SAM time series, making the SAM appear more persistent, while the SAM-ENSO teleconnection may occur via the stratosphere, being mediated by the vortex breakdown.

Berrisford et al. (2007) suggested that variations in the wintertime SAM index are linked with high latitude atmospheric blocking, akin to the relationship of the NAO and Greenland blocking (Woollings et al., 2008). Blocking is generally less frequent in the SH because of the stronger winds and more zonally orientated flow, though it still can have a substantial impact on circulation variability and weather (e.g. Müller and Ambrizzi, 2007; Mendes et al., 2008; Rodrigues and Woollings, 2017; Risbey et al., 2019) and is most frequent over my study region, the South Pacific (e.g. Sinclair, 1996; Renwick and Revell, 1999; Parsons et al., 2016). Berrisford et al. (2007) found that the high latitude blocking correlation with SAM is particularly strong to the south of New Zealand, a finding corroborated by (Parsons et al., 2016). I will investigate the relationship between the jet and blocking in chapter 5.

Variations in the SAM modulates surface winds and hence it has been linked to variability in ocean circulation, mixed-layer depth and sea-ice (Hall and Visbeck, 2002; Sen Gupta and England, 2006; Ciasto and Thompson, 2008; Sallée et al., 2010; Thompson et al., 2011). Consequently, the SAM has been shown to modulate biological productivity (Lovenduski and Gruber, 2005; Sallée et al., 2010) and ocean carbon uptake (Le Quéré et al., 2007). The different phases have also been connected to regional weather impacts. The positive phase is correlated with cooling over most of Australia and Antarctica; warming in West Antarctica, Argentina and New Zealand;

anomalously wet conditions over Australia and South Africa; and dry anomalies over New Zealand, Tasmania and South America (Gillett et al., 2006; Hendon et al., 2007). However, it has been noted that there is considerable seasonal variation to these impacts as this covariability is much stronger during summer than winter (Hendon et al., 2007, 2014; Spensberger et al., 2019). As a result of the weaker weather impacts and non-annular pattern of the winter SAM, some have questioned the physical interpretation of the winter SAM (Spensberger et al., 2019; Spensberger and Spengler, 2020). Ding et al. (2012) suggested that EOF analysis, which attempts to maximise the variance explained by each pattern, captures a combination of Indian Ocean jet variability and the Pacific South America (PSA) modes.

In addition to the SAM, which has a barotropic signature in geopotential height, a mode known as the Baroclinic Annular Mode (BAM) has recently been identified in the SH extratropics (Thompson and Woodworth, 2014; Thompson and Barnes, 2014). The BAM is typically defined as the first EOF of eddy kinetic energy between 20S and 70S. Intriguingly, it is associated with a 25-30 day periodicity (Thompson and Woodworth, 2014) and appears to vary largely independently of the SAM (Boljka et al., 2018). This latter finding is somewhat unexpected given that barotropic and baroclinic processes are linked through the lifecycle of baroclinic eddies. That is, transient eddies in mid-latitudes typically exhibit baroclinic growth, extracting available potential energy from the background flow, before undergoing a barotropic decay with an associated flux of momentum. This discrepancy can be resolved by considering that on timescales of ten days or longer, which exceeds that of a baroclinic lifecycle, eddy kinetic energy is correlated with heat fluxes, but not with momentum fluxes (Boljka et al., 2018). As of yet, the BAM is not as well understood as the SAM, but its apparent periodicity is likely to yield enhanced predictability on sub-seasonal timescales (Boljka and Shepherd, 2020).

The PSA modes are another set of SH extratropical circulation patterns and like

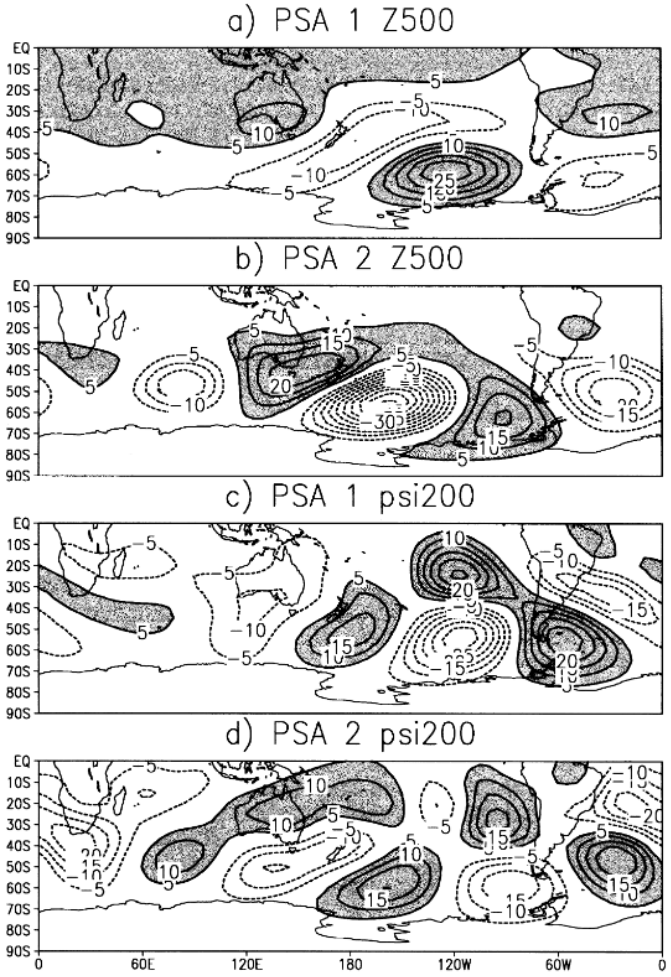


Figure 2.8: The Pacific South America modes, defined as the 2nd and 3rd EOFs of 500hPa monthly geopotential height data in the SH using NCEP-NCAR reanalysis data. The top two panels show 500hPa geopotential height anomalies, while the bottom two panels show 200hPa stream function anomalies. Figure reproduced from Mo (2000).

the SAM they have also attracted a considerable amount of discussion regarding their physical interpretation. The PSA patterns were originally defined as the 2nd and 3rd EOF patterns of SH geopotential height anomalies (Mo and Ghil, 1987; Mo et al., 1998; Mo and Paegle, 2001), shown in figure 2.8. However, they have since been defined using a variety of methods including Fourier analysis (Irving and Simmonds, 2016; O'Kane et al., 2017) and singular spectrum analysis (Robertson and Mechoso, 2003). EOF 2 and EOF 3 are in quadrature and hence a common interpretation is that

the PSA modes describe a propagating wave. Others have argued that geographically fixed patterns of variability are a better description (Robertson and Mechoso, 2003). On interannual timescales, the PSA patterns modulate the ENSO teleconnection with the South-East Pacific (Karoly, 1989; Mo, 2000) and provide a link between tropical and Antarctic variability (Ding et al., 2011; Schneider et al., 2012; Li et al., 2015), affecting the Amundsen Sea Low (Turner et al., 2013) and West Antarctic temperatures (Ding et al., 2011; Schneider et al., 2012; Clem and Fogt, 2015). On an intraseasonal timescale, recent studies have found that PSA variability is mostly internal to the mid-latitudes and uncorrelated with tropical convection (Irving and Simmonds, 2016; O'Kane et al., 2017).

2.2.4 Coupling with the stratosphere

The stratosphere is the region of the atmosphere between the top of the troposphere and the base of the mesosphere, spanning approximately 10-50km above the surface of the Earth. Stratospheric temperatures increase with height, making the stratosphere relatively stable in comparison to the troposphere. During the SH wintertime, a strong westerly jet forms in the stratosphere, known as the polar vortex, and persists until late spring or early summer (Black and McDaniel, 2007). Unlike its NH counterpart, the SH polar vortex rarely undergoes Sudden Stratospheric Warmings, in which the polar vortex breaks down in the winter, before reforming. This is because planetary waves, which act to disrupt the vortex, are relatively weak in the SH, with respect to the NH (Gray et al., 2005; Roscoe et al., 2005).

A number of studies have demonstrated that the SH stratosphere may be a source of seasonal predictability for SH tropospheric circulation in austral spring and summer (Roff et al., 2011; Son et al., 2013; Seviour et al., 2014; Lim et al., 2018; Byrne et al., 2019). The rarity of Sudden Stratospheric Warmings means that this skill primarily comes via predictability of the final warming date in late spring or early summer

(Lim et al., 2018; Byrne et al., 2019). Specifically, following the vortex breakdown, the tropospheric eddy-driven jet tends to shift equatorwards (Byrne et al., 2017; Byrne and Shepherd, 2018) and a number of different mechanisms have been proposed which may mediate such stratosphere-troposphere linkages (see Tripathi et al., 2015, for a review). However, this thesis primarily concerns the SH winter, when the stratosphere has relatively little effect on the tropospheric circulation. Hence, my discussion of the stratosphere will be limited. The stratosphere has played an important role in recent tropospheric jet trends which I will discuss in the next section.

2.2.5 Response to climate change

Anthropogenic-induced changes to greenhouse gas concentrations, aerosols, and ozone can have an indirect impact on atmospheric circulation, often by changing the temperature structure of the atmosphere. I here provide a summary of the major SH extratropical circulation changes which have been observed and changes that are projected as a result of anthropogenic climate change, alongside a brief survey of the potential mechanisms involved in such changes.

Observational data shows that changes to ozone concentrations in the SH stratosphere and increasing greenhouse gas concentrations have had a considerable influence on the SAM and Hadley cell over the last 50 years, particularly during SH summer (Thompson et al., 2002; Arblaster and Meehl, 2006; Son et al., 2010; Gerber and Son, 2014). While both ozone depletion (Polvani et al., 2011) and enhanced greenhouse gas forcing (Butler et al., 2010; Wu et al., 2012) have been shown to individually produce a positive SAM trend, the current consensus is that the ozone trend has contributed more strongly (Son et al., 2008; Polvani et al., 2011; Lee and Feldstein, 2013; Schneider et al., 2015). Ozone depletion has radiatively cooled the polar lower stratosphere, enhancing the equator to pole temperature gradient and resulting in a strengthened polar vortex (Randel and Wu, 1999; Waugh et al., 1999). This signal has descended

to the troposphere, resulting in a strengthened and poleward jet (Thompson et al., 2002; Son et al., 2008). Meanwhile, there has been a notable expansion of the tropics and SH Hadley cell which has been linked to both ozone forcing and SST changes (e.g. Waugh et al., 2015; Grise et al., 2019).

On the other hand, in light of global efforts to ban the emission of ozone depleting substances, the SH ozone hole has begun to recover (Solomon et al., 2016) and total column ozone over Antarctica is expected to return to 1980 levels by around 2045-2060 (Eyring et al., 2010). Indeed, Banerjee et al. (2020) linked reductions in ozone-depleting substances to a pause in the poleward trend of the SH summer jet between 2000 and the present day. Furthermore, ozone recovery is expected to continue to oppose the tendency for a poleward shift imposed by greenhouse gas forcing, and depending on the particular forcing scenario used in a given model, the summertime jet is likely to experience only a slight poleward shift over the next 50-100 years (McLandress et al., 2011; Polvani et al., 2011; Eyring et al., 2013; Bracegirdle et al., 2013).

Outside of summertime, the trends in SH jets during the period from 1979 to present exhibit considerably less certainty (Swart et al., 2015). This is likely because considerable ozone changes are only seen in summer. Waugh et al. (2020) showed that there is variation in the sign of 1980-2018 winter and spring jet latitude trends between ocean basins. In particular, they found a poleward jet shift over the Indian and Atlantic Oceans, and an equatorward shift over the South Pacific, attributing the latter to large internal variability. In terms of future changes, the subtropical jet is projected to strengthen slightly over the course of the 21st century during JJA (Chenoli et al., 2017), while the zonal-mean eddy-driven jet is expected to shift polewards and strengthen in all seasons due to greenhouse gas forcing (Swart and Fyfe, 2012; Bracegirdle et al., 2013).

However, the exact mechanism by which the eddy-driven jet shifts polewards with

greenhouse gas forcing remains a source of debate (see Shaw, 2019, for an extensive review on the topic). Some studies have suggested that changes to lower level eddy heat fluxes due to tropical heating are responsible for the shift (Lu et al., 2010; Butler et al., 2011). Also concerning lower levels, Kidston et al. (2010, 2011b) suggest that changes to lower tropospheric static stability cause a change in eddy length scale which promotes the jet shift via changes to regions of eddy dissipation. On the other hand, many authors have emphasised the role of meridional temperature gradient increases in the upper troposphere. These upper tropospheric changes have been linked to changes in the propagation of upper level eddy activity (Simpson et al., 2009; Chen et al., 2013; Wu et al., 2013), changes to eddy length scale (Rivière, 2011) and changes to eddy phase speed (Chen et al., 2008). Lorenz and DeWeaver (2007) also suggested that the jet shift is related to the increase in tropical tropopause height, which is a robust feature of climate model simulations (Vallis et al., 2015). Finally, in recent years there has been increasing interest in the role that CO_2-induced cloud radiative effects may play in the poleward jet shift. For instance, increasing CO_2 leads to an upward shift in high clouds which may shift the jet by altering the longwave cloud radiative effect (Voigt and Shaw, 2015; Shaw and Voigt, 2016; Li et al., 2019), while cloud-liquid water is enhanced in the extratropics with global warming, affecting the shortwave cloud radiative effect (Ceppi et al., 2016; Voigt and Shaw, 2016).

Regardless of the exact mechanisms causing the jet shift, Barnes and Polvani (2013) showed that increases in eddy-driven jet speed and changes in jet latitude are likely to affect the variability of the SH jet, causing it to vary less in latitude and more in speed (pulsing). They explained these findings in terms of Rossby wave-breaking in that a more poleward jet tends to exhibit less wave-breaking on its poleward flank for geometric reasons. This weakens the feedback which maintains the jet at a given latitude and hence variability in latitude becomes a less dominant component of the low frequency variability (Barnes and Hartmann, 2012).

Another important factor underlying circulation changes outside of DJF, is the fact that the mean circulation is not zonally symmetric. Simpson et al. (2014) showed that the zonally varying basic state leads to differing future responses to anthropogenic climate change between the seasons. For instance, simulations of future extratropical circulation change in JJA show a substantially zonally asymmetric response (e.g. Grose et al., 2017) while circulation changes are zonally symmetric in DJF. One explanation for this was provided by Freitas and Rao (2014), who analysed CMIP3 model data and showed that stationary wave propagation becomes less favourable under a basic state modified by climate change, while Freitas et al. (2017) showed that changes to the SH Hadley cell also alter stationary wave propagation. I will investigate the extratropical circulation response to climate change in chapter 7 with a particular focus on zonal asymmetries. Following this, I will seek to understand the mechanisms driving the circulation response in chapter 8.

Chapter 3

Data and methods

This chapter outlines the data sources used in this thesis including the ERA-Interim reanalysis dataset, Coupled Model Intercomparison Project (CMIP) and idealised models. Common diagnostics are also described.

3.1 Reanalysis data

Reanalysis is the process of combining a range of historical weather observations to generate a physically consistent dataset with global coverage. This is achieved by assimilating observations, which may come from ground-based measurements, radiosondes or satellites, using a weather model. The use of a weather model ensures dynamical consistency and provides a 'best estimate' of the true atmospheric state. Furthermore, this process effectively 'fills in the gaps' created by regions in which the data coverage is sparse. However, these datasets should be treated with caution as the quality and number of observations has greatly changed over time, making analysis of trends difficult. For instance, in the SH, there are relatively few observations available before the satellite era, which began in 1979 and before this period reanalysis datasets often tend to regress towards the climatology of the weather model (Tennant, 2004). For this reason, in this thesis I only utilize reanalysis data from 1979 onward. Consequently, there are only around 40 years of data meaning that there may be insufficient data for some analyses. For example, the identification of atmospheric

regimes is frequently hampered by short data records (e.g. Hannachi, 2007).

In this thesis, I regularly show analysis of ERA-Interim reanalysis data (Dee et al., 2011). ERA-Interim was initially released to improve upon data assimilation issues encountered in production of ERA-40 (Uppala et al., 2005) including with regard to the hydrological cycle, stratospheric circulation and consistency in time of various fields (Dee et al., 2011). In the SH, it provided a substantial advance on ERA-40 with regard to synoptic scale processes (Hodges et al., 2011) and high southern latitude surface variability (Bracegirdle and Marshall, 2012). On the other hand, Swart et al. (2015) noted that all modern reanalysis datasets, including ERA-Interim, show spurious trends in SLP and 10 metre zonal wind with respect to ground and satelite measurements. Considering both variables, in their study ERA-Interim performed slightly better than the alternatives, though the point remains that caution should be exercised when interpreting trends in reanalysis data. ECMWF has recently released the ERA-5 dataset which succeeds ERA-Interim and features both higher spatial and temporal resolution. However much of the analysis was completed before its release and I do not believe that the results presented here are likely to change using the updated dataset. ERA-Interim data was obtained via the ECMWF website-

https://www.ecmwf.int/en/forecasts/datasets/reanalysis-datasets/era-interim.

3.2 Idealised modelling

3.2.1 General principles

The climate system is complex and to aid understanding of it, it is necessary to construct and study climate models. These are sets of equations ranging from simple analytically tractable systems to systems which must be solved numerically on computers. At the higher end of this scale are the coupled climate models and Earth system models which make up the Coupled Model Intercomparison Project (CMIP). These often comprise millions of lines of computer code with representations of many

different aspects of the climate system in order to achieve accurate simulations. These are computationally expensive to run and whilst in many respects they represent the observed climate well, separating 'cause' from 'effect' is often challenging. Additionally, accurate simulation is not necessarily equated with better understanding of the system in question (Held, 2005). For these reasons, idealised models which are sufficiently accurate in resolving key processes, yet inexpensive to run and more easily analysed, are frequently useful. These idealised models can then form part of a hierarchy of models varying in complexity (Maher et al., 2019). Idealised models can often help to isolate important mechanisms by including some processes and excluding others. For instance, a simplified model of mid-latitude storm tracks could demonstrate whether moist effects are important through the inclusion or exclusion of latent heating. Furthermore, if a given mechanism is seen in both idealised and more comprehensive models, it is more likely to be robust (Maher et al., 2019). In this thesis I will utilize data from models of varying complexity including simple barotropic models (chapters 4 and 8) and a semi-realistic AGCM (chapter 4). The details of these models will be documented in the relevant chapters, however as barotropic models feature in two chapters, I provide a brief introduction to barotropic modelling here.

3.2.2 Barotropic modelling

The barotropic vorticity equation describes the "evolution of a constant density, non-divergent, incompressible flow on the surface of a sphere" (GFDL, 2020). This equation does not allow for sources of vorticity or the conversion of available potential energy, however it does represent large-scale features such as Rossby waves and non-linear wave-breaking. In a frictionless, incompressible fluid rotating with angular velocity vector, $\mathbf{\Omega}$, the momentum equation can be written, following Vallis (2017),

as

$$\frac{\partial \mathbf{u}}{\partial t} + \mathbf{u} \cdot \nabla \mathbf{u} = -2\boldsymbol{\Omega} \times \mathbf{u} - \frac{\nabla p}{\rho} - \nabla \phi \tag{3.1}$$

in which $\mathbf{u}$ is the wind vector, p the pressure, ρ is the density and ϕ is the geopotential. Using the identity

$$\mathbf{A} \times (\nabla \times \mathbf{A}) = \nabla(\mathbf{A} \cdot \mathbf{A}/2) - \mathbf{A} \cdot \nabla \mathbf{A}, \tag{3.2}$$

allows equation 3.1 to be re-written

$$\frac{\partial \mathbf{u}}{\partial t} + (2\boldsymbol{\Omega} + \omega_{\mathbf{r}}) \times \mathbf{u} = -\frac{\nabla p}{\rho} - \nabla(\phi - \frac{1}{2}\mathbf{u} \cdot \mathbf{u}), \tag{3.3}$$

where $\omega_{\mathbf{r}} = \nabla \times \mathbf{u}$ is the relative vorticity. Then, taking the curl of equation 3.3 and applying the identity

$$\nabla \times (\mathbf{A} \times \mathbf{B}) = (\mathbf{B} \cdot \nabla)\mathbf{A} - (\mathbf{A} \cdot \nabla)\mathbf{B} + \mathbf{A}\,\nabla \cdot \mathbf{B} - \mathbf{B}\,\nabla \cdot \mathbf{A}, \tag{3.4}$$

yields the vorticity equation

$$\frac{D\omega_{\mathbf{r}}}{Dt} = [(2\boldsymbol{\Omega} + \omega_{\mathbf{r}}) \cdot \nabla]\mathbf{u} + \frac{1}{\rho^2}(\nabla\rho \times \nabla p). \tag{3.5}$$

Taking the vertical component of equation 3.5, performing some algebraic manipulation and bearing in mind that the unit vectors are functions of position, the following equation can be obtained

$$\frac{D}{Dt}(\xi + f) = \left(\frac{\partial u}{\partial z}\frac{\partial w}{\partial y} - \frac{\partial v}{\partial z}\frac{\partial w}{\partial x}\right) + \frac{1}{\rho^2}\left(\frac{\partial \rho}{\partial x}\frac{\partial p}{\partial y} - \frac{\partial \rho}{\partial y}\frac{\partial p}{\partial x}\right). \tag{3.6}$$

Here ξ is the vertical component of the relative vorticity and $f = 2\Omega\, sin(\theta)$ is the Coriolis parameter. The first and second terms on the right hand side are respectively known as the tilting and baroclinic terms, which act as sources of vorticity. If the fluid is then constrained to motion only in the horizontal directions and taking the

density to be constant everywhere, equation 3.6 simplifies further with both terms on the right hand side vanishing. Consequently, equation 3.6 reduces to

$$\frac{D}{Dt}(\xi + f) = \frac{D\zeta}{Dt} = 0, \tag{3.7}$$

in which ζ is the absolute vorticity. The non-divergence of the flow means that a stream function, ψ, can be defined as the unique solution to the Poisson equation, $\nabla^2\psi = \zeta$. The zonal and meridional components of velocity, u and v respectively, are then given by

$$u = -\frac{1}{a}\frac{\partial\psi}{\partial\theta}, \qquad v = \frac{1}{a\,cos(\theta)}\frac{\partial\psi}{\partial\lambda}. \tag{3.8}$$

Writing the barotropic vorticity equation (equation 3.7) in spherical co-ordinates, with λ the zonal co-ordinate and θ the meridional co-ordinate, yields

$$\frac{\partial\zeta}{\partial t} = -J(\psi,\zeta) = -\beta v - J(\psi,\xi) = -\frac{2\Omega}{a^2}\frac{\partial\psi}{\lambda} - J(\psi,\xi) \tag{3.9}$$

where $J(\psi,\zeta)$ is the Jacobian:

$$J(\psi,\zeta) = \frac{1}{a^2\,cos(\theta)}\left(\frac{\partial\psi}{\partial\lambda}\frac{\partial\zeta}{\partial\theta} - \frac{\partial\zeta}{\partial\lambda}\frac{\partial\psi}{\partial\lambda}\right). \tag{3.10}$$

Here a represents the radius of the Earth. It is then necessary to discretise this equation in order to solve it numerically. In the case of 2D turbulence, enstrophy cascades towards smaller and smaller scales which poses a problem because of the finite resolution of the model. This issue can be resolved by introducing a hyperdiffusion term of the form $-\nu(-1)^n\nabla^{2n}\zeta$, where n is an integer. This term then provides dissipation at the smallest unresolved scales. The code used to solve this equation is based on the GFDL barotropic model code (GFDL, 2020). The code uses a standard

leapfrog scheme whereby equation 3.9 is written

$$\frac{\zeta_{i+1} - \zeta_{i-1}}{2\Delta t} = -J(\psi_i, \zeta_i) - \nu(-1)^n \nabla^{2n} \zeta_{i+1}, \tag{3.11}$$

where i is the timestep label and Δt is the length of the timestep. The vorticity is expressed as a sum of spherical harmonics and solved in spectral space. That is,

$$\zeta(\theta, \lambda) = \sum_{l=0}^{\infty} \sum_{m=-l}^{l} \zeta_{lm} Y_{lm}(\lambda, \theta) = \sum_{l=0}^{\infty} \sum_{m=-l}^{l} \zeta_{lm} P_{lm}(sin(\theta)) e^{im\lambda} \tag{3.12}$$

where l is the total wave-number, m is the zonal wave-number, Y_{lm} are the eigenfunctions of the Laplacian and P_{lm} are the associated Legendre polynomials. Further information on the specifics of the model code can be found in the GFDL barotropic model manual (GFDL, 2020). Additionally, the specific formulation of the barotropic model used for each set of experiments will be described in the relevant chapters.

3.3 Coupled Model Intercomparison Project

The Coupled Model Intercomparison Project (CMIP) is a co-ordinated set of climate model experiments to support assessments of climate change. This thesis utilizes data from phase 5 of CMIP, referred to as CMIP5 (Taylor et al., 2012). CMIP5 model data was extensively used to inform the fifth assessment report of the Intergovernmental Panel on Climate Change (IPCC; Stocker et al., 2013).

According to the World Climate Research Programme (WCRP, 2008), the experiments are designed to be useful in:

1. *"assessing the mechanisms responsible for model differences in poorly understood feedbacks associated with the carbon cycle and with clouds"*

2. *"examining climate 'predictability' and exploring the ability of models to predict climate on decadal time scales, and, more generally"*

3. *"determining why similarly forced models produce a range of responses."*

Initially, 20 modelling groups participated in CMIP5. The project required each group to perform a core set of experiments, while groups could then choose to perform other experiments, which were prioritised into two tiers. A schematic of the long-term experiments for CMIP5 can be seen in figure 3.1, showing the core experiments in the centre, with tier 1 and tier 2 experiments outside. These cover scenarios which are comparable with observations or can be used as projections (upper hemisphere) and also idealised experiments such as abrupt quadrupling of CO_2 (lower hemisphere). In the former group are the Representative Concentration Pathways (RCPs), a set of radiative forcing scenarios based on various policy responses to climate change (Meinshausen et al., 2011). Each of these scenarios is denoted by the radiative forcing imposed by the RCP in the year 2100, i.e. RCP4.5 means that under this scenario the radiative forcing in the year 2100 will be $4.5 W m^{-2}$, relative to the pre-industrial era. RCP2.6 is thus a scenario in which strong climate change mitigation is employed, while RCP8.5 is a high emissions scenario assuming high population growth and little climate change mitigation (Riahi et al., 2011). In this thesis I use RCP8.5 runs when considering the atmospheric circulation response to climate change. The use of RCP8.5 as a 'business as usual' scenario in the scientific literature has recently been criticised because of its pessimistic outlook on future carbon emissions (Ritchie and Dowlatabadi, 2017; Hausfather and Peters, 2020). Hausfather and Peters (2020) argue that this scenario is increasingly unlikely given reductions in the growth of coal-use and falling clean energy prices, and its use in studies can often overstate the risk of certain extreme impacts. However, I recognise that RCP8.5 has been widely used in the scientific literature and so it is useful for making comparisons between studies. The high radiative forcing also provides a large signal-to-noise ratio. Therefore, I use RCP8.5 in this work, but refrain from the use of language like 'business as usual'.

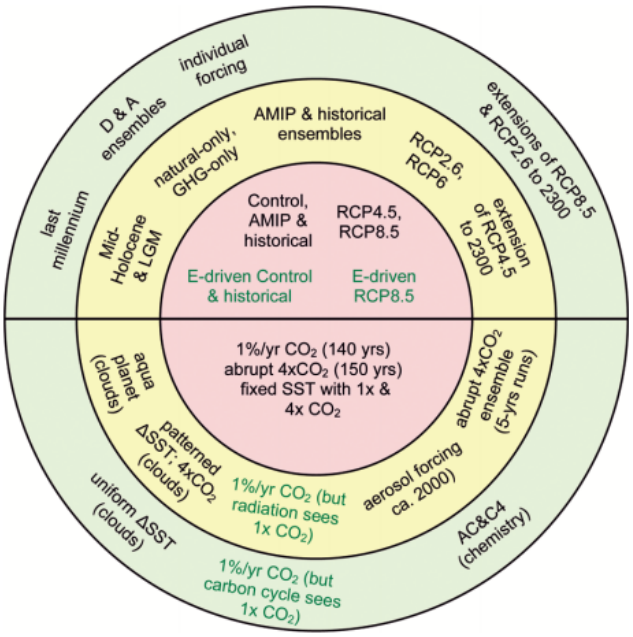


Figure 3.1: Schematic of long-term experiments in CMIP5. Experiments are organised into a central core, with tier 1 and tier 2 experiments outside. Experiments in the upper hemisphere are comparable with observations or can be used as projections while those in the lower hemisphere are idealised. In the core experiments, 'E' stands for emissions. Figure reproduced from Taylor et al. (2012).

The models themselves are all coupled atmosphere-ocean GCMs, representing atmospheric and oceanic physics as well as sea-ice and land surface processes (Flato et al., 2013). Furthermore, many models are termed Earth System Models because of the inclusion of additional processes, such as interactive aerosols, atmospheric chemistry, land carbon processes and ocean biogeochemistry. Few of these additional components were featured in CMIP3, the predecessor of CMIP5. On the other hand, CMIP5 models are based on models which participated in CMIP3 and share many of the same features. In spite of the inclusion of new Earth System components, Knutti and Sedláček (2013), Knutti et al. (2013) and Collins et al. (2013) all concluded that CMIP5 is an advance on CMIP3, but not a radically different ensemble.

The ensemble of CMIP5 models should not be considered to sample the full range of model uncertainty in climate change projections. Models differ in many ways including with respect to horizontal and vertical resolution, inclusion of Earth system

components, and in terms of their formulation of sub-gridscale paramerisations, such as representation of clouds. However, some institutions contributed multiple models to the project, while other models share a significant portion of code (e.g. ACCESS1 and HadGEM2 models) meaning that many models are not truly independent. This can be seen in figure 3.2a, a dendrogram showing the relative similarity of different model outputs. Models with similar code or produced by the same institution are shown in the same colours and it is clear that these tend to show a higher degree of similarity. Interestingly this doesn't always translate to similar climate projections as the pairs 'HadGEM2-ES'/'HadGEM2-CC' and 'Fgoals-s2'/'Fgoals-g2' are each well separated in figure 3.2b.

As a result of the lack of systematic exploration of model uncertainty, the CMIP5 ensemble is often termed an 'ensemble of opportunity' (Knutti et al., 2010). Some models also represent the observed climate more successfully than others. It would therefore appear sensible to apply a weighting to climate model projections based on a metric which quantifies the model's relative ability to correctly simulate climate. Unfortunately, constructing such a weighting is fraught with difficulty because the choice of metric is heuristic and depends on the field of interest (Chandler, 2013). Studies have also found that an unweighted average performs as well or better than a weighted average of all models (Déqué and Somot, 2010; Christensen et al., 2010). Consequently, in this thesis I will use unweighted multi-model means and include hatching on plots to indicate the degree of model agreement.

In my evaluation of CMIP5 models, my particular focus will be the large scale dynamics of the SH extratropical atmosphere. A common feature in the CMIP5 models with respect to atmospheric circulation is that SH jet streams are frequently equatorward-biased when compared to observational data (Kidston and Vallis, 2010; Bracegirdle et al., 2013; Lee, 2015; Simpson and Polvani, 2016). This is also found in CMIP3 models (Swart and Fyfe, 2012) and in atmosphere-only simulations (Brace-



Figure 3.2: a) CMIP3/CMIP5 (CMIP5 marked by asterisks) dendrogram based on Historical simulations of precipitation and temperature. Observations are also shown using ERA-40/GPCP and NCEP/CMAP datasets. Models with similar code or produced by the same modelling centre are shown in the same colours. b) as in a) but for precipitation and temperature changes in RCP8.5 at the end of the 21st century. Figure reproduced from Knutti et al. (2013), while the methodology is described in Masson and Knutti (2011).

girdle et al., 2013), indicating that the bias is likely to be generated internally within the model atmosphere. Relatedly, many models fail to capture the observed split jet structure in the South Pacific (Arakelian and Codron, 2012; Bracegirdle et al., 2013). These systematic biases reduce the confidence which I may have in future projections of circulation in the SH.

In this thesis I will particularly seek to investigate the wintertime split jet bias in models. I will also examine projected changes to the split jet under climate change and attempt to explain these changes mechanistically. With respect to CMIP5 data,

I will make use of the Historical control experiment, RCP8.5 and a number of AMIP experiments. The full list of models used in this thesis can be found in appendix A. The CMIP5 model data was obtained from the British Atmospheric Data Centre (BADC) archive on the Centre for Environmental Data Analysis (CEDA) data server (available at *http://data.ceda.ac.uk/badc/*).

3.4 Diagnostics and indices

Throughout this thesis a number of diagnostics and indices are consistently used. For reference I define them here and provide a brief discussion of their relative advantages and disadvantages.

3.4.1 Jet latitude and speed indices

In order to identify variations in jet latitude and speed, I calculate the indices of Woollings et al. (2010a), applied to the South Pacific region. Any given day is identified with a particular jet latitude and speed. Their methodology is as follows:

1. Vertically average the zonal wind between the 700 and 925hPa levels.
2. Perform a zonal average within the region in question
3. Apply a 10-day low pass Lanczos filter (Duchon, 1979)
4. The jet latitude is identified as the maximum zonal average wind on each day, while the jet speed is the magnitude of the wind at this latitude.

Woollings et al. (2014) stated that using 850hPa winds gives almost identical results and so I use only this level to limit the data required. The indices have the advantages of being simple and well studied, having been extensively used in other work (e.g. Anstey et al., 2013; Barnes and Polvani, 2013; Davini and Cagnazzo, 2014; Baker et al., 2017). On the other hand, jet stream variability is complex and these

indices cannot fully capture the variability of the jet (Madonna et al., 2017). For instance, the index is unable to account for the horizontal tilt of the North Atlantic jet or presence of double eddy-driven jets (Woollings et al., 2010a).

3.4.2 Southern Annular Mode (SAM) index

As described in chapter 2, there are a number of different methods of calculating a SAM index including using SLP measurements from stations or constructing the first EOF from reanalysis data. The advantage of the former is that the data record in the SH is unreliable before the satelite era and hence the use of station-based observations allows one to extend time series well before 1979 (Marshall, 2003). On the other hand, I am interested in the large scale circulation and the Marshall (2003) station-based index takes in only a handful of observations at each time, with few of these in the South Pacific region. I therefore opt for an EOF-based index and define the SAM as the principal component time series associated with the first EOF of daily, standardised 850hPa geopotential height anomalies. Before calculating the EOFs, I apply a 10-day low pass Lanczos filter to the daily geopotential height data. To account for the decreased spacing between gridpoints at high latitudes, I also weight the data by $\sqrt{cos(\phi)}$, where ϕ is the latitude.

3.4.3 Eliassen-Palm (EP) flux

The zonal mean zonal wind is maintained by both the direct effect of eddy momentum flux convergence and the indirect effect of eddy heat fluxes. That is, because of the requirement of thermal wind balance, eddy heat fluxes have an impact on the zonal wind and their influence is communicated via the development of a thermally indirect meridional circulation (Hoskins and James, 2013). The EP flux, F, takes into account the effects of both momentum and heat fluxes on the mean zonal wind. It is defined

under the quasi-geostrophic approximation, following Edmon et al. (1980), as

$$F = a\,cos(\phi)\left(-[u^*v^*], f\frac{[v^*\theta^*]}{\theta_p}\right), \tag{3.13}$$

where u and v are respectively the daily zonal and meridional wind, f is the Coriolis parameter and θ the potential temperature. The radius of the Earth is a, while p and ϕ are the pressure and meridional co-ordinates. Square brackets represent the zonal mean, asterisks indicate departures from the zonal mean and θ_p is the derivative of the potential temperature climatology with respect to pressure.

F is a useful diagnostic for wave propagation in a zonal mean framework and for small amplitude waves it represents the wave activity flux. In Transformed Eulerian Mean co-ordinates (Andrews and McIntyre, 1976), the combined effects of eddies and friction on the zonal mean zonal wind can be seen:

$$\frac{\partial[u]}{\partial t} = f[v_r] + \frac{1}{\rho}\nabla \cdot F + [\mathscr{F}], \tag{3.14}$$

where $v_r = v - \frac{[v^*\theta^*]}{\theta_p}$ is the meridional component of the residual circulation and $[\mathscr{F}]$ is the zonal mean frictional force.

3.4.4 E vectors

E vectors (Hoskins et al., 1983) provide a measure of transient wave activity flux on a given pressure level and have been widely used (e.g. Trenberth, 1991; Limpasuvan and Hartmann, 1999; Rivière and Orlanski, 2007; Fogt et al., 2011). The diagnostic is designed to provide an approximate extension of Eliassen-Palm flux theory (e.g. Edmon et al., 1980) to the 3D circulation, though E vectors are calculated using anomalies from the time mean rather than from the zonal mean. More specifically, the mechanical effect of eddies on the mean flow is given by the eddy vorticity flux

divergence. This can be written following Hoskins et al. (1983), as

$$\nabla \cdot \overline{\mathbf{v}'\zeta'} = -2M_{xy} + N_{xx} - N_{yy}, \tag{3.15}$$

in which ζ is the absolute vorticity and $\mathbf{v}$ is the velocity vector. Primes indicate that the data has been high pass filtered (with a 10-day Lanczos filter), over-bars represent time averages and subscripts represent partial derivatives. M and N are given by

$$M = \frac{1}{2}\overline{u'^2 - v'^2} \qquad N = \overline{u'v'}. \tag{3.16}$$

According to Hoskins et al. (1983), the term N_{xx} may be neglected if either the x-length scale of N is much larger than its y-length scale or the M term dominates over the N terms. For high pass eddies in storm tracks, the former criterion is usually satisfied. Assuming that N_{xx} can be neglected, equation 3.15 becomes

$$\nabla \cdot \overline{\mathbf{v}'\zeta'} = -2M_{xy} - N_{yy} = \partial_y \nabla \cdot \mathbf{E}, \tag{3.17}$$

where $\mathbf{E}$ is defined by

$$\mathbf{E} = \left(\overline{v'^2 - u'^2}, -\overline{u'v'}\right). \tag{3.18}$$

Hence, under the given assumptions, E vectors represent the eddy vorticity flux and their divergence is proportional to the westerly acceleration of the flow by transient eddies.

3.4.5 Wave activity flux

The wave activity flux vectors of Takaya and Nakamura (2001), W, diagnose the propagation of stationary or transient Rossby waves. Under the Wentzel–Kramers–Brillouin (WKB) approximation, W is parallel to the group velocity of linear Rossby waves.

Their formulation extends the work of Plumb (1985) to a zonally varying background flow and has been widely used (e.g. Inatsu and Hoskins, 2004; Lin et al., 2009; Trenberth and Fasullo, 2012; Gastineau and Frankignoul, 2015). The WKB approximation assumes that the basic state varies slowly in the horizontal and vertical directions, such that the length scales over which the background flow varies are much larger than the length scales of any perturbations to that flow. Potter et al. (2013) investigated the WKB assumption in an idealised barotropic framework and found it to be accurate in describing tropical-extratropical propagation. However, Wirth (2020) recently argued that the WKB conditions are unlikely to be satisfied in the case of mid-latitude jets because of their narrow meridional extent. However, they concluded that the theory still provides qualitatively, though not quantitatively accurate predictions. Hence, the wave activity flux vectors remain useful, but in this thesis, I focus on qualitative aspects of the diagnostic and plot vectors alongside other wave diagnostics such as stationary eddy stream function. The horizontal components of W are calculated as follows,

$$W = \frac{p}{p_0}\begin{bmatrix} \frac{\partial\overline{\psi*}}{\partial x}\frac{\partial\overline{\psi*}}{\partial x} - \overline{\psi*}\frac{\partial^2\overline{\psi*}}{\partial x^2} \\ \frac{\partial\overline{\psi*}}{\partial x}\frac{\partial\overline{\psi*}}{\partial y} - \overline{\psi*}\frac{\partial^2\overline{\psi*}}{\partial x\partial y} \end{bmatrix}, \tag{3.19}$$

in which p is the pressure, p_0 is the surface pressure and ψ is the horizontal stream function. An asterisk indicates that the zonal mean has been removed, while overbars represent the time-mean and x and y are the zonal and meridional coordinates respectively.

3.4.6 Wave-breaking / blocking index

I also investigate the connection between jet variability and high latitude atmospheric blocking following Masato et al. (2012, 2013a). Many different indices have been employed to study blocking, though most of these can be grouped into two categories;

persistent positive anomaly indices and reversal-based indices (Woollings et al., 2018). The first of these defines a persistent anticyclone as the key feature of a block and the blocking index is constructed to look for persistent positive geopotential height or SLP anomalies (Renwick and Revell, 1999; Parsons et al., 2016). The second considers that a persistent reversal of the geopotential height or potential vorticity (PV) gradient better characterises blocking (Tibaldi et al., 1994; Davini et al., 2012). I use an adaptation of the reversal method of Masato et al. (2012). The original index from Masato et al. (2012) extended the method of Pelly and Hoskins (2003) to two dimensions. It used PV on the dynamical tropopause, however Masato et al. (2013a) showed that the use of geopotential height at 500hPa (Z500), which is a readily available field, produced similar results.

The algorithm calculates the difference in daily mean Z500 integrated over a line 11° to the north and 11° to the south of each gridpoint. For regions where the difference is negative and thus the usual meridional Z500 gradient is reversed, a 'blocking centre' is defined and tracked over the following days. If the blocking centre continues to exist and remains sufficiently close to the original location then this is defined as a blocking event. For a more complete description of the algorithm see Masato et al. (2013a). In the original paper, Z500 was integrated polewards and equatorwards of each gridpoint by 15° and not 11°, however the frequency of SH blocking is considerably lower than in certain regions of the NH and so I choose 11° to improve the signal to noise ratio. Experiments comparing 11° with 15° for the SH show similar blocking frequency distributions, though the frequency is increased by about 30% (not shown). In accordance with Berrisford et al. (2007), I also set the threshold for persistence of the Z500 gradient reversal to four days rather than five days because of the typically lower persistence of SH blocks.

An example blocking detection is shown in figure 3.3. The figure shows the overturning of geopotential height contours associated with wave-breaking. A high geopo-

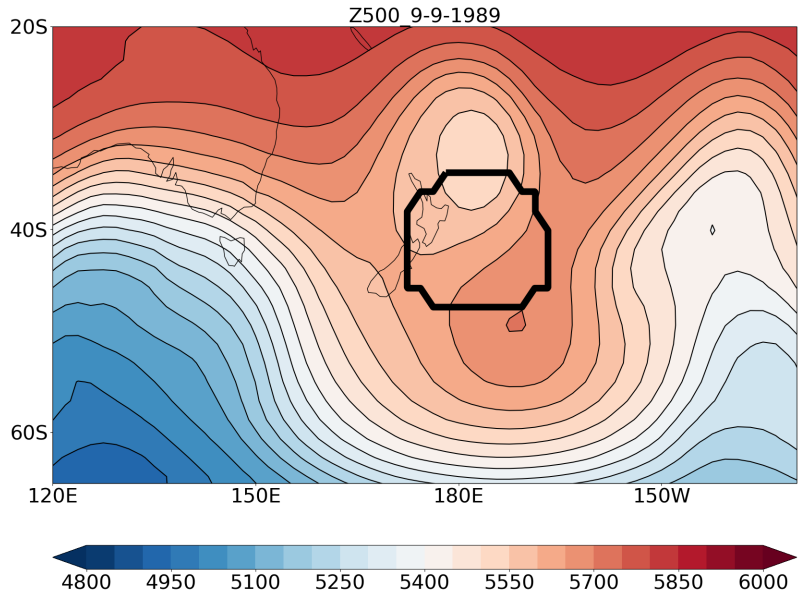


Figure 3.3: A blocking event detected on 9th September 1989 in the Australia - New Zealand sector. Colours and thin contours show the daily mean geopotential height, while the thick black line denotes the region in which the blocking algorithm detects a block.

tential height anomaly is located to the south-east of New Zealand, disrupting the flow, while a low geopotential height anomaly to its north-west is cut-off from the flow. The thick black line shows the region in which blocking is detected, that is, the algorithm detects the region in which the reversal occurs, which is smaller than the actual block itself.

Chapter 4

The structure of the southern hemisphere mean state

The wintertime SH extratropical circulation exhibits considerable zonal asymmetries. I investigate the roles of various surface boundary conditions in shaping the mean state using a semi-realistic AGCM. I find, in agreement with previous literature, that tropical SST patterns are an important contributor to the mean state, while mid-latitude SSTs and sea ice extent play a smaller role. My main finding is that Antarctic orography has a first order effect on the structure of the mid-latitude circulation. In the absence of Antarctic orography, equatorward eddy momentum fluxes associated with the orography are removed and hence convergence of eddy momentum in mid-latitudes is reduced. This weakens the Indian Ocean jet, making Rossby wave propagation downstream to the South Pacific less favourable. Consequently the flow stagnates over the mid to high-latitude South Pacific and the characteristic split jet pattern is destroyed. Removing Antarctic orography also results in a substantial warming over East Antarctica partly because transient eddies are able to penetrate further polewards, enhancing poleward heat transport. However, experiments in which a high latitude cooling is applied indicate that these temperature changes are not the primary driver of circulation changes in mid-latitudes. Instead, I invoke a simple barotropic mechanism in which the orographic slope creates an effective potential vorticity gradient which alters the eddy momentum flux.

4.1 Introduction

Many of the key zonal mean features of the Earth's atmospheric circulation, such as eddy-driven jets and Hadley cells, can be understood under zonally symmetric surface boundary conditions. Time-mean zonal asymmetries to the atmospheric flow can then largely be explained by the addition of zonally varying SSTs, land-sea contrasts and orography (e.g. Wang and Ting, 1999; Held et al., 2002; Brayshaw et al., 2009, 2011). The atmospheric circulation of the SH during winter is notably asymmetric and characterised by an upper level jet spiraling in towards Antarctica (Hoskins and Hodges, 2005; Williams et al., 2007). This can be seen in figure 4.1, plotted using winter (JJA) ERA-Interim reanalysis data for the years 1979-2014. A strong mid-latitude jet exists over the Indian Ocean which subsequently bifurcates into subtropical and polar branches, forming the split jet over the South Pacific (e.g. van Loon et al., 1972; Karoly and Vincent, 1998; Bals-Elsholz et al., 2001). This behaviour contrasts strongly with the summer season, in which the atmospheric circulation is largely zonally symmetric.

I have already considered some explanations of the zonally asymmetric circulation in chapter 2, but revisit some of the relevant studies here. Inatsu and Hoskins (2004) performed a set of AGCM experiments in which they altered aspects of the surface boundary conditions which may contribute to the structure of the SH winter storm tracks. Their experiments included removing orography over Southern Africa, removing orography over South America, setting SSTs to the zonal mean in the tropics and finally, setting SSTs to the zonal mean in the extratropics. They concluded that removing tropical SST asymmetry had the largest impact and hypothesised that convection related to the Asian monsoon induces a stationary Rossby wave which creates the split atmospheric flow over the South Pacific.

Other authors have emphasised the role of the subtropical jet, which forms in late spring (Williams et al., 2007; Nakamura and Shimpo, 2004). This acts as a waveguide

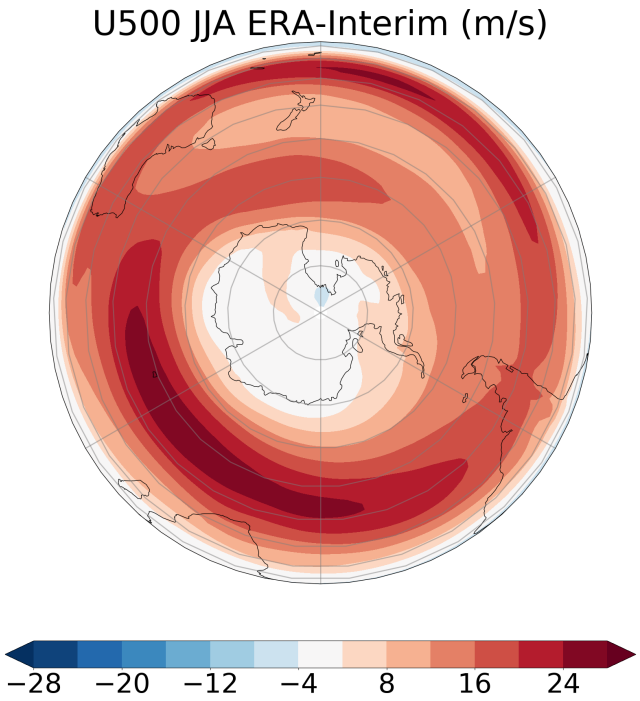


Figure 4.1: ERA-Interim mean zonal wind on the 500hPa level for the SH during JJA. The units are ms^{-1}.

and suppresses the eddy-mean flow feedback of the eddy-driven jet (Nakamura and Sampe, 2002). However, sufficient eddy activity persists at high latitudes to maintain a weak polar jet. Therefore the atmospheric flow is split between a strong subtropical jet and a weak polar jet.

Furthermore, Ogawa et al. (2016) suggested that the location of the mid-latitude SST front is crucial for the South Pacific split jet structure. The strong temperature gradients associated with the SST front give rise to large baroclinicity and hence can provide a source of transient eddies. Ogawa et al. (2016) argued that as the SST front over the South Pacific is located at high latitudes (around 55S), there is sufficient separation from the subtropical jet for an eddy-driven jet to form. Conversely the Indian Ocean jet is located at approximately 40S and thus the eddy-driven jet does not separate from the subtropical jet.

Additionally, a significant perturbation to the SH circulation is provided by Antarctica. The year-round presence of snow and ice keeps the air above cold, maintaining

a strong equator-to-pole temperature contrast. Moreover, much of the Antarctic continent is covered with over 3km of ice and the presence of this orography enhances longwave cooling to space (Ogura and Abe-Ouchi, 2001; Singh et al., 2016), further cooling the surface. Longwave cooling at the top of the Plateau drives a strong and relatively persistent drainage flow which is sharply constrained by topography (Parish and Bromwich, 2007). The drainage flow is fed by a meridional overturning circulation which rises between 60S and 70S, moves polewards at upper levels and subsides over the continent (Parish and Bromwich, 2007). Whilst the overturning circulation is thermally direct, eddy fluxes of momentum and heat are necessary to maintain the balance with the easterly Coriolis torque (Juckes et al., 1994).

Several studies have examined the effect of removing Antarctic orography on high-latitude climate. Some consistent findings have included an increase in poleward heat flux (Mechoso, 1980, 1981; Parish and Bromwich, 2007; Quintanar and Mechoso, 1995; Walsh et al., 2000; Ogura and Abe-Ouchi, 2001; Singh et al., 2016), an increase in poleward momentum flux (Egger, 1991; Parish et al., 1994; Singh et al., 2016) and a reduction in high latitude cyclogenesis (Mechoso, 1980; Simmonds and Law, 1995; Walsh et al., 2000). Additionally, Lachlan-Cope et al. (2001) noted that the Antarctic Plateau is displaced by over 10° from the South Pole, resulting in a significant non-axisymmetric perturbation to the flow. Using AGCM experiments they found that the displacement of the orography is responsible for the existence of the Amundsen Sea Low, a highly variable region of sea level pressure near the West Antarctic coastline. It is clear that Antarctic orography influences the circulation at high latitudes, but how much of a role does it play in shaping the flow in the mid-latitudes?

With respect to past climates, topography of the Antarctic ice sheet has varied considerably over timescales of order 10,000 years or longer. The West Antarctic ice-sheet was likely around 1000m higher at the Last Glacial Maximum (LGM, approx. 21,000 years before present, Peltier, 2004) and Justino et al. (2015) found that low-

ering of the LGM ice sheet towards present day conditions, in an idealised coupled model, produced a weakening of the SH westerly winds. On the other hand, Chavaillaz et al. (2013) examined six PMIP3 models (Braconnot et al., 2012) and found that some models exhibited a jet weakening and others a jet strengthening. Wind anomalies from this period are also poorly constrained by proxy evidence (Kohfeld et al., 2013). Considering much longer timescales, Justino et al. (2014) performed simulations with Antarctic orography lowered by 25%, mimicking conditions in the mid to late Miocene (approx. 15 million years ago) and found weakened zonal–mean winds in mid-latitudes.

In this study I build on the work of Inatsu and Hoskins (2004) and investigate the influence that altering various surface boundary conditions has on the zonally asymmetric structure of the SH wintertime circulation. I particularly consider the importance of Antarctic orography for the configuration of jet streams and demonstrate that without the Plateau, the split jet does not form over the South Pacific.

In section 4.2 the model and experiments are described followed by a comparison of the CONTROL experiment with ERA-Interim reanalysis in section 4.3. The circulation in each of the model runs is then discussed in section 4.4 before going into more depth on the role of Antarctic orography in section 4.5. Subsequently, in section 4.6 a barotropic model is employed to explain some of the effects of orography on circulation and conclusions are given in section 4.7.

4.2 Data and methodology

Isca

For this study I perform a set of idealised AGCM experiments using the modelling framework, Isca (Vallis et al., 2018). My CONTROL experiment is broadly similar to the setup used by Thomson and Vallis (2018) except I use prescribed SSTs rather than a slab ocean. The model integrates the primitive equations using a spectral

dynamical core with 40 levels in the vertical and at T42 horizontal resolution. This translates to a grid-point spacing of approximately 2.8° at the equator. The model is run on uneven sigma co-ordinates, with the distribution of model levels weighted towards the troposphere and a model top at $\sigma = 0.0003$. For each of the plots in this chapter, the sigma levels have been interpolated onto regular pressure levels. The radiation scheme is the Rapid Radiative Transfer Model (RRTM, Clough et al., 2005) which divides longwave and shortwave radiation into 16 and 14 contiguous bands, respectively, with the bands based on the main absorption features of atmospheric gases. It utilises the correlated-k method which has been shown to be both computationally efficient and accurate when compared to line-by-line radiative transfer codes (Clough et al., 2005). In each run, I set the carbon dioxide concentration to be fixed at 350ppmv and prescribe a zonal mean ozone profile, set at 1990 levels. Clouds are not represented in this model, though evaporation from the surface is parameterised as in Frierson et al. (2006) and Thomson and Vallis (2018). Water vapour is thus present in the atmosphere and is advected with the flow, interacting with the atmosphere via latent heating effects and absorption of longwave and shortwave radiation. The model features a fast condensation scheme, again following Frierson et al. (2006), in which water vapour, removed as precipitation, instantaneously reaches the surface. Convection is parameterised using the Betts-Miller scheme (Betts and Miller, 1986) and the boundary layer is represented via a Monin–Obukhov scheme (Frierson et al., 2006). To include the effect of gravity wave drag on the upper stratosphere, Rayleigh damping with a timescale of 0.5 days is applied in a sponge layer above 1.5hPa, similar to Polvani and Kushner (2002) and Jucker and Gerber (2017). However, sub-grid orographic effects and orographic gravity wave-drag are excluded from the model. In terms of surface boundary conditions, the same SSTs and ice fraction as used for AMIP (Taylor et al., 2000) are averaged for each month of the year to produce a monthly varying climatology, which is then used to force the model. The effect of ice

on the atmosphere is primarily distinguished from that of land and SSTs by a higher albedo (taken as 0.7 for regions of ice). The low horizontal resolution means that the model will not fully capture sharp SST gradients (Brayshaw et al., 2008; Sampe et al., 2010). However as I will show, the model is able to represent the key features of the SH circulation relatively well and SST perturbations in my experiments are large and hence should be easily captured by the model atmosphere. Finally, land is differentiated from the sea surface by differing parameter values for the albedo, roughness length and evaporative resistance, with values following Thomson and Vallis (2018). The land mask and topographic height field are both taken from ERA-Interim (Dee et al., 2011).

Model experiments

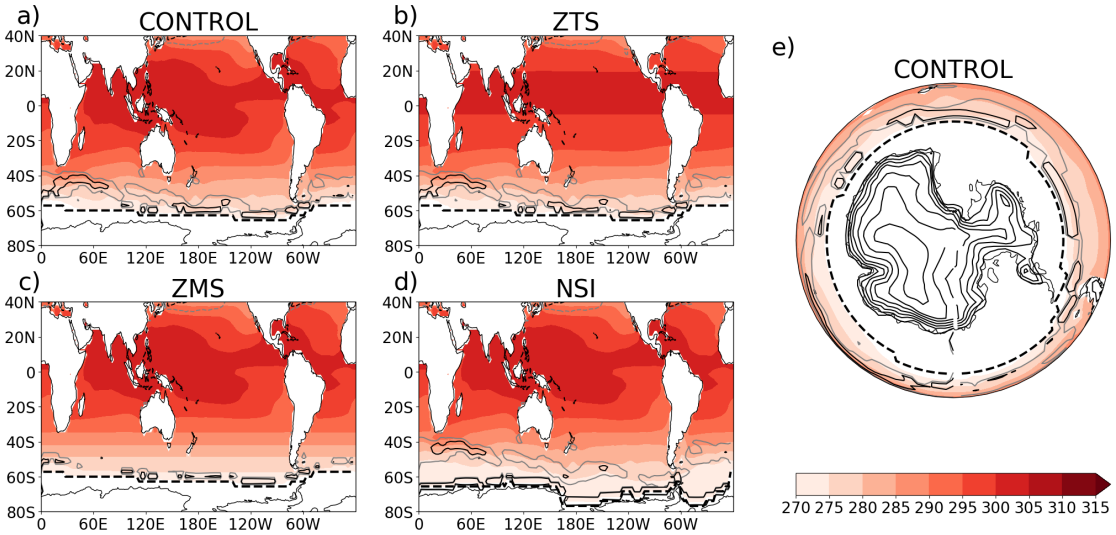


Figure 4.2: A comparison of boundary conditions used in experiments. JJA SSTs are shown by colours for the a) CONTROL, b) ZTS, c) ZMS and d) NSI runs, alongside the 50% sea ice edge indicated by a dashed, black line. Meridional SST gradients above $5 \times 10^{-7} Km^{-1}$ and $8 \times 10^{-7} Km^{-1}$ are indicated by solid grey and black curves respectively. Panel e) shows topography over Antarctica in the CONTROL run with contours drawn every 500m starting at 500m.

Following Inatsu and Hoskins (2004) I alter various boundary conditions and examine the impact of these changes on the atmospheric circulation. An obvious caveat

is that the real atmosphere is coupled with the ocean, so in the real Earth system many of the changes imposed here may be mitigated by changes to ocean circulation. Indeed, Singh et al. (2016) emphasised that including an ocean model reduces the change in atmospheric energy transport upon flattening Antarctica, with the largest reduction occurring in the tropics (their figure 4). However, my focus is on mid to high-latitudes where the change is less significant. Imposing different boundary conditions at the surface also allows us to draw more conclusions about the causality of changes in the model.

A CONTROL experiment is integrated for 30 model years with the first two years taken as spin-up. As in Inatsu and Hoskins (2004), I perform a run with SSTs between 20N and 20S set to the zonal mean and a run with SSTs south of 35S set to the zonal mean. These are respectively labelled ZTS and ZMS. The SST patterns for both of these runs are shown in figure 4.2, along with the region of high SST gradients. It is clear that in the ZMS run, the mid-latitude SST gradients are substantially diminished. In order to test the sensitivity of the jet latitude to the latitude of the sea ice edge, I retreat the sea ice edge back to the edge of the land mass calling this run NSI (figure 4.2d). In regions where sea ice is removed, the SSTs are taken to be 273K. Finally, to test the role of Antarctic orography in SH circulation, I run the model with Antarctic orography removed. Figure 4.2e shows the CONTROL orography contoured every 500m. The height and steepness of surface elevation are most significant over East Antarctica where it rises steeply from the coast to over 3000m above sea level. I create two runs without Antarctic orography, the first with SSTs as in the CONTROL (NOROG) and the second with the same SSTs as in the ZTS run (NOROG_ZTS). A summary of the model boundary conditions for each run is given in table 4.1.

Table 4.1: A summary of the boundary conditions used for all experiments.

Experiment	SSTs and sea ice	Land and orography
CONTROL	Seasonally varying climatology, taken from AMIP (Taylor et al., 2000)	As in ERA-Interim
ZTS	SSTs 20N to 20S set to zonal mean with a smooth transition to 35N/S	As in CONTROL
ZMS	SSTs south of 35S set to zonal mean with a smooth transition 20S to 35S	As in CONTROL
NSI	Sea ice edge moved back to the edge of land	As in CONTROL
NOROG	As in CONTROL	Antarctic orography removed
ZTS_NOROG	As in ZTS	Antarctic orography removed
COOL	As in CONTROL	Antarctic orography removed

4.3 Comparison of the control run with ERA-Interim reanalysis

The experiments that I perform are idealised, however I still require that the model CONTROL run represents the atmosphere sufficiently well for my results to map onto the real Earth system. Therefore, I here plot a number of diagnostics showing the performance of the Isca CONTROL run against reanalysis data. The Hadley cell is a crucial feature of the global circulation in that it regulates poleward energy and

momentum transport. The winter zonal mean overturning stream function, $\psi(\phi, p)$, is shown in figure 4.3 for both ERA-Interim and CONTROL. $\psi(\phi, p)$ is defined, following Oort and Yienger (1996), as

$$\psi(\phi, p) = \frac{2\pi\, a\, cos\phi}{g} \int_{p}^{p_s} [\overline{v}(p', \phi)] dp', \tag{4.1}$$

where a is the radius of the Earth, g is the acceleration due to gravity, p_s is the surface pressure and $\overline{v}$ is the zonal mean meridional wind.

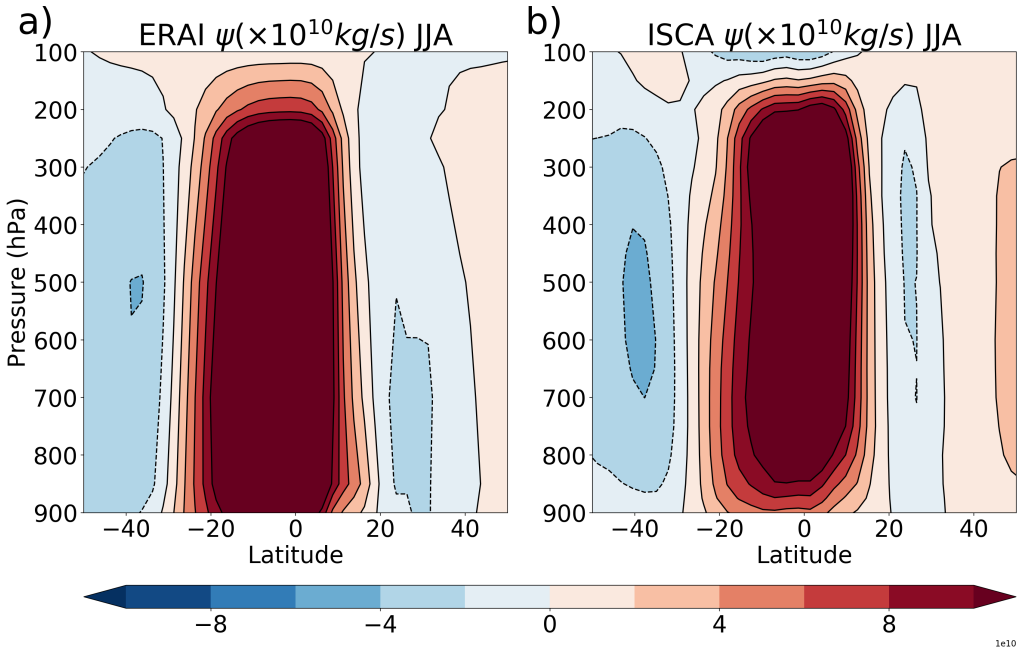


Figure 4.3: Zonal mean overturning stream function, ψ, in winter (JJA) for a) ERA-Interim and b) CONTROL.

Broadly speaking, the structure of the dominant winter Hadley cell is well captured in CONTROL, with an anti-clockwise cell rising at about 10N and descending in the SH subtropics. However, the descending branch of the Hadley cell is located slightly further equatorward than in ERA-Interim. The Ferrel cell on the poleward side of the winter Hadley cell also appears to be relatively well represented, though is slightly too strong. Continuing to examine the zonal mean, figure 4.4 shows a comparison of the JJA zonal mean temperature and zonal mean zonal wind between the CONTROL run

and ERA-Interim. Much like coupled climate models in CMIP5 (Taylor et al., 2012), the model extratropical troposphere is cold-biased and the jet is overly equatorward (Bracegirdle et al., 2013; Simpson et al., 2014; Lee, 2015). The temperature bias has a magnitude of around 1-2K in most of the troposphere, but is substantially higher in the lower stratosphere, reaching 9K. It is likely that the lack of gravity wave drag in the model's lower stratosphere contributes to these biases (e.g. McFarlane, 1987). With respect to the zonal wind structure, the mid-latitude jet over the Indian Ocean is too strong and equatorwards, while the polar front jet over the South Pacific is too weak, the latter being a result found in many CMIP5 models (Arakelian and Codron, 2012; Bracegirdle et al., 2013).

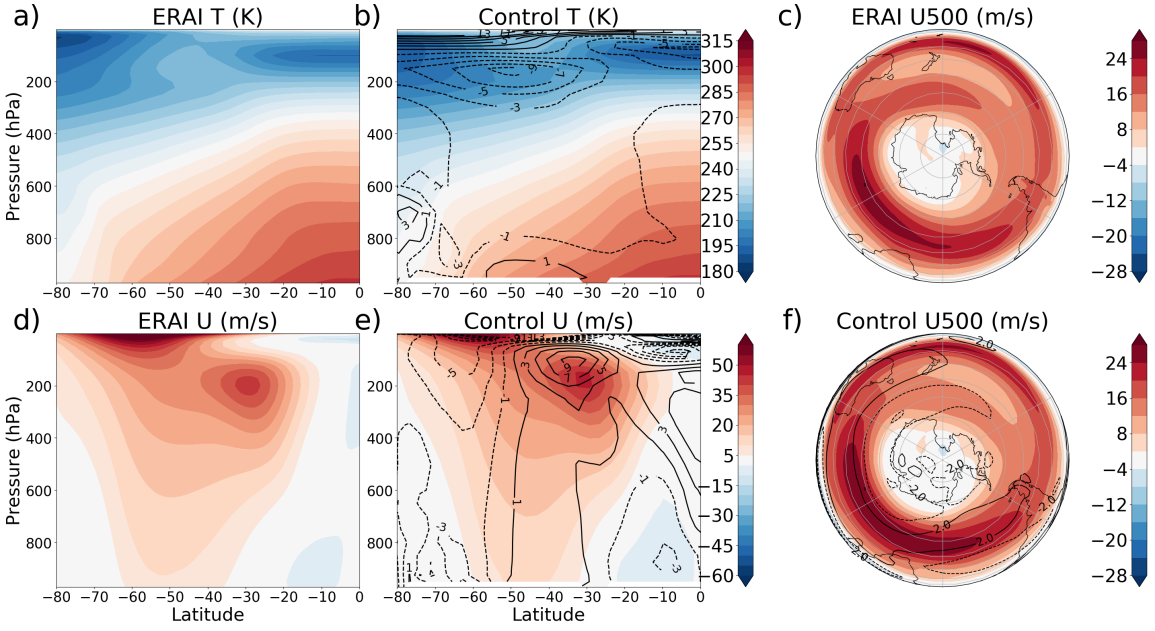


Figure 4.4: Comparison of wintertime (JJA) zonal wind and temperature in the CONTROL run with ERA-Interim (1979-2014). Zonal mean temperature is shown by colours for a) ERA-Interim and b) CONTROL with contours in b) indicating the model bias, CONTROL - ERA-Interim (contour interval $2K$, beginning at $\pm 1K$). Panels d) and e) are the same as a) and b) respectively, but for zonal mean zonal wind (bias contour interval of $2ms^{-1}$, beginning at $\pm 1ms^{-1}$). The 500hPa zonal wind is shown for c) ERA-Interim and f) CONTROL with contours again showing the bias (contour interval $2ms^{-1}$)

This chapter is primarily concerned with the wintertime circulation, but for com-

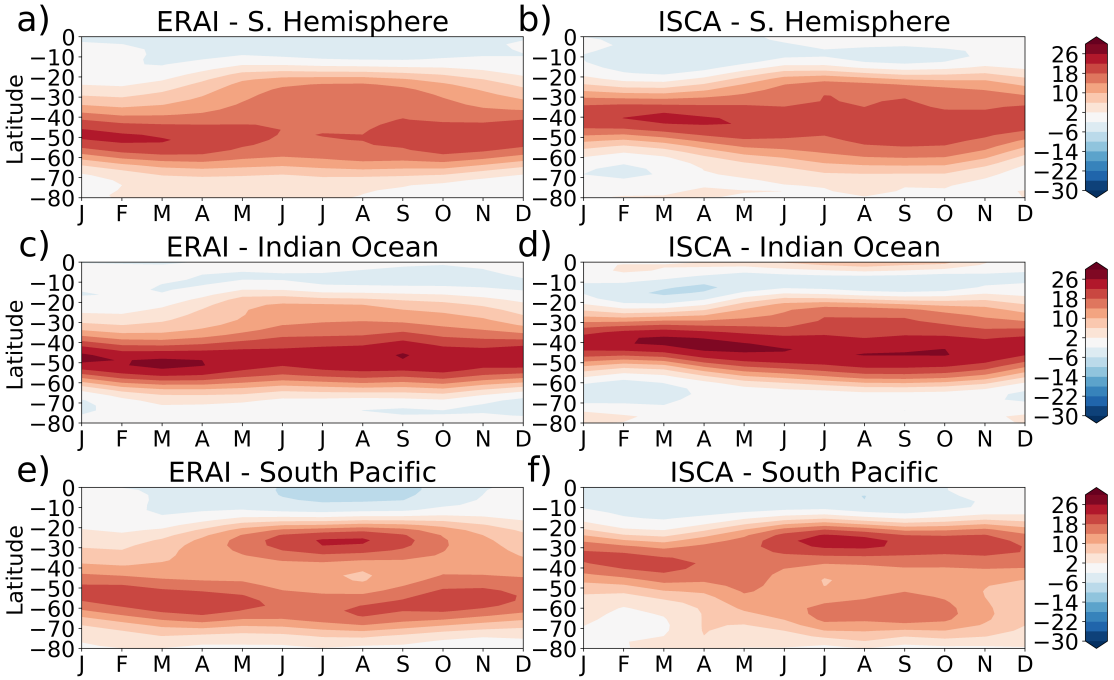


Figure 4.5: The seasonal cycle of sector zonal mean 500hPa zonal wind for a,c,e) ERA-Interim and b,d,f) CONTROL. The sector zonal mean is shown for a,b) the entire southern hemisphere, c,d) the Indian Ocean sector (30E-120E) and e,f) South Pacific sector (150E-240E). Units are ms^{-1}.

pleteness I also show the seasonal cycle of 500hPa zonal wind in figure 4.5. These plots are constructed by taking the zonal mean within three sectors; over all of the SH, over the Indian Ocean sector (30E to 120E) and over the South Pacific sector (150E-240E). Generally, the observed seasonal cycle of the SH (figure 4.5a) shows a broadening in latitude and weakening of the westerlies in wintertime. The broadening of the westerlies is replicated in CONTROL (figure 4.5b), however the zonal mean jet remains too strong in winter, with little variation across the season in jet speed. The Indian Ocean jet (figure 4.5c,d) varies little across the year apart from a slight equatorward expansion of the westerlies from around May to October, which is relatively well captured in CONTROL. However, the equatorward bias seen in figure 4.4e is also apparent when comparing ERA-Interim and CONTROL in the Indian Ocean sector. Unfortunately, the summertime South Pacific mid-latitude jet is not particularly well captured, as the mid-latitude jet is strongly equatorward-biased, while the

high latitude flow is too weak (figure 4.5e,f). Around May, a double jet structure forms in ERA-Interim (figure 4.5e), however this is not a clear feature until around July in CONTROL.

It is clear that the CONTROL run is a far from perfect representation of the SH circulation and its summertime jet, in particular, is placed considerably equatorward of its position in ERA-Interim. However, the model captures most of the salient features of the wintertime circulation including the split jet and the stronger Indian Ocean jet. Considering that this study is idealised, I conclude that it represents the wintertime SH circulation sufficiently well enough for my purposes.

4.4 Tropical SST asymmetries and stationary Rossby waves

The key result of Inatsu and Hoskins (2004) was that the observed stationary wave pattern and much of the zonally asymmetric structure to the SH winter circulation is forced by tropical SST asymmetries. In order to show that this is reproduced in my experiments, I now plot the 300hPa stationary eddy stream function, $\psi*$, calculated as the zonally asymmetric component of the stream function, along with wave activity flux vectors (Takaya and Nakamura, 2001), W, in figure 4.6. Under the WKB approximation, W vectors are parallel to the Rossby wave group velocity. Here I calculate W using monthly-mean data to isolate the stationary wave activity flux. The definition of W can be found along with further details in section 3.4.5. The CONTROL run (figure 4.6a) is dominated by zonal wavenumber 1 waves with wave activity propagating south-eastwards from the Indian Ocean and refracting equatorwards to the east of the dateline. This is consistent with Inatsu and Hoskins (2006) (their figure 3c). In most of the runs this pattern of wave propagation remains largely the same as in CONTROL, however in agreement with Inatsu and Hoskins (2004) and Quintanar and Mechoso (1995), the stationary wave pattern and wave activity flux is

severely diminished in the runs with zonally symmetric SSTs in the tropics (4.6b and 4.6c). The stationary waves are more subtly modified by the removal of Antarctic orography (figure 4.6d) as the pattern of cyclonic and anticyclonic anomalies remains broadly the same, but the centre of action over the Indian Ocean is diminished and the wave activity flux is weakened. The Antarctic Plateau clearly does exert some influence on stationary wave propagation as the pattern of wave activity flux found in ZTS (figure 4.6b) is much weaker in ZTS_NOROG (figure 4.6c).

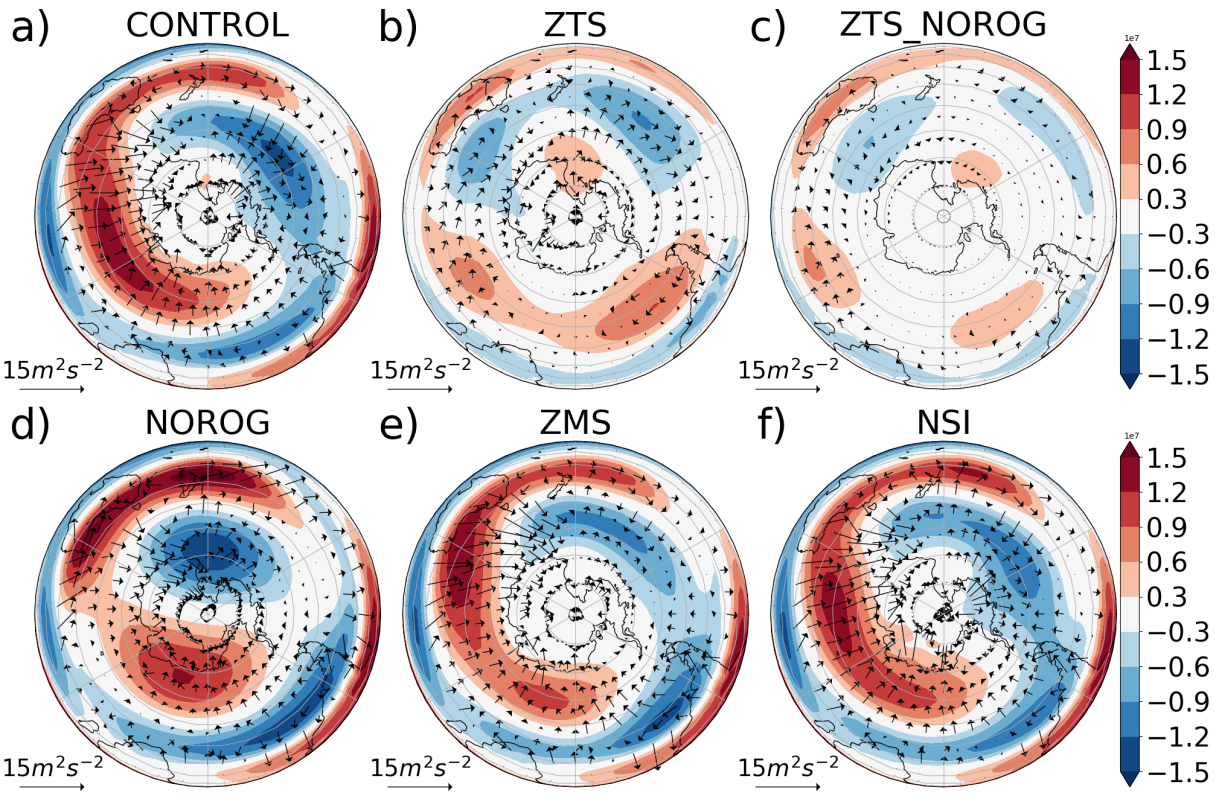


Figure 4.6: Time-mean stationary waves for the different model runs during JJA. Each panel shows the 300hPa stationary eddy stream function in colours with contour interval $0.3 \times 10^{-7} m^2 s^{-1}$ alongside wave activity flux vectors on the same level. Red and blue colours indicate anomalously cyclonic and anticyclonic flow respectively.

Figure 4.7 shows the 500hPa wind and provides a complementary picture to the stationary wave changes in figure 4.6. In spite of the changes to surface temperature gradients and thus local baroclinicity in the ZMS experiment (figure 4.7e), the circulation is relatively unchanged. This appears to contradict the results of Ogawa et al.

(2016) who found considerable differences between runs with and without strong SST gradients. However a key difference lies in the fact that Ogawa et al. (2016) modified SST gradients by changing the meridional structure of the zonal mean SST (see their figure 1), whereas in my experiments the zonal mean SST is preserved. In the latter case, the zonal mean temperature profile will be largely the same as in the CONTROL state, however in the former case this will change, altering the zonal mean winds in line with thermal-wind balance. Hence, it may be that some of the changes observed by Ogawa et al. (2016) relate more to the change in equator-to-pole temperature gradient than to local SST gradients. The NSI run (figure 4.7f) shows a slight weakening of the eddy-driven jet in the South-East Pacific, off the Antarctic peninsula. It is notable that the South Pacific jet in CONTROL is located at high latitudes where it may be affected by removal of the proximal sea ice edge.

As expected, the circulation in the ZTS run is much more zonally symmetric than CONTROL, with the subtropical jet no longer a distinct feature and hence the South Pacific split jet pattern is destroyed (figure 4.7b). However, the split jet pattern is also absent in the NOROG experiment, but for a different reason, as the high latitude winds over the South Pacific are severely weakened and the subtropical jet is enhanced (figure 4.7d). Over the South Pacific, the anomalies seen in these two runs with respect to CONTROL are almost equal and opposite, though both runs show a weakening over the Indian Ocean. Close examination of zonal wind changes in the ZTS_NOROG run (figure 4.7c) reveals that the responses to removal of tropical SST asymmetries and flattening Antarctica, do not add linearly over the high latitude South Pacific. That is, taken individually, removing tropical SST asymmetries and flattening Antarctica are both associated with a reduction in the strength of high latitude westerlies over the South Pacific (figure 4.7b,d), but this is not the case in ZTS_NOROG (figure 4.7c). Note that this study does not assume linearity, rather, I am demonstrating that the observed structure is contingent upon certain key bound-

ary conditions. Another way in which to view the non-linear behaviour is to say that removal of Antarctic orography has a larger impact on atmospheric circulation in the presence of a stationary wave induced by tropical SSTs. Regarding the cause of non-linearity, this requires either non-linear interaction between stationary wave patterns induced by tropical and high-latitude sources or that transient eddy momentum fluxes play an important role. Seeing that the ZMS and NSI runs do not differ as markedly from the CONTROL run and the role of tropical SST asymmetry has been extensively discussed elsewhere (e.g. Inatsu and Hoskins, 2004, 2006), I now focus on the runs without Antarctic orography.

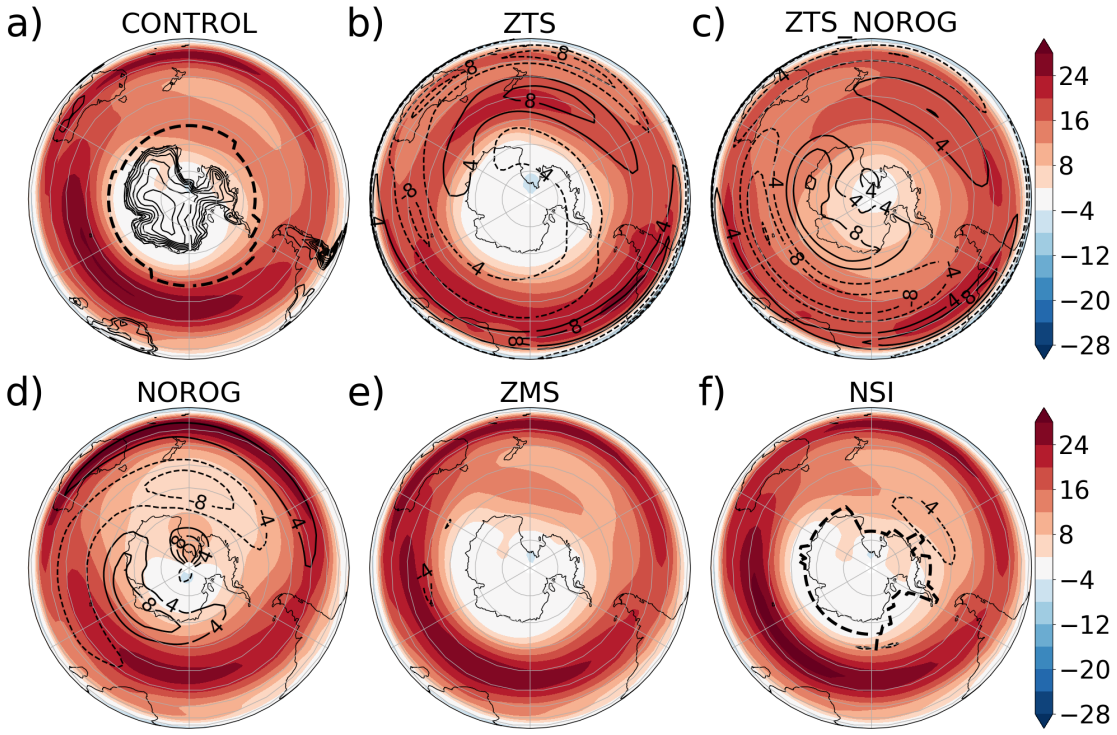


Figure 4.7: Same as figure 4.6 but for 500hPa zonal wind. All panels show the climatology for the given run in colours and panels b) - f) show the climatology minus the CONTROL run in contours, with contour interval $4ms^{-1}$. Panel a) shows the 50% sea ice edge and topography (contoured every 500m) and panel f) the 50% sea ice edge for their respective runs.

4.5 Effects of removing Antarctic orography

Effect on temperature

Previous studies on the effect of removing Antarctic orography have shown that the surface and air temperatures at high latitudes increase when the Plateau is removed (Ogura and Abe-Ouchi, 2001; Singh et al., 2016). Figure 4.8a, which shows the temperature difference between the NOROG and CONTROL runs, illustrates this point. The largest changes to the zonal mean temperature occur below 500hPa (figure 4.8a). However, it is clear from figure 4.8c that there is a substantial zonal asymmetry to these temperature changes, with increases in 500hPa temperature of 6K over parts of East Antarctica and no significant change over West Antarctica. These regionally varying changes closely correspond with the changes to elevation between the NOROG and CONTROL runs (figure 4.2).

The temperature changes occur for two reasons. Firstly, in the absence of orography, the column of air is deepened and hence there is more mass to absorb longwave radiation from the surface. This in turn heats the atmosphere which re-emits and warms the surface. Secondly, the removal of the Plateau allows transient eddies, which would normally be confined to the coastline, to access the continent and hence transport heat from lower latitudes, balancing the enhanced loss of energy to space. It therefore appears that there are two main ways in which removal of the Antarctic Plateau could alter the circulation, namely effects relating directly to the removal of the orography and effects through changes to the temperature gradients at high southern latitudes.

To try and understand which of these effects is more important in explaining the circulation changes seen in figures 4.6e and 4.7e, I perform a run without the Antarctic orography, but imposing a cooling tendency at high latitudes. This cooling is designed to cancel the temperature effects of removing the Plateau. The cooling tendencies are calculated first by performing a run like NOROG, but with Newtonian

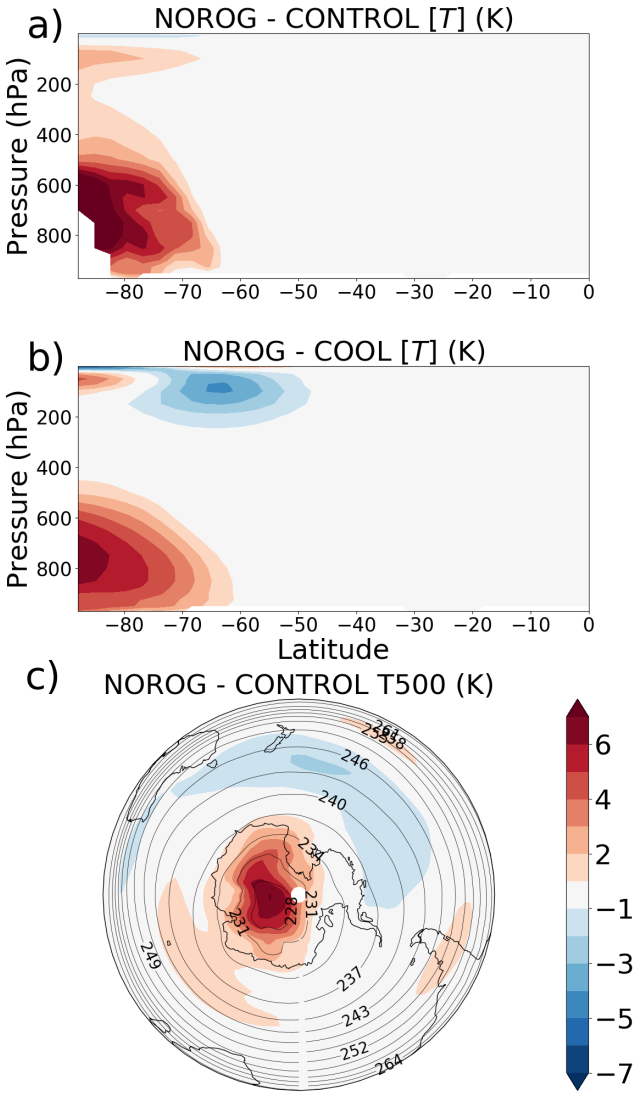


Figure 4.8: Temperature differences between the CONTROL, NOROG and COOL runs in JJA. The zonal mean temperature difference is shown for a) NOROG - CONTROL and b) NOROG - COOL, and in c) temperature difference on the 500hPa level is shown for NOROG - CONTROL. In c), contours indicate the CONTROL climatology values, with contour interval 3K.

relaxation of the temperature field south of 65S at all pressure levels, to a seasonally varying climatology calculated from CONTROL. For regions in the CONTROL run which are masked out by orography, I set the relaxation temperature to follow a dry adiabatic lapse rate to the surface. The Newtonian cooling tendencies saved from this run are then used to create a climatology. Finally, a run without the Plateau is performed with the seasonally varying cooling tendencies imposed, named COOL.

The advantage of using this method is that it doesn't damp out eddy activity at high latitudes as is the case in the Newtonian relaxation run. Figure 4.8b shows the temperature difference between NOROG and COOL, which is similar to the difference between NOROG and CONTROL. The main difference is a cold anomaly in the lower stratosphere between 60S and 70S. The lower tropospheric temperature perturbation is of the same magnitude in both cases, with a peak of 6-7K. It should be noted that while only the zonal mean temperature difference between COOL and NOROG is shown, the applied cooling is substantially zonally asymmetric.

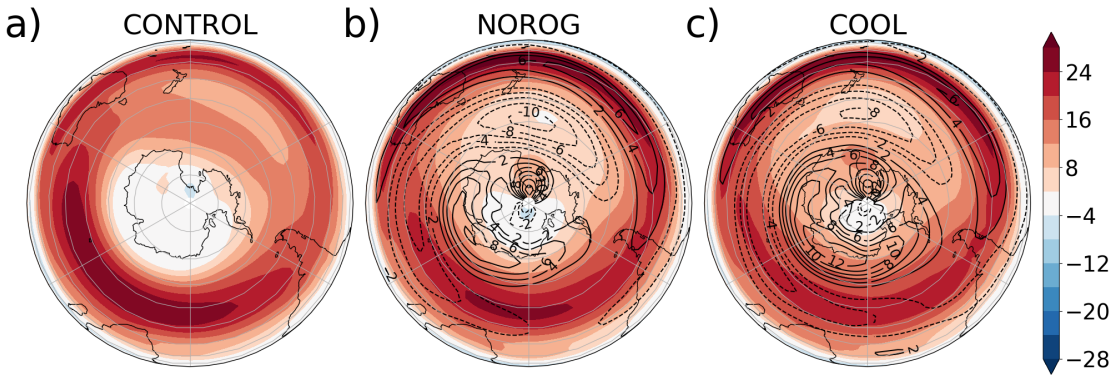


Figure 4.9: 500hPa zonal wind in the run with cooling imposed. The climatology is shown by colours for a) CONTROL, b) NOROG and c) COOL, and in b) and c) contours indicate the difference from CONTROL with contour interval $2ms^{-1}$.

In figure 4.9, a comparison is made of the 500hPa zonal wind fields in CONTROL, NOROG and COOL. It is clear that even with strong cooling of polar temperatures, the wind change from the CONTROL run is very similar to NOROG (figure 4.9b,c). For instance in figure 4.9c, the weakening of the flow over the South Pacific region remains much the same, as does the strengthening of the flow near the East Antarctic coastline. It might be expected that cooling would increase the local baroclinicity and promote stronger winds, but this only occurs at high latitudes and the flow in the mid-latitudes remains severely weakened with respect to CONTROL. This indicates that the removal of the mechanical effects of the orography itself and the subsequent effects on eddy propagation are likely more important in altering the mid-latitude

circulation than the associated temperature perturbation.

Effect on circulation

I have so far noted that the circulation changes associated with flattening Antarctic orography are zonally asymmetric, with significant weakening of zonal wind over the South Pacific (figure 4.7). However, following many of the previous papers which have studied the effect of Antarctic orography on circulation I start by focussing on the zonal mean.

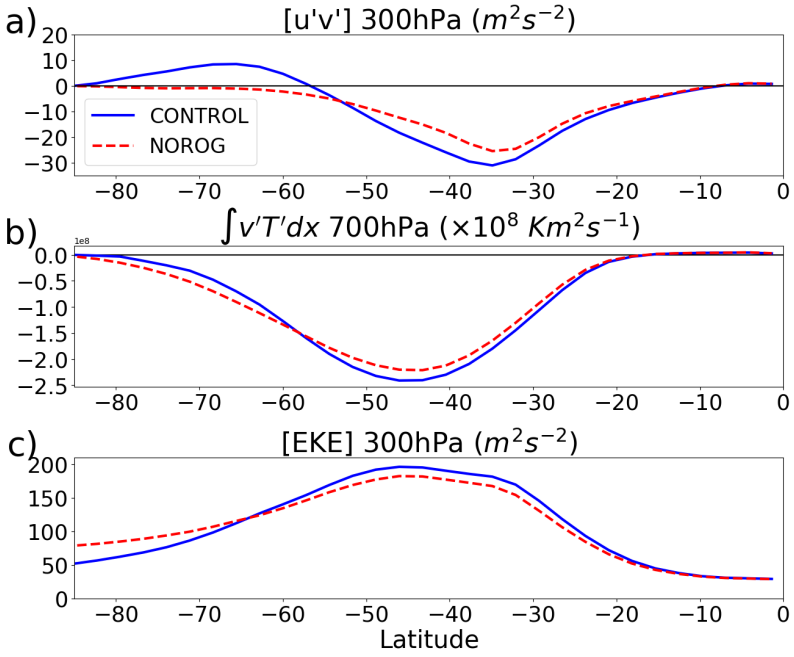


Figure 4.10: Zonal mean eddy statistics for CONTROL and NOROG. a) Zonal mean transient northward eddy momentum flux, $u'v'$, at 300hPa, b) zonally integrated transient northward eddy heat flux, $v'T'$, at 700hPa and c) transient eddy kinetic energy, $u'^2 + v'^2$, at 300hPa. In b), $v'T'$ is undefined under orography, hence $v'T'$ is integrated over all valid longitudes to show total transient eddy heat transport.

In figure 4.10, I plot the zonal mean momentum flux, heat transport and kinetic energy, associated with transient eddies. In calculating each of these quantities, daily-mean u, v and T have each been high pass filtered using a 10-day Lanczos filter (Duchon, 1979), indicated by primes. At high latitudes the CONTROL run sees an equatorward flux of eddy momentum (figure 4.10a) which is absent in NOROG. This

reduces the convergence of eddy momentum in mid-latitudes, hence the weakened mid-latitude winds in NOROG (figure 4.7d,4.9b), consistent with Singh et al. (2016). I suggest that the changes to high latitude eddy momentum flux are likely linked to the removal of the orographic slope and will investigate this further in section 6. High latitude eddy heat flux is enhanced in NOROG as eddies are no longer confined to the coastline around Antarctica (figure 4.10b). However, eddy heat flux is also reduced in mid-latitudes with respect to CONTROL, which is consistent with the decrease in eddy kinetic energy seen in figure 4.10c. The changes to mid-latitude heat flux are in contrast to Mechoso (1981), who found much more substantial increases in eddy heat flux associated with removing the Antarctic Plateau. Interestingly, eddy kinetic energy is greater at high latitudes in NOROG, even though the momentum flux is very weak there. It appears that even if the magnitude of high latitude eddy kinetic energy is lower in CONTROL, the eddies are more efficient at transporting momentum northward than in NOROG. A similar picture is seen in figure 4.11 with zonal wind and EP flux diagnostics (Edmon et al., 1980), which indicate the propagation of wave activity. The definition of EP flux can be found along with further information in section 3.4.3. No time-frequency filtering is applied to u and v in figure 4.11, though if a high pass filter is used, the resulting figures are similar, whereas vectors are substantially diminished when using monthly-mean data. This indicates that transient eddies dominate the observed changes over stationary eddies. For visual clarity, the vertical component of the vectors is multiplied by a factor of 10 when plotting.

In the CONTROL run, the zonal mean zonal wind peaks at around 50S in the lower troposphere and is close to zero over Antarctica. EP flux vectors indicate that waves propagate upwards in the lower troposphere and then mostly equatorwards, strengthening the surface westerlies and eddy-driven jet. On the poleward side of the jet, vectors are directed polewards suggesting an equatorward flux of momentum

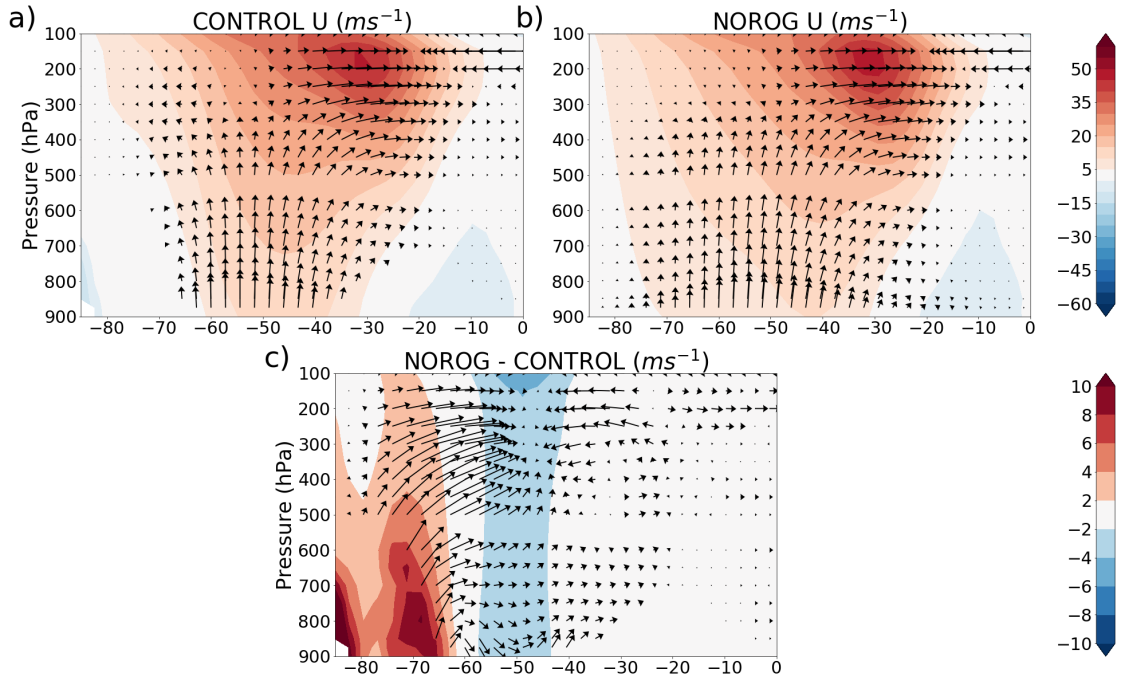


Figure 4.11: EP flux vectors and zonal mean zonal wind for a) CONTROL b) NOROG and c) NOROG - CONTROL. EP flux vectors are not plotted in regions of significant orography.

which helps to maintain the jet on the poleward side. In agreement with previous authors, flattening Antarctica increases the zonal mean zonal wind south of 65S and decreases it in mid-latitudes (Mechoso, 1981; Singh et al., 2016). This is consistent with the fact that in NOROG, there is no equatorward momentum flux reinforcing the poleward flank of the jet (figure 4.10a).

However, the zonal mean masks the considerable zonal structure to the changes seen in figure 4.12. In the CONTROL run, 700hPa $v'T'$ is strongest over the Indian Ocean with weaker, though still significant, heat transport at mid to high latitudes over the South Pacific. Without Antarctic orography, transient eddy heat transport is extended polewards over the South Atlantic and South Indian Oceans as in the zonal mean (figure 4.10b), but $v'T'$ is considerably diminished in the South Pacific region (figure 4.12b,c). Surprisingly, it thus appears that removal of the zonally asymmetric orography creates an even more asymmetric storm track. Figure 4.12

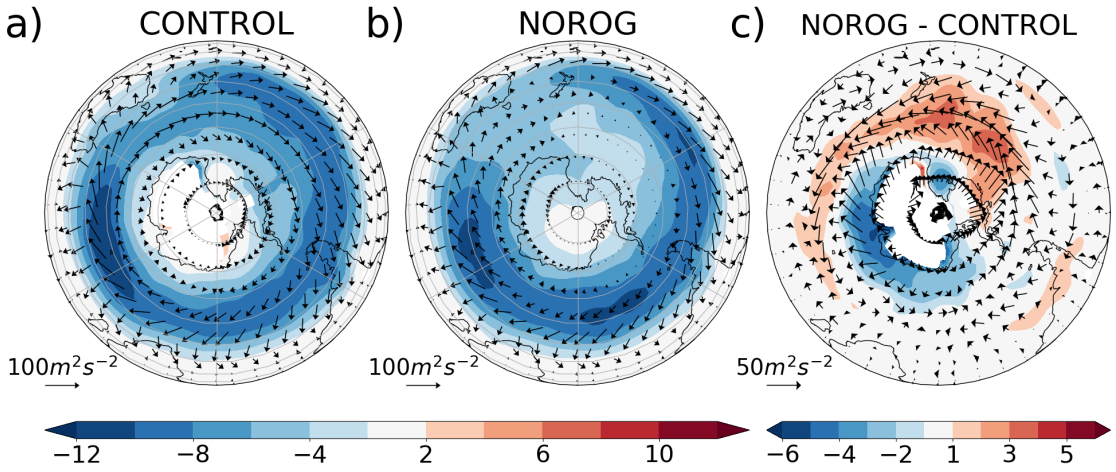


Figure 4.12: Horizontal 300hPa E vectors and 700hPa transient eddy heat flux, $v'T'$ (colours) for a) CONTROL, b) NOROG and c) NOROG - CONTROL. Transient eddy heat flux has units Kms^{-1}. As before, primes indicate filtering with a 10-day high pass filter.

also shows horizontal E vectors (Hoskins et al., 1983) which provide a useful measure of transient wave activity flux on a given pressure level. The westerly acceleration by transient eddies is proportional to the horizontal divergence of the E vectors in a given region. E vectors are defined in section 3.4.4. As was the case with $v'T'$, wave activity is abruptly reduced over the high latitude South Pacific upon flattening Antarctica. The meridional component of E indicates the transient meridional flux of eddy momentum and this dominates the differences between the two runs at high latitudes (figure 4.12c), consistent with figures 4.10a and 4.11.

Thus far it has become clear that the largest mid-latitude circulation changes in response to flattening Antarctica, occur in the South Pacific region (figures 4.7,4.12), downstream of the most significant orography. In addition to the development of local instabilities, the eddies which reinforce the mean flow are often generated from further west by the process of downstream development (Chang and Orlanski, 1993; Hoskins and Hodges, 2005). To investigate the role that Rossby waves from upstream might play, I plot lagged correlations of meridional wind in figure 4.13 as in Chang (1993, 1999). A base-point is chosen (here 180E, 62S, indicated by the white cross)

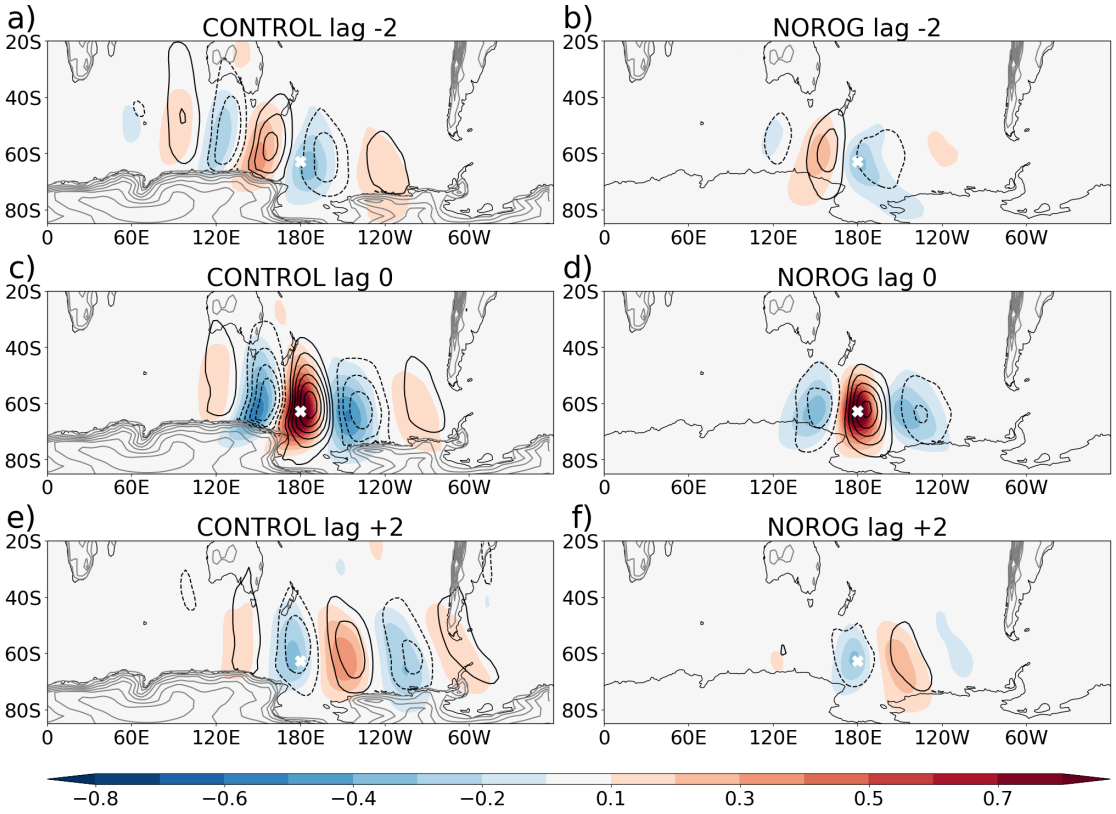


Figure 4.13: Lagged correlations of meridional wind, as described in the text. Correlations of 300hPa meridional wind at the point 180E, 62S (denoted by a cross), with 300hPa wind (colours) and 850hPa wind (contours) are shown in all panels. In both cases the contour interval is 0.1. Topographic contours are also displayed in light grey with contours every 500m, beginning at 500m.

before correlations between 300hPa meridional wind at that point and meridional wind at 850hPa and 300hPa, at all other grid-points are calculated and plotted. In the CONTROL run, meridional wind anomalies over the South Pacific are associated with a Rossby wave train from the Indian Ocean. This initially propagates south-east and continues eastwards toward South America, refracting equatorwards past about 200E. Comparing correlations with 850hPa and 300hPa, there is a close correspondence between anomalies at the two levels, with a slight westward tilt with height indicating the wave has a small baroclinic component. In contrast to the clear Rossby wave train in CONTROL, anomalies in the NOROG run are more localised. This absence of coherent wave activity over the South Pacific in NOROG is consistent with the

weakened mid-latitude flow there (figure 4.7e). It is likely that the equatorward momentum flux on the poleward side of the jet seen in the CONTROL run (figures 4.10a, 4.11 and 4.12a,c), reinforces the jet and enables it to act as a waveguide for transient waves. Removing the orography removes this momentum flux, weakens the Indian Ocean jet and hence makes Rossby wave propagation into the South Pacific less favourable. This is consistent with Codron (2007), who found that South Pacific eddy forcing is strongly influenced by zonal wind anomalies upstream, over the Indian Ocean. I therefore suggest that the reduced transient eddy heat flux and weak E vectors seen over the South Pacific in figure 4.10b, are related to the decrease in wind strength upstream via reductions in downstream development.

4.6 A barotropic model of orographic effects on transient eddies

In the absence of Antarctic orography, the jet stream weakens substantially in the Indian Ocean region (figure 4.7e) with implications for the South Pacific downstream (figure 4.12). My argument so far, concerning reductions in eddy momentum flux changing the circulation, has a degree of circularity to it. This is because the interaction between eddies and the mean flow is a two way process; eddies generate the mean winds and the mean winds alter eddy propagation and also affect eddy generation through baroclinic instability. I now suggest an explanation for the influence of orography on eddy momentum fluxes using a barotropic model with bottom orography, stirred over a range of wavenumbers. Using this model has the advantages that it is conceptually simple and allows a better understanding of causality, as the eddy momentum fluxes generate the zonal winds in this model, but the winds do not affect the stirring which generates the eddies. It is worth noting that the differing mean-wind profiles will have some effect on eddy propagation. However, the key point is that the stirring itself has the same properties in each run meaning that any differences

between runs can ultimately be attributed to the presence or absence of orography.

The model is the same as in Vallis et al. (2004) and Barnes and Hartmann (2011) with the exception that I allow the depth of the fluid layer to vary in the meridional direction. The result of this is to add another term to the barotropic vorticity equation which effectively modifies the planetary vorticity gradient along gradients of orography. The key idea is that the presence of an orographic slope at high southern latitudes means that meridional mixing across the orographic slope will result in a northward flux of vorticity / westerly momentum (e.g. James, 1989; Egger, 1991). That is, an air column moving southward will be squashed and by conservation of potential vorticity, will become more anticyclonic. Conversely, an air column moving northward will be stretched and thus become anomalously cyclonic. I will demonstrate this effect by comparing runs with and without high latitude orography and then explain how the northward vorticity flux is achieved.

I begin with a layer of fluid with depth, H and relative vorticity, ζ. I write the depth of the fluid as $H(\phi) = H_T - h_B(\phi)$ in which H_T is the height of the tropopause, set as 10km, and h_B is the bottom topography. Potential vorticity, P is given by the following,

$$P = \frac{\zeta + f}{H}, \tag{4.2}$$

as in Vallis (2017). Bottom topography is given a profile which is zero to the north of 65S and then slopes upward to a maximum at 90S. A cosinusoidal profile is used for the slope which is shown by a thick curve in figure 4.14c and mathematically described as follows

$$h_B(\phi) = \begin{cases} h_0 \, cos\left(\frac{90}{\phi_w}\left(\phi + 90\right)\right) & \phi \leq -90 + \phi_w \\ 0 & \phi > -90 + \phi_w, \end{cases} \tag{4.3}$$

with $\phi_w = 25^\circ$ and $h_0 = 3km$. The model is integrated on a sphere and takes the following form

$$\frac{\partial \zeta}{\partial t} + \frac{u}{a\cos\phi}\frac{\partial \zeta}{\partial \lambda} + \frac{v}{a}\frac{\partial \zeta}{\partial \phi} + \left(\beta + \frac{\zeta + f}{aH}\frac{\partial h_B}{\partial \phi}\right) v = S - r\zeta + \kappa\nabla^4\zeta, \tag{4.4}$$

where λ and ϕ are the zonal and meridional co-ordinates respectively. Similar to Vallis et al. (2004) and Barnes and Hartmann (2011), I apply stirring, S which parameterises baroclinic instability. S is an Ornstein-Uhlenbeck process defined as

$$S_{lm} = (1 - e^{2dt/\tau})^{1/2} Q^i + e^{-dt/\tau} S_{lm}^{i-1}, \tag{4.5}$$

where l and m are respectively, the total and zonal wavenumber, dt is the timestep (900 seconds), i is an index for the current timestep and τ is a decorrelation timescale equal to 2 days. Q^i is a random number drawn from a uniform distribution in the range $[-7 \times 10^{-11}, 7 \times 10^{-11}]$. The stirring is only applied in mid-latitudes and this is achieved by multiplying S by a Gaussian function of half width 12°, centred on 45S. Linear Ekman damping is employed with coefficient, $r = \frac{1}{5} day^{-1}$ and the loss of vorticity at the smallest, unresolved scales is simulated via 4th order hyperdiffusion.

4.6.1 Barotropic model results

Like in the full Isca model, the barotropic model runs with and without orography are notably different in terms of momentum fluxes near the pole. Figure 4.14 shows the zonal mean zonal wind and transient eddy momentum transport, $u'v'$, in both models. In both Isca and barotropic runs, the model without orography exhibits either weak or poleward momentum fluxes at high latitudes in contrast to the runs with orography, which show substantial equatorward momentum fluxes. With the enhanced equatorward momentum fluxes, there is a clear impact on the jet in both runs with orography, as the wind is reduced at high latitudes and enhanced in mid-latitudes. Note that in the Isca runs, momentum fluxes are shown at 300hPa as these

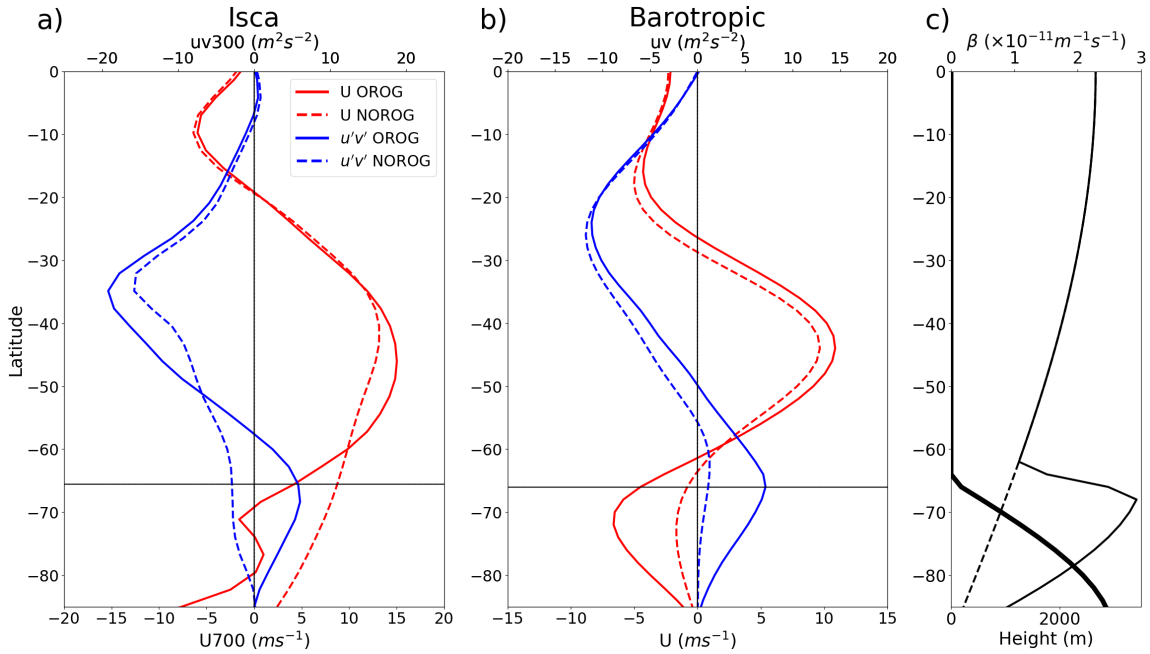


Figure 4.14: Zonal mean momentum flux (blue) and zonal mean zonal wind (red) for a) Isca and b) barotropic model runs. Runs with Antarctic orography are shown by solid curves, while runs without orography are indicated by dashed curves. In a) eddy momentum flux, $u'v'$, is shown on the 300hPa level and zonal mean zonal wind shown at 700hPa. A horizontal line in a) marks the most northward latitude of the Antarctic continent and a similar line in b) marks the edge of the orography. Finally in c), orographic height in the barotropic model is shown by the thick curve and β is plotted as a function of latitude (dashed) with an estimation of the effective 'orographic β' (solid). The orographic β term is a function of vorticity so the time-mean value is shown.

are largest at this level, whereas winds are shown at 700hPa to isolate the eddy-driven jet (e.g. Woollings et al., 2010a). The effective planetary vorticity gradient is also shown in figure 4.14c, defined as

$$\beta_{eff} = \frac{2\Omega\cos(\phi)}{a} + \frac{\zeta + f}{aH}\frac{\partial h_B}{\partial \phi}. \tag{4.6}$$

Figure 4.14c shows the sharp increase in β_{eff} that the orography generates in the barotropic model.

The total wavenumber framework of Hoskins and Karoly (1981) is helpful here in understanding the propagation of waves and hence the momentum fluxes which

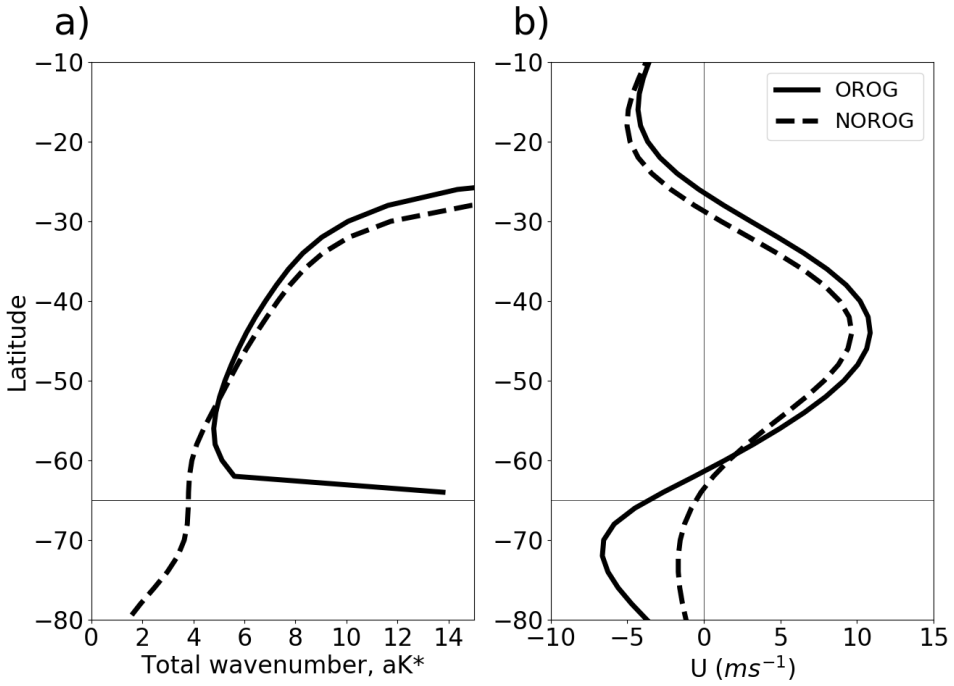


Figure 4.15: a) Total wavenumber and b) zonal wind in the barotropic model runs. A horizontal line at 65S indicates the beginning of the bottom orography.

generate the mean flow. The total wavenumber, K^*, is given by

$$K^* = \cos(\phi) \left(\frac{\beta - \frac{\partial^2 u}{\partial y^2}}{\overline{u} - c} \right)^{\frac{1}{2}}, \tag{4.7}$$

in which $\overline{u} - c$ is the zonal mean zonal wind minus the wave phase speed. In general, waves propagate towards higher K^* until they encounter a turning latitude, where $K^* = k$, or a critical latitude, $\overline{u} = c$, at which K^* becomes infinite and simple barotropic wave theory breaks down, sometimes associated with non-linear wave-breaking (Hoskins and Ambrizzi, 1993). I replace β with β_{eff} as defined above, in the definition of K^*, to account for the additional orographic β effect. Hence K^* becomes

$$K^* = \cos(\phi) \left(\frac{\beta_{eff} - \frac{\partial^2 u}{\partial y^2}}{\overline{u} - c} \right)^{\frac{1}{2}}. \tag{4.8}$$

In figure 4.15a, it can be seen that without bottom orography, K^* generally de-

creases with increasing latitude and so any waves propagating polewards will tend to encounter a turning latitude and refract equatorwards, breaking in the subtropics. Hence the jet will mostly only be enhanced on its equatorward flank by eddy momentum fluxes. On the other hand, waves generated in mid-latitudes in the presence of high latitude orography, can also refract polewards towards higher K^*. For this reason, there will also be a significant equatorward momentum flux in this case, in agreement with figure 4.14 and the full 3D model runs. The profile of K^* is partly shaped by the orographic β term, but the critical latitude at 65S is set by the latitude at which $\overline{u} = c$. Hence, the mean winds largely determine the propagation of transient eddies. However, it is worth emphasising that the only difference between the runs with and without orography is the orographic β term, $\frac{\zeta+f}{aH}\frac{\partial h_B}{\partial \phi}v$, as the eddy stirring is statistically identical. It can therefore be said that the increase in the jet speed is entirely due to the presence of high latitude orography.

In order to check that both Isca and the barotropic models are achieving momentum fluxes in a similar way, I plot correlations of meridional wind in figure 4.16, as in figure 4.13, but for the base-point (110E, 62S) and at lag 0. This base-point is close to the most significant orography which rises steeply over East Antarctica. I also plot correlations for ERA-Interim to connect the results back to observational data. The two models show a remarkable correspondence for both experiments and the orography runs agree well with ERA-Interim.

For runs with orography, correlations show a Rossby wave train, centred on the base-point, with a distinctive southwest-northeast tilt to the positive meridional wind anomaly. This tilted pattern is characteristic of equatorward momentum flux. Downstream, the negative anomaly appears to follow the topographic gradient eastwards and remains at high latitudes. This is less obvious in the barotropic model (with orography), but is clearer at lag +1 (figure 4.17). The waves do not appear to break, but may be propagating along the effective potential vorticity gradient which results

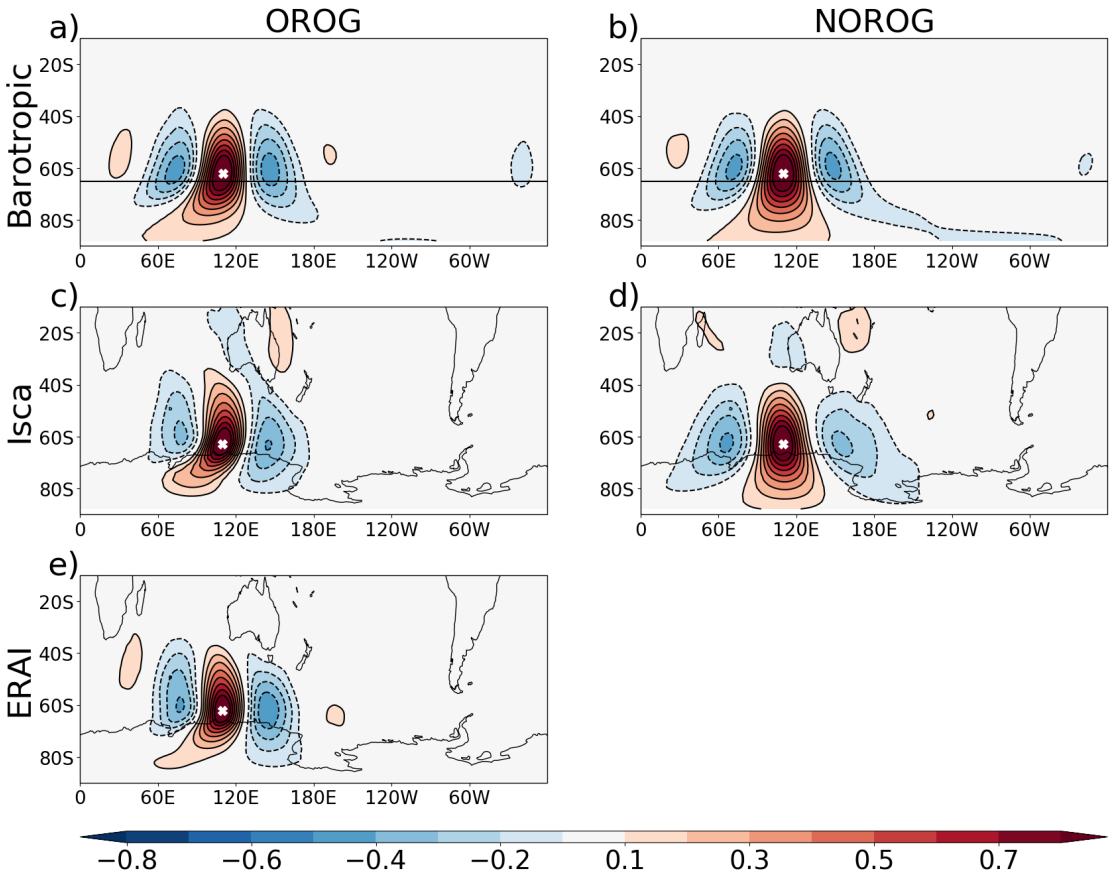


Figure 4.16: 300hPa meridional wind correlation maps as in figure 4.13 but for ERA-Interim, barotropic model runs and Isca runs and using the base-point, 110E, 62S (marked by a white cross).

from the orographic slope (Egger and Fraedrich, 1987). The tilt is caused by the propagation of eddies towards higher K^* as suggested by the poleward critical latitude in figure 4.15a. In contrast to these cases, the correlation patterns in runs without orography (figure 4.16b,d) show a Rossby wave propagating south-eastwards from the west of the base-point, reaching the base-point and then refracting equatorwards. Whilst the waves exhibit a slight southwest-northeast tilt on reaching the base-point, the poleward momentum flux associated with the equatorward refraction cancels this out. Correlations for the runs without orography also appear to pick out a lower wavenumber. This is particularly the case when comparing the Isca runs, as the CONTROL has a typical wavenumber of 4-5 while NOROG exhibits a wavenumber

of around 3-4. Typical wavenumbers of 4-5 at high latitudes in the CONTROL run are in agreement with the observational study of Chang (1999, his figure 3). Generally only the lowest wavenumber waves are able to propagate to high latitudes, but it is likely that the increase in potential vorticity gradient associated with orography allows waves of a higher wavenumber to reach polar latitudes.

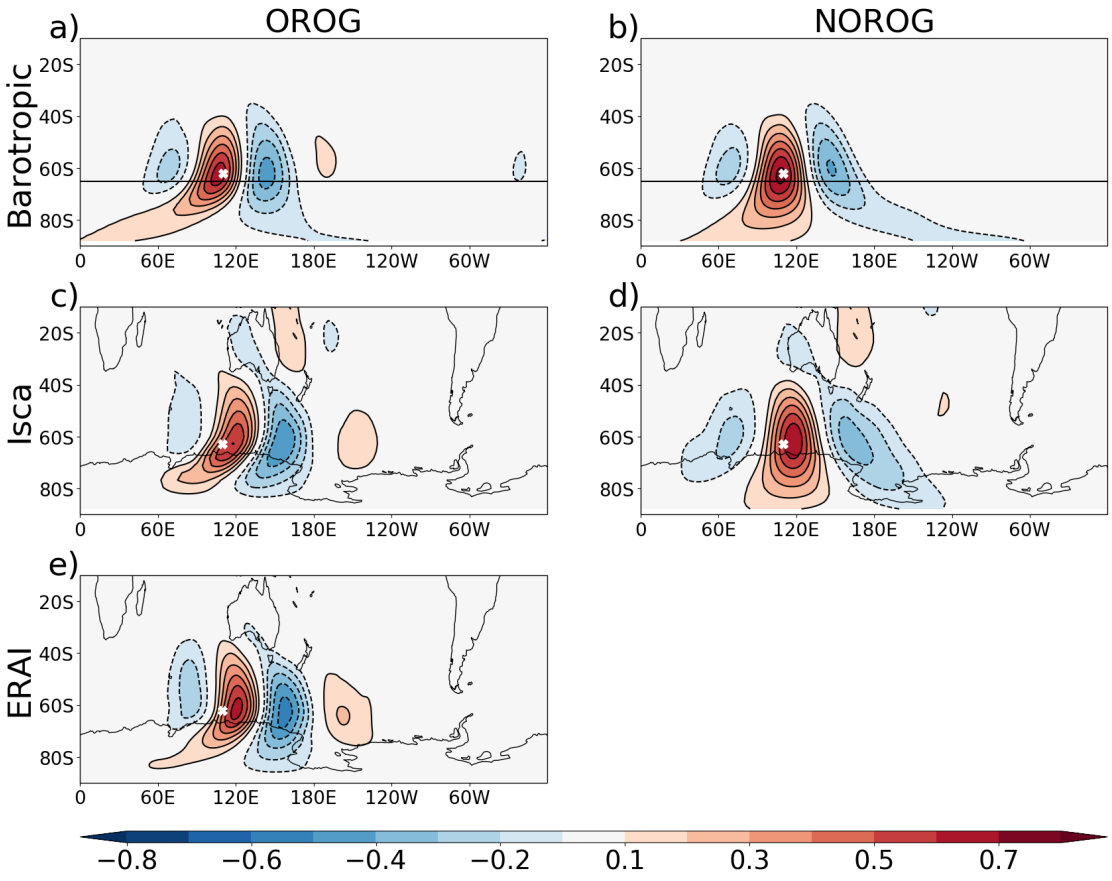


Figure 4.17: As in figure 4.16 but for lag +1.

In summary, when a high latitude orographic slope is imposed in a barotropic model with stochastic forcing, mixing across the orographic slope results in a vorticity flux away from the orography. In the steady state, transient eddies, generated by stirring in mid-latitudes, propagate towards a critical latitude which is set by the presence of high latitude easterlies along the orographic slope. The poleward propagation of eddies results in an equatorward momentum flux and thus the maintenance

of a stronger eddy-driven jet. This is similar to the Indian Ocean sector where there is a steep orographic slope at high latitudes and a strong mid-latitude jet. Conversely, in the barotropic model run with no orography, waves encounter a turning latitude at high latitudes, preventing poleward wave propagation on the poleward side of the jet, consistent with lagged correlation plots in the Isca NOROG run (figure 4.16b).

4.7 Discussion and conclusions

In this chapter I have investigated the processes shaping the wintertime SH circulation by altering various boundary conditions in an idealised model. In agreement with previous work, the longitudinal structure of tropical SSTs was found to be critical for the formation of a quasi-stationary Rossby wave which creates the South Pacific split jet (Inatsu and Hoskins, 2004, 2006). In contrast, removing the zonally asymmetric components of mid to high latitude SSTs resulted in relatively weak changes to the overall circulation. Retreating sea ice back to the Antarctic continent made only a small difference, as in the experiments of Kidston et al. (2011a), though it did weaken the high latitude jet over the South-East Pacific.

In addition to tropical SSTs, I found the presence of orography over Antarctica to have a leading order effect on mid-latitude circulation. Without the Antarctic Plateau, eddy activity over the Indian Ocean increased and was able to penetrate further polewards. However, high-latitude equatorward momentum fluxes also ceased, weakening the eddy driven jet. The largest changes occurred downstream in the South Pacific region as the storm track abruptly terminated over the Indian Ocean (illustrated by $v'T'$ in figure 4.12). Concomitantly, the mid to high latitude winds over the South Pacific severely weakened and the split jet was destroyed. Whilst idealised, these experiments illustrate the dependence of the wintertime South Pacific circulation on the flow upstream over the Indian Ocean (e.g. Chang, 1999; Codron, 2007). Propagation of Rossby waves from the Indian Ocean to the South Pacific became less

favourable in the absence of Antarctic orography (figure 4.13), likely because of the weakening of the Indian Ocean jet, making it less effective as a waveguide (Hoskins and Ambrizzi, 1993). These results appear all the more intriguing when considering that Antarctic orography is itself considerably zonally asymmetric, and yet removing this feature results in an even more zonally asymmetric atmospheric circulation. I also noted that circulation anomalies associated with removal of tropical SST asymmetries and anomalies associated with flattening Antarctica, do not add linearly when both changes are imposed in the same run (figure 4.7c). This non-linearity is particularly seen over the South Pacific and could be related to the dependence of the South Pacific on downstream propagation of transient Rossby waves, as discussed above.

My results have broadly been in agreement with those of previous studies investigating the effect of Antarctic orography on circulation. For instance, I found a large warming at high latitudes and an increase in poleward heat flux at high latitudes upon flattening Antarctica (Mechoso, 1981; Simmonds and Law, 1995; Ogura and Abe-Ouchi, 2001; Singh et al., 2016). At the same time, I found an increase in high latitude westerly winds and a decrease in wind strength in mid-latitudes (Mechoso, 1981; Singh et al., 2016). Furthermore, I showed substantial zonal asymmetries to the mid-latitude circulation response, with the largest changes occurring in the South Pacific region, a finding which was alluded to in Simmonds and Law (1995). However, in contrast to Simmonds and Law (1995), I have found that the temperature perturbation resulting from flattening Antarctica, is of lesser importance in determining changes to large-scale atmospheric dynamics (figure 4.9). Rather, I have shown that it is the presence of the orographic slope itself which altered the dynamics of eddies, increasing the convergence of eddy momentum in mid-latitudes. Flattening the orography in Isca enabled transient eddies to penetrate further south over the Antarctic continent, as measured in eddy kinetic energy and heat transport. Despite this, the eddy momentum fluxes over Antarctica are considerably stronger in the case

with orography.

I have provided an explanation for this influence of Antarctic orography on mid-latitudes using a simple barotropic model with bottom topography varying in latitude. The effect of this was to add an additional orographic β term which modified high latitude eddy momentum fluxes, enhancing the eddy-driven jet in mid-latitudes. β is relatively weak at high latitudes (figure 4.14c), but as a result of the orographic β effect and changes to the zonal mean wind profile, it appears that waves tend to refract polewards towards the greater potential vorticity gradient (figure 4.16). The eddies thus exhibit a southwest-northeast tilt at high latitudes, which is effective at transporting momentum equatorwards, strengthening the jet. Whilst simplified, I have shown that the output of this model corresponds closely, at least in a qualitative sense, with effects seen in the full 3D model. I have also shown that the eddy tilt seen in the barotropic and 3D models is present in observations (figure 4.16). The importance of eddy momentum fluxes over Antarctica was also emphasised by Juckes et al. (1994). Surface cooling over the continent results in downslope winds from the centre of the continent towards the coast. The Coriolis torque acting on these generates surface easterly winds, and the drag on these constitutes a source of westerly momentum for the atmosphere over Antarctica. Equatorward transient eddy momentum fluxes play an important role in balancing this source term, and my results suggest that eddy refraction by the orographic potential vorticity gradient is a key mechanism which provides these fluxes.

Many CMIP5 models struggle to capture the polar front branch of the South Pacific split jet seen in reanalysis data. The fine details of Antarctic orography may be smoothed out due to the coarse resolution of climate models, but the orographic effects on eddies that I have considered are unlikely to be sensitive to these details. However, the present study does suggest that both the strength of the wind and the nature of Rossby wave propagation over the Indian Ocean are important for the split

jet. Consequently, I have shown that in order to correctly capture the South Pacific jet structure, a model must adequately capture the processes governing the upstream flow.

This work has concerned the asymmetry of the SH mean state, however studies have noted that the response of wintertime SH circulation under climate change is also considerably zonally asymmetric (Simpson et al., 2014; Grose et al., 2017). It would be of interest to investigate which forcing mechanisms are responsible for driving these responses and how they relate to the mean state. I will address these questions in chapters 7 and 8. The results of this chapter lead us to speculate that changes to tropical SSTs are likely to be important, while sea ice retreat and mid-latitude SSTs are less likely to play a major role in driving changes in the asymmetry. Indeed, several studies have shown links between observed high southern latitude circulation changes and tropical SST trends (Simpkins et al., 2014; Li et al., 2015). My findings concerning the dependence of the South Pacific eddy-driven jet on the flow upstream are also relevant here, as any changes to the Indian Ocean region could potentially have an even greater impact on the Pacific.

Chapter 5

Low frequency eddy-driven jet variability

I have thus far considered the structure of the mean wintertime circulation and the surface boundary conditions that give rise to it. This chapter investigates the variability of the South Pacific eddy-driven jet about that mean state. The aim of this chapter is to characterise this variability, with a particular focus on austral winter, and examine connections with related phenomena such as the SAM and high latitude blocking / wave-breaking (HLB). I show that the jet undergoes a semi-annual oscillation in both latitude and speed with the jet being strongest and located furthest poleward during Spring (SON) and Autumn (MAM). During austral winter, interannual variations in jet latitude and speed are both highly correlated with the frequency of HLB, similar in some ways to the North Atlantic. I also investigate whether dynamical regimes can provide a helpful perspective on South Pacific jet variability. However, I find that the equatorward jet state is not persistent, nor is it regularly visited suggesting that dynamical regimes is not a viable model. Finally, I suggest that the Indian Ocean jet may play an important role in determining the state of the South Pacific eddy-driven jet downstream.

5.1 Introduction

Eddy-driven jets tend to vary in latitude and speed and the nature of this variability is largely dependent on the region in question. For instance, variations in jet latitude have been found to explain considerably more of the variance in North Atlantic circulation than jet speed, while these are roughly equally important for the North Pacific (Barton and Ellis, 2009; Barnes and Polvani, 2013). Additionally, jet variability is dependent on the season, particularly in the case of the North Atlantic. The amplitude of the summertime NAO is weaker and its centres of action are located further northward than in winter (Folland et al., 2009). The summer jet does not exhibit the trimodal jet latitude structure seen in winter (Woollings et al., 2014) and variations in the summer jet are driven by different factors than in winter (Hall et al., 2017). The South Pacific eddy-driven jet also exhibits considerable seasonal variation, with the summer jet dominated by a shifting behaviour and the winter jet characterised by a pulsing (Kidston et al., 2009; Barnes and Hartmann, 2010b). On the other hand, the nature of Indian Ocean jet variability varies less between the seasons, as the jet remains strong and the dominant mode is a latitudinal shift throughout the year (Barnes and Hartmann, 2010b).

Many of these seasonal and regional differences can be understood by considering the locations of Rossby wave propagation and breaking (Barnes and Hartmann, 2011; Barnes and Polvani, 2013). Within the mid-latitudes, Rossby waves tend to break on the flanks of the eddy-driven jet, locally decelerating the flow and consequently shifting the jet (Strong and Davis, 2008; Kunz et al., 2009). In general, anticyclonic wave breaking tends to occur on the equatorward flank and is associated with poleward jet shifts, whilst cyclonic wave-breaking occurs on the poleward flank and shifts the jet equatorwards (Orlanski, 2003). Hence, the frequency of occurrence of large-scale wave-breaking events is linked to jet variability (Benedict et al., 2004; Woollings et al., 2008; Davini et al., 2012). Large-scale wave-breaking events are also closely linked

to atmospheric blocking (Masato et al., 2012). Woollings et al. (2008) provided a new interpretation of the NAO, arguing that low frequency variations in the jet are synonymous with variations in high latitude blocking (HLB) occurrence (sometimes termed high latitude wave-breaking, Berrisford et al., 2007). Similarly, large-scale wave-breaking has been used to explain the trimodal pattern of North Atlantic jet latitude (Woollings, 2010; Woollings et al., 2011). In this chapter I will suggest a similar interpretation of variations in the South Pacific jet.

The SAM is the dominant mode of large-scale SH atmospheric variability on time scales of ten days or greater. The dominance of the SAM is understood as resulting from an eddy-mean flow feedback process (Lorenz and Hartmann, 2001). That is, baroclinic eddies are preferentially generated near the jet and subsequent propagation of eddies away from the jet fluxes momentum back towards it, maintaining the jet, and hence, creating a positive feedback loop. However, the variability and structure of the SAM varies seasonally and while the feedback mechanism thus described applies readily at all longitudes during austral summer, some authors have suggested that it acts during the winter in the Indian Ocean region only (Barnes and Hartmann, 2010b; Ding et al., 2012). Its variability also varies regionally as can be seen from figure 5.1. During summer both South Pacific and Indian Ocean regions primarily exhibit a latitudinal shifting with respect to variations in the SAM index. On the other hand, wintertime Indian Ocean jet variability manifests as a shifting, but South Pacific jet variations are identified by changes in jet strength and secondarily in latitude. This asymmetry is likely a result of the formation of a thermally-driven, subtropical jet over the wintertime South Pacific, which modifies the propagation and breaking of waves (Nakamura and Shimpo, 2004; Williams et al., 2007; Barnes and Hartmann, 2010b). Rossby waves propagate meridionally away from their source region until they encounter a turning latitude, where their meridional group velocity changes sign, or a critical latitude where the wave breaks (Hoskins and Karoly, 1981; Hoskins

and Ambrizzi, 1993). In the absence of a strong subtropical jet, critical latitudes are set by the wind profile of the eddy-driven jet itself, contributing to an eddy-mean flow feedback. On the other hand, a strong subtropical jet creates a strong gradient in absolute vorticity and gives rise to a critical latitude in the subtropics (Barnes and Hartmann, 2011). This means that the equatorward critical latitude is no longer tied to the eddy-driven jet and consequently, the wave-mean flow feedback is weakened (Eichelberger and Hartmann, 2007). Spensberger et al. (2019) also found that while the SAM describes mid-latitude variability well in summer, it does this less effectively in winter, predominantly capturing polar variations. In the case of the South Pacific winter, it is therefore useful to consider other indices of mid-latitude variability including jet latitude and speed.

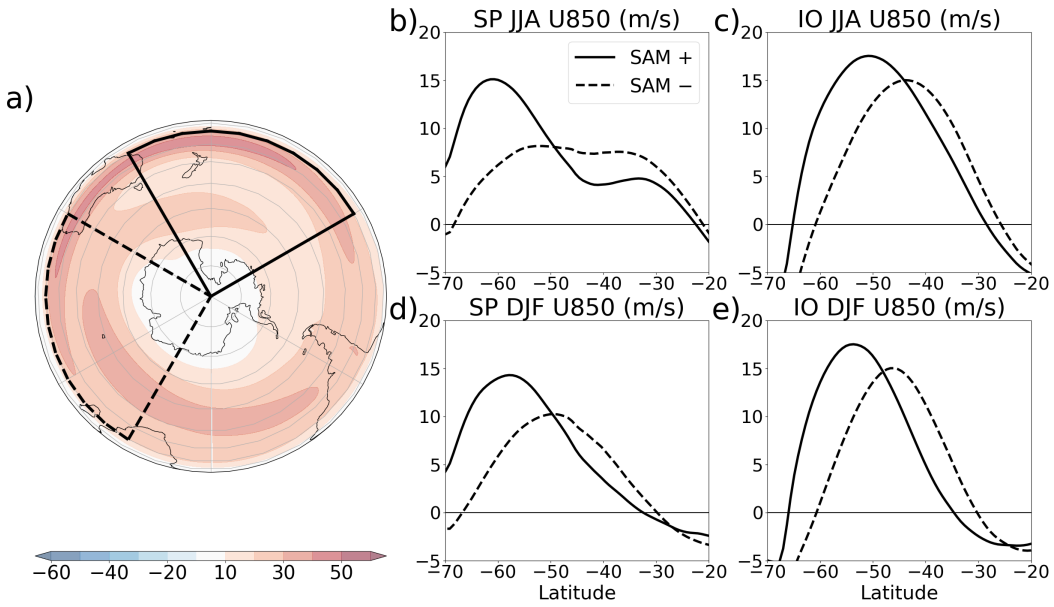


Figure 5.1: Seasonal and regional differences in SAM variability: In a) the sector definitions are shown with the Indian Ocean region delineated by dashed lines and the South Pacific by solid lines. 300hPa zonal wind is also indicated by colours. In b) to e), solid and dashed curves indicate the sector zonal mean zonal wind for positive and negative phases of the SAM, respectively, with these phases being defined as at least ±1 standard deviation from the mean. The plots show b) South Pacific winter, c) Indian Ocean winter, d) South Pacific summer and e) Indian Ocean summer.

A number of authors have suggested that the wintertime SH circulation can be

described using the framework of dynamical regimes. There is an extensive literature on this topic with several definitions of regimes, particularly for the North Atlantic region (see Hannachi et al., 2017, for a review on dynamical regimes). I consider dynamical regimes to be defined as distinct circulation states which are both persistent and regularly visited. For instance, the trimodal structure of the North Atlantic jet latitude distribution (Woollings et al., 2010a) is simple and yet compelling evidence for jet regime structure with the peaks representing preferred jet states. The regime perspective has the potential to improve sub-seasonal forecasts (Robertson et al., 2015) and has been used in studying circulation responses to climate change (Corti et al., 1999; Palmer, 2001; Hsu and Zwiers, 2001) and in model evaluation (Dawson et al., 2012; Dawson and Palmer, 2015).

With regard to regime detection in the SH, Yoden et al. (1987), Itoh et al. (1999) and Koo et al. (2002) all diagnosed alternating split and merged jet regimes using SH zonal mean zonal wind from reanalysis datasets. However, the short data period prevented any statistically robust conclusions from being drawn. In the case of Koo et al. (2002), the data spanned 1948 to 1998, though their results are less likely to be reliable given satellite data was not available for the majority of this period. These studies also failed to account for the regional asymmetry in wintertime SH variability (Yang and Chang, 2006; Codron, 2007; Kidston et al., 2009; Barnes and Hartmann, 2010b). Ogawa et al. (2016) showed that the winter jet latitude distribution in the South Pacific sector is strongly skewed, if not weakly bimodal, a finding suggestive of preferred regime states (Woollings et al., 2010a). Ogawa et al. (2016) performed a series of aqua-planet GCM simulations with different SSTs in order to understand these jet latitude states. They found that if the SST front was sufficiently separated from the subtropical jet, the eddy-driven jet tended to jump between two different regimes - one in which the jet was tied to the SST front and another in which it merged with the subtropical jet. They emphasised the role played by the location of the SST front

in creating baroclinicity at high latitudes which generates the eddies to maintain the jet. In particular, they noted that shifting the SST gradient polewards caused the jet latitude in the positive phase of the annular mode to shift poleward, whereas the jet in the negative phase remained at the same latitude. Several studies have also attempted to identify SH regimes using cluster analysis or similar unsupervised learning techniques on atmospheric fields. For instance, using k-means clustering of 500hPa geopotential height data, Robertson and Mechoso (2003) found 3-4 geographically fixed regime patterns in the South Pacific region. Examining the entire SH, Mo and Ghil (1987), Farrara et al. (1989) and Hansen and Sutera (1991) all identified either two or three regimes, with wavenumber 3 patterns being particularly prominent. Pohl and Fauchereau (2012) also employed k-means clustering and identified regimes corresponding to the opposing phases of the SAM, while O'Kane et al. (2013), using a more complex clustering method, identified two 'blocking regimes' and a SAM regime. However, it has been shown that cluster analysis of atmospheric data is often highly sensitive to the choice of clustering method and data period (Christiansen, 2007). In this study, to avoid these issues with cluster analysis and in the interest of parsimony, I prefer to utilise simpler diagnostics like jet latitude to investigate whether regime dynamics provides a helpful model of South Pacific jet variability.

In this chapter, I investigate the variability of the South Pacific eddy-driven jet. The data and methods are briefly described in section 5.2. I first consider the seasonal variation of jet speed and jet latitude indices in section 5.3 and the relationship of these diagnostics with the SAM in section 5.4 and with HLB in section 5.5. Following this, I examine composites of equatorward and poleward jet states and consider the hypothesis of dynamical regimes in section 5.6 and then examine connections between the South Pacific and Indian Ocean jets in section 5.7. Finally conclusions are given in section 5.8.

5.2 Data and methods

5.2.1 Reanalysis data

Daily-mean zonal wind, meridional wind, temperature and geopotential height data from the ERA-Interim dataset are used for all plots, covering the years 1979-2015. ERA-Interim and reanalysis in general is discussed further in section 3.1.

5.2.2 SAM

The SAM is defined as the principal component time series associated with daily 10-day low pass filtered 850hPa geopotential height data, south of 20S. Before calculating the first principal component time series, the values at each grid-point are standardised and weighted by $\sqrt{(cos\phi)}$, where ϕ is the latitude. This definition is discussed in more detail in section 3.4.2

5.2.3 Jet indices

The method of Woollings et al. (2010a) discussed in section 3.4.1 is used to calculate the jet latitude and speed indices. Briefly, the jet latitude is defined each day as the latitude of the maximum 850hPa sector zonal mean zonal wind on that day. Prior to this the zonal mean zonal wind is low pass filtered with a 10-day Lanczos filter to remove the influence of transient baroclinic systems. The jet speed is then defined as the 850hPa sector zonal mean wind speed at the jet latitude. The South Pacific and Indian Ocean regions are defined as the longitudes 150E-240E and 30E-120E respectively and these are shown in figure 5.1a).

5.2.4 Blocking index

Blocking is calculated using a modified version of Masato et al. (2012) using 500hPa geopotential height (Z500) data rather than potential temperature on the dynamical tropopause as in Masato et al. (2013a). In short, the method involves integrating

Z500, 11° to the north and south of a given grid-point and taking the difference. If the integral to the south exceeds the integral to the north, i.e. there is a reversal, that grid-point is defined as instantaneously blocked. This is repeated for all grid-points between 70S and 30S and where several reversals are clustered together, a blocking centre is defined for the largest reversal. If this blocking centre persists for at least four days without moving outside a given region, this is defined as a blocking event. Further details and an example detection can be found in section 3.4.6.

5.3 Seasonality of jet indices

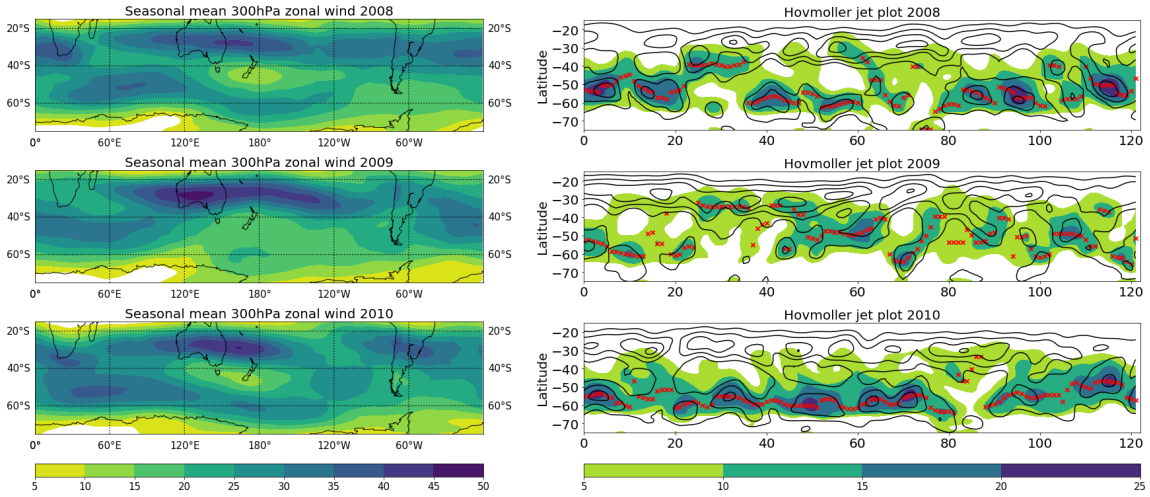


Figure 5.2: South Pacific jet variability: (left) Mean 300hPa zonal wind for the years 2008-2010 for JJA and (right) Hovmöller plots of zonal mean zonal wind within the South Pacific sector (150E-240E) for each of those years. In the latter, 300hPa zonal wind is shown by contours (contour interval of $10ms^{-1}$), 850hPa zonal wind is shown with colours (contour interval $5ms^{-1}$) and the jet latitude (see section 3.4.1) index is denoted by a red cross for each day. Day 0 is 1st June and day 120 is the 30th September.

The wintertime zonal flow in the South Pacific region is notably variable on sub-seasonal and interannual timescales. Variations in latitude and speed of the jet are illustrated in figure 5.2, which compares the mean zonal wind for three consecutive winters and Hovmöller plots showing the intra-seasonal variability of the jet. In two of the three years, a clear time-mean split jet was observed, whereas in 2009 the

eddy-driven jet merged with the subtropical jet, and had only weak winds over the high latitude Pacific. Breaking this down into sub-seasonal variability, the Hovmöller diagrams show the sector zonal mean 300hPa (contours) and 850hPa (colours) winds, while small crosses indicate the jet latitude. These diagrams indicate that there is often a large amount of variability on shorter timescales. The years 2009 and 2010 showed almost opposing behaviour in that the eddy-driven jet was weak and variable during 2009, while it was strong and consistently found at high latitudes in 2010. What is also striking about these plots is the abruptness of many of the transitions. For instance, around day 25 in the 2009 Hovmöller, the jet latitude shifts from its position around 55S to a position at the edge of the subtropics, around 30-35S. This may be the result of new features moving into the South Pacific region from the west. These plots also show that double eddy-driven jets are relatively rare (shown by the colours), justifying the use of a single jet latitude on each day.

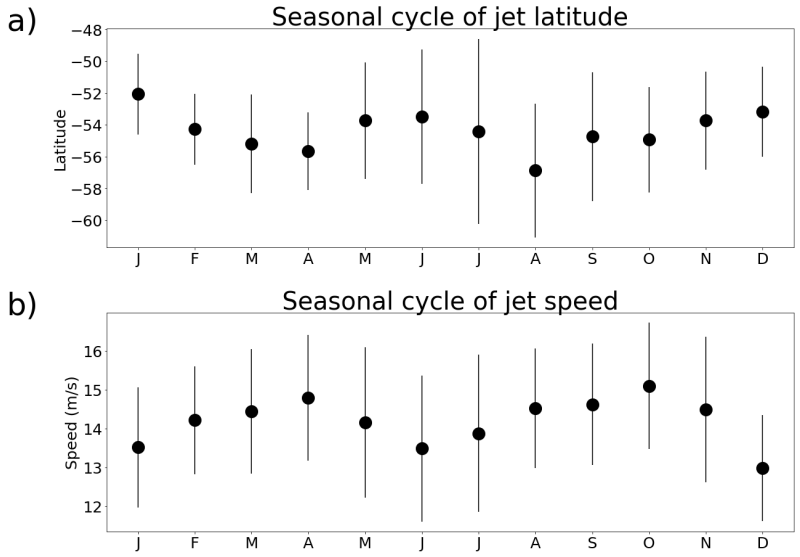


Figure 5.3: Seasonality of mean eddy-driven jet latitude and speed in the South Pacific sector: Markers show the mean eddy-driven jet a) latitude and b) speed, calculated using daily data for each of the twelve months of the year. Bars indicate ± 1 standard deviation of the monthly means of daily jet latitude / speed.

I now examine the seasonality of South Pacific jet latitude and speed. Figure 5.3 shows the seasonal cycle of jet latitude and speed within the South Pacific sector, with

filled circles showing the mean of the jet indices, calculated on a daily basis. In both jet latitude and speed, there is a clear semi-annual cycle, with the greatest jet speeds in April and October, and mean jet latitude being furthest poleward in April and August. This is likely a signature of the SH semiannual oscillation (SAO) described by Schwerdtfeger and Prohash (1956) and van Loon (1967). van Loon (1967) considered that the reason behind this semiannual periodicity concerns the differential rates of sea surface heating and cooling at mid and high latitudes during March and September, a finding corroborated by Meehl (1991) and Meehl et al. (1998). The magnitude of the SAO also varies on an interannual timescale as a result of stratosphere-troposphere coupling in late summer / early autumn and late winter / early spring (Kuroda and Kodera, 1998; Bracegirdle, 2011; Byrne and Shepherd, 2018). Putting figure 5.3 into context, the magnitude of the seasonal cycle in South Pacific jet speed is around half of that seen in the North Atlantic, while the magnitude of variations in jet latitude are similar (see figure 3 of Woollings et al., 2014). The muted seasonal cycle in jet speed is unsurprising given the circumpolar band of ocean and hence large thermal inertia in the SH (Nigam and DeWeaver, 2015). The bars give an indication of the spread within each month, calculated as ± 1 standard deviation of the monthly mean jet latitude / speed. Jet speed variability is relatively constant throughout the year, however jet latitude varies considerably more between May and September than at other times of the year. It is also worth noting that the magnitude of this variability is large compared with the seasonal cycle, similar to the North Atlantic (Woollings et al., 2014).

To explore seasonal variations in jet latitude further, I plot distributions of the South Pacific jet latitude index for the four seasons in figure 5.4. The jet latitude in summer (DJF) is strongly peaked between 50S and 55S, in contrast to the winter (JJA) in which jet latitude is considerably more variable, with autumn (MAM) and spring (SON) lying between these extremes. The equivalent figure for the Indian

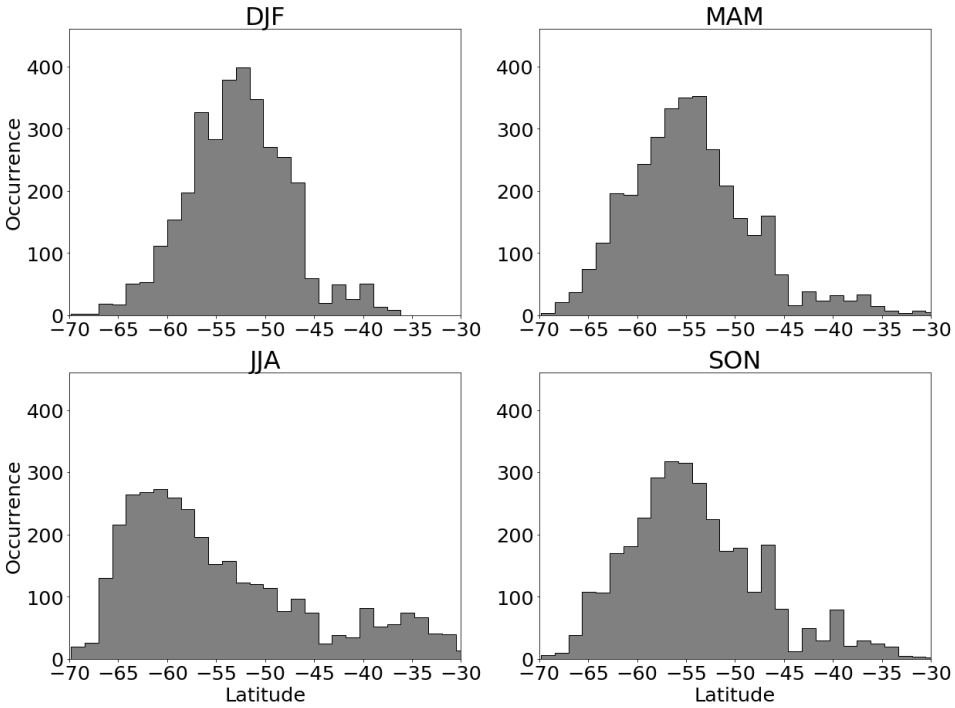


Figure 5.4: Histograms showing the distributions of eddy-driven jet latitudes in the South Pacific sector for different seasons.

Ocean region resembles the DJF South Pacific in all seasons and is more distinctly peaked (not shown). As has been noted by Woollings et al. (2010a) and Ogawa et al. (2016), the wintertime South Pacific jet latitude is weakly bimodal, or at least strongly skewed, with a large peak between 65S and 60S and a small bump between 40S and 30S. They each suggested that this could be an example of regime structure in which the different jet latitudes represent different dynamical states of the jet. To check whether this structure is region dependent, I varied the longitude bounds of the sector and broadly speaking the structure remains similar. For the longitudes 180E-240E, for instance, the high latitude peak is broadened and reduced in magnitude by around 25%, and there are more jet latitude events at low latitudes. Admittedly, the skewed structure is not as obviously regime-like as the trimodal North Atlantic jet latitude, however the non-Gaussian nature of the distribution could still be evidence for regime structure (Sura and Hannachi, 2015). In the following sections I will focus on the variability of the wintertime jet and investigate the question of dynamical

regimes.

5.4 Split jet - SAM covariability

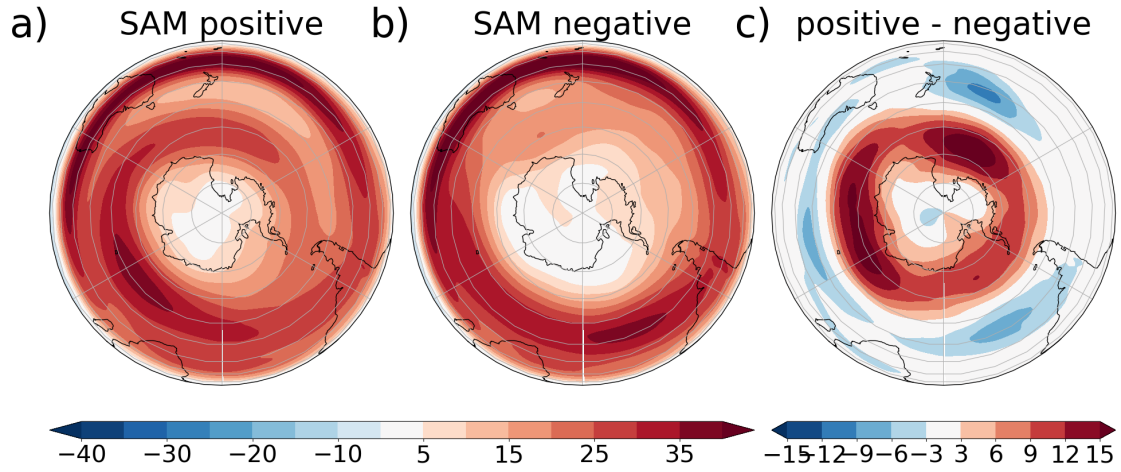


Figure 5.5: 300hPa zonal wind composites for a) positive SAM, b) negative SAM and c) positive SAM - negative SAM.

The SAM describes variations in both jet latitude and speed, though the amount of SAM variability explained by each of these varies regionally (Codron, 2007; Barnes and Hartmann, 2010b). Composites of 300hPa zonal wind are shown in figure 5.5 indicating the overall structure of these two phases. Here, the positive and negative phases are defined as days on which the SAM index is greater than 1 standard deviation from the mean. The Indian Ocean jet can be seen to be shifted poleward and equatorward in the positive and negative phases of the SAM, respectively. The South Pacific eddy-driven jet is strong and poleward in the positive phase, whereas the eddy-driven jet is merged with the subtropical jet in the negative phase, with weaker winds at high latitudes. The subtropical jet core is largely unaffected by variations in the SAM index.

To relate the jet latitude and speed indices to the SAM, I plot a scatter plot of jet speed against latitude for different phases of the SAM in figure 5.6. SAM positive days are marked by high values of the jet speed index and high jet latitudes. Conversely,

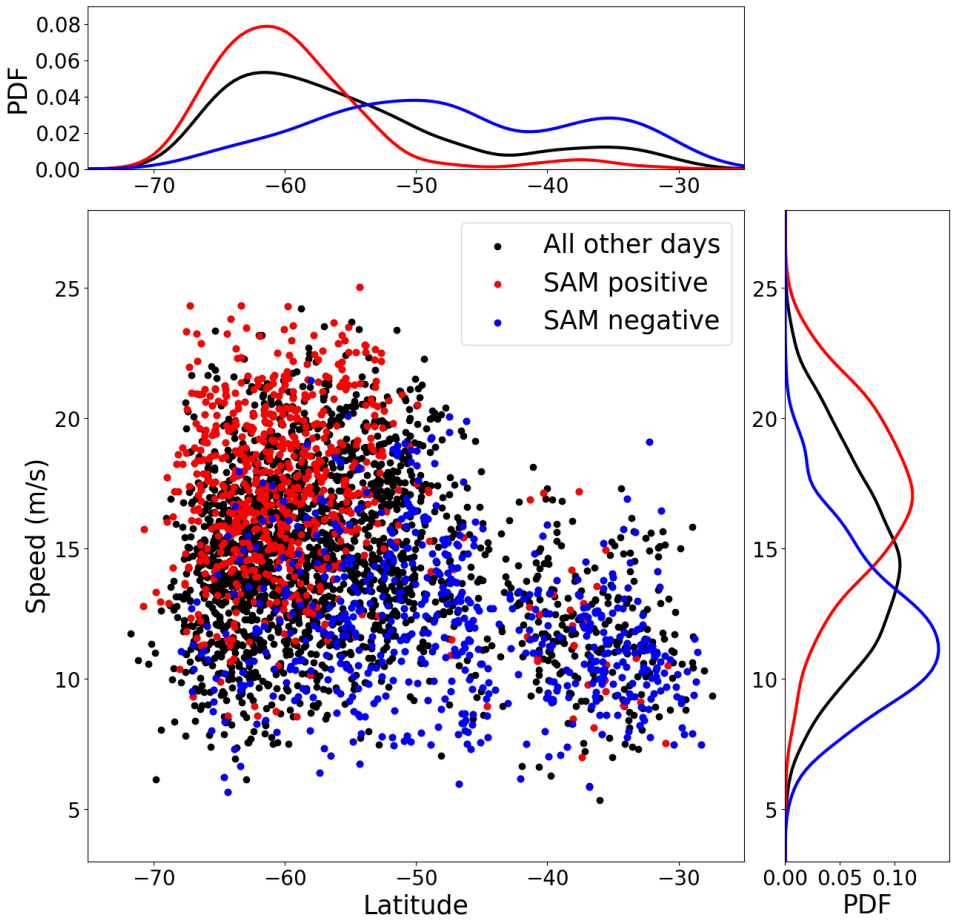


Figure 5.6: Scatter plot of South Pacific jet speed against jet latitude for days in which the SAM index is greater than 1 standard deviation above the mean (red), greater than 1 standard deviation below the mean (blue) and all other days (black). The same data is shown for jet latitude and speed individually as probability density functions.

SAM negative days are associated with slower jet speeds and more equatorward jet latitudes. However, the spread of latitudes in the negative phase of the SAM is notable and is consistent with the observations of Woollings et al. (2017) that weaker jets tend to be more variable. It is clear that *both* jet latitude and speed capture a substantial fraction of observed SAM variability in this sector, unlike the Indian Ocean region where shifts in the jet characterise a much higher proportion of the variance (Codron, 2007). Interestingly, on an interannual basis, jet latitude and jet speed are highly anti-correlated for the winter South Pacific, with a correlation coefficient of $R = -0.66$

(not shown). That is, a poleward jet is generally strong, while an equatorward jet is anomalously weak. This is not the case for the summer South Pacific nor for the Indian Ocean or North Atlantic in any season.

I noted in section 5.1 that variations in the NAO are closely linked to episodes of Rossby wave-breaking and so I now investigate whether this is also the case for the SAM.

5.5 Blocking and high latitude wave-breaking

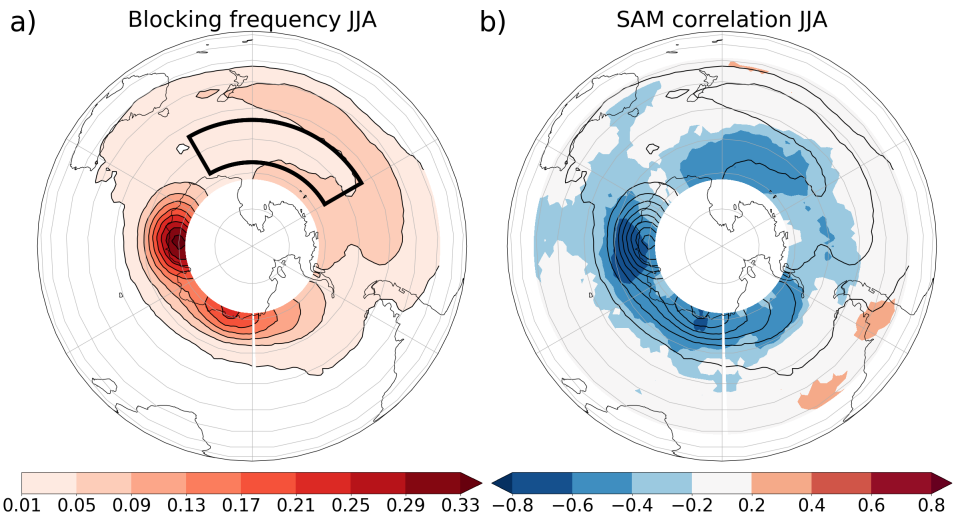


Figure 5.7: (a) Blocking frequency climatology and b) correlations with SAM for JJA. In b), only correlations with p values, calculated from a two-sided t-test, which lie below 0.05 are plotted. In a), a black box indicates the South Pacific high latitude blocking region used for correlation analysis in figure 5.8.

Figure 5.7 shows the frequency of blocking occurrence in the SH winter. In agreement with previous literature, the algorithm detects the highest mid-latitude blocking frequency over the South Pacific (Trenberth and Mo, 1985; Sinclair, 1996; Renwick, 2005; Berrisford et al., 2007; Parsons et al., 2016). This is likely because the South Pacific lies at the end of the mid-latitude storm track, where the flow has a reduced capacity for carrying waves (Nakamura and Huang, 2018). Consequently, large-scale waves tend to break in these regions. The winter blocking frequency maximum, east

of New Zealand, is shifted slightly equatorward with respect to studies such as Renwick (2005), which use persistent positive anomaly methods, as these locate blocking events at the anticyclonic anomaly rather than at the location of the Z500 reversal. In addition, there is no local maximum south-east of South America as in Trenberth and Mo (1985) and Renwick (2005). There are a significant number of high latitude events detected, particularly around the coast of East Antarctica from the South Atlantic round to the South Indian Oceans. Berrisford et al. (2007) also found a large number of high latitude events using a reversal-based index, though they found a higher proportion in the South Pacific region and fewer events around East Antarctica. It is possible that this difference from my results arises from their use of potential temperature on the dynamical tropopause rather than 500hPa geopotential height, as indices calculated from these variables may differ at high latitudes. These HLB events do not meet the traditional criterion of blocking in that they do not block the main westerly flow, but they can have an important role to play in jet variability (Berrisford et al., 2007; Woollings et al., 2008).

Berrisford et al. (2007) and Parsons et al. (2016) reported significant correlations between the SAM and blocking and so to confirm this I plot a correlation map between blocking frequency and the SAM index in figure 5.7b. Ostensibly, positive SAM values are associated with a decrease in high latitude blocking events around Antarctica, with particularly high concentrations near the climatological maximum, south of the Indian Ocean and to the south of New Zealand.

To relate high latitude blocking more directly to the South Pacific eddy-driven jet, I calculate a HLB index and plot it alongside jet latitude and speed in figure 5.8. The index is defined as the total number of daily blocked grid-points in the South Pacific between 150E and 240E, 65S and 55S (shown by a black box in figure 5.7a) during a given winter (i.e. if a grid-point is blocked on 10 days, it will be counted 10 times). The index is then standardised and plotted for each year. It is clear that there is a

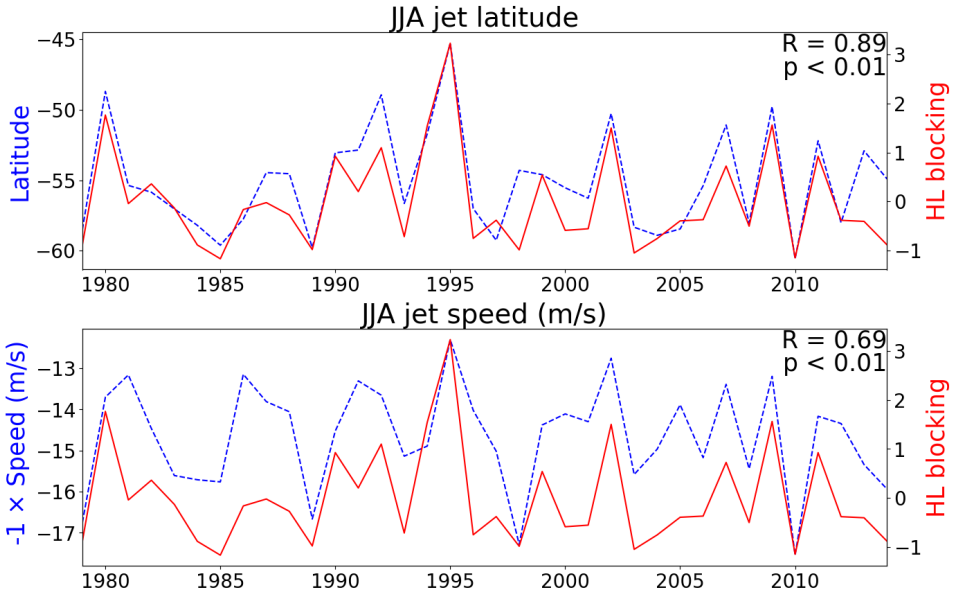


Figure 5.8: Interannual variability of jet latitude, jet speed and high latitude blocking. See text for details of the high latitude blocking index calculation. Correlation values and p values from a t-test are shown in the top right hand corner.

very high correlation between the HLB index and both jet indices. Jet latitude and HLB are positively correlated with coefficient $R = 0.89$ and, jet speed is negatively correlated with $R = -0.69$. This indicates that when HLB occurs frequently during a season, the jet is likely to be weaker and generally located closer to the equator than usual, with the opposite occurring in the absence of HLB. Note that the years 2009 and 2010, shown by Hovmöller plots in figure 5.2, are typical examples of these two extremes respectively. The picture thus emerging is one similar to the North Atlantic in which variations in the jet are strongly linked to the presence of wave-breaking at high latitudes (Woollings et al., 2008). The behaviour of the South Pacific does appear to be unique in the SH as a similar correlation analysis for the Indian Ocean region (HLB over 30E - 120E) gives much lower values of $R = 0.51$ for jet latitude and $R = 0.39$ for jet speed (not shown). However, a question arises, are these two different extremes of a strong, poleward jet and a weak, equatorward jet, merely opposite tails of a distribution or are they in some sense different dynamical states? I investigate this in the following section.

5.6 Dynamical regimes

As discussed previously, the subtropical jet alters the dynamics of the eddy-driven jet. Using the barotropic model described in section 4.6, Barnes and Hartmann (2011) imposed a subtropical jet by relaxing the zonal wind towards a Gaussian profile in the subtropics and found that when the stirring is imposed sufficiently far polewards, the eddy-driven jet can exist in two regimes. The regimes consist of one in which the eddy-driven jet merges with the subtropical jet and another in which the two jets are split. This is similar to the results found by Ogawa et al. (2016) described in section 5.1 and motivates my study of the South Pacific jet at high and low latitudes (see figure 5.4). In the next few figures, I plot composites defined as the 500 days closest to the two jet latitude 'peaks'. Recall that the jet latitude is defined based on 850hPa winds as this isolates the eddy-driven component of the wind from the thermally driven subtropical jet. For the poleward jet composite, the jet latitude is mostly between 62S and 59S and the equatorward composite, between 45S and 30S.

Initially, I plot zonal wind maps using data on the 850hPa and 300hPa levels in figure 5.9 alongside blocking frequency anomalies. In the equatorward jet phase, the eddy-driven jet is located on the flank of the subtropical jet, with weak near surface winds at higher latitudes. The eddy-driven jet itself is relatively weak at only around $10ms^{-1}$ at 850hPa. Given the weak westerlies at high latitudes, it is unsurprising that the equatorward jet composite is associated with an anomalously high frequency of HLB, consistent with figures 5.7 and 5.8. The region of anomalous HLB extends westwards from the South Pacific to about 60E. On the other hand, the eddy-driven jet is stronger in the poleward phase with a clear split jet at upper levels. The upper level subtropical jet is similar between the two composites as in figure 5.5.

Examining the vertical structure of the composites, figure 5.10a,b demonstrates that the South Pacific zonal wind anomalies are barotropic, consistent with the eddy-driven nature of the flow. A marked feature of the equatorward jet phase is the

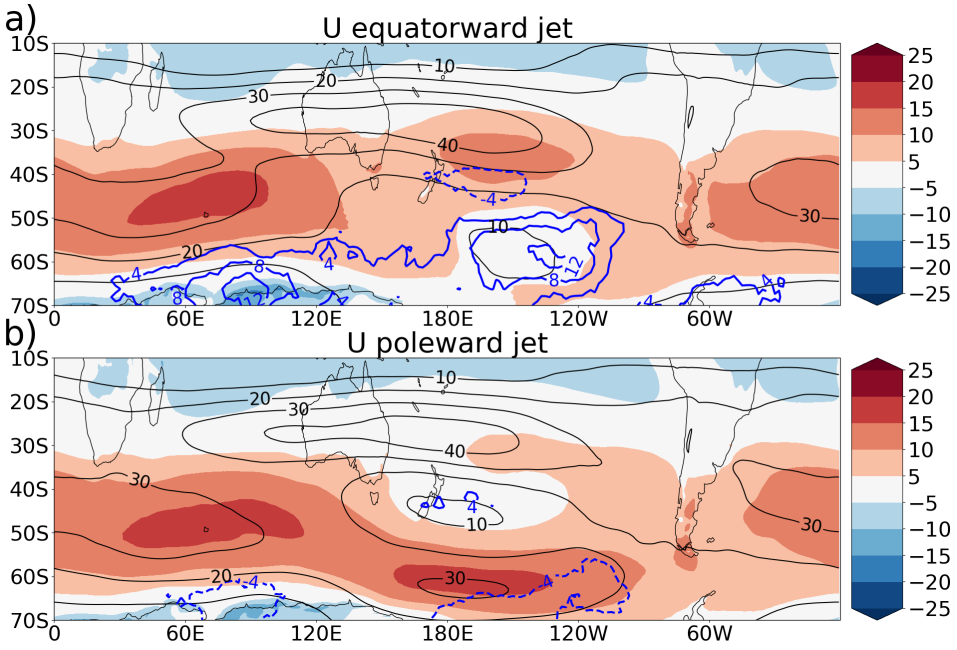


Figure 5.9: Composites of zonal wind for a) equatorward and b) poleward states of the South Pacific jet. Zonal wind is shown on the 850hPa and 300hPa levels by colours and black contours respectively, with units of ms^{-1}. Blocking frequency anomalies from the winter climatology are also shown by thick blue contours with units of events per 100 days. Composites are defined in the text.

absence of a westerly jet at high latitudes as well as the slightly strengthened winds between 40S and 30S. I also plot transient momentum fluxes, $\overline{u'v'}$, in which primes indicate 2-6 day bandpass pass filtering with a Lanczos filter. In general, eddies flux momentum polewards at upper levels between around 55S and 30S, with corresponding equatorward fluxes between 75S and 65S. Anomalies from the climatology are shown in colours and it is clear from figure 5.10c that equatorward jet events are associated with a substantial reduction in poleward momentum flux, while poleward jet events are similar to momentum fluxes in the mean state. However, the region of momentum flux anomalies in the equatorward jet composite is very broad, consistent with a weak, unfocused feedback of eddies onto the jet.

To further examine eddy statistics in the two composites, I plot E vectors (see section 3.4.4) and their divergence (colours) in figure 5.11. Note that the divergence has been smoothed using a Gaussian filter of width 6° in latitude / longitude, as

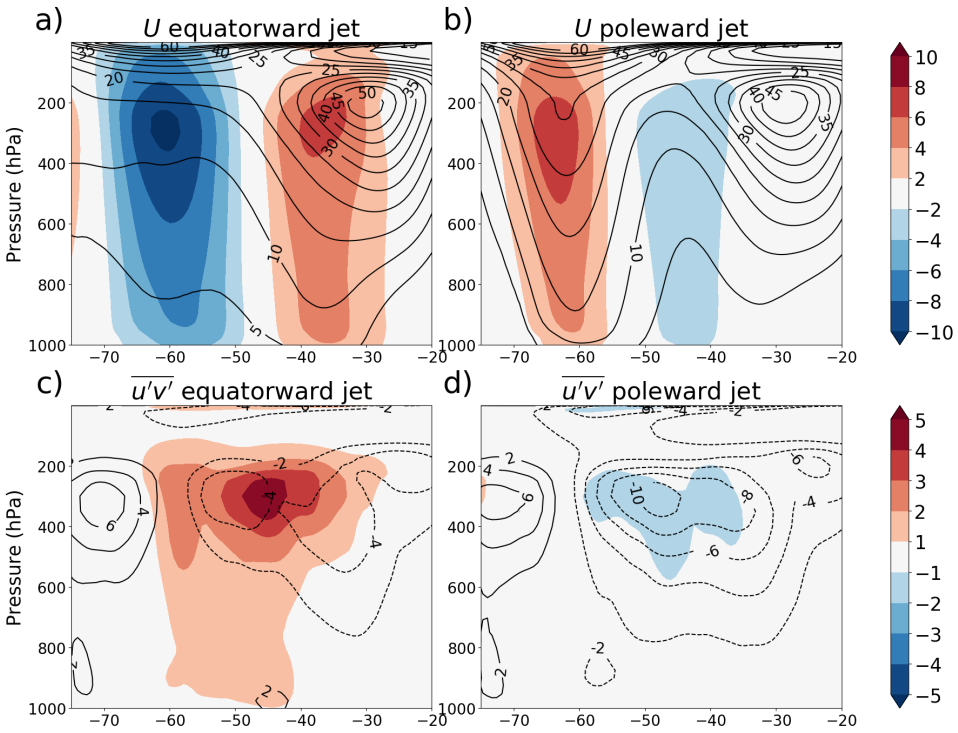


Figure 5.10: Vertical structure of composites of the equatorward and poleward eddy-driven jet states: a) and b) show the zonal mean wind within the South Pacific sector for these two states with contours showing the full field and colours the anomalies. c) and d) show the eddy momentum flux in the same sector with the same plotting convention. The units of U and $\overline{u'v'}$ are ms^{-1} and m^2s^{-2} respectively.

the E vector divergence is a relatively noisy field. The major features of the plots are not substantially altered by reasonable variations of the Gaussian smoothing parameter. For the poleward South Pacific jet case, there is strong divergence at high latitudes, across all longitudes, indicating strong transient eddy forcing of the mean flow. Conversely, in the equatorward jet composite, eddy forcing in the western South Pacific maintains the jet at a similar latitude to New Zealand and the high latitude forcing is diminished at these longitudes. E vector divergence at equatorward jet latitudes appears to suggest a mechanism for maintenance of an equatorward jet regime. However, like Woollings et al. (2010a), I find that similar composites using other latitude bands (e.g. 45S- 50S) also show anomalous divergence at those latitudes (not shown), indicating that the eddies simply tend to reinforce the jet at its current

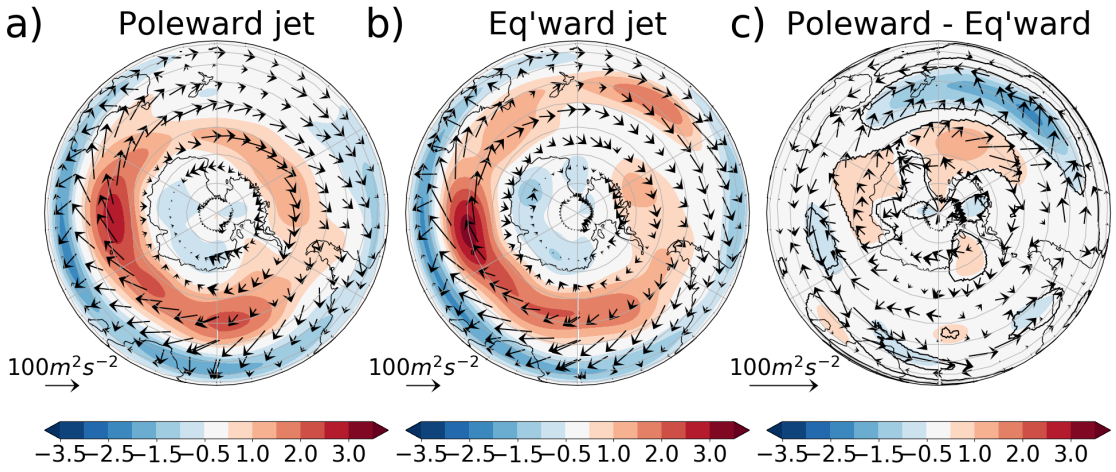


Figure 5.11: E vectors and $\nabla \cdot E$ calculated using 2-6 day bandpass filtered zonal and meridional winds on the 300hPa level for a) poleward South Pacific jet, b) equatorward South Pacific jet and c) poleward - equatorward composites. Divergence is shown in units of $ms^{-1}day^{-1}$. For visual clarity, only 1 in every 15 E vectors is plotted. In a,b), $\nabla \cdot E$ is smoothed with a Gaussian filter of width 6°. In c), black contours indicate the regions which show statistically significant differences with a p-value of 0.05 or less. The method for calculating the p-values is described in the text.

location.

The difference between these composites is shown in figure 5.11c. Black contours indicate the regions in which differences are deemed statistically significantly different, with p-values less than 0.05. P-values are calculated by creating two synthetic composites, each composed of a random selection of days, with the number of days being the same as in the poleward and equatorward jet composites. The difference in the E vector divergence between the two synthetic composites is then calculated before comparing with the difference between the original composites. This procedure is repeated 1000 times. The p-value at each grid-point is defined to be the fraction of synthetic composite pairs with a larger difference between them than the difference between the original composites. Unsurprisingly the largest differences in figure 5.11c are over the western South Pacific. However, there is also a region of anomalous eddy forcing at high latitudes, to the west of the South Pacific. That is, eddy forcing over the high latitude Indian Ocean region, is significantly stronger in the poleward jet

composite than in the equatorward jet composite. This provides a hint that forcing from the flow upstream may be important for the maintenance of the high latitude zonal flow.

A key property of dynamical regimes is that they must exhibit some level of persistence. This is important because it could potentially enable enhanced predictability of the atmospheric circulation (Robertson et al., 2015). In order to test this, I calculate a measure of persistence in three latitude bands by counting the number of days that the South Pacific jet latitude index remains in that band. I count from the first day that the jet latitude lies within each band. The fraction of events that last a certain number of days or longer is then plotted in figure 5.12. This method is similar to that used by Barnes and Hartmann (2010a) to study the persistence of the different phases of the NAO.

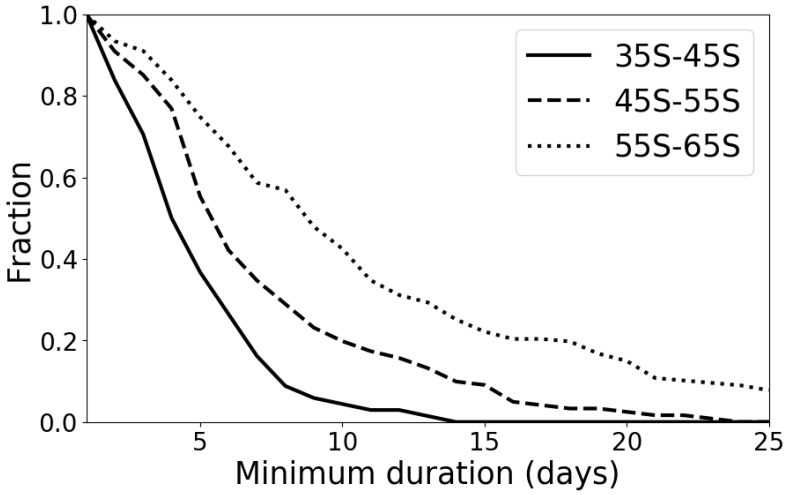


Figure 5.12: The fraction of jet latitude events that persist within a given latitude band for at least a certain number of days. See text for further details of the method.

Here the hypothesis of regime structure begins to look somewhat weak. Figure 5.12 shows that the equatorward jet latitude band, 35S-45S, is much less persistent than either of the other two more poleward bands, with few events persisting beyond 5-6 days. Blocking systems typically persist for around 5 days or more, hence a persistent jet would be expected to remain in that state for longer than 5 days. On

the other hand, in about 20% of cases, the jet latitude index remains in the band 55S-65S for 15 days or longer. Qualitatively similar results are obtained for narrower latitude bands.

The short persistence time of the equatorward jet phase indicates that there is unlikely to be a significant eddy feedback in this state. The equatorward jet state therefore does not fulfill my requirement that dynamical regimes must be persistent, suggesting that the regime paradigm is not a helpful model of South Pacific eddy-driven jet variability. It is also notable that the poleward jet states are more persistent in this case than the equatorward jet, as equatorward jets have been associated with greater persistence in other studies (Barnes et al., 2010; Barnes and Hartmann, 2010a; Woollings et al., 2010b). The time-mean South Pacific eddy-driven jet is located at high latitudes, therefore some of this apparent persistence at high latitudes relates to this being the mean or 'undisturbed' jet location. Furthermore, the studies cited above, which find higher persistence at lower latitudes, concern setups with a strong eddy-mean flow feedback, which is weak or absent over the South Pacific in winter (Barnes and Hartmann, 2010b).

5.7 Influence of the Indian Ocean sector

I have noted that jet variability with the winter SAM varies regionally, with a positive eddy feedback process only having a strong effect over the Indian Ocean, while it is ubiquitous in the summer. If the feedback process is only dominant in the Indian Ocean sector, why is the winter SAM pattern hemispheric in nature (figure 5.5c) rather than confined regionally like the NAO? One possibility is that this is an artifact of the use of EOFs, as these merely attempt to maximise the explained variance, rather than reflecting true physical patterns (Ambaum et al., 2001). However Codron (2007) suggested that this is unlikely to be the case as principal component time series' calculated over both the Indian Ocean and South Pacific region separately, are well

correlated. Instead he suggested that positive wind anomalies from the Indian Ocean region are necessary to maintain a strong polar front jet downstream.

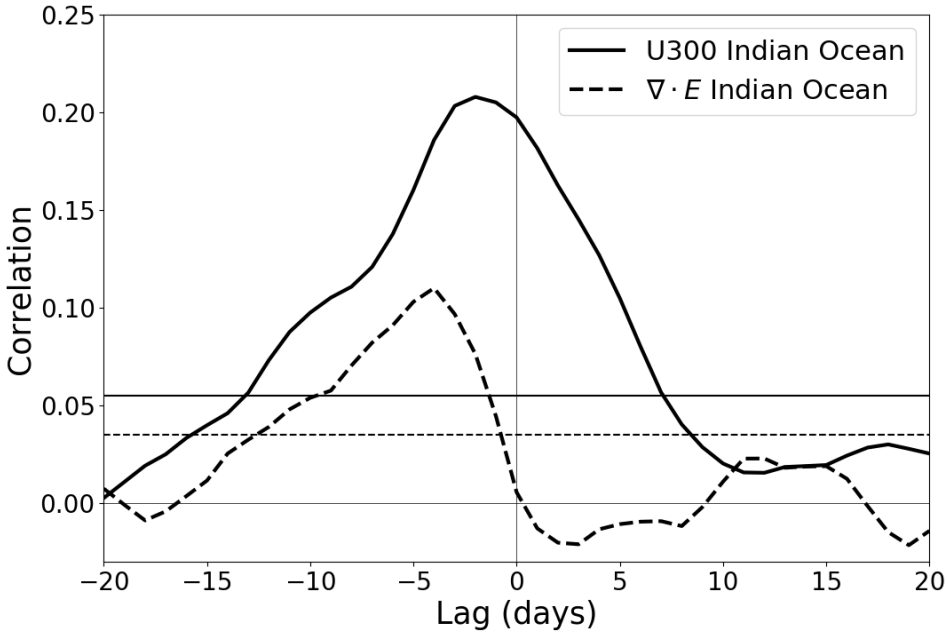


Figure 5.13: Lagged cross-correlation between daily-mean, high latitude zonal wind in the South Pacific sector (50S-65S, 150-240E) and high latitude zonal wind in the Indian Ocean sector (solid curve, 50S-65S, 30E-120E) and with high latitude $\nabla \cdot E$ (dashed curve, 50S-65S, 30E-120E). The left hand side of the figure shows the Indian Ocean leading the South Pacific and on the right hand side, the Indian Ocean is lagging the South Pacific. Horizontal lines show 95% significance levels for the zonal wind (solid) and $\nabla \cdot E$ (dashed) correlation plots. The method for calculating the significance levels is detailed in the text.

I provide some corroboration of this hypothesis by considering lagged correlations of high latitude South Pacific zonal wind, defined by 50S-65S and 150-240E, with transient eddy forcing and zonal wind over the high latitude Indian Ocean. The high latitude Indian Ocean region is defined by 50S-65S and 30E-120E, and the transient eddy forcing is taken to be $\nabla \cdot E$, spatially smoothed with a Gaussian filter. On the left hand side of figure 5.13, South Pacific zonal wind anomalies lag Indian Ocean zonal wind and eddy forcing anomalies, while on the right hand side, the South Pacific wind anomalies lead the Indian Ocean. The solid and dashed lines indicate the 95% significance levels for lagged cross-correlations with the Indian Ocean zonal wind and

eddy forcing anomalies, respectively. These are each calculated by generating 1000 synthetic time series, each with the same auto-correlation properties as the Indian Ocean anomalies, and then calculating the correlations between the synthetic time series' and the South Pacific wind anomalies. The two-tailed 95% significance level is then the 97.5th percentile of the correlations. Figure 5.13 shows that Indian Ocean wind anomalies are significantly correlated with South Pacific wind anomalies, up to 14 days prior to the appearance of the latter. At positive lags, Indian Ocean anomalies remain correlated with the South Pacific wind anomalies for a further 7 days. Inspecting cross-correlations with Indian Ocean eddy forcing anomalies indicates that South Pacific zonal wind is correlated with upstream eddy forcing at lags -1 to -13. However, upstream eddy forcing is not significantly correlated at positive lags, likely because of the short eddy forcing auto-correlation timescale. Both of these lagged cross-correlations indicate Indian Ocean flow anomalies have a significant impact on the South Pacific polar front jet strength downstream. This is consistent with figure 5.11c, which shows a positive eddy forcing over the Indian Ocean when the South Pacific jet is in its poleward phase.

Further evidence for this perspective is provided by considering the idealised model results of chapter 4. In the NOROG simulations without Antarctic orography, the Indian Ocean jet is substantially weakened, while the flow downstream over the South Pacific is weak in comparison to the CONTROL run, with no distinct eddy-driven jet present (figure 4.7). The steepest Antarctic orography is located to the south of the Indian Ocean (figure 4.2e) and the orography south of the South Pacific Ocean is less significant. Hence, if these results are best explained by a *local* weakening of the Indian Ocean jet resulting from changes to orography, then changes in the South Pacific are likely a consequence of these changes upstream. In particular, the lagged correlation plots of meridional wind anomalies (figure 4.13) illustrate that there is less downstream propagation of wave activity in the NOROG run, with a weak Indian

Ocean jet, than in the CONTROL run in which the Indian Ocean jet is stronger.

5.8 Discussion and conclusions

In this chapter I have considered the low frequency variability of the wintertime South Pacific eddy-driven jet using simple jet latitude and speed indices alongside more involved diagnostics such as a blocking index. Both jet latitude and speed indices undergo a marked semi-annual oscillation with the jet being strongest and located furthest polewards in April and October (figure 5.3). This is unsurprising given the well known semi-annual oscillation in the SH surface pressure field (Schwerdtfeger and Prohash, 1956; van Loon, 1967). I have also noted that the latitude of the jet is considerably more variable between May and September, while jet speed variability is constant through the year.

I then examined the relationship between South Pacific jet indices and the phases of the SAM, concluding that positive SAM events are associated with a strong and poleward eddy-driven jet, while negative SAM events are linked to a weaker eddy-driven jet (figure 5.6). The jet latitude is much more variable in the negative SAM state, consistent with Woollings et al. (2017) who show that weaker jets tend to vary more in latitude. Examining the jet latitude distribution for winter (figure 5.4), it is clear that the eddy-driven jet is most commonly located around 57-64S with occasional excursions further equatorwards. These equatorward jet events are strongly linked with the presence of high latitude blocking (figures 5.7, 5.8 and 5.9), much like the negative phase of the NAO (Woollings et al., 2008).

However, unlike the NAO, I showed that the equatorward phase of the South Pacific eddy-driven jet is not persistent (figure 5.12). A requirement of the dynamical regime perspective is that the jet must show some degree of persistence in each regime state (Hannachi et al., 2017), hence it appears that this is not a good model for variability of the South Pacific eddy-driven jet. This is contrary to the hypothesis of

Ogawa et al. (2016), however it should be noted that in their experiments they only considered a zonally symmetric framework and it is likely that zonally asymmetric effects play a significant role in this region. For example, the Indian Ocean Rossby wave (Inatsu and Hoskins, 2006) clearly is important in determining the winter South Pacific mean jet structure (see chapter 4), while I showed in chapter 4 that Antarctic orography is also a necessary condition for the observed split jet.

The lack of persistence in the equatorward state may result from the presence of the subtropical jet which weakens the eddy-mean flow feedback (e.g. Nakamura and Shimpo, 2004). A key element of the eddy mean flow feedback is that the wind profile, set by the eddy-driven jet, determines the propagation of eddies and the regions at which they break, known as critical latitudes. The meridional propagation of the eddies away from the jet acts to reinforce the jet. However, a strong subtropical jet will modify the regions of wave-breaking in the subtropics, weakening the feedback between the eddies and the eddy-driven jet (Barnes and Hartmann, 2011).

Finally, I raised the question of the extent to which the Indian Ocean sector exerts an influence on the state of the South Pacific eddy-driven jet. E vector composites of poleward and equatorward South Pacific eddy-driven jet states (figure 5.11) indicated that there is a larger amount of transient wave propagation from the Indian Ocean at high latitudes when the South Pacific jet is in its poleward phase, consistent with Codron (2007). I also showed that South Pacific wind anomalies are significantly correlated with Indian Ocean wind and eddy forcing anomalies up to two weeks in advance of the South Pacific anomalies. Further evidence for the importance of the Indian Ocean jet in the variability of the South Pacific jet is provided by the results of chapter 4. Namely, in the absence of a strong Indian Ocean jet, the South Pacific jet does not form. On the other hand, a more robust confirmation of this hypothesis would require more detailed modelling work. For instance, the atmospheric circulation over the Indian Ocean could be nudged to a particular state and the effects on the

South Pacific sector noted. I leave investigations such as this for future work.

In conclusion, the South Pacific eddy-driven jet does not conform to the paradigm of regime dynamics. A better perspective is to consider the poleward jet state as representing the basic state with occasional departures from this state linked to high latitude blocking diverting the jet and possibly a reduction in wave propagation from upstream over the Indian Ocean.

Chapter 6

Split jet and atmospheric blocking representation in CMIP5

The representation of SH circulation and atmospheric blocking in the historical experiments of 23 CMIP5 models is examined. I find that the SH equatorward jet bias is most prominent in the summer season, with the models in the ensemble showing both equatorward and poleward jet biases in the winter season. The winter season bias has a significant stationary wave component, centred to the south of Australia. Unlike the Euro-Atlantic sector, wintertime blocking frequency underestimation is not found in all models, indeed many models strongly overestimate the frequency of blocking occurrence. Implications for future projections of atmospheric circulation and blocking are also discussed.

6.1 Introduction

Climate models are frequently utilized for the purpose of making projections of future climate, however their use requires that they can accurately simulate relevant climate processes. The models within the CMIP framework (see section 3.3), which will be the focus of this chapter, have grown vastly in complexity since the project's inception in 1995. For instance, many models in CMIP5 (Taylor et al., 2012) simulate aerosols, the terrestrial carbon cycle, ocean biogeochemistry and atmospheric chemistry; processes which were not represented in earlier iterations (Flato et al., 2013).

With the advent of more powerful supercomputers, CMIP5 models have also been run at higher resolutions in the atmosphere and ocean than was possible previously. On the other hand, these grid resolutions remain relatively coarse and coupled with incomplete scientific understanding and the need for parameterisation of sub-gridscale processes, these models will always exhibit some biases with respect to observations. The prevalence of biases within a given model then informs the confidence which one may have in the results of simulations with that model.

In this chapter, I focus on atmospheric circulation biases in the SH mid-latitudes of CMIP5 model simulations. This will provide the context for chapter 7 on climate projections using these models. Material in these chapters concerns work completed before data from CMIP6 (Eyring et al., 2016) became available. In the coming months and years, the latest generation of models within CMIP6 will supersede CMIP5. However, it is likely that CMIP5 will continue to be widely used and compared with more recent simulations. As such, CMIP5 simulations are likely to remain relevant for the foreseeable future.

Atmospheric circulation in the SH extratropics has an important influence on many aspects of SH climate including ocean circulation, mixed-layer depth and sea-ice distribution (Hall and Visbeck, 2002; Sen Gupta and England, 2006; Ciasto and Thompson, 2008), carbon uptake (Lovenduski and Gruber, 2005; Le Quéré et al., 2007; Lovenduski et al., 2007; Sallée et al., 2010) and precipitation (e.g. Marshall et al., 2017; Rodrigues and Woollings, 2017; Grose et al., 2017). Consequently, jet biases may have a significant effect on each of these systems. It has been noted that CMIP5 models exhibit a systematic equatorward bias of the SH jet (Swart and Fyfe, 2012; Simpson and Polvani, 2016), a problem which is also evident in CMIP3 (Barnes and Hartmann, 2010d; Gerber et al., 2010) and in atmosphere-only models (Bracegirdle et al., 2013), indicating that SST biases are not the primary cause. The jet bias has been linked to an overly persistent SAM (Kidston and Gerber, 2010),

shortwave cloud forcing biases (Ceppi et al., 2012; Grise and Polvani, 2014a) and underestimated low level orographic drag (Pithan et al., 2016).

The SH jet bias has also received particular attention because it is apparent that model jets with a larger bias tend to shift further poleward under increased greenhouse gas forcing (Kidston and Gerber, 2010; Son et al., 2010; Bracegirdle et al., 2013). This could potentially provide an emergent constraint on future projections (Collins et al., 2012), though more recent work has shown that the relationship is restricted to the winter season and the reasons for this correlation are unclear (Simpson and Polvani, 2016). Encouragingly, studies have indicated that there is a substantial reduction in the SH jet biases of CMIP6 models with respect to CMIP5 (Bracegirdle et al., 2020; Curtis et al., 2020), giving greater confidence in the reliability of future projections.

In addition to the zonal mean jet, it is also worth noting that the extent of the wind bias may vary regionally (Bracegirdle et al., 2013; Lee, 2015). For instance, Lee (2015) found that CMIP5 models exhibit a weakened stationary wave pattern from the Indian Ocean to the South Pacific and speculated that this may be related to tropical precipitation biases. This stationary wave pattern is generally strongest in austral winter and hence this bias has the effect of diminishing the distinct split jet pattern found in observations. Recently, Garfinkel et al. (2020) showed that the combination of the double ITCZ bias in models (e.g. Bellucci et al., 2010) and biases in the Agulhas current explain most of the SH stationary wave bias in the annual mean.

Furthermore, evaluation of circulation variability about the mean state is also important in determining how well a model represents the observed climate. I have shown in chapter 5 that atmospheric blocking is a significant feature of the South Pacific region, in agreement with previous studies (Trenberth and Mo, 1985; Renwick and Revell, 1999; Sinclair, 1996; Renwick, 2005; Berrisford et al., 2007). Blocking events have a notable effect on SH weather and have been shown to be associated

with heatwaves over New Zealand (Salinger et al., 2019) and Australia (Pezza et al., 2012; Perkins-Kirkpatrick et al., 2016; Risbey et al., 2018), and persistent frost events in Australia (Risbey et al., 2019) and South America (Müller and Berri, 2007). The occurrence of blocks also modulates precipitation over South America (Mendes et al., 2008; Rodrigues and Woollings, 2017) and Australia (Pook et al., 2006, 2013; Cowan et al., 2013; Grose et al., 2017; Tozer et al., 2018).

Many studies have noted that blocking occurrence is generally underestimated in the NH of CMIP5 models, particularly in the Euro-Atlantic region (Anstey et al., 2013; Masato et al., 2013b; Dunn-Sigouin and Son, 2013; Zappa et al., 2014; Davini and D'Andrea, 2016). However, fewer papers have examined the SH and none have performed a systematic study of all available models over the entire SH. Using the reversal-based method of Tibaldi and Molteni (1990), Grose et al. (2017) performed an evaluation of blocking in CMIP5 models for the Australia region, concluding that there is no systematic blocking bias in this region. This is in agreement with Parsons et al. (2016) who examined four CMIP5 models over the entire hemisphere using a persistent positive anomaly method and found positive blocking biases around most of the hemisphere in three models and negatives biases in the other.

In this chapter, I evaluate the mean state biases in CMIP5 models as well as atmospheric blocking. The data and methods are outlined in section 6.2 and then mean state biases are discussed in section 6.3, paying particular attention to zonally asymmetric biases, given the asymmetry of the wintertime basic state. I also extend previous work on CMIP5 blocking biases in the SH by considering the ensemble of all available CMIP5 models over the entire hemisphere in section 6.4. Finally, conclusions are given in section 6.5.

6.2 Data and methods

6.2.1 Data

I utilize daily-mean and monthly-mean data from the historical experiments of 23 CMIP5 models for the period 1979-2005 and compare this with ERA-Interim reanalysis data over the same period. This period is chosen to coincide with the beginning of the satellite era, as reanalysis data before this date is less reliable in the SH (Bromwich and Fogt, 2004), while most of the CMIP5 simulations end in 2005. Models are chosen which have provided daily geopotential height on the 500hPa level, which is used for the blocking calculations. Model output is interpolated onto a standard N48 Gaussian grid ($1.875^\circ \times 1.875^\circ$) before blocking calculations are performed. Monthly-mean geopotential height, and zonal and meridional wind are used for calculations of stationary eddy stream function and wave-activity flux. The full list of models used in this study is given in appendix A.

6.2.2 Methods

In this chapter, I use the horizontal component of wave activity flux, W (Takaya and Nakamura, 2001), to show the propagation of stationary Rossby waves. Under the WKB approximation, W is parallel to the wave group velocity. The definition of W, along with further details, can be found in section 3.4.5.

I also detect blocking events using an adaptation of the reversal-based method of Masato et al. (2012). The original paper used PV on the dynamical tropopause, however Masato et al. (2013a) showed that the use of geopotential height at 500hPa, which is a readily available field in CMIP5 models, produced similar results. Details of the method can be found in section 3.4.6.

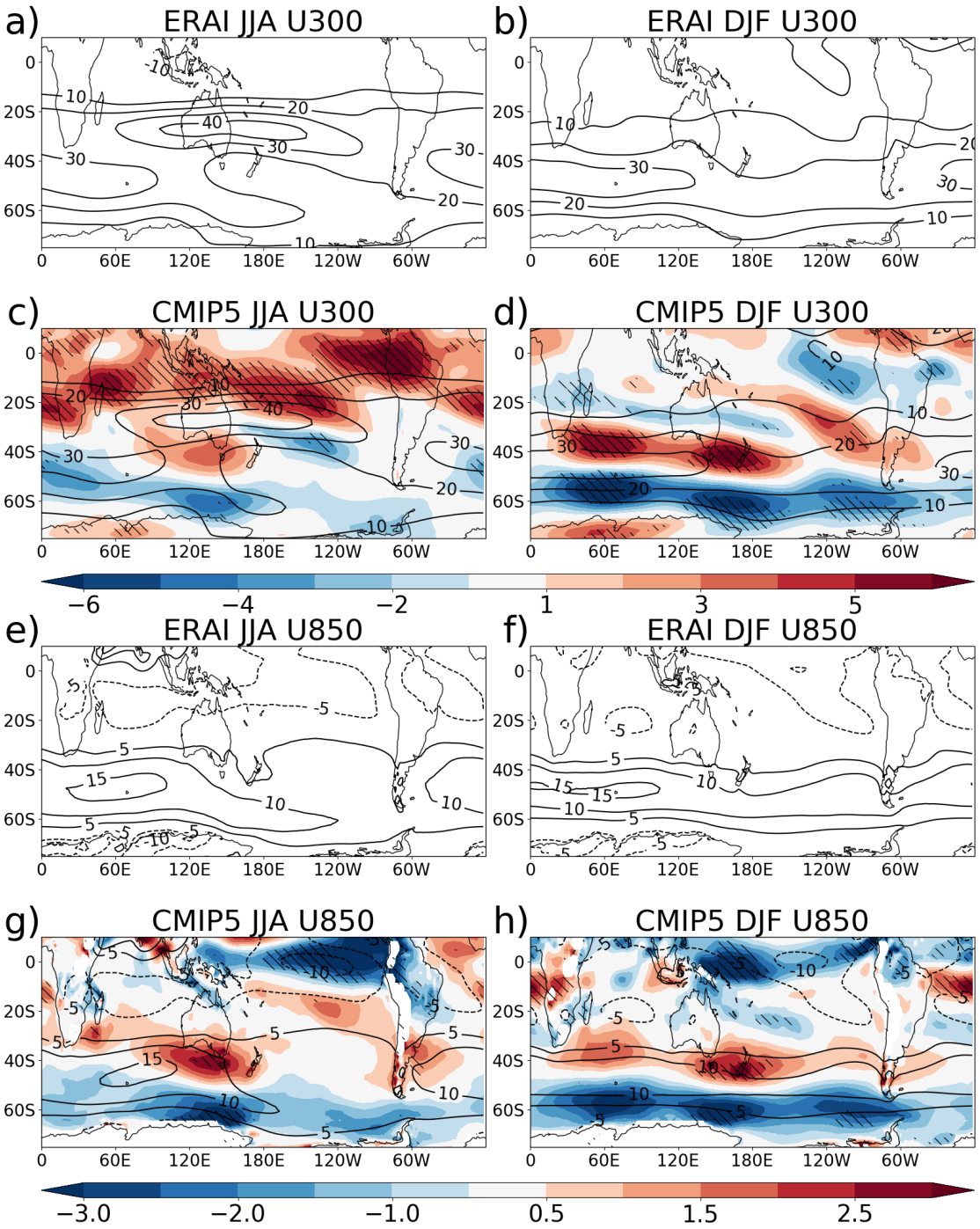


Figure 6.1: Zonal wind biases in CMIP5 with respect to ERA-Interim reanalysis: Mean zonal wind is shown for ERA-Interim at 300hPa for a) winter and b) summer and at 850hPa for e) winter and f) summer. The CMIP5 ensemble-mean zonal wind is also shown on the 300hPa level for c) winter and d) summer and at 850hPa for g) winter and h) summer. In each of these panels, contours show the climatology, colours show CMIP5 - ERA-Interim, while hatched regions show where the models agree on the sign of the bias in greater than 80% of cases. Units are ms^{-1}.

6.3 Mean state representation

Figure 6.1 shows the zonal wind biases in CMIP5 with respect to ERA-Interim reanalysis for both winter and summer. In the tropical upper troposphere during austral winter, there is a systematic positive wind bias in excess of $5ms^{-1}$ over the eastern Pacific, while there is also a positive bias in the subtropics from the Indian Ocean to the central Pacific (figure 6.1c). This is coincident with a negative wind bias at lower levels in the eastern Pacific (figure 6.1g), consistent with Grose et al. (2014). Circulation biases in the eastern Pacific are likely to be related to the pervasive cold-tongue bias (e.g. Bellucci et al., 2010; Li and Xie, 2014; Oueslati and Bellon, 2015) as circulation is closely linked to the east-west Pacific SST gradient (e.g. Meng et al., 2012).

In mid-latitudes, the equatorward jet bias can be seen for both seasons and in both the upper and lower troposphere (figure 6.1c,d,g,h). The wintertime split jet structure is less pronounced than in observations, as shown by the positive wind bias south of Australia and the relatively weak eddy-driven jet at high latitudes (figure 6.1c,g). However, the lack of hatching at upper levels indicates that this bias is not shared by all models. Rather than a zonally symmetric equatorward jet bias, the winter wind bias is localised to the south of Australia, with weaker winds at high latitudes, upstream over the Indian Ocean. This is consistent with the results of chapter 4, that the South Pacific jet strength depends on the strength of the upstream flow. The bias to the south of Australia was also noted by Bracegirdle et al. (2016) who showed that it was also a feature of atmosphere-only models, indicating that it is likely to be generated internally within the model atmosphere. It is also a feature of Spring (SON, not shown) and to a lesser extent Autumn (MAM, not shown).

The equatorward jet bias is both stronger, more consistent across different models (as shown by hatching) and more zonally symmetric in summer (figure 6.1). It is likely that this is the result of the more zonally symmetric jet in summer, while stationary

wave biases may play a larger role in winter as stationary waves are stronger during this season (Inatsu and Hoskins, 2006).

To investigate stationary wave biases in SH winter, I plot the 300hPa stationary eddy stream function, $\psi*$, in figure 6.2. This is calculated by removing the zonal mean from the stream function. I also plot wave activity flux vectors in panels a) and b) to indicate the propagation of energy associated with the stationary waves. In ERA-Interim reanalysis, figure 6.2a shows that wave activity propagates south-eastwards from the Indian Ocean region, refracting equatorward from around 110-120E and towards the subtropical central Pacific, consistent with the findings of Inatsu and Hoskins (2006). The associated stationary wave pattern is composed of a pair of anticyclones to the north-west of Australia and south of Madagascar, a cyclone centred at (100E,60S), an anticyclone to the south of New Zealand and a cyclone to its north.

This pattern is largely captured by the CMIP5 model ensemble (figure 6.2b). However, there appears to be insufficient wave activity propagating northwards from the high latitude South Pacific, consistent with the weakened split jet pattern (figure 6.1c). Figure 6.2c shows the CMIP5 stationary eddy stream function bias (colours) with the ERA-Interim climatology plotted for comparison (contours). At mid to high latitudes, the bias takes a wave-2 form with a prominent cyclonic anomaly to the south of Australia as observed in figure 6.1c. The anticyclone to the north-west of Australia is overly deep and extended further east in CMIP5 (figure 6.2b) giving an anticyclonic bias from the subtropical Indian Ocean to eastern Australia (figure 6.2c). Wave activity over the tropical-subtropical Indian Ocean is also stronger than in ERA-Interim (compare figure 6.2a,b), coincident with the westerly wind bias in figure 6.1c. It may be that the cyclonic anomaly to the south of Australia is forced by these tropical-subtropical wave activity flux biases.

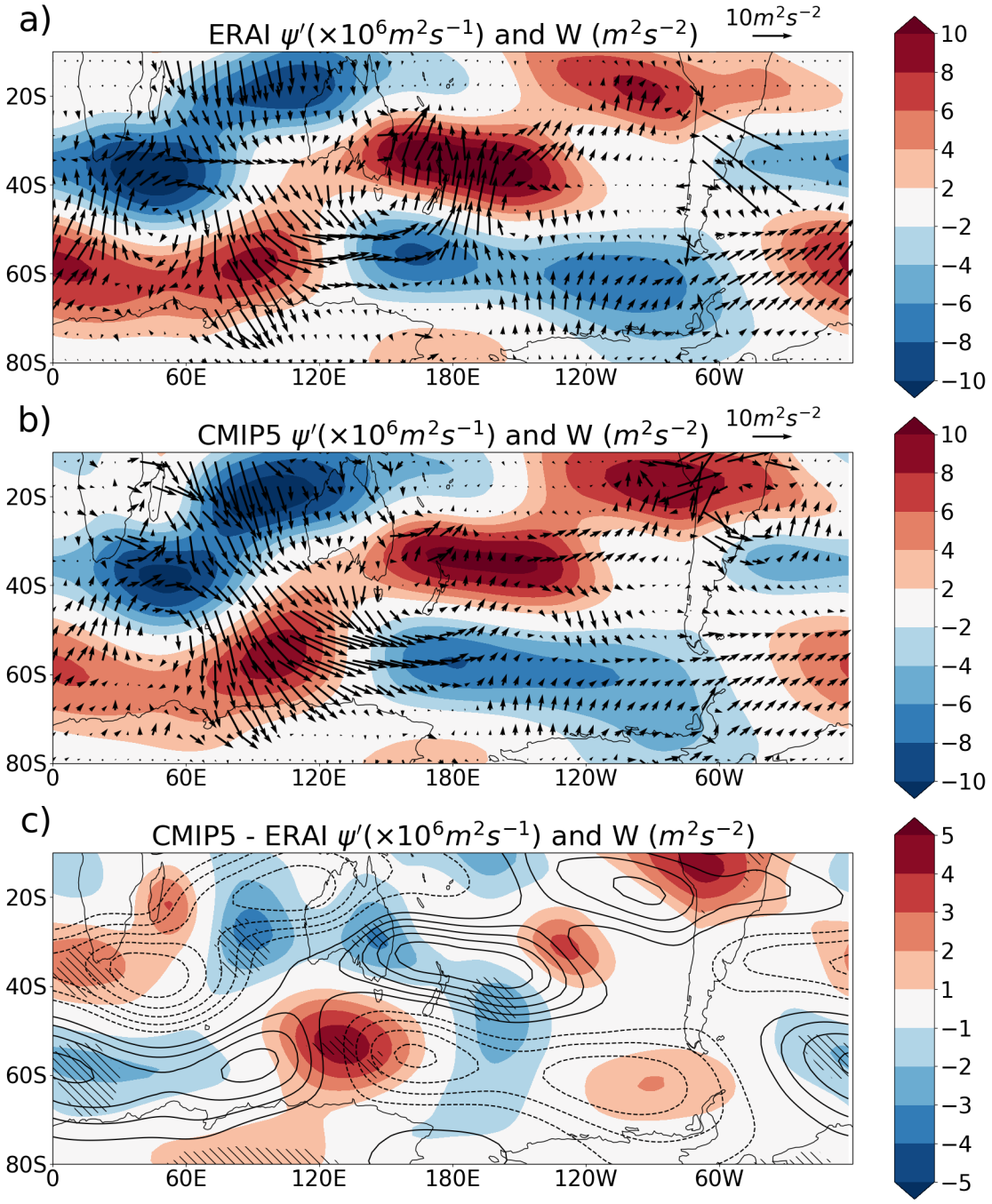


Figure 6.2: Stationary wave biases on the 300hPa level in CMIP5 with respect to ERA-Interim for winter. a) ERA-Interim stationary eddy stream function is shown in colours with wave activity flux vectors b) is the same as a) but for the CMIP5 ensemble-mean of these quantities. In c) CMIP5 - ERA-Interim stationary eddy stream function is shown by colours with contours indicating the ERA-Interim climatology. Red colours indicate cyclonic anomalies, while blue indicates anticyclonic anomalies. In c), regions with hatching indicate model agreement on the sign of the bias in greater than 80% of cases.

6.4 Blocking representation

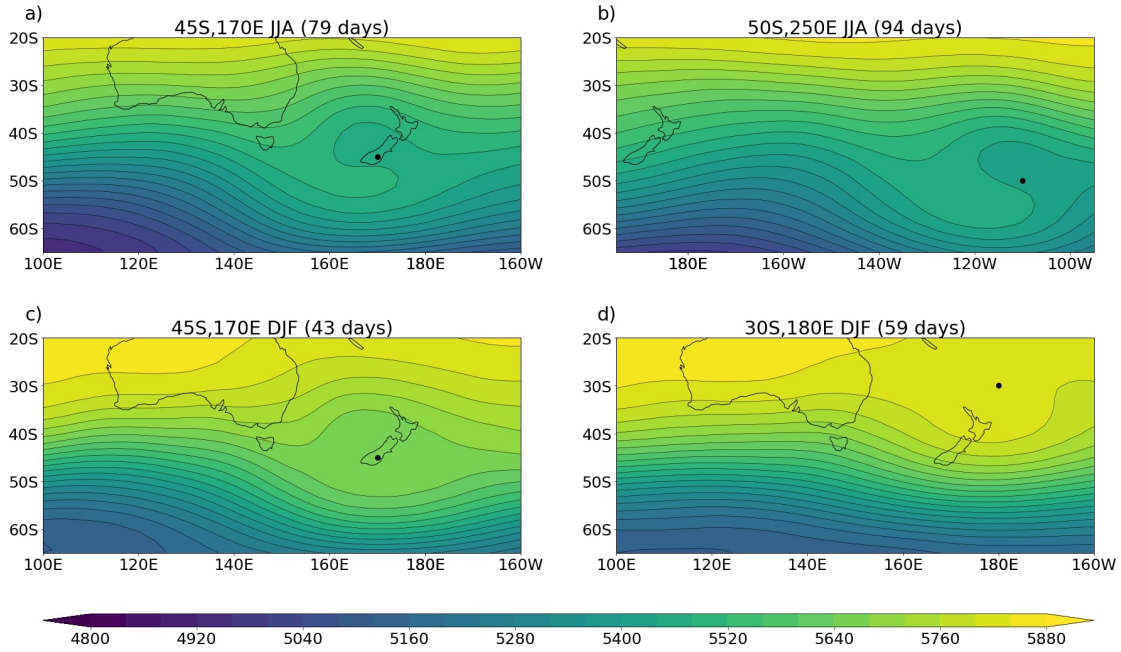


Figure 6.3: (a–d) Composites of daily mean Z500 for the onset day of blocking occurring at different locations. In each figure the location of the block is denoted by a black dot, with the location of that point noted in the title. The units are m.

Having examined the mean state biases in CMIP5, I will now investigate the representation of blocking in the same models. To ensure that the blocking algorithm correctly identifies blocking events, I show composites of daily mean Z500 on the onset day of blocking events occurring at a few particular locations. Figure 6.3a,b, show composites of blocking events during winter over New Zealand and in the south-east Pacific with a clear pattern of anticyclonic wave-breaking. In both cases the events clearly disrupt the mean flow, justifying them being labelled as blocking. The same point over New Zealand during summer in figure 6.3c does not show a clear overturning of contours but rather shows a poleward ridge and equatorward trough. Examination of individual events (not shown) indicates that detections by the algorithm normally do correspond to wave-breaking, though they are split between anticyclonic and cyclonic wave-breaking events which may explain the smoothed-out composite.

Finally, figure 6.3d shows composites of events occurring at or near a point in the subtropics. Unlike the other cases, the main flow does not appear to be significantly altered by the block. There has been some debate about whether low latitude events constitute blocking (Davini et al., 2012), though Rodrigues and Woollings (2017) showed that similar events over South America can have important impacts on local weather. Similarly, the index detects a high frequency of blocking events at high latitudes, in agreement with other studies (Berrisford et al., 2007; Masato et al., 2013a). In this chapter, I take the approach of focusing on events in mid-latitudes as these cohere more strongly with the traditional view of blocking.

Figure 6.4 shows the blocking climatologies (contours) for ERA-Interim and the CMIP5 ensemble-mean for both winter and summer, along with biases (colours). The maps are plotted in cylindrical rather than orthographic formats to better emphasise the mid-latitudes. In agreement with previous studies, blocking occurs most frequently during winter (figure 6.4a) and predominantly over the South Pacific Ocean (Trenberth and Mo, 1985; Sinclair, 1996; Renwick, 2005; Berrisford et al., 2007; Parsons et al., 2016). There are also a large number of events at high-latitudes, particularly at 60-120E. As discussed in section 5.5, these events do not match the traditional definition of blocking, though they are strongly linked to jet variability, especially in the South Pacific sector. Broadly speaking, the CMIP5 ensemble-mean represents the main features of wintertime SH blocking relatively well (figure 6.4b). Interestingly, the lack of hatching indicates that models have biases of differing signs, with no systematic underestimation, in contrast with the Euro-Atlantic sector. If anything, blocking occurrence is overestimated slightly as shown by the positive bias south of New Zealand. There is also a slight underestimation of blocking occurrence in the south-east Pacific.

Blocking in the summer season is far less frequent than in winter with few events occurring in mid-latitudes (figure 6.4c). This is likely a result of the more zonal jet

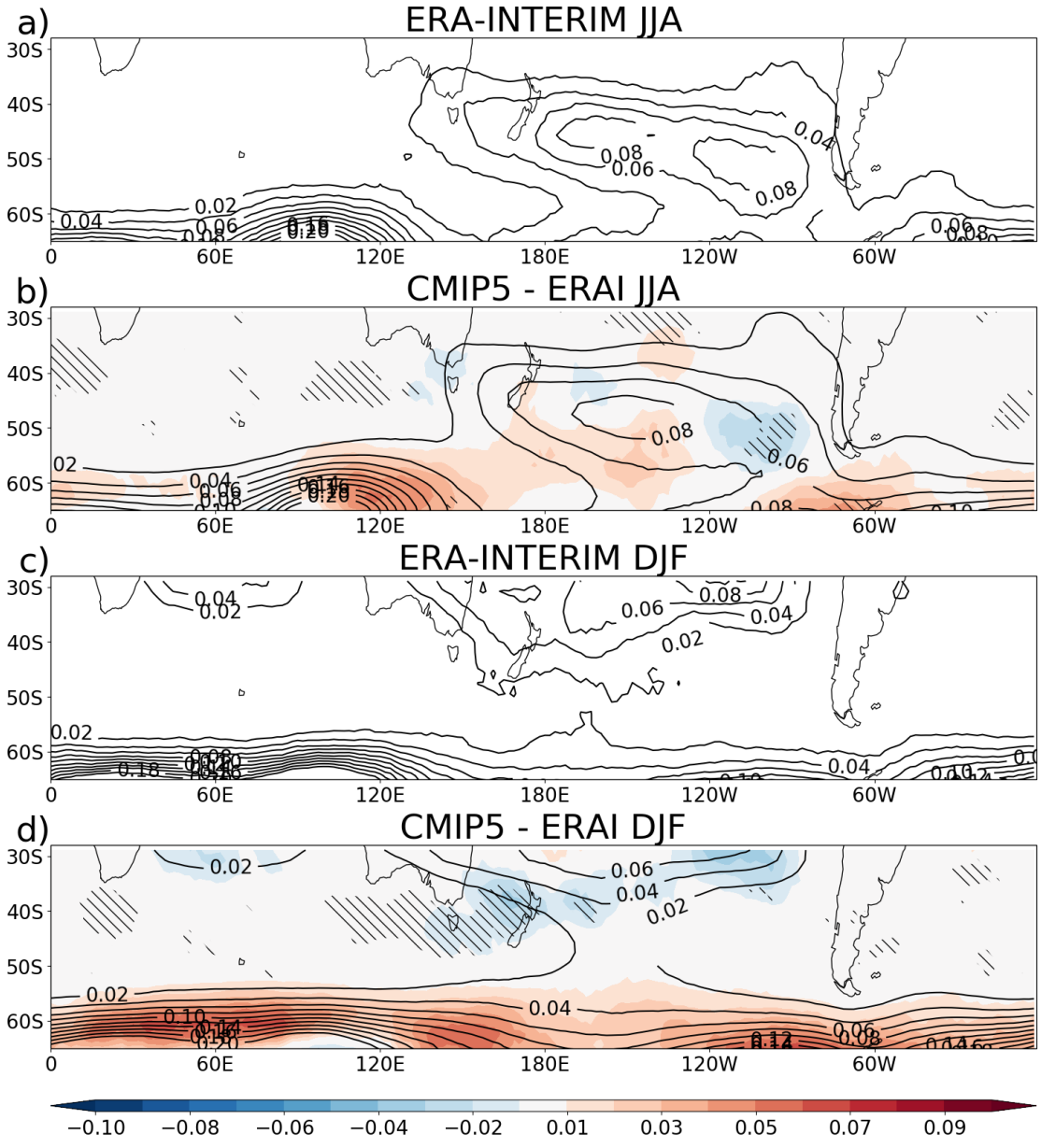


Figure 6.4: Blocking frequency biases for winter (a,b) and summer (c,d): (a, c) The ERA-Interim mean blocking frequency for each grid-point; (b, d) the mean of all CMIP5 models (contours) minus ERA-Interim (colours). The contour interval for each climatology is 0.02, while it is 0.01 for differences, and hatching indicates that 80% of models agree on the sign of the difference. The blocking frequency is given as the fraction of blocked days.

and stronger westerlies in the South Pacific sector. The CMIP5 jet bias in summer is more consistently equatorward and this is reflected in the blocking bias (figure 6.4d). That is, blocking occurrence is consistently underestimated to the south of Australia, as indicated by hatching, where the westerlies are anomalously strong (figure 6.1d,h). At the same time, high latitude blocking events occur too frequently relative to ERA-Interim reanalysis, consistent with the anomalously weak flow there (figure 6.1d,h).

Taking the CMIP5 ensemble-mean masks out the variation across different models. In figure 6.5, I plot the blocking biases for each individual model for the winter season. There is a large amount of interannual variability in blocking occurrence from year to year and the relatively short, 27 year period being examined means that there is a substantial uncertainty in observed blocking frequency. To quantify this, I performed a bootstrapping procedure in which the ERA-Interim blocking climatology was recalculated 10,000 times, but each time taking a random 27 years from the period 1979-2005, with replacement. This allowed calculation of 95% confidence intervals for each grid-point as the 2.5th and 97.5th percentile of these 10,000 climatologies. Biases in figure 6.5 are only plotted where the bias exceeds these confidence intervals.

It is clear that there is a wide variety of model representations of blocking. Some models such as 'bcc-csm1-1', 'bcc-csm1-1-m', 'BNU-ESM' and 'CanESM2', which have an overly strong jet in mid-latitudes (not shown), exhibit very little blocking at all. It is worth noting that all of these are run at low horizontal resolution (each is approx. $2.8^\circ \times 2.8^\circ$ at the equator) which is known to produce a low occurrence of blocking (e.g. Matsueda et al., 2010; Berckmans et al., 2013). On the other hand some models such as the 'IPSL' and 'CMCC' models have a large equatorward jet bias (not shown) and instead considerably overestimate blocking occurrence. Of these, 'IPSL-CM5A-LR', 'IPSL-CM5B-LR' and 'CMCC-CESM' are run at a similarly low resolution to the models which strongly underestimate blocking, suggesting that low resolution does not guarantee that the model will have a low rate of blocking occur-

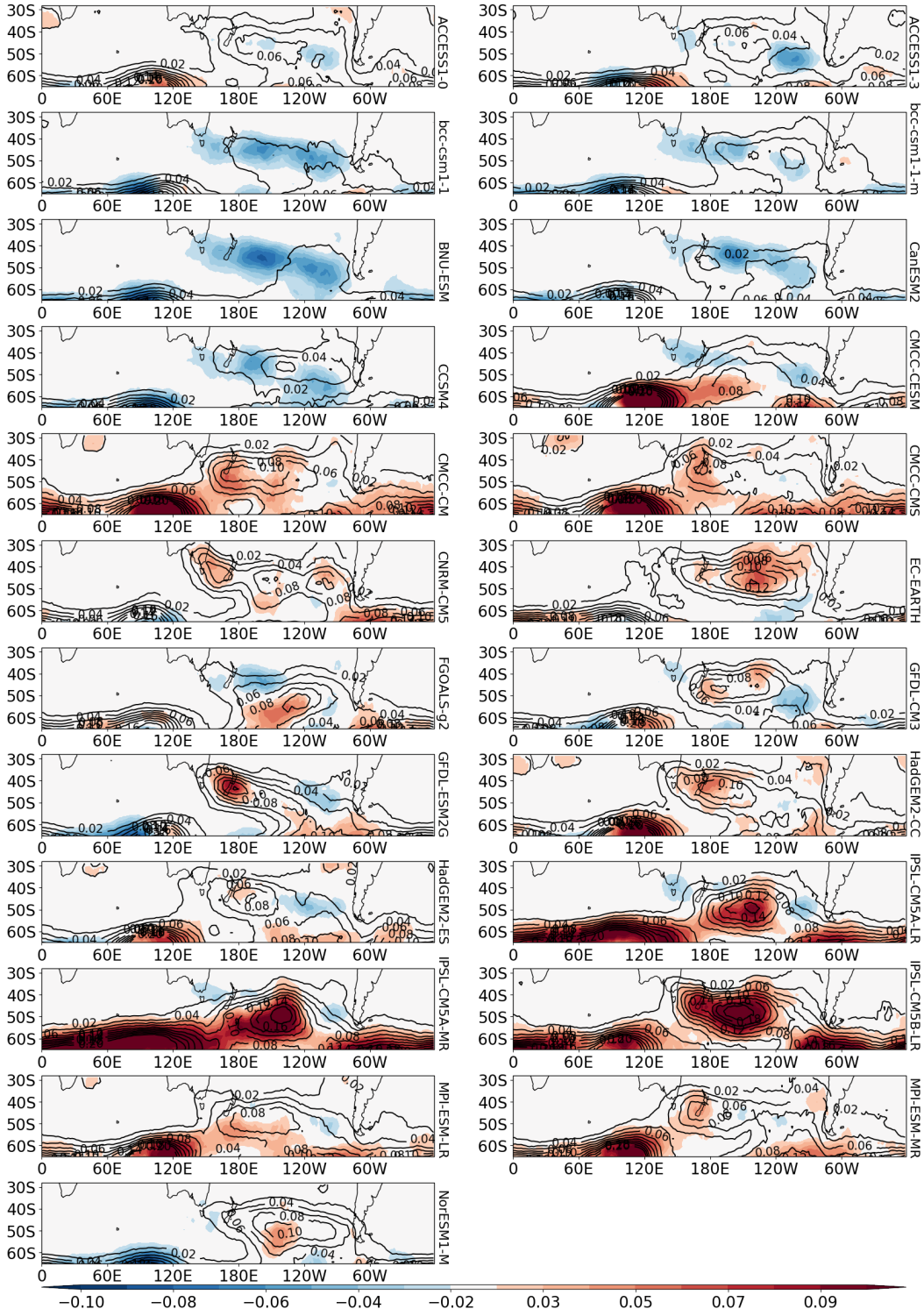


Figure 6.5: Blocking frequency biases for winter for all models. In each plot the climatology is shown by contours and the bias by colours with contour interval 0.02 for the climatologies (contours) and 0.01 for the biases (colours), with the latter beginning at 0.02. The blocking frequency is given as the fraction of blocked days.

rence. Rather, the mean state is likely to be important in determining the blocking frequency (Scaife et al., 2010). It is of course the case that blocking events will contribute to the mean state itself, but given that the frequency of blocking events is relatively low, this is likely to be a small effect. Other models such as the 'ACCESS' and 'HadGEM2' models, and 'NorESM1-M', capture the observed distribution of blocking relatively well. Overall, only a small subset of models simulate South Pacific blocking well, though the CMIP5 ensemble-mean bias appears low because roughly as many models overestimate as underestimate blocking occurrence.

6.5 Discussion and conclusions

In this chapter, I have examined the mean state and blocking biases in the historical experiments of 23 CMIP5 models with respect to ERA-Interim reanalysis. In general, the CMIP5 ensemble-mean eddy-driven jet is equatorward-biased in both summer and winter (figure 6.1c,d,g,h), though in the latter case some individual models have the opposite bias and the bias is largely restricted to the region to the south of Australia. On the other hand, the summer jet bias is equatorward in almost all models and more zonally symmetric in nature. The wintertime circulation bias has a notable stationary wave component to it (figure 6.2c), which is unsurprising given the significant zonal asymmetry in the mid-latitudes during this season. Again, the locus of the bias pattern is to the south of Australia and hence likely has implications for simulation of current and future circulation and climate in the Australia-New Zealand sector, a topic which will be examined in chapter 7. The cause of the stationary wave bias is unclear, though I noted that it is likely to be generated internally within the model atmosphere as it is also a feature of atmosphere-only simulations.

I have also examined SH atmospheric blocking using an adaptation of the index of Masato et al. (2012) which has previously been used to study NH blocking in CMIP5 (Masato et al., 2013a). Unlike the Euro-Atlantic sector, blocking is not systemati-

cally underestimated in SH winter, instead models are roughly equally split between those that have positive and negative biases with respect to ERA-Interim (figure 6.5). Most models do not represent the observed distribution of blocking well, but there is a cancellation within the ensemble-mean between models which underestimate and those which overestimate observed blocking frequency (figure 6.4b). On the other hand, models such as the 'ACCESS' models, 'HadGEM2' and 'NorESM1-M' simulate blocking successfully (figure 6.5). These models also are successful in capturing the typical timescales of blocking in the SH (not shown). Summertime blocking is relatively infrequent in the SH, though there is a consistent underestimation of blocking frequency to the south of Australia (figure 6.4d). This is consistent with the pervasive equatorward jet bias found in the summer season.

In spite of these blocking biases, the CMIP5 ensemble still provides important information regarding potential future changes in blocking. This is particularly the case if there is a link between the magnitude of the bias and that of the projected change as this provides an emergent constraint (Collins et al., 2012). I will investigate this in the following chapter.

Chapter 7

Split jet and atmospheric blocking response to forcing

In this chapter I analyse the SH circulation response to anthropogenic forcing under the RCP8.5 scenario using CMIP5 models. I find that the circulation changes differ between summer and winter, with a zonally symmetric poleward jet shift characterising the summer response and a more zonally asymmetric response in winter. In the latter case, this consists of a strengthening of the subtropical jet over the eastern South Pacific and strengthened atmospheric flow to the south of Australia, making the split jet pattern less distinct. I also examine atmospheric blocking and find a robust reduction in wintertime blocking frequency to the south of Australia, with the total number of blocking days reduced by around one third for the period 2070-2099.

7.1 Introduction

Anthropogenic-induced changes to the climate system have already had a considerable impact on society including through increasing the frequency of extreme events (Hartmann et al., 2013) and increasing the severity of droughts (e.g. Murphy and Timbal, 2008; Williams et al., 2020). These changes have been influenced both by increases in global mean temperature associated with enhanced radiative forcing and the resultant dynamical changes to the Earth system, including changes to atmospheric circulation.

In this chapter, I consider the response of the SH circulation in mid-latitudes to a future high greenhouse gas emissions scenario. In the background chapter (section 2.2.5), I discussed the main projected SH circulation changes including a continued poleward shifting of the eddy-driven jet (e.g. Swart and Fyfe, 2012; Barnes and Polvani, 2013) and expansion of the Hadley cell (e.g. Grise et al., 2019). Similar to the previous chapter, I seek to document not only the zonally symmetric response to forcing, but to focus on the zonally asymmetric or stationary wave component, which is larger in austral winter.

Stationary waves in the extratropics are generally forced by orography, diabatic heating and land-sea thermal contrast (e.g. Held et al., 2002). These can have a large effect on regional hydrology and temperature, particularly during winter. According to barotropic Rossby wave theory, the amplitude, phase and propagation of stationary waves depends critically on the background flow (Hoskins and Karoly, 1981; Hoskins and Ambrizzi, 1993). A key quantity in this regard is the stationary wave number,

$$K_S = cos(\theta) \sqrt{\frac{\beta - \partial_{yy} U}{U}}, \tag{7.1}$$

in which β is the planetary vorticity gradient, U is the background zonal flow and $\partial_{yy} U$ is the background meridional vorticity gradient. The $\cos(\theta)$ term also accounts for the effect of k decreasing with latitude. Rossby waves tend to refract towards higher K_S and cannot propagate through regions where $U = 0$, where K_S becomes imaginary. Changes to stationary waves may thus arise through changes to the background flow, which alters K_S, or through changes to the Rossby wave sources. In the latter case, the location of orography and land-sea contrast are fixed, but changes to tropical convection can alter the strength or location of diabatic heating (Haarsma and Selten, 2012), while the magnitude of land-sea contrast will also change with climate change (Sutton et al., 2007). Additionally, orographic forcing of stationary

waves depends strongly on the impinging background flow (e.g. Son et al., 2009) so any changes to U could have a substantial effect on orographic stationary waves.

Only a few studies have examined the SH stationary wave response to climate change and this knowledge gap provides motivation for this work. Freitas and Rao (2014) diagnosed a weakening of the SH winter climatological stationary wave pattern in CMIP3 simulations with increased greenhouse gas forcing and attributed this to changes to the background flow. However, they did not consider changes to Rossby wave sources and so could not rule these out as a significant factor. In idealised experiments with the CSIRO Mk3 model, Freitas et al. (2017) found a similar stationary wave response to Freitas and Rao (2014) upon uniformly increasing tropical SSTs and suggested that changes to the Hadley cell may mediate this response. Simpson et al. (2014) examined the longitudinally varying component of RCP8.5 circulation changes with respect to Historical simulations. Their analysis of the 700hPa wind field (their figure 6e) shows that the wind changes show a significant degree of zonal asymmetry. Rather than a zonally symmetric poleward jet shift, the zonal wind is strengthened locally to the south of Australia, with a similar result being found in CMIP3 simulations (Lorenz and DeWeaver, 2007).

The changing background circulation is also likely to result in changes to transient phenomena. For instance, previous studies have examined changes to cyclone frequency, finding a poleward shift and intensification of the storm track under climate change (e.g. Chang et al., 2012; Lee, 2015; Mindlin et al., 2020). However, relatively few papers have considered changes to atmospheric blocking in the SH. I have shown in chapter 5, that this is a key feature in the South Pacific region, hence in this chapter I investigate changes to blocking frequency.

Several studies have shown that in response to anthropogenic forcings, the number of cutoff lows over Australia decreases during all seasons (Grose et al., 2012; Dowdy et al., 2013). This is consistent with Matsueda et al. (2010), who found blocking

frequency decreases in the Australia-New Zealand sector using the Japanese Meteorological Research Institute model, while they found no change in blocking over the south-east Pacific. Similarly, Grose et al. (2017) examined blocking within the Australia region in 26 CMIP5 models and found blocking frequency to be reduced in future simulations. More broadly, a study by Parsons et al. (2016) using four GCMs from the CMIP5 ensemble showed that blocking frequency was generally reduced across most of the SH in future climate simulations, with some seasonal variations in the location of the largest changes. I build on this literature by considering a large range of models over the entire SH to assess whether these changes are robust across all models.

In this chapter, I analyse SH extratropical circulation and blocking frequency differences between the Historical and RCP8.5 experiments within CMIP5. My focus is primarily on austral winter, but I also show summer differences for comparison. In section 7.2 I describe the data and methods, then in section 7.3 I document changes to the large-scale circulation. Following this I investigate changes to atmospheric blocking in section 7.4, while section 7.5 examines changes in the Australia-New Zealand region and I then provide conclusions in section 7.6.

7.2 Data and methods

In this chapter, I compare data from RCP8.5 and Historical experiments within CMIP5. As I discussed in chapter 3, RCP8.5 is likely to represent an unrealistically high forcing, as global coal-use is beginning to plateau and clean energy prices are continuing to fall (Ritchie and Dowlatabadi, 2017; Hausfather and Peters, 2020). However, I recognise that RCP8.5 has been widely used in the scientific literature and so it is useful for making comparisons between studies. Moreover, high radiative forcing provides a large signal-to-noise ratio.

I utilize daily-mean and monthly-mean data from the Historical and RCP8.5 simulations of the same 23 CMIP5 models as in chapter 6 (full model list given in appendix A). To be consistent with the previous chapter, I also use the period 1979-2005 for the Historical simulations and compare this to the period 2070-2099 in the RCP8.5 simulations. I only use one ensemble member (r1i1p1) for each model, apart from in 7.5 where I include all ensemble members for which daily geopotential height was available in both Historical and RCP8.5 simulations.

I calculate blocking frequency, stationary eddy stream function and wave-activity flux as in the previous chapter (see section 3.4 for details on the calculation of these diagnostics). As before, model output is interpolated onto a standard N48 Gaussian grid ($1.875^\circ \times 1.875^\circ$) before blocking calculations are performed. Monthly-mean geopotential height, and zonal and meridional wind are used for calculations of stationary eddy stream function and wave-activity flux.

7.3 Circulation response to forcing

I show differences in zonal wind at upper and lower levels in figure 7.1 for both winter and summer. In summer, there is a clear poleward shift of the mid-latitude jet (figure 7.1d,h), with the large regions of hatching indicating substantial model agreement on the response to forcing, at least in the sign of the response. This result is consistent with many previous studies on the SH summer jet (e.g. Swart and Fyfe, 2012; Wilcox et al., 2012; Barnes and Polvani, 2013) and the zonal symmetry of the response is unsurprising given the largely symmetric basic state. Also of note is the baroclinic response over the eastern South Pacific between the equator and subtropics with anticyclonic and cyclonic anomalies at upper and lower levels respectively. This is consistent with reduced downwelling and a weakened Walker circulation (e.g. Vecchi and Soden, 2007).

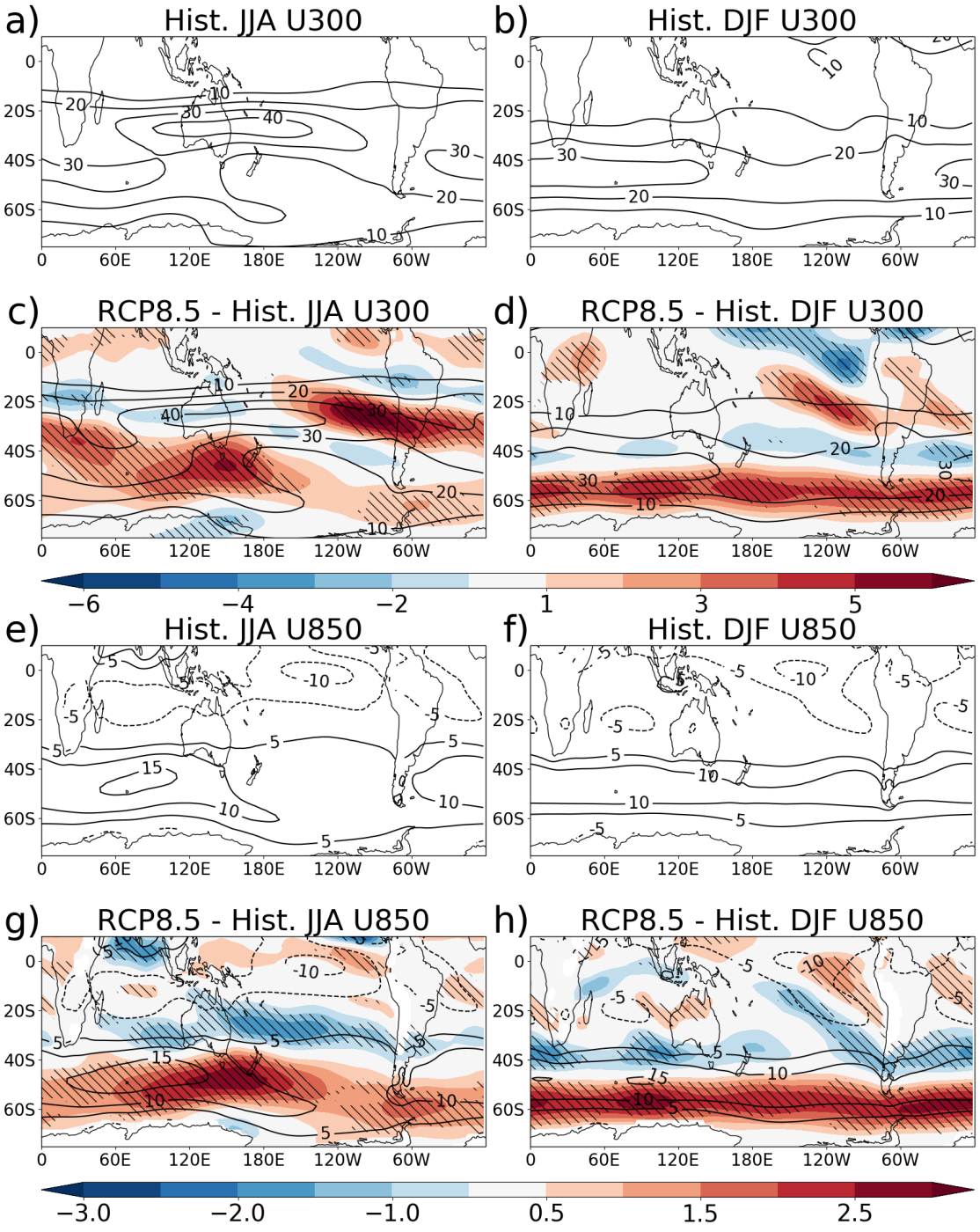


Figure 7.1: Zonal wind in the CMIP5 Historical (1979-2005) and RCP8.5 (2070-2099) simulations: CMIP5 ensemble-mean zonal wind is shown for the Historical simulation at 300hPa for a) winter and b) summer and at 850hPa for e) winter and f) summer. The ensemble-mean zonal wind for RCP8.5 is shown on the 300hPa level for c) winter and d) summer and at 850hPa for g) winter and h) summer. In each of these panels, contours show the climatology, colours show RCP8.5 - Historical, while hatched regions show where the models agree on the sign of the difference in greater than 80% of cases. Units are ms^{-1}

The wintertime response shows considerably more structure as expected from the zonally asymmetric basic state (figure 7.1c,g). At upper levels (figure 7.1c), the subtropical jet strengthens between the central Pacific and over the South Atlantic, linking up with a strengthened jet in mid-latitudes. As in summer, there is a barotropic strengthening of the jet in mid-latitudes which may give the appearance of a poleward shift in the zonal mean. In agreement with previous studies, mid-latitude jet changes are not zonally symmetric, with the largest changes occurring to the south of Australia and west of New Zealand (Lorenz and DeWeaver, 2007; Simpson et al., 2014; Grose et al., 2017). Interestingly, this is co-located with the region of the largest wintertime circulation bias (see figure 6.1c,g). I will investigate the possibility of a connection between the bias and response in this region in section 7.5. The location of this response is between the subtropical and polar front jets, reducing the 'splitting' of the two jets. Given the range of SH winter zonal wind climatologies in the CMIP5 models, with some models capturing the split jet and others exhibiting only a single subtropical jet (Bracegirdle et al., 2013), it is interesting that the sign of the zonal wind response is fairly consistent across models (shown by large regions of hatching).

To investigate the stationary wave component to the circulation change, I plot the stationary eddy stream function and wave activity vectors in figure 7.2. I only consider the stationary wave response in winter when stationary waves are strongest (Inatsu and Hoskins, 2006). The largest mid-latitude response consists of anticyclonic and cyclonic anomalies over south Australia and further south at around (150E, 60S), respectively (colours, figure 7.2c). This could stem from a modification of the climatological stationary Rossby wave emanating from the Indian Ocean region as seen by wave activity vectors in figure 7.2a,b. Concomitantly, the stationary cyclone over the central Pacific at about 35S in the Historical climatology, is extended further eastwards towards South America in the RCP8.5 simulation. As with the zonal wind changes (figure 7.1c,g), there is substantial model agreement over the sign of the

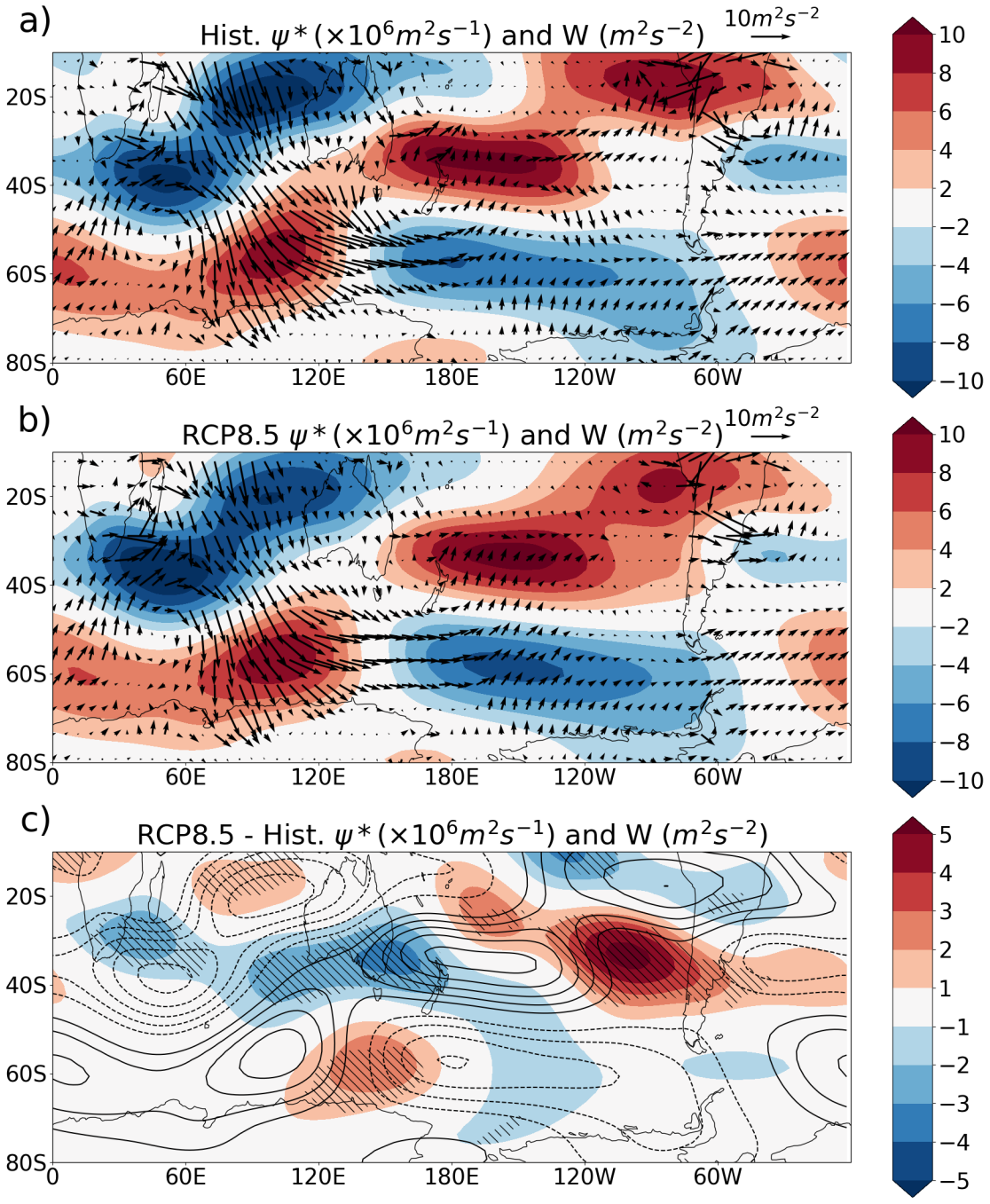


Figure 7.2: Winter ensemble-mean stationary waves in Historical (1979-2005) and RCP8.5 (2070-2099) simulations: a) Historical stationary eddy stream function is shown in colours with wave activity flux vectors, b) is as in a) but for RCP8.5. In c) RCP8.5 - Historical stationary eddy stream function is shown by colours, with contours indicating the Historical climatology. In c), regions with hatching indicate model agreement on the sign of the difference in greater than 80% of cases.

changes to stationary waves, suggesting that the response is relatively robust. On the other hand, it is unclear whether these changes arise from changes to the background flow modifying K_S or whether an alteration of the Rossby wave sources plays a larger role. I will investigate the mechanisms behind this stationary wave response in chapter 8. As discussed previously, changes to the mean atmospheric circulation are likely to drive changes in blocking frequency (Woollings, 2010; de Vries et al., 2013) and I now examine whether this is the case in CMIP5.

7.4 Blocking changes

Figure 7.3 compares the blocking frequency in the Historical and RCP8.5 simulations for both winter and summer. For both seasons, ensemble-mean blocking occurrence generally decreases with anthropogenic forcing. Previous work (Matsueda et al., 2010; Parsons et al., 2016) has shown this to be the case in a small subset of models, but using a larger ensemble allows us to rule out the influence of natural variability, which is considerable for blocking frequency, and to show that the result is robust to model choice. In particular, there is strong intermodel agreement on reduced high-latitude blocking in summer, which is consistent with the strengthening of high-latitude winds (figure 7.1d), and on blocking reductions south of Australia and over New Zealand during winter (shown by hatching). The latter result is in agreement with Parsons et al. (2016), who used a persistent positive pressure anomaly method and found the largest winter changes in that region (see their Figure 6b) and with Grose et al. (2017). This result is also consistent with the reductions in cutoff low events found by Grose et al. (2012) and Dowdy et al. (2013). Reductions in overall blocking frequency may be the result of a decrease in the number of blocking events or a reduction in the mean duration of blocking events. A decomposition of this (not shown), indicates that both effects play a role; however changes in the number of events are more important.

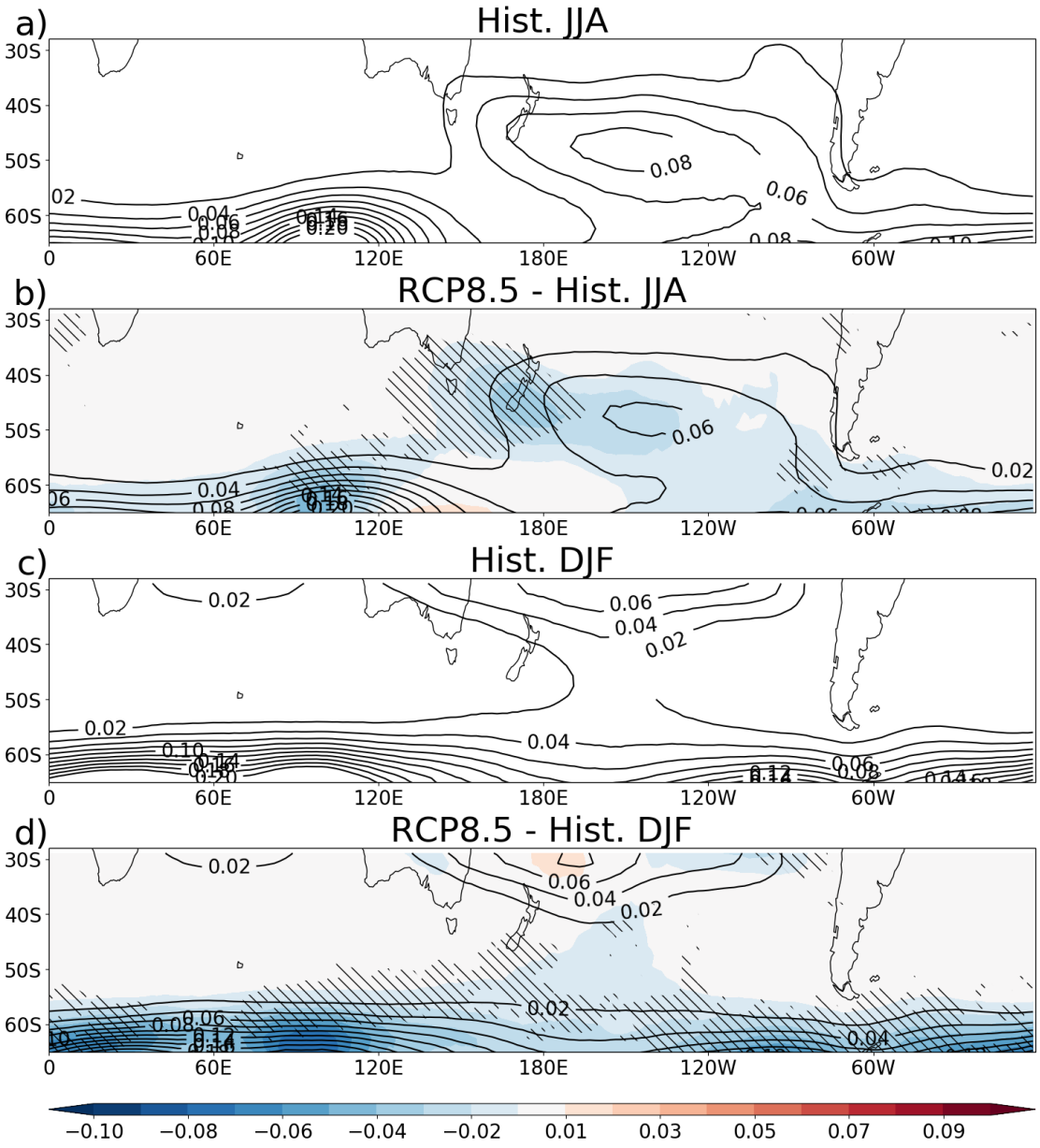


Figure 7.3: Blocking frequency in the Historical (1979-2005) and RCP8.5 (2070-2099) simulations for winter (a,b) and summer (c,d): (a, c) The Historical CMIP5 ensemble-mean blocking frequency for each grid-point; (b, d) the RCP8.5 ensemble-mean (contours) minus Historical ensemble-mean (colours). The contour interval for each climatology is 0.02, while it is 0.01 for differences, and hatching indicates that 80% of models agree on the sign of the difference. The blocking frequency is given as the fraction of blocked days.

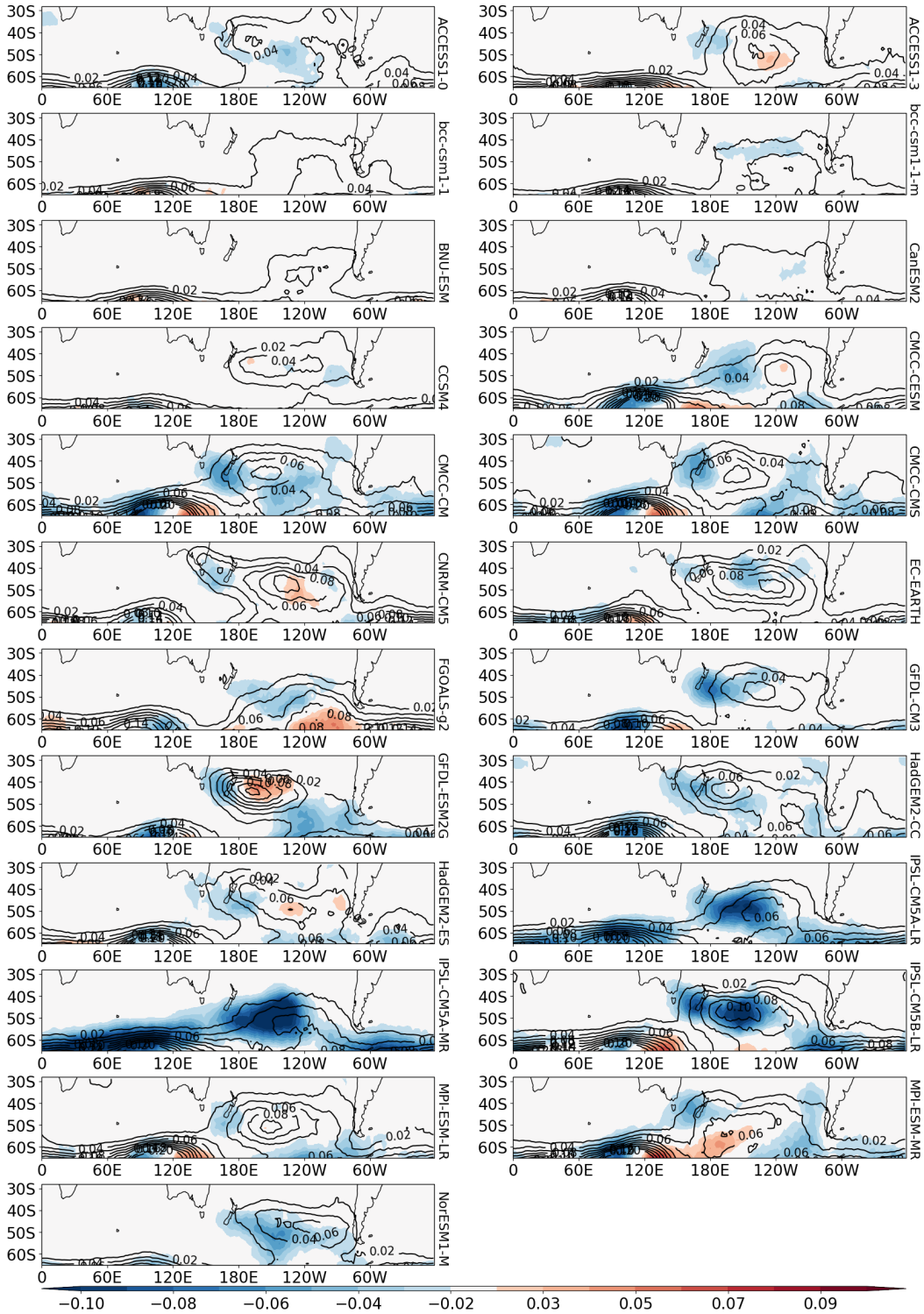


Figure 7.4: Winter blocking frequency in RCP8.5 (2070-2099) for all models: In each plot the climatology is shown by contours and RCP8.5 - Historical by colours with contour interval 0.02 for the RCP8.5 climatologies and 0.01 for the differences, with the latter beginning at 0.02. The blocking frequency is given as the fraction of blocked days.

As was the case with blocking biases (section 6.4), taking the multimodel mean in figure 7.3 masks considerable variation between models (figure 7.4). For instance, models such as 'bcc-csm1-1' and 'CanESM2', which greatly underestimate the number of South Pacific blocking events, show little change in blocking occurrence (figure 7.4). On the other hand, models which overestimate blocking frequency such as the 'IPSL' models, show a marked decrease. Overall, the trend is clearly a general reduction in the number of blocking events, but particularly in the Australia-New Zealand sector, which I investigate further in the next section.

7.5 Changes in the Australia-New Zealand sector

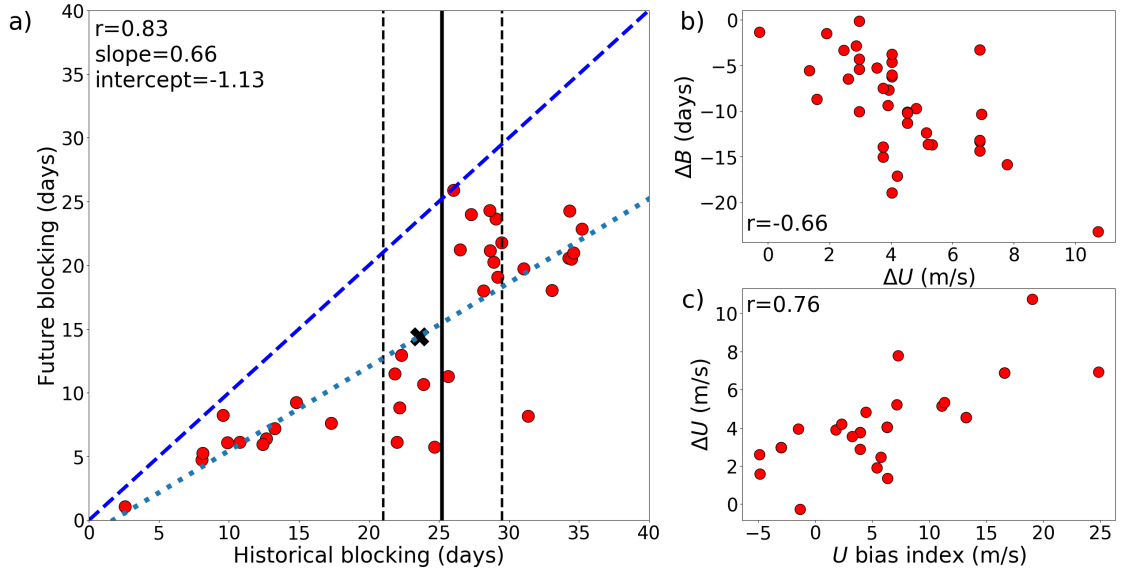


Figure 7.5: Changes in the number of blocked days per season in the Australia-New Zealand region (AusNZ) during winter: a) Mean blocking days per season for RCP8.5 and Historical simulations for all ensemble members. The cross represents the multi-model mean, the dashed line is the line with the y value equal to the corresponding x value, the dotted line is the line of best fit, the solid black line is the ERA-Interim mean, while the dashed vertical lines are the 95% confidence intervals (see text for details). b) Blocking days per season change against the change in 300-hPa zonal wind. c) The change in 300-hPa zonal wind against the zonal wind bias index (see text for details).

The largest anthropogenically forced changes to the winter midlatitude circulation

in the SH occur to the south of Australia (figure 7.1c), coincident with blocking frequency decreases seen in figure 7.3b. To investigate this further, I define the region between 120–180E and 40–55S to be the Australia-New Zealand region (AusNZ) and count the number of blocked days, which occur within this area each season. For a day to be defined as "blocked" there must be at least one blocked gridpoint within this region.

In Figure 7.5a, I plot the mean number of blocked days per winter season for the RCP8.5 scenario in the period 2070–2099 against the Historical period. Significantly, all ensemble members but one show a decrease in blocking frequency as they all lie below the blue dashed line (the exception being EC-Earth r2i1p1, which remains virtually the same). This is all the more remarkable given the spread of Historical blocking frequency among CMIP5 (figure 6.5). Blocking frequency varies substantially from year to year and so sampling uncertainty may play a role. In order to quantify this, I plot the 95% confidence intervals on the ERA-Interim value, calculated by resampling the number of blocking days for each year with replacement 1,000 times, calculating the mean each time and taking the confidence intervals as the 2.5th and 97.5th percentiles. Interestingly, the multimodel mean Historical blocking lies close to the ERA-Interim mean and within the confidence intervals, even though upper tropospheric wind speed is generally significantly overestimated in this region in models (Figure 6.1c). This is in contrast to central Europe where a positive wind bias results in strongly underestimated blocking (Scaife et al., 2010).

In general, the best fit line in figure 7.5a indicates that the blocking frequency in a future simulation decreases by about a third in comparison to the corresponding Historical simulation. This exceeds the internal variability in mean blocking days between ensemble members of the same model (not shown). However, there is a considerable spread in RCP8.5 blocking frequency and even for the Historical simulations, which lie close to the ERA-Interim value (black line), the spread in future projections

is large at between 5 and 25 days per season. Blocking frequency changes are likely to be driven by changes to the large-scale circulation (Woollings, 2010; de Vries et al., 2013). To investigate if this is the case, the relationship between blocking changes in the AusNZ region and changes in mean zonal wind for each model is shown in Figure 7.5b. From this, it is clear that larger wind increases result in larger reductions in blocking frequency with the wind change accounting for about $0.66^2 \times 100 = 44\%$ of the intermodel variance in blocking change.

In addition, several authors have noted a relationship between the zonal mean Historical jet latitude and the magnitude of the future poleward jet shift/jet strengthening (Kidston and Vallis, 2010; Barnes and Polvani, 2013; Bracegirdle et al., 2013; Simpson and Polvani, 2016) suggesting that there is a relationship between the Historical winds and the wind change. There is both a strong wind bias and a strong response within the AusNZ sector, and as the blocking change is linked to the wind response, it may be that the wind bias seen in figure 6.1c influences this. To quantify the strength, locally, of the relationship between the zonal wind response and the Historical wind bias, I construct a wind bias index. This is defined as the difference between the winter mean zonal wind at 300 hPa over the latitudes 35–45S and 55–65S, both between 120E and 180E, minus the same index in ERA-Interim. Figure 7.5c shows that the zonal wind response in the AusNZ region is strongly related to the Historical wind bias as models with a strong bias index show an enhanced response. While it is apparent that all models show an increase in wind speed, considering the bias-response relationship, the true wind response may lie closer to 2–3 m/s than the 4–5 m/s seen in Figure 7.1c. Hence, with the strong correlation between zonal wind changes and blocking frequency changes in 7.5b), the reduction in blocking days per winter season is unlikely to be more than 10 days. These results also seem to be consistent with Grose et al. (2017), who found that models with a more positive blocking bias, tended to show a greater reduction in winter blocking days.

7.6 Discussion and conclusions

In this chapter I have investigated the response of the SH circulation to anthropogenic forcing in 23 CMIP5 models. Most research on this topic has focused on the zonally symmetric poleward shift of the summertime jet or on the annual-mean. I have shown that while the wintertime response also shows a strengthening of the winds at high latitudes, there are substantial zonal asymmetries to this response (figure 7.1c,g). The largest mid-latitude change is a zonal wind speed increase to the south of Australia, reducing the splitting of the split jet. Concomitantly, the subtropical jet over the eastern South Pacific strengthens. The models studied agree well on the sign of both of these responses, suggesting that these results are relatively robust. Analysis of the stationary eddy stream function (figure 7.2) provides a similar picture. This shows anticyclonic and cyclonic anomalies over southern Australia and further south at 60S, respectively. These anomalies may result from a modification of the stationary Rossby wave discussed in Inatsu and Hoskins (2006) and I will investigate this further in chapter 8. Local changes to the circulation will affect precipitation over Australia and New Zealand and so understanding and constraining the magnitude of these changes is of practical interest.

Linked to the mean circulation changes, I examined changes to atmospheric blocking frequency under the RCP8.5 scenario. In general, blocking frequency is reduced in both summer and winter (figure 7.3b,d) in line with Parsons et al. (2016). It is worth noting that the most significant changes to summer blocking occur primarily at high latitudes, well away from regions, such as Australia, which are affected by heat waves (Figure 7.3d). However, this does not imply that the frequency and severity of heat waves will not change. First, it is likely that the driving force behind the increased occurrence of heat waves (Perkins-Kirkpatrick et al., 2016) is thermodynamic rather than dynamic in origin. Second, the Masato et al. (2013b) index only captures large-scale events, and it may be that smaller wave breaking events are important for

heat waves. For example, heat waves over south-east Australia are often associated with wave-breaking in which a large anticyclonic air mass is encircled by a relatively thin filament of cyclonic air (Parker et al., 2014).

The most robust decreases in the winter season occur to the south of Australia in agreement with Matsueda et al. (2010) and Grose et al. (2017). A closer examination of individual models revealed that there is, however, a wide spread in the blocking frequency changes between different models (figure 7.4), even if they all agree on the sign of that change. Examining this further, I showed that the change in blocking frequency is linked to the blocking frequency bias in the Historical simulations. The inability of many models to successfully capture the observed blocking climatology does reduce the confidence I may have in their projected changes. However, Grose et al. (2017) note that the relationship between the bias and future projections of blocking in the Australia-New Zealand sector creates an emergent constraint on future changes.

Finally, in this chapter I have only examined a single high emissions scenario, RCP8.5, a scenario which thankfully is unlikely to be fully realised (Ho et al., 2019). This scenario was chosen for comparison with previous studies and to provide a large a signal-to-noise ratio. There is uncertainty as to the exact magnitude of future changes to atmospheric temperatures, and therefore circulation, partially because of uncertainty in future greenhouse gas emissions. The use of other scenarios such as RCP4.5 in CMIP5 and the shared socioeconomic pathways (SSPs, O'Neill et al., 2017) in CMIP6 would therefore provide additional information to better constrain future changes.

Chapter 8

Modelling the SH winter response to forcing

In this chapter I investigate the mechanisms behind the zonally asymmetric changes to the extratropical circulation in the SH winter noted in chapter 7. I find that the stationary wave response pattern is also found in atmosphere-only experiments with uniformly raised SSTs and is most likely linked to weakening of the Pacific Walker circulation. I perform a set of barotropic model experiments in which the Rossby wave source (RWS) change between Historical and RCP8.5 experiments, is used to force the model. I find that the stationary wave response can be successfully reproduced by forcing the model with RWS anomalies over the eastern Pacific, which are associated with a reduction in the strength of the descending branch of the Walker circulation.

8.1 Introduction

It is virtually certain that global precipitation will increase with climate change, however changes on a regional scale exhibit considerably more uncertainty (Collins et al., 2013). A key source of this uncertainty arises from a relative lack of understanding of atmospheric circulation changes, particularly on a regional scale (Shepherd, 2014; Zappa and Shepherd, 2017). Therefore, developing a mechanistic understanding of regional circulation changes allows the drivers of uncertainty in local precipitation changes to be better identified and constrained.

In chapter 4, I showed that stationary waves driven by zonal SST asymmetries in the tropics, contribute strongly to the structure of the SH extratropical circulation. Then, in chapter 7, I demonstrated that projected circulation changes in CMIP5 models in the SH winter have a strong zonally asymmetric component (figures 7.1, 7.2). This stationary wave response appears to be robust across many models and features a region of enhanced zonal flow to the south of Australia and a strengthened subtropical jet over the eastern Pacific.

Climate change may affect stationary waves either through modification of the sources of Rossby waves in the tropics and subtropics, or via changing the background flow in mid-latitudes. The Rossby wave source (RWS), is a useful diagnostic of the forcing of stationary Rossby waves. Following Sardeshmukh and Hoskins (1988), the RWS, S, is given by

$$S = -\nabla \cdot (v_\chi \zeta) = -v_\chi \cdot \nabla \zeta - \zeta D, \tag{8.1}$$

where v_χ is the divergent wind, ζ is the absolute vorticity and D is the divergence. The terms on the right hand-side are often referred to as absolute vorticity advection and vortex squashing respectively. Alterations to the strength of tropical circulations such as the Hadley cell or Pacific Walker circulation would change the magnitude of the upper level divergence field and thus affect the RWS via the vortex squashing term. I will show that anthropogenically-forced tropical and subtropical circulation changes also affect the absolute vorticity advection term, but these changes are smaller than the changes to the vortex squashing term.

Model future projections suggest a weakening of both the Walker (Power and Kociuba, 2011a,b) and Hadley circulations (Lu et al., 2007; Vecchi and Soden, 2007), with these results appearing to be robust across models. These changes have been explained on the basis of simple arguments concerning the relative differences between projected changes to global precipitation and changes to atmospheric moisture content

(Held and Soden, 2006; Vecchi and Soden, 2007). However, Plesca et al. (2018) found that different Walker circulation indices produce trends of different signs in the same models and that internal variability in the Walker circulation is substantial even over a 70 year period. Kociuba and Power (2015) also found that CMIP5 models failed to capture the recent strengthening trend, dampening confidence in future projections. Concomitantly, observations of recent tropical SST trends have shown greater warming in the western Pacific, in contrast to climate model projections which show a greater warming in the eastern Pacific. The SST warming and Walker circulation trends are likely to be linked and Seager et al. (2019) attributed the former to the pervasive equatorial cold tongue bias (e.g. Xie et al., 2007; Li and Xie, 2014) in CMIP5.

Stationary waves can also be altered by changes to the background flow. Under the WKB approximation of a slowly varying background flow, Hoskins and Ambrizzi (1993) showed that the stationary wave number, K_S (equation 7.1), controls the patterns of stationary waves in the extra-tropics. Slight changes to the background flow as a result of changes to the eddy-driven jet, can have a significant impact on K_S and thus alter stationary wave patterns. For example, Simpson et al. (2016) examined changes to circulation over North America seen in CMIP5 models using a stationary wave model. They prescribed the projected background state with historical forcing and showed that the altered background state was sufficient to explain the changes in stationary waves.

There is some disagreement over whether changes to the RWS (e.g. Stephenson and Held, 1993; Selten et al., 2004; Haarsma and Selten, 2012) or background flow (e.g. Joseph et al., 2004; Brandefelt and Körnich, 2008; Simpson et al., 2016) are more important in explaining NH changes. On the other hand, stationary waves and the transient eddy momentum fluxes which shape mid-latitude jets do not act independently. Consequently, the effects of changing both the RWS and background flow are

not always separable and a more complete understanding of stationary wave changes will require a theory of the mutual interaction between transient and stationary waves (Wills et al., 2019).

With regard to the SH, Freitas et al. (2017) examined the influence of different SST changes on the Hadley cell and stationary waves in a warming climate. They performed a fully coupled simulation with quadrupled CO_2 as well as a set of experiments with different patterns of raised SSTs and found similar stationary wave patterns in many of the simulations. They found that SST forcing within the deep tropics (5S-5N) provided the largest contribution towards the zonally asymmetric extratropical circulation change and attributed these changes to weakening of upper level divergence associated with the winter Hadley cell.

In this chapter, I investigate the mechanisms behind this stationary wave response. In particular, I aim to test whether the SH stationary wave response to climate change in CMIP5 can be modelled by only considering changes in the RWS. To do this I force the barotropic vorticity equation with the changes in the RWS between RCP8.5 and the Historical runs. This follows the method of Haarsma and Selten (2012) who studied stationary wave changes in the NH. The model data used and method are described in section 8.2, then the results of regression analysis and barotropic modelling experiments are presented in section 8.3. Finally, a discussion of the results and conclusions are given in section 8.4.

8.2 Data and methods

8.2.1 Model data

In this chapter I utilize monthly mean data from the Historical and RCP8.5 experiments in the same set of CMIP5 models as in the previous chapters, using the same periods. In particular, the variables I use are surface temperature, air temperature, specific humidity, sea level pressure (SLP) as well as zonal, meridional and vertical

wind velocity. In addition, I use data from 10 models which performed both AMIP and AMIP 4K simulations within the CMIP framework. These are atmosphere-only experiments forced with observed SSTs and sea-ice from 1979 to 2008 (Taylor et al., 2012). In AMIP 4K the SSTs have been uniformly raised by 4K. The full list of models used from both the fully coupled and atmosphere-only runs can be found in appendix A.

8.2.2 Indices

I calculate an index for the Walker circulation as the difference in annual-mean SLP between eastern and western Pacific boxes, following Vecchi et al. (2006). Both boxes are defined by the latitudes 5S-5N and the longitudes 80E-160E and 80W-160W for the western and eastern boxes respectively. I define the winter Hadley cell edge similarly to Kang and Lu (2012) and Vallis et al. (2015) as the latitude at which the 500hPa meridional overturning stream function falls to 10% of its absolute maximum value between 40S and the equator. Its strength is then defined as the maximum 500hPa meridional stream function value within these bounds. The meridional overturning stream function, $\psi(\phi, p)$, is defined following Oort and Yienger (1996) as

$$\psi(\phi, p) = \frac{2\pi a cos\phi}{g} \int_{p}^{p_s} [\overline{v}(p', \phi)] dp', \tag{8.2}$$

in which a is the radius of the Earth, g is the acceleration due to gravity, p_s is the surface pressure and $\overline{v}$ is the zonal mean meridional wind.

8.2.3 Barotropic vorticity equation

Following Hoskins and Ambrizzi (1993), the barotropic vorticity equation, may be written as

$$\left(\frac{\partial}{\partial t} + v_\psi \cdot \nabla \right) \zeta = F - \lambda\zeta - \mu\nabla^4\zeta, \tag{8.3}$$

where v_ψ is the rotational component of the wind and F is a forcing term. The second term on the right hand side is a linear damping term with a timescale of 10 days, while the third term represents the loss of vorticity variance at small scales with $\mu = 2.4 \times 10^{16} m^4 s^{-1}$. The variable, F, is separated into two components,

$$F = F_0 + \Delta S, \tag{8.4}$$

in which F_0 is a forcing designed to exactly match the background state of a given CMIP5 model, while ΔS represents the change in the RWS between the RCP8.5 and Historical simulations. ΔS is therefore given by

$$\Delta S = S_{RCP8.5} - S_{Hist.} = -v'_\chi \cdot \nabla\overline{\zeta} - \overline{v_\chi} \cdot \nabla\zeta' - \overline{\zeta} D' - \zeta'\overline{D} \tag{8.5}$$

with primes representing differences between RCP8.5 and the Historical experiments, and overbars representing the Historical climatology. In practice, terms involving ζ' are small and hence these terms have been omitted from the barotropic model calculations. In my experiments, I find that to first order, changes to ΔS can be approximated by $-\overline{\zeta} D'$, however I include the absolute vorticity advection term as it is often of considerable magnitude in the vicinity of a strong subtropical jet (Sardeshmukh and Hoskins, 1988).

The background state is chosen to be the vorticity field at 400hPa given that this level is closest to the equivalent barotropic level (Held et al., 1985; Held and Kang, 1987), though similar results are obtained if the 500hPa level is used and to a lesser extent for the 300hPa level. The climatological RWS peaks at around 200hPa and is shown as a multi-model mean in figure 8.1a. However, Haarsma and Selten (2012) noted that the Walker circulation not only weakens in future projections, but also becomes shifted in the vertical direction. This could be problematic for choosing a particular level at which to calculate RWS differences. Figure 8.1a shows that there are large RWS features in the southern subtropics of each of the three Ocean basins,

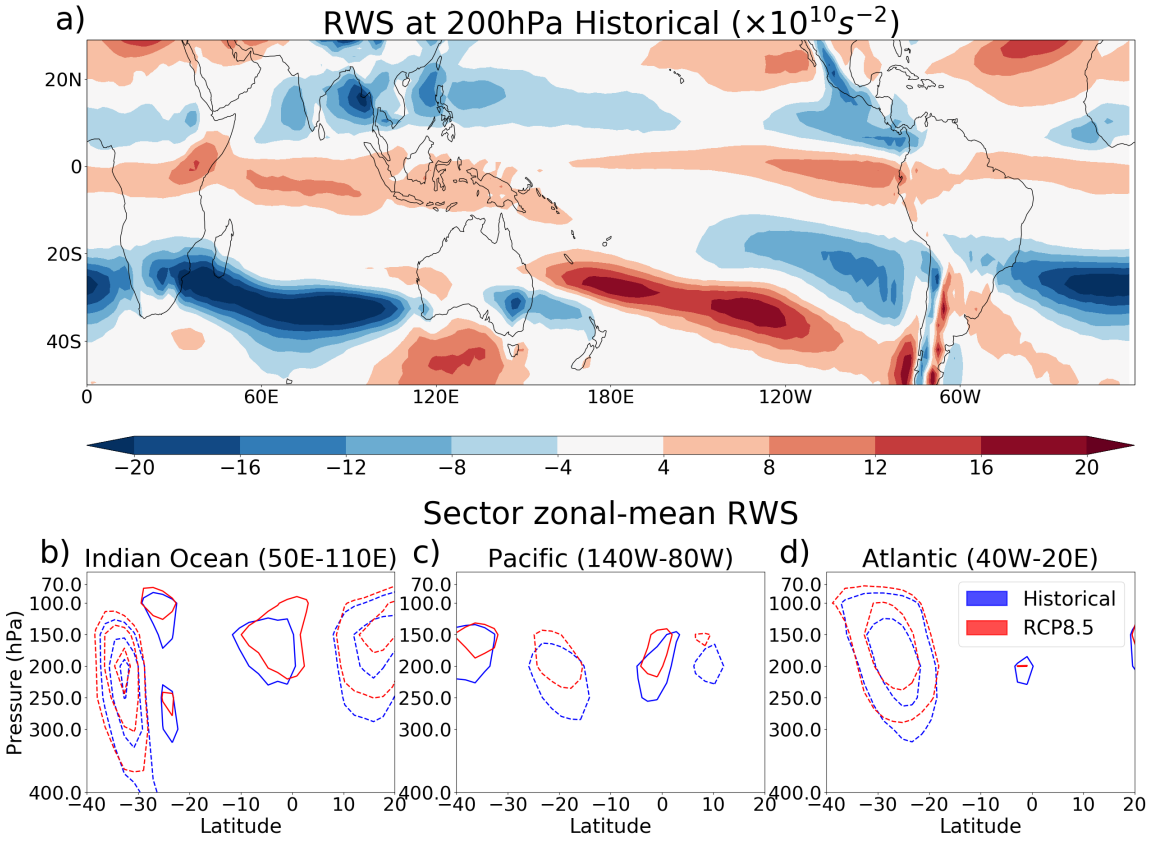


Figure 8.1: In a) the multi-model mean RWS calculated at 200hPa using Historical CMIP5 data is plotted, while b-d) show the zonal-mean RWS within three regions as a function of latitude and pressure level. In b-d), blue contours show the Historical climatology, while red contours show the RCP8.5 climatology with the contour interval $5 \times 10^{-11} s^{-2}$ in both cases and the zero contour omitted.

so I plot the change in the vertical structure in each of these basins. It is apparent that the sector zonal-mean RWS is indeed shifted upwards by up to 50hPa in RCP8.5 runs in comparison to the Historical experiment (figure 8.1b-d). For this reason, I force the model with the differences in the vertical average RWS for each CMIP5 model, calculated between 70hPa and 400hPa. The RWS is also restricted to the latitudes 35S to 15N to avoid directly putting in the mid-latitude response I am attempting to re-create. I integrate the model for 100 days, finding that the solution becomes steady after about 15 days. Finally, the response is averaged from day 25 to day 100.

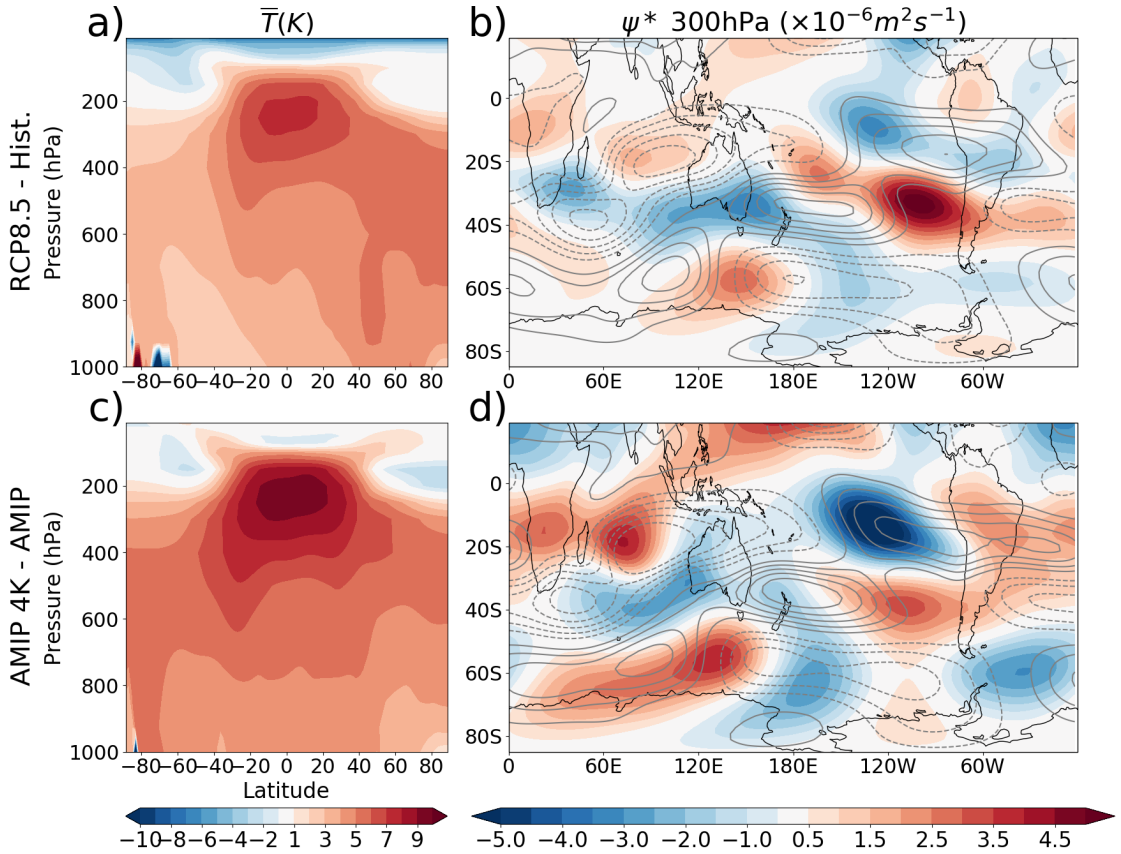


Figure 8.2: Wintertime zonal mean temperature and stationary wave changes: a) time-mean zonal mean temperature difference RCP8.5 (2070-2099) - Historical (1979-2005), b) the same, but for stationary eddy stream function difference (colours) with Historical stationary eddy stream function climatology (contours), c) time-mean zonal mean temperature difference AMIP 4K - AMIP, d) is the same as c) but for stationary eddy stream function difference (colours) and AMIP stationary eddy stream function climatology (contours). Each climatology in b) and d) has contour interval $2 \times 10^6 m^2 s^{-1}$.

8.3 Results

SST warming patterns represent a significant source of uncertainty in future circulation and precipitation changes (Ma and Xie, 2013; Xie, 2020). It is therefore useful to examine whether the SST warming patterns in the CMIP5 models play an important role in the stationary wave response seen in the previous chapter. I investigate this by comparing the stationary wave response in the RCP8.5 run (RCP8.5 - Historical) with that in the AMIP 4K experiment (AMIP 4K - AMIP), in which the SST warm-

ing is uniform. Uniformly raising the SSTs results in a similar pattern of zonal-mean temperature change throughout the atmosphere as in RCP8.5 (figure 8.2a,c). For instance, tropical upper-tropospheric warming is a major feature of both as a result of increased water vapour concentrations reducing the saturated lapse rate (Manabe and Wetherald, 1980; Vallis et al., 2015). It can also be seen that AMIP 4K is a larger forcing than RCP8.5 as the associated atmospheric temperature changes are larger (figure 8.2a,c).

Figure 8.2 also shows the stationary eddy stream function response to climate change in RCP8.5 and for AMIP 4K. Whilst there are some differences in the details of the patterns, the circulation responses are remarkably similar between the two experiments. The largest differences appear to be in the eastern tropical Pacific, where an anticyclonic anomaly is more prominent in AMIP 4K - AMIP, while the amplitude of the pattern is also larger for AMIP 4K - AMIP because of the larger forcing imposed. Seeing as the stationary wave response patterns in these different experiments are similar, it appears that to first order the response is not generated by changes in SST patterns. However, it is not unlikely that different SST warming patterns will act to accentuate or diminish various aspects of the pattern. Ma et al. (2012) found that both Hadley and Walker circulations are weakened in uniformly increased SST runs. However, they also showed that unlike the Walker circulation change, the Hadley cell change was also strongly influenced by the structure of SST changes when patterned SST warming was imposed. For this reason, the similarity of the difference patterns in AMIP 4K - AMIP and RCP8.5 - Historical suggests that the Walker circulation may be more important for the stationary wave changes.

In order to investigate the role of various tropical and subtropical circulation changes in shaping the extratropical SH stationary wave pattern, I show changes between RCP8.5 and Historical climatologies in 200hPa velocity potential, 500hpa omega (vertical velocity) and surface temperatures in figure 8.3. I am particularly

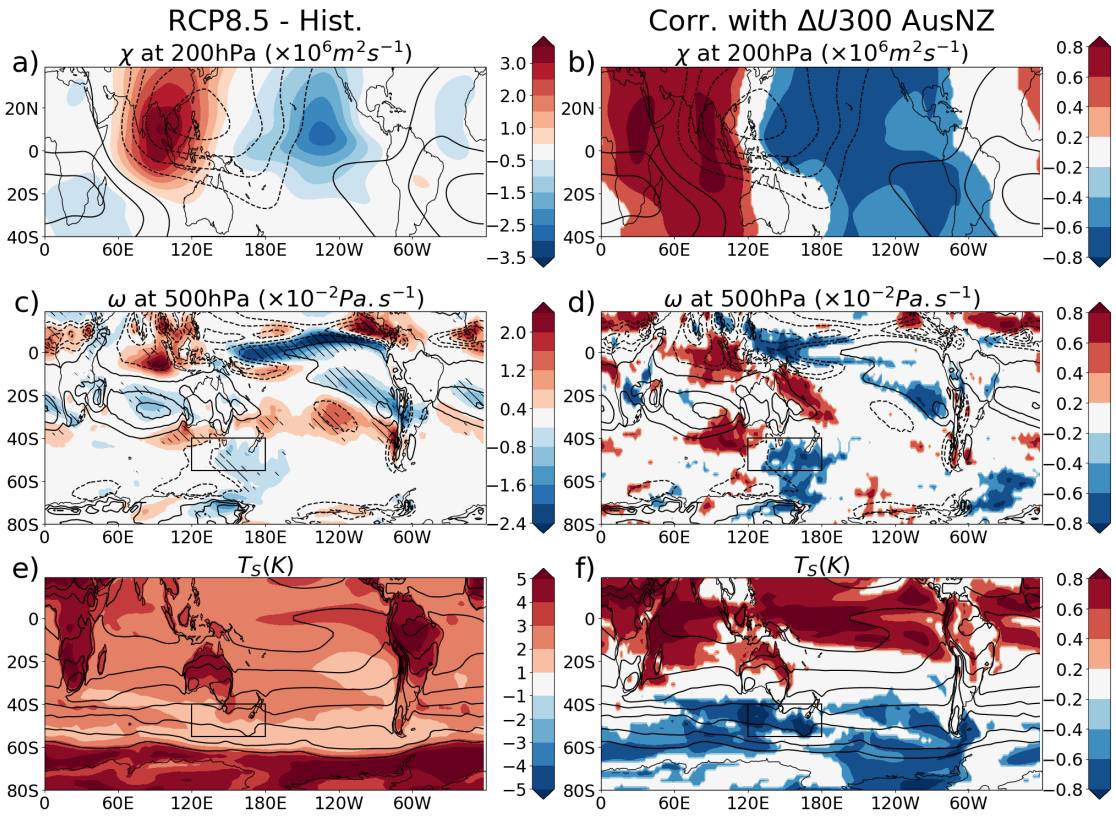


Figure 8.3: Multi-model mean differences in a) 200hPa velocity potential, c) 500hPa omega and e) surface temperature between RCP8.5 (2070-2099) and the Historical simulations (1979-2005) in JJA. Differences are shown by colours, while the Historical climatology is shown by contours. In c), hatching shows regions in which at least 80% of models agree on the sign of the difference. Also plotted in b), d) and f) are correlations between the change in 300hPa zonal wind in the AusNZ region (shown by the box in c-f) and the change in the variable at each grid-point. Correlations are shown by colours in b), d) and f), with the Historical climatology shown by contours. The variables regressed onto the AusNZ wind change are scaled by the global-mean warming in each model before correlations are calculated following Zappa and Shepherd (2017). Only correlations with p-values below 0.05 are plotted.

interested in the zonal wind change to the south of Australia as this is the location where the split jet bifurcates and was shown to be the region containing the largest wintertime blocking changes in chapter 7 (figure 7.3). It is worth noting that the zonal wind response in this region is similar in AMIP 4K - AMIP and RCP8.5 - Historical (figure 8.2b,d). Hence, I also show correlations between the AusNZ zonal wind index from the previous chapter (section 7.5) and each of the three variables, scaled by

the global-mean surface temperature change, following Zappa and Shepherd (2017). Velocity potential and omega both show a general reduction in ascending air over the maritime continent, as well as a reduction in descent over the eastern Pacific (figures 8.3a,c). Indeed, the magnitude of vertical velocity is reduced at almost all locations in the tropics and subtropics, with the exception of an equatorial band from 160E to around 100W, which is likely to be related to the narrowing of the Intertropical Convergence Zone (Byrne et al., 2018). These findings are similar to those of Vecchi and Soden (2007) concerning 500hPa vertical velocity changes in CMIP3. These changes are also mostly consistent in sign across the models (hatching in figure 8.3c), in spite of the relative noise associated with the vertical velocity field. In particular, the enhanced ascent near the equator and the reduction in descent at 20S, to the west of South America, are large regions of model consensus.

The correlation patterns of zonal wind changes south of Australia with velocity potential and vertical velocity changes are similar to the multi-model mean changes (figure 8.3b,d), suggesting a possible link between tropical circulation weakening and changes in zonal wind to the south of Australia. The fields have been scaled by global warming, and hence, climate sensitivity does not explain these correlations. Figure 8.3e also shows the multi-model mean pattern of surface temperature change, which is characterised by greater warming over land, relatively less warming over the Southern Ocean and an El Niño-like warming in the equatorial Pacific. Figure 8.3f shows that larger zonal wind increases to the south of Australia are characterised by enhanced tropical SST warming at all longitudes and a slower warming of the Southern Ocean. This is consistent with an enhanced equator-to-pole temperature gradient and hence stronger winds, though it is worth noting that regression of the AusNZ index directly onto the wind field produces a largely zonally asymmetric pattern rather than a symmetric jet strengthening (not shown).

To connect these results more directly to the Walker and Hadley circulations, I

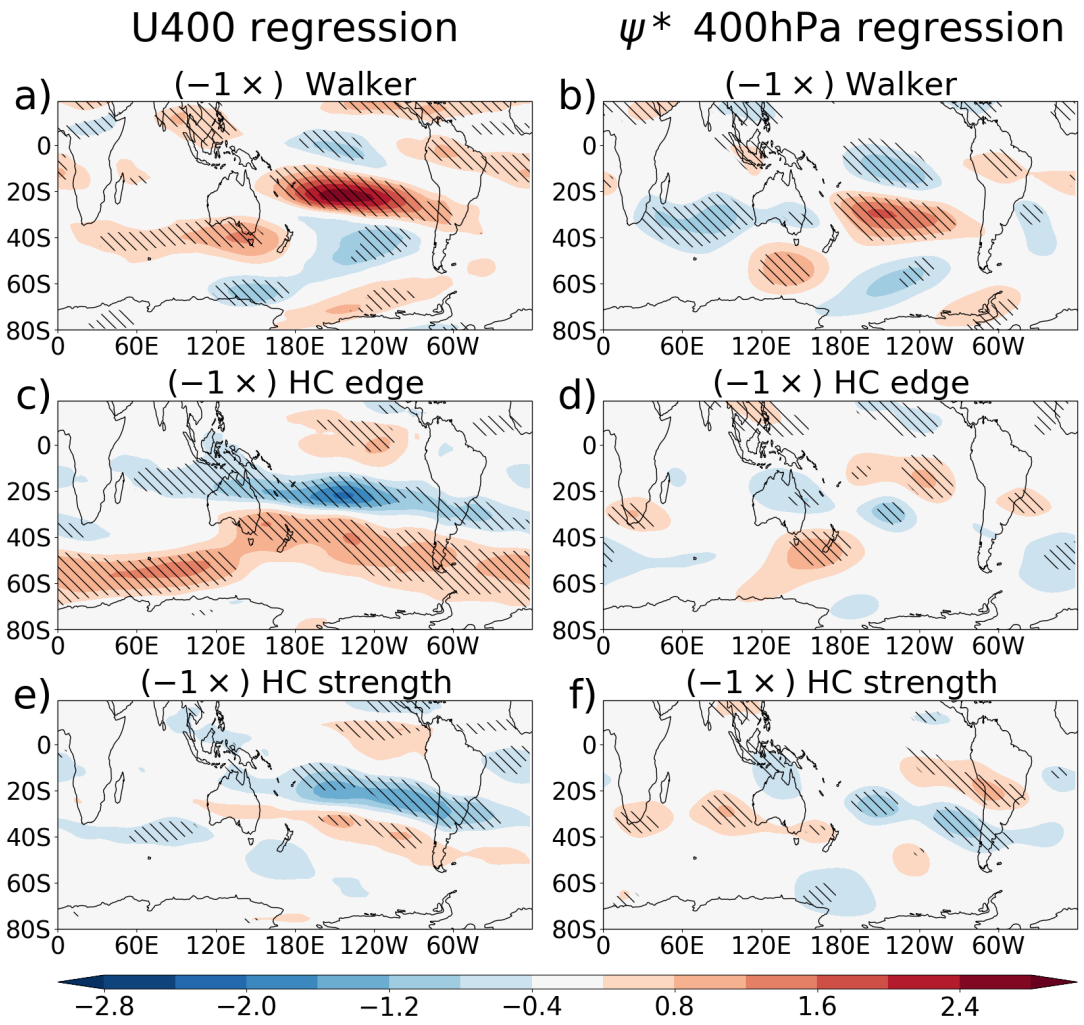


Figure 8.4: 400hPa zonal wind and stationary eddy stream function changes in each model between RCP8.5 and Historical runs regressed onto the change in the Walker circulation and Hadley cell indices. The zonal wind changes and stream function fields have been divided by the global-mean warming between RCP8.5 and Historical runs for each model. The indices have also been standardised and multiplied by a factor of -1 to reflect the fact that each of these indices is decreasing and thus to aid comparison with other figures. That is, the SH Hadley cell edge is moving southward and therefore decreasing in latitude. Therefore, multiplying by -1 means a more positive Hadley cell edge index corresponds to a more poleward shifted Hadley cell edge. The units for each plot are therefore a,c,e) $ms^{-1}K^{-1}$ per standard deviation of index change and b,d,f) $m^2s^{-1}K^{-1}$ per standard deviation of index change. Hatching shows where p-values are below 0.05.

regress the zonal wind and stationary eddy stream function fields onto Walker and Hadley circulation indices. I do this for the fields at 400hPa because this is the

level at which the barotropic model runs are performed, however similar results are obtained using fields at 300hPa (not shown). It can be seen from figure 8.4 that the regression pattern associated with changes to the Walker circulation (figure 8.4a,b) most closely match the stationary wave pattern seen in figure 8.2b and the zonal wind changes in figure 7.1c. This includes an enhancement of the subtropical jet over the eastern Pacific flanked by reductions in wind strength to the north and south, and strengthening of the zonal wind to the south of Australia (figure 8.4a). On the other hand, the Walker circulation regression pattern only captures the stationary wave and not the zonally symmetric component of wind strengthening in mid-latitudes (figure 7.1c).

Plesca et al. (2018) noted discrepancies between the signs of trends using different Walker cell indices. The vertical velocity-based Walker circulation index of Wang (2002) is similar to Vecchi et al. (2006) in that it is defined by the difference between west and east Pacific boxes, but these are further west than in the Vecchi et al. (2006) index, with the boxes bounded by longitudes 120E-160E and 120E-160W for the west and east Pacific respectively. Regression plots using the Wang (2002) index bear little resemblance to the plots using the SLP index of Vecchi et al. (2006, not shown). Using vertical velocity but with the same boxes as the SLP index, namely 80E-160E and 80W-160W, produces similar results to the SLP index, suggesting that it is the choice of region rather than the variable which is most sensitive, with the region over the eastern Pacific being most important.

Regressions of the Hadley cell indices do not correspond to the stationary wave pattern in figure 8.2, however the Hadley cell edge gives a similar pattern of jet strengthening to that found in figure 7.1c. This is consistent with the work of Ceppi and Hartmann (2013) who found a correlation between the Hadley cell edge and eddy-driven jet speed in the SH, with the eddy-driven jet affecting the Hadley cell edge via modulation of subtropical critical latitudes. Hence, in this case it is more likely to be

the mid-latitude jet affecting the circulation in the subtropics, than vice-versa.

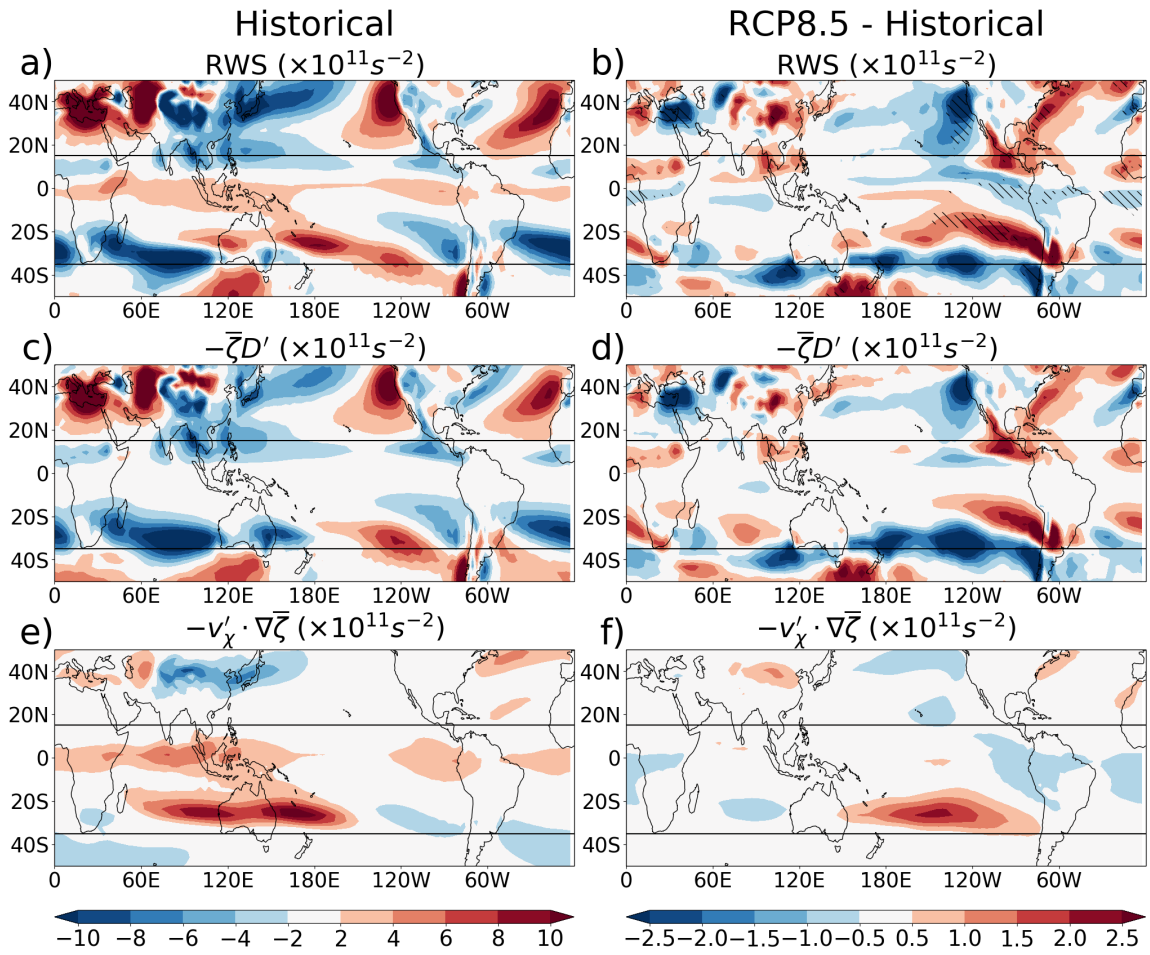


Figure 8.5: Multi-model mean RWS in a) the Historical experiment and b) RCP8.5 - Historical. The RWS is calculated as a vertical average between 70hPa and 400hPa (see text for further details). In b) hatching indicates where at least 80% of models agree on the sign of the difference. c) and e) are the same as a) but only showing changes to the vortex squashing and advection terms respectively. Similarly, d) and f) are the same as b) but for differences in the vortex squashing and advection terms respectively. Horizontal lines indicate the region in which the RWS is used to force the barotropic model.

Having investigated correlations between tropical and extratropical circulation features from CMIP5 model data, I now test whether it is possible to reproduce the extratropical circulation features using a simple barotropic model. The multi-model mean RWS change (RCP8.5 - Historical) is shown in figure 8.5b. Like with vertical velocity, RWS changes are largely of the opposite sign to that of the Historical RWS

climatology (figure 8.5a), that is, a reduction in RWS magnitude. The largest and most consistent changes across models (shown by hatching) are found in the south-east Pacific. Specifically, there is a tripole pattern of negative RWS anomalies at around 35S, positive from 30S to around 10S and negative closer along the equator. However, it should be noted that the zonal flow is weak or easterly from around 10S to 10N at all longitudes in austral winter (e.g. figure 7.1a) and as a consequence, Rossby wave propagation is unfavourable from these latitudes (Ambrizzi et al., 1995). Examining the change in vortex squashing and absolute vorticity advection terms, the former clearly dominates over the latter in the south-east Pacific. The changes in vortex squashing at 20S and 40S are likely associated with regions of weakening descent and ascent, respectively, as can be seen in figure 8.3c.

I now force the model with the RWS changes in figure 8.5b between 35S and 15N, and the results are shown in figure 8.6b, with the actual stationary wave difference shown in figure 8.6a for comparison. Many of the features seen in the full CMIP5 models are captured by the model including a cyclonic anomaly centred on (120W, 35S) with an anticyclonic anomaly on the equatorward side, as well as a cyclonic anomaly to the south of Australia and anticyclonic anomaly to its south-east. However, the pattern over the Indian Ocean is, in general, too horizontally tilted in comparison with CMIP5 models, while the cyclonic anomaly south of Australia is centred too far north and the anticyclonic anomaly over Australia is not captured. Intriguingly, forcing the model with only the RWS in the South Pacific reproduces the full stationary wave pattern even more successfully (figure 8.6c) as the Indian Ocean anomalies are more zonally orientated and there is an anticyclonic feature over Australia. The most robust changes in RWS occur over the South Pacific (figure 8.5b) and it is possible that including RWS at other longitudes merely adds noise to the solution. In addition, Rossby waves in the polar waveguide tend to refract equatorward eastwards of South America (e.g. figure 17 of Ambrizzi et al., 1995; Mo et al.,

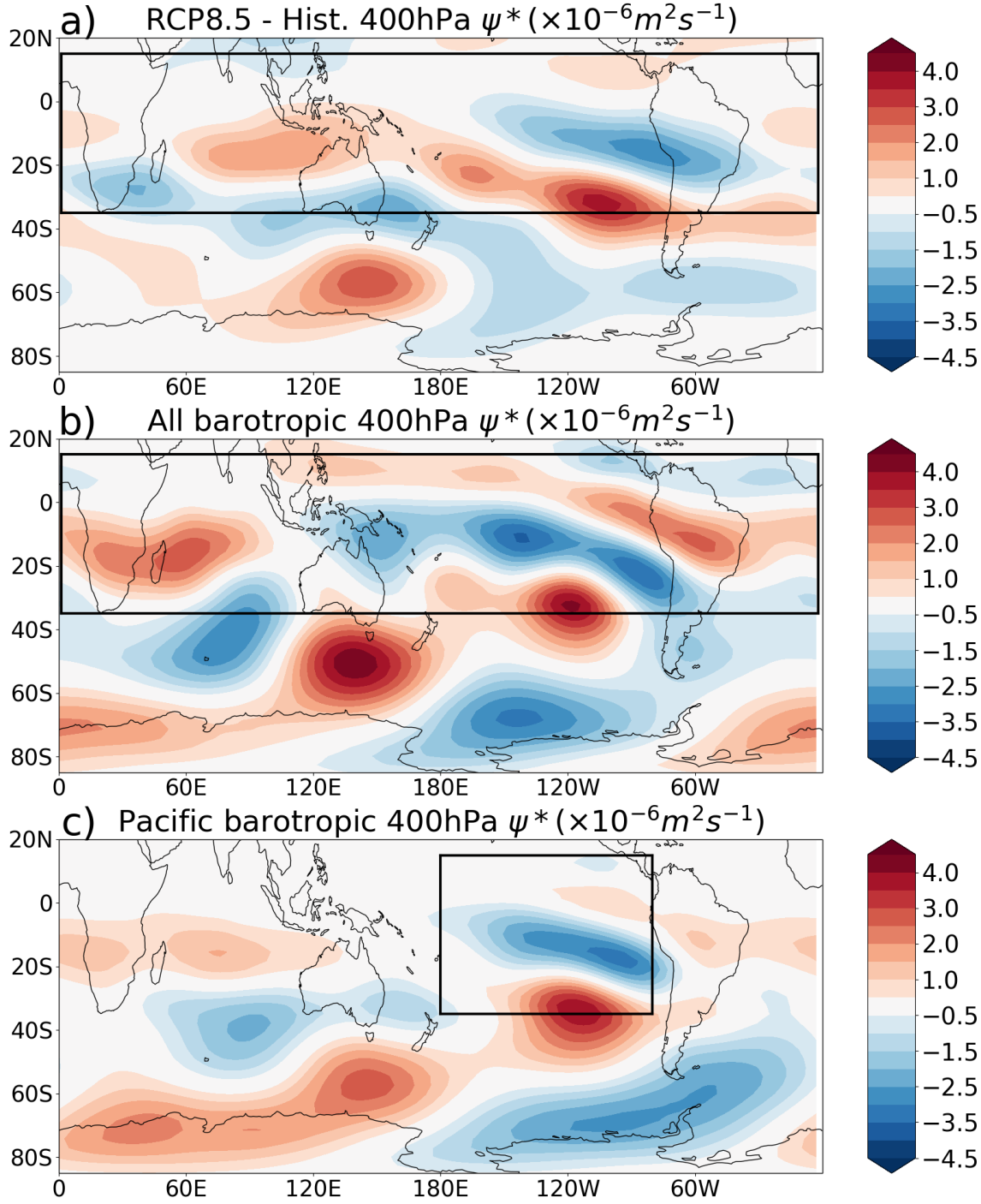


Figure 8.6: The stationary wave response to forcing: a) multi-model mean stationary eddy stream function, $\psi*$, at 400hPa for RCP8.5 - Historical, b) $\psi*$ response in the barotropic model forced with the anomalous RWS between 35S and 15N, c) $\psi*$ response in the model forced with the anomalous RWS over the South Pacific region (shown by the box).

1998; Müller and Ambrizzi, 2007). Hence it may be that RWS changes over the Atlantic or Indian Ocean basins, are responses to wave activity refracting equatorward, rather than sources of new wave activity. The panels in figure 8.6 are each showing multi-model means, but examining barotropic responses for individual models tells a fairly similar story (not shown). That is, in general the barotropic model captures the key extratropical features seen in the RCP8.5 - Historical pattern, when forced with RWS changes in the tropics and subtropics. However, the fine details of the response for individual models are often not captured, which is not unexpected given the crudeness of the barotropic modelling technique.

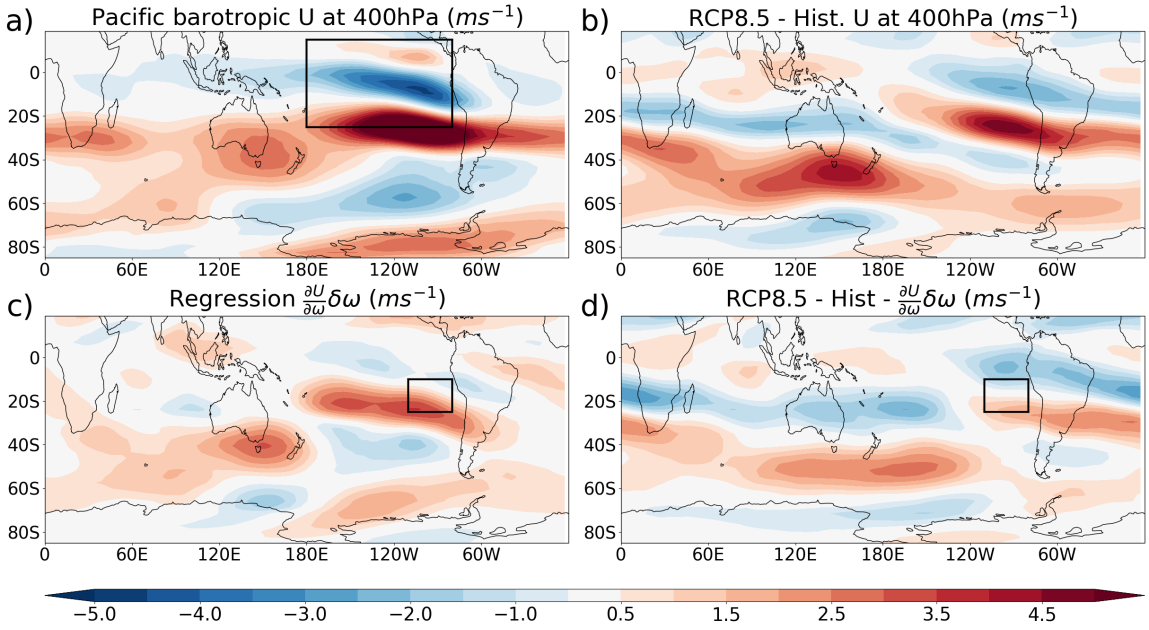


Figure 8.7: Zonal wind responses: a) Multi-model mean zonal wind response in the barotropic model , b) multi-model mean 400hPa zonal wind change, RCP8.5 - Historical, c) regression of the 400hPa zonal wind change in CMIP5 models onto the standardised 500hPa vertical velocity in the eastern Pacific (see text for details), d) as in b) but with the vertical velocity changes in the eastern Pacific regressed out.

In spite of the simplicity of the barotropic model approach, it is clear that the model can capture the stationary wave response to climate change with relative success. Crucially, it establishes the connection between tropical / subtropical dynamics and mid-latitudes changes, suggesting that the former is more important than

background wind changes for reproducing the stationary wave response. It should be noted however, that the barotropic modelling method does not reproduce the changes to the zonal wind field, as this has a substantial zonally symmetric component. The barotropic model zonal wind change is shown in figure 8.7a with the full CMIP5 zonal wind change in figure 8.7b. The barotropic model successfully reproduces a strengthening of the jets over southern Africa, to the south of Australia and over the eastern Pacific, but features in mid-latitudes are not well represented (figure 8.7b). This is unsurprising because although the wintertime jet structure is substantially zonally asymmetric, Simpson et al. (2014) showed that changes in transient eddy forcing in the winter season under climate change are largely zonally symmetric. Consequently, it appears that the SH extratropical zonal wind response to climate change, is forced by both zonally symmetric and stationary wave components.

In order to isolate the stationary wave component of the zonal wind, I regress the change in the zonal wind field of different models onto an index of 500hPa vertical velocity over the eastern Pacific, shown in figure 8.7c. The region is defined by the longitudes 80W-110W and latitudes 10S-25S, as shown by the black box (figure 8.7c,d), and is associated with reduced descent (figure 8.3c,d) and positive RWS anomaly (figure 8.5b) over the eastern Pacific. The index has been standardised and the regression coefficients scaled by the mean change in the index between Historical and RCP8.5 experiments. This pattern bears a close correspondence to the barotropic model response in figure 8.7a, with the largest discrepancies over the high-latitude South Pacific. The regression pattern in figure 8.7c is also similar to the Walker circulation regression pattern in figure 8.4a. Removing the vertical velocity regression pattern from the full CMIP5 response produces a slightly more zonally symmetric pattern (figure 8.7d), though the jet change is larger over the western and central Pacific than at other longitudes. The lack of complete zonal symmetry in 8.7d) suggests that the zonally symmetric and stationary wave components do not combine linearly

to give the total zonal wind pattern, which is to be expected given the stationary wave dependence on the background flow.

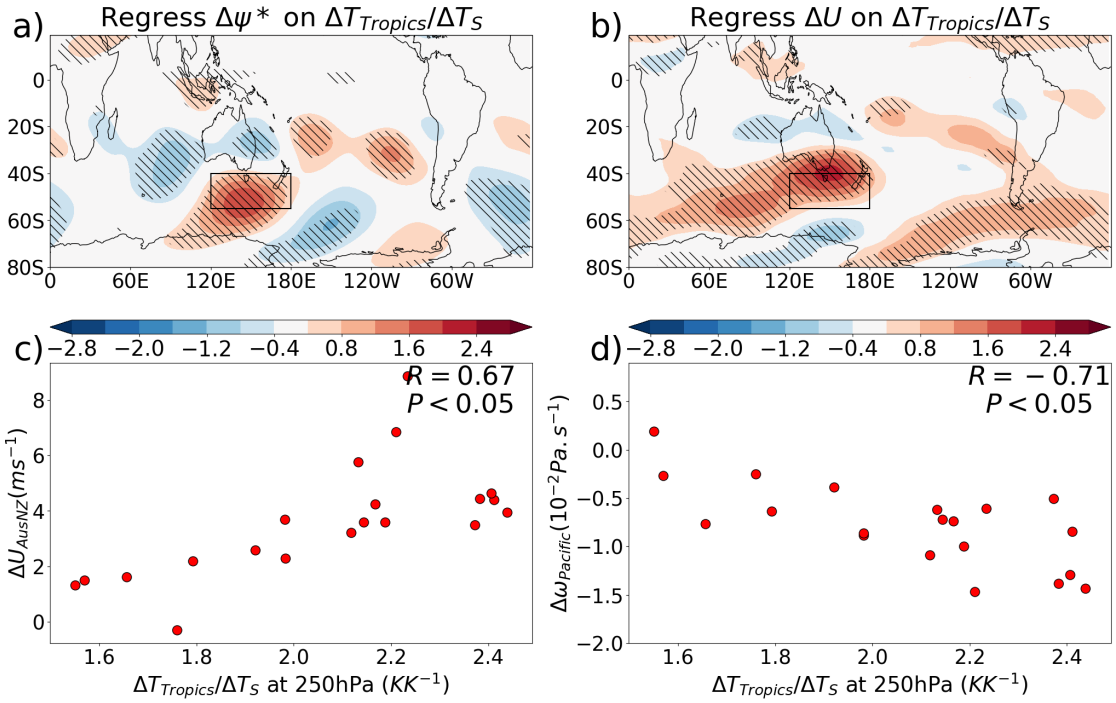


Figure 8.8: Relationship between tropical upper tropospheric warming and extratropical circulation changes: a) Regression of stationary eddy stream function changes at 400hPa onto the mean tropical upper-tropospheric warming (see text for details, units: $\times 10^6 m^2 s^{-1}$ per standard deviation $\Delta T_{Tropics}/\Delta T_S$) with hatching showing regions in which p-values are less than 0.05 b) as in a), but for 400hPa zonal wind (units: ms^{-1} per standard deviation $\Delta T_{Tropics}/\Delta T_S$) , c) scatter plot showing change in AusNZ zonal wind change against tropical upper-tropospheric warming d) scatter plot showing change in the vertical velocity index (from figure 8.7c,d) against tropical upper-tropospheric warming. In each case tropical upper-tropospheric warming has been scaled by the mean global-warming at the surface.

The recent study of Mindlin et al. (2020) found that the magnitude of tropical upper-tropospheric warming between Historical and RCP8.5 simulations is strongly correlated with zonal wind changes to the south of Australia. This result is helpful in understanding the drivers of uncertainty in future circulation change, although the mechanism for this relationship is not yet clear. Regressions of stationary eddy stream function and zonal wind onto their index of tropical tropospheric warming (figure 8.8a,b) show a distinctly zonally asymmetric pattern, similar to those seen in

figures 8.7c and 8.4a,b. This is suggestive that the tropical upper tropospheric warming connection with zonal wind changes is primarily associated with a stationary wave response, rather than through an enhancement of the equator-to-pole temperature gradient. The tropical upper-tropospheric warming index is defined following Zappa and Shepherd (2017) and Mindlin et al. (2020) as the change in zonal-mean temperature at 250hPa, averaged 15S-15N and scaled by the global-mean surface temperature change between the Historical and RCP8.5 experiments. Furthermore, this index is well correlated with the vertical velocity index (R = -0.71) used in figure 8.7c,d as can be seen in figure 8.8d. The link between reduced descent over the eastern Pacific and tropical upper-tropospheric warming can be explained using the arguments of Held and Soden (2006) and Vecchi and Soden (2007). Tropical upper-tropospheric warming is driven by reductions in the saturated lapse rate due to the increase in water vapour content of the atmosphere, following the Clausius-Clapeyron relationship. Meanwhile, Held and Soden (2006) and Vecchi and Soden (2007) argue that tropical circulation weakens because of the differential rate of change of precipitation (which is constrained by the radiative energy budget, Allen and Ingram, 2002) and water vapour, with climate change. Hence, both tropical upper tropospheric warming and the weakening of tropical vertical motions are correlated with increases in atmospheric water vapour concentration. Correlations of global-mean total column water vapour changes with tropical upper-tropospheric warming and the eastern Pacific vertical velocity change index (as in figure 8.8) appear to be consistent with this explanation, as shown in figure 8.9.

8.4 Discussion and conclusions

In this chapter, I have examined mechanisms concerning the SH stationary wave response to climate change. The stationary wave pattern is not generated by the pattern of SST warming, as similar patterns are obtained in AMIP runs with the

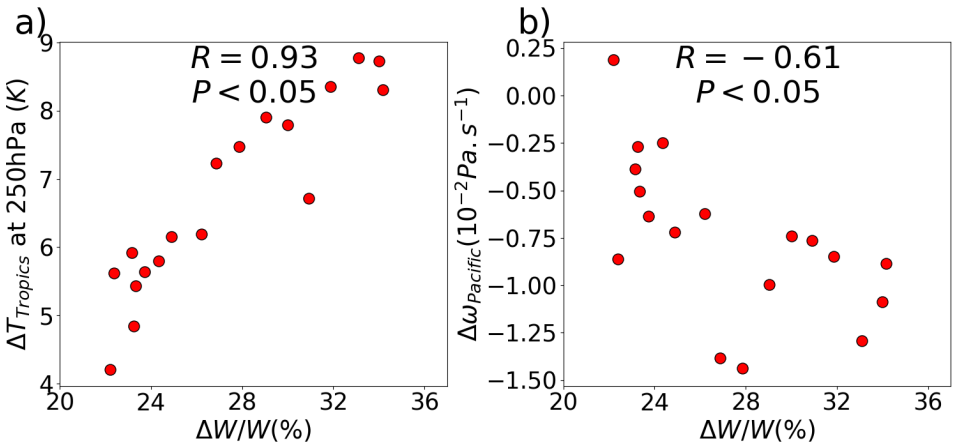


Figure 8.9: Scatter plots of a) tropical upper-tropospheric warming at 250hPa (not scaled by surface warming) and b) the eastern Pacific vertical velocity change index (as in figure 8.8) with the global-mean, total column water vapour content (W) % change. Correlation coefficients and p-values are also shown.

SSTs uniformly raised by 4K (figure 8.2). This suggests that the wintertime SH stationary wave pattern may be relatively robust, which is encouraging as CMIP5 models fail to capture the SST trends found in observations (Seager et al., 2019) and there is considerable uncertainty concerning future SST changes. However, I also noted that differing SST warming patterns may still affect some of the details of the stationary wave pattern. Under the RCP8.5 anthropogenic emissions scenario, there is a tendency for the Hadley and Pacific Walker circulations to weaken (Vecchi and Soden, 2007), with reductions in the speed of ascending or descending air (figure 8.3a-d). Consequently upper level divergence or covergence is weakened, changing the RWS in the tropics and subtropics. I have shown that the pattern of stationary eddy stream function change is more closely correlated with changes to the Walker circulation than to Hadley cell changes (figure 8.4). In particular it appears that changes to the descending branch of the Walker circulation over the eastern Pacific, have the largest effect on the extratropical circulation changes. This result is somewhat at odds with the interpretation of Freitas et al. (2017), who focused on the role of Hadley circulation changes in generating a stationary wave response to climate change. The stationary

wave response patterns found in their experiments with quadrupled CO_2 and tropical SST warming, are consistent with those presented in this study, but they did not demonstrate that it was changes to the Hadley cell which altered the RWS rather than the Walker circulation. On the basis of my regression analysis (figure 8.4), I argue that a better interpretation of their results is likely to involve changes to the Walker circulation.

I then performed barotropic model runs with the model forced each time by RWS changes in a given CMIP5 model between the Historical and RCP8.5 experiments. In each case, the winds from the Historical climatology were set as the basic state for the barotropic model, hence, I implicitly assumed that the changes to that basic state resulting from the RWS changes would be small. Forcing the barotropic model with RWS changes at all longitudes reproduced many of the salient features of the full RCP8.5 response, however there were significant discrepancies over the Indian Ocean and Australia (figure 8.6b). Forcing the model with only RWS changes over the south-east Pacific, where the RWS changes were strong and robust across models (figure 8.5b), more successfully reproduced the full pattern. The importance of RWS changes over the south-east Pacific is perhaps surprising given that the climatological Rossby wave which sets up the split jet is associated with the Indian Ocean (Inatsu and Hoskins, 2004, 2006), but the barotropic modelling result is consistent with regressions across the CMIP5 models (figures 8.3, 8.4). Changes in the Indian Ocean RWS are also small because of a cancellation between the vortex squashing and absolute vorticity advection terms (figure 8.5b,d,f).

This work provides a mechanistic understanding of zonally asymmetric SH extratropical circulation changes with climate change. Understanding circulation changes is important because these are a key source of uncertainty in future precipitation change (Shepherd, 2014). Consequently, the links I have found between Walker circulation changes and extratropical circulation patterns provide extra motivation for

understanding and better constraining tropical circulation changes.

The barotropic modelling in this chapter was remarkably successful, given its simplicity, however it would be of interest to test this mechanism in a more complex stationary wave model which includes baroclinic effects. I also ignored the effects of zonally symmetric changes to the background flow in RCP8.5 simulations and so the importance of this could be better quantified in future work.

Chapter 9

Conclusions

Large scale circulation features, such as jet streams, play an important role in shaping the weather and climate of different extratropical regions. This thesis has focused on the South Pacific split jet, a system consisting of subtropical and polar front branches, situated between western Australia and the central South Pacific. The split jet is primarily a feature of austral winter as zonal winds are largely zonally symmetric in the summer season, with spring and autumn somewhere between these two extremes. Its location means that it contributes to the climate of Australia and New Zealand, while the polar front jet affects both coastal Antarctica and southern South America. In this concluding chapter we revisit the original aims of this thesis and summarise the key findings of each chapter. Following this, we state a number of implications resulting from these findings and suggest some avenues for further work.

9.1 Key findings

We now return to the aims of this thesis outlined in section 1.3 and summarise the findings of each chapter. These were:

1. To establish the boundary conditions responsible for the wintertime South Pacific split jet structure.

2. To characterise and seek to explain the variability of the split jet from weekly to inter-annual timescales.

3. To characterise the ability of current climate models to represent the observed split jet structure.

4. To investigate the response of the split jet system to external forcing.

Chapter 4 addressed the first aim using an idealised, atmosphere-only model. We followed the approach of Inatsu and Hoskins (2004), which consisted of modifying various boundary conditions which may contribute to the split jet structure and examining the effect on atmospheric circulation. In agreement with the studies of Inatsu and Hoskins (2004) and Quintanar and Mechoso (1995), we found that zonally asymmetric SSTs in the tropics were a key factor in the formation of the split jet via generation of a wavenumber 1 pattern in the extratropics. However, the novel finding of this chapter was that Antarctic orography also has a first order impact on the split jet structure. Specifically, flattening Antarctica weakened the eddy-driven jet over the Indian Ocean and destroyed the polar front branch of the split jet downstream. Interestingly, responses to removing tropical SST asymmetry and lowering orography, did not add linearly when both changes were imposed together. Following this, we explored the mechanisms generating the orographic effects on circulation, concluding that the high latitude temperature increase on flattening Antarctica, was insufficient to explain the jet response. Rather, we advanced a mechanism entailing vortex squashing by Antarctic orography creating an effective potential vorticity gradient, allowing poleward eddy refraction and therefore, equatorward momentum fluxes. We provided evidence for these claims with a set of barotropic model runs with bottom orography varying as a function of latitude. On the other hand, modifying other boundary conditions including setting mid-latitude SSTs to the zonal mean and removing Antarctic sea-ice, had comparatively small impacts on the jet structure.

Following our investigation of the factors maintaining the mean-circulation in SH winter, chapter 5 examined the second aim, namely characterising the low frequency variability of the split jet. This chapter particularly focused on the variability of the polar front jet, with our analysis showing that this is largely captured by the SAM. That is, in the positive phase of the SAM, the South Pacific polar front jet is strong and distinct from the subtropical jet, while in the negative SAM phase, the polar front jet is weak and located further equatorward. This is in agreement with previous studies (Bals-Elsholz et al., 2001; Inatsu and Hoskins, 2006; Babian et al., 2018). Similar to the North Atlantic, variations in South Pacific jet latitude were found to be strongly related to the relative frequency of high latitude wave-breaking. A number of studies, using idealised models of split subtropical and eddy-driven jet systems, have suggested that under certain conditions, variability of such a system may be governed by a form of regime dynamics (e.g. Barnes and Hartmann, 2011; Ogawa et al., 2016). However, we showed that this paradigm was not a good model for variations in the South Pacific split jet as the equatorward jet state does not exhibit persistence.

The final three chapters considered the split jet in CMIP5 climate models with chapter 6 evaluating representation of the split jet in these models and thus addressing the third aim. Due to the strong link between jet variability and blocking in the South Pacific region, we also examined blocking in CMIP5. In general the SH jet was found to have a prevalent equatorward bias in both winter and summer, though in the former case the bias is largely localised to the region south of Australia. Unlike the Euro-Atlantic sector, atmospheric blocking was not systematically biased in the models. However, relatively few models attained a blocking climatology close to ERA-Interim reanalysis, with some models featuring very few blocking events and others wildly overestimating blocking occurrence.

Chapter 7 examined the fourth aim in terms of the zonal wind, stationary wave and

blocking responses to anthropogenic forcing under the RCP8.5 scenario. In general, the jet shifts poleward and strengthens under this scenario, however there is significant zonal asymmetry in the winter season, including an enhanced subtropical jet over the eastern Pacific and a pronounced jet strengthening to the south of Australia, making the split jet pattern appear less distinctive. The winter season is therefore characterised by both zonal-mean and stationary wave changes, unlike the summer season in which the former dominates. Overall, blocking frequency was shown to be reduced in the RCP8.5 runs, with the locus of winter changes again to the south of Australia, where blocking frequency was reduced by about a third on average. A correlation analysis suggested that winter circulation biases and responses, co-located to the south of Australia, were connected.

Finally, chapter 8 provided an attempt to understand, mechanistically, the wintertime SH stationary wave response to climate change, using a barotropic model forced with Rossby Wave Source (RWS) changes in the tropics and subtropics. The stationary wave pattern was found to be linked to Walker circulation weakening, particularly the reduction in descending air over the eastern Pacific. However, stationary wave changes were unable to account for the pattern of extratropical zonal wind changes. Hence a full understanding of SH wintertime circulation changes requires combining a zonally symmetric jet strengthening, with a zonally asymmetric stationary wave response.

9.2 Implications and future work

9.2.1 Role of Antarctic orography in shaping the mean-state

The role of Antarctic orography in shaping the mean-state atmospheric circulation has implications for a number of different areas of research. Firstly, this has implications for studies of paleoclimate as the structure and height of Antarctic ice-sheets changes considerably over million-year timescales. For example, Justino et al. (2014) studied

the effect of reducing Antarctic orography by around 25%, similar to that found in the mid to late Miocene (approx. 15 million years ago). On the other hand, our study has only considered full flattening of Antarctic orography, hence a less dramatic lowering of orography could provide an interesting extension of this work which would be more directly applicable to paleoclimate research.

Secondly, the mechanism we have suggested underlines the importance of Antarctic orography in capturing the observed circulation in comprehensive climate models. It is unclear from the present study how sensitive the circulation is to the particular details of the orography, however there is reason to believe that the horizontal resolution may become important if this affects the representation of the topographic gradient. Sensitivity studies with varying orographic resolution and topographic structure could provide clarification on this. This study was also performed using an idealised model, with prescribed sea-ice and SSTs, simple parameterisations of convection and no representation of clouds or gravity wave drag (beyond a simple Raleigh drag in the upper stratosphere). Whilst results, such as enhanced heat transport and warming at high latitudes, are consistent with Singh et al. (2016) who used a more advanced climate model (CCSM4, Gent et al., 2011), it is possible that the changes to the split jet would not be observed when including these additional processes. Therefore, it would be important to test the robustness of these results using a more complex model which features a good representation of gravity waves, the stratosphere and ocean dynamics.

Thirdly, many idealised modelling studies consider zonally symmetric aquaplanet simulations to present an analogue of the SH (e.g. Williams et al., 2007; Wu et al., 2012, 2013; Ogawa et al., 2016). Our results suggest that orography has a first order effect on SH circulation, while recent studies on the effect of orographic drag (Pithan et al., 2016; van Niekerk et al., 2017; Pithan and Polichtchouk, 2020) corroborate this. Hence the analogy between aquaplanet simulations and the SH circulation may not be

so clean. That being said, such idealised simulations will always be important for the mechanistic understanding which they allow, regardless of whether they omit major features of the climate system. It is worth noting that the barotropic modelling results of chapter 8 do not explicitly include orography, however this is implicitly included by forcing the background state to match the Historical climatology.

Finally, whilst we did not explore this in detail, the non-linear response of SH circulation to both flattening Antarctic orography and removing tropical SST asymmetries suggests that each change should not solely be considered in isolation. That is, on paleo timescales, changes to both tropical SST patterns and Antarctic orography could combine in non-linear ways to affect SH jet streams. In addition, tropical SST biases can contribute to extratropical circulation biases (e.g. Lachlan-Cope et al., 2007), hence non-linear interactions between high latitude orography and tropically generated waves could exacerbate these extratropical circulation biases or indeed affect the response to forcing.

9.2.2 Low frequency variability

Previous research has shown that the winter SAM is notably less symmetric than its summertime counterpart (Codron, 2007; Kidston et al., 2009) and only exhibits a conventional eddy-mean flow feedback process (e.g. Lorenz and Hartmann, 2001) over the Indian Ocean region (Barnes and Hartmann, 2010b). Our hypothesis is that variations in the SAM index are reflected in the South Pacific region primarily by variations in the frequency of high latitude wave-breaking. This provides a simple interpretation of this mode of variability on a local scale and is similar to that of Woollings et al. (2008) concerning the North Atlantic.

The fact that variability of the South Pacific eddy-driven jet does not conform to the dynamical regime paradigm, suggests that the zonally symmetric aquaplanet model of Ogawa et al. (2016) may be too simple. The jet is not persistent in its

equatorward jet state and hence affords no added predictability. A further argument against the existence of regimes concerns the response to forcing. Under the regime framework, when a forcing is applied, the rate of occupancy of each regime should change, however the structure of the regimes states should remain the same (Palmer, 1999; Branstator, 2009). However, in chapter 8, we showed that the response of the split jet to climate change can instead be understood via a stationary response to tropical / subtropical forcing. The pattern of zonal wind changes in the South Pacific sector also does not project strongly onto either equatorward or poleward jet states, with the largest zonal wind changes at the location of the zonal wind minimum, between the subtropical and polar front jets.

On the other hand, the results of chapter 4 suggest that the Indian Ocean jet may be important in providing sufficient wave-forcing via downstream propagation. This hypothesis was also suggested by Codron (2007) and it is consistent with our results. It would be of interest to test this mechanism more rigorously, for instance via nudging experiments with the Indian Ocean jet nudged towards a particular jet state.

9.2.3 Climate model biases and responses

Wintertime circulation biases in CMIP5 models are largely zonally asymmetric suggesting that the source of this bias is not itself zonally symmetric. In this thesis, we did not attempt to account for this bias, however this could present an interesting avenue for future work. In particular, asymmetry of the bias suggests that stationary wave biases could play a role. Nie et al. (2019) showed that a RWS bias is present in most CMIP5 models over the eastern tropical Pacific, hence a similar approach to chapter 8, but with a bias-corrected RWS, could test whether this is the source of extratropical circulation biases.

The poor representation of blocking in many of the models somewhat dampens

the confidence which one might have in future projections. However, the correlation between wind bias and change, and the correlation of wind change with blocking change in the Australia region, suggest that the full ensemble of models is useful for forming an emergent constraint. Equally, the fact that models systematically see a reduction in blocking frequency in this region, suggests that this finding is robust. Furthermore, our results concerning blocking changes under climate change, are consistent with the study of Parsons et al. (2016), who examined SH blocking using a considerably different method of blocking detection (persistent positive surface pressure anomalies). Finally, the findings of chapter 8 give a mechanistic understanding of the background wind changes which contribute to the reductions in blocking.

Concerning circulation changes, heat waves are expected to increase under climate change, but the slight reduction in summer blocking events suggests that these increases are primarily driven by thermodynamical processes. The weakening of the split jet pattern / strengthening of zonal wind to the south of Australia has implications for precipitation in both southern Australia and New Zealand. This has already been shown by Mindlin et al. (2020), with this pattern associated with drying over south-west Australia and enhanced precipitation over New Zealand. Therefore, constraining these wind changes is of practical interest to decision makers in these countries. Our result that split jet changes are linked to Walker circulation weakening via a stationary wave pattern thus underlines the importance of better constraining changes in tropical circulation. However, this result should be tested in a more complex, baroclinic stationary wave model for further confirmation. Moreover, the Walker circulation has varied in strength throughout the 20th century. Hence, it could prove fruitful to test whether the Walker circulation is correlated with SH stationary wave variability in the Historical runs of CMIP5 models and with satelite-era reanalysis data.

Lastly, data from CMIP6 is now widely available and early signs are that the equa-

torward jet bias has been reduced considerably (Bracegirdle et al., 2020; Curtis et al., 2020), while there have been improvements in storm track representation (Priestley et al., 2020) and tropical SST biases have also seen a slight reduction (Grose et al., 2020). It would be of interest to compare the results of this thesis with similar analyses of CMIP6 models. In particular, it would be interesting to examine whether the response to forcing in these models is modified from CMIP5, given the reductions in jet biases.

9.3 Final remarks

This thesis has examined the South Pacific split jet using a combination of idealised modelling, reanalysis data and comprehensive climate models. We have shown that the split jet structure is shaped by both tropical SSTs and by the presence of Antarctic orography. This changes the way in which one conceptualises the SH circulation, as the orography is no longer a detail of the high latitudes, but becomes an important element shaping the flow. We examined the variability of the split jet jet and found that the jet variability is not regime-like, as others have suggested, but is instead closely connected with the presence of wave-breaking at high latitudes. Finally, we have shown that the split jet is expected to become less distinct under high emissions climate change scenarios. Our barotropic model simulations and regression analysis indicate that this is a result of Walker circulation changes, however further work using a more complex modelling framework could be used to confirm this.

Appendix A

List of CMIP5 models

Table A.1: The full list of AMIP models used in this thesis along with their horizontal resolutions. Each model listed provided data for both AMIP and AMIP 4K experiments.

Model Name	Institute ID	Horiz. res. (lat. × lon.)
bcc-csm1-1-m	BCC	2.79 × 2.81
CanAM4	CCCMA	2.79 × 2.81
CNRM-CM5	CNRM-CERFACS	1.40 × 1.41
HadGEM2-A	MOHC	1.25 × 1.88
IPSL-CM5A-LR	IPSL	1.89 × 3.75
IPSL-CM5A-MR	IPSL	1.25 × 2.5
MIROC5	AORI-NIES-JAMSTEC	1.40 × 1.40
MPI-ESM-LR	MPI-M	1.87 × 1.88
MPI-ESM-MR	MPI-M	1.87 × 1.88
MRI-CGCM3	MRI	1.12 × 1.13

Table A.2: The full list of CMIP5 models used in this thesis along with the number of ensemble members with daily Z500 data available and their horizontal resolutions.

Model Name	Institute ID	Ens. members. (Hist./RCP 8.5)	Horiz. res. (lat. × lon.)
ACCESS1-0	CSIRO-BOM	1/1	1.25 × 1.88
ACCESS1-3	CSIRO-BOM	1/1	1.25 × 1.88
bcc-csm1-1	BCC	1/1	2.79 × 2.81
bcc-csm1-1-m	BCC	1/1	2.79 × 2.81
BNU-ESM	GCESS	1/1	2.79 × 2.81
CanESM2	CCCMA	5/5	2.79 × 2.81
CCSM4	NCAR	1/1	0.90 × 1.25
CMCC-CESM	CMCC	1/1	3.44 × 3.75
CMCC-CM	CMCC	1/1	0.75 × 0.75
CMCC-CMS	CMCC	1/1	3.71 × 3.75
CNRM-CM5	CNRM-CERFACS	1/1	1.40 × 1.41
EC-EARTH	EC-EARTH	4/4	1.12 × 1.12
FGOALS-g2	LASG-CESS	2/1	2.79 × 2.81
GFDL-CM3	NOAA GFDL	3/1	2.00 × 2.50
GFDL-ESM2G	NOAA GFDL	1/1	2.02 × 2.00
HadGEM2-CC	MOHC	3/3	1.25 × 1.88
HadGEM2-ES	MOHC	1/1	1.25 × 1.88
IPSL-CM5A-LR	IPSL	6/4	1.89 × 3.75
IPSL-CM5A-MR	IPSL	3/1	1.25 × 2.5
IPSL-CM5B-LR	IPSL	1/1	1.89 × 3.75
MPI-ESM-LR	MPI-M	3/3	1.87 × 1.88
MPI-ESM-MR	MPI-M	3/1	1.87 × 1.88
NorESM1-M	NCC	3/1	1.89 × 2.50

Bibliography

Allen, M. R. and W. J. Ingram, 2002: Constraints on future changes in climate and the hydrologic cycle. *Nature*, **419**.

Ambaum, M. H. P., B. J. Hoskins, and D. B. Stephenson, 2001: Arctic Oscillation or North Atlantic Oscillation? *Journal of Climate*, **14**, 3495–3507.

Ambrizzi, T., B. J. Hoskins, and H.-H. Hsu, 1995: Rossby Wave Propagation and Teleconnection Patterns in the Austral Winter. *Journal of the Atmospheric Sciences*, **52**, 3661–3672.

Andrews, D. G. and M. E. McIntyre, 1976: Planetary Waves in Horizontal and Vertical Shear: The Generalized Eliassen-Palm Relation and the Mean Zonal Acceleration. *Journal of the Atmospheric Sciences*, **33**, 2031–2048.

Anstey, J. A., P. Davini, L. J. Gray, T. J. Woollings, N. Butchart, C. Cagnazzo, B. Christiansen, S. C. Hardiman, S. M. Osprey, and S. Yang, 2013: Multi-model analysis of Northern Hemisphere winter blocking: Model biases and the role of resolution. *Journal of Geophysical Research Atmospheres*, **118**, 3956–3971.

Arakelian, A. and F. Codron, 2012: Southern Hemisphere Jet Variability in the IPSL GCM at Varying Resolutions. *Journal of the Atmospheric Sciences*, **69**, 3788–3799.

Arblaster, J. M. and G. A. Meehl, 2006: Contributions of External Forcings to Southern Annular Mode Trends. *Journal of Climate*, **19**, 2896–2905.

Austin, J. F., 1980: The blocking of middle latitude westerly winds by planetary waves. *Quarterly Journal of the Royal Meteorological Society*, **106**, 327–350.

Babian, S., J. Grieger, and U. Cubasch, 2018: A new index for the wintertime southern hemispheric split jet. *Atmospheric Chemistry and Physics*, **18**, 6749–6760.

Baker, H. S., T. Woollings, and C. Mbengue, 2017: Eddy-Driven Jet Sensitivity to Diabatic Heating in an Idealized GCM. *Journal of the Atmospheric Sciences*, **30**.

Baldwin, M. P. and T. J. Dunkerton, 2001: Stratospheric harbingers of anomalous weather regimes. *Science*, **294**, 581–4.

Bals-Elsholz, T. M., E. H. Atallah, L. F. Bosart, T. A. Wasula, M. J. Cempa, and A. R. Lupo, 2001: The wintertime southern hemisphere split jet: Structure, variability, and evolution. *Journal of Climate*, **14**, 4191–4215.

Banerjee, A., J. C. Fyfe, L. M. Polvani, D. Waugh, and K. L. Chang, 2020: A pause in Southern Hemisphere circulation trends due to the Montreal Protocol. *Nature*, **579**, 544–548.

Barnes, E. A. and D. L. Hartmann, 2010a: Dynamical Feedbacks and the Persistence of the NAO. *Journal of the Atmospheric Sciences*, **67**, 851–865.

— 2010b: Dynamical Feedbacks of the Southern Annular Mode in Winter and Summer. *Journal of the Atmospheric Sciences*, **67**, 2320–2330.

— 2010c: Influence of eddy-driven jet latitude on North Atlantic jet persistence and blocking frequency in CMIP3 integrations. *Geophysical Research Letters*, **37**.

— 2010d: Testing a theory for the effect of latitude on the persistence of eddy-driven jets using CMIP3 simulations. *Geophysical Research Letters*, **37**.

— 2011: Rossby Wave Scales, Propagation, and the Variability of Eddy-Driven Jets. *Journal of the Atmospheric Sciences*, **68**, 2893–2908.

— 2012: Detection of Rossby wave breaking and its response to shifts of the midlatitude jet with climate change. *Journal of Geophysical Research Atmospheres*, **117**, 1–17.

Barnes, E. A., D. L. Hartmann, D. M. W. Frierson, and J. Kidston, 2010: Effect of latitude on the persistence of eddy-driven jets. *Geophysical Research Letters*, **37**.

Barnes, E. A. and L. Polvani, 2013: Response of the Midlatitude Jets, and of Their Variability, to Increased Greenhouse Gases in the CMIP5 Models. *Journal of Climate*, **26**, 7117–7135.

Barton, N. P. and A. W. Ellis, 2009: Variability in wintertime position and strength of the North Pacific jet stream as represented by re-analysis data. *International Journal of Climatology*, **29**, 851–862.

Bellucci, A., S. Gualdi, and A. Navarra, 2010: The double-ITCZ syndrome in coupled general circulation models: The role of large-scale vertical circulation regimes. *Journal of Climate*, **23**, 1127–1145.

Benedict, J. J., S. Lee, S. B. Feldstein, J. J. Benedict, S. Lee, and S. B. Feldstein, 2004: Synoptic View of the North Atlantic Oscillation. *Journal of the Atmospheric Sciences*, **61**, 121–144.

Benjamin, S. G., J. M. Brown, G. Brunet, P. Lynch, K. Saito, and T. W. Schlatter, 2018: 100 Years of Progress in Forecasting and NWP Applications. *Meteorological Monographs*, **59**, 13.1–13.67.

Berckmans, J., T. Woollings, M.-E. Demory, P.-L. Vidale, and M. Roberts, 2013: Atmospheric blocking in a high resolution climate model: influences of mean state, orography and eddy forcing. *Atmospheric Science Letters*, **14**, 34–40.

Berrisford, P., B. J. Hoskins, and E. Tyrlis, 2007: Blocking and Rossby Wave Breaking on the Dynamical Tropopause in the Southern Hemisphere. *Journal of the Atmospheric Sciences*, **64**, 2881–2898.

Betts, A. K. and M. J. Miller, 1986: A new convective adjustment scheme. Part II: Single column tests using GATE wave, BOMEX, ATEX and arctic air-mass data sets. *Quarterly Journal of the Royal Meteorological Society*, **112**, 693–709.

Black, R. X. and B. A. McDaniel, 2007: The Dynamics of Northern Hemisphere Stratospheric Final Warming Events. *Journal of the Atmospheric Sciences*, **64**, 2932–2946.

Boljka, L. and T. G. Shepherd, 2020: Multiscale extratropical barotropic variability on the subseasonal-to-seasonal time-scale. *Quarterly Journal of the Royal Meteorological Society*, **146**, 301–313.

Boljka, L., T. G. Shepherd, and M. Blackburn, 2018: On the coupling between barotropic and baroclinic modes of extratropical atmospheric variability. *Journal of the Atmospheric Sciences*, **75**, 1853–1871.

Bordoni, S. and T. Schneider, 2008: Monsoons as eddy-mediated regime transitions of the tropical overturning circulation. *Nature Geoscience*, **1**, 515–519.

— 2010: Regime Transitions of Steady and Time-Dependent Hadley Circulations: Comparison of Axisymmetric and Eddy-Permitting Simulations. *Journal of the Atmospheric Sciences*, **67**, 1643–1654.

Bracegirdle, T., S. Hosking, and J. Turner, 2016: CMIP5 wind biases over the Adelie Land sector of the Southern Ocean: the role of resolution. *Scientific Committee on Antarctic Research: Biennial meetings and open science conference*, Scientific Committee on Antarctic Research, Kuala Lumpur, 101.

Bracegirdle, T. J., 2011: The seasonal cycle of stratosphere-troposphere coupling at southern high latitudes associated with the semi-annual oscillation in sea-level pressure. *Climate Dynamics*, **37**, 2323–2333.

Bracegirdle, T. J., C. R. Holmes, J. S. Hosking, G. J. Marshall, M. Osman, M. Patterson, and T. Rackow, 2020: Atmospheric Circulation in CMIP6 Compared to CMIP5. *Journal of Earth and Space Science*, **7**.

Bracegirdle, T. J. and G. J. Marshall, 2012: The reliability of antarctic tropospheric pressure and temperature in the latest global reanalyses. *Journal of Climate*, **25**, 7138–7146.

Bracegirdle, T. J., E. Shuckburgh, J. B. Sallee, Z. Wang, A. J. S. Meijers, N. Bruneau, T. Phillips, and L. J. Wilcox, 2013: Assessment of surface winds over the atlantic, indian, and pacific ocean sectors of the southern ocean in cmip5 models: Historical bias, forcing response, and state dependence. *Journal of Geophysical Research Atmospheres*, **118**, 547–562.

Braconnot, P., S. P. Harrison, M. Kageyama, P. J. Bartlein, V. Masson-Delmotte, A. Abe-Ouchi, B. Otto-Bliesner, and Y. Zhao, 2012: Evaluation of climate models using palaeoclimatic data. *Nature Climate Change*, **2**, 417–424.

Brandefelt, J. and H. Körnich, 2008: Northern Hemisphere Stationary Waves in Future Climate Projections. *Journal of Climate*, **21**, 6341–6353.

Branstator, G., 2009: "Modes of Variability" and Climate Change. *Journal of Climate*, **22**, 2639–2658.

Brayshaw, D. J., B. Hoskins, and M. Blackburn, 2008: The Storm-Track Response to Idealized SST Perturbations in an Aquaplanet GCM. *Journal of the Atmospheric Sciences*, **65**, 2842–2860.

— 2009: The Basic Ingredients of the North Atlantic Storm Track. Part I: Land–Sea Contrast and Orography. *Journal of the Atmospheric Sciences*, **66**, 2539–2558.

— 2011: The Basic Ingredients of the North Atlantic Storm Track. Part II: Sea Surface Temperatures. *Journal of the Atmospheric Sciences*, **68**, 1784–1805.

Bromwich, D. H. and R. L. Fogt, 2004: Strong Trends in the Skill of the ERA-40 and NCEP–NCAR Reanalyses in the High and Midlatitudes of the Southern Hemisphere, 1958–2001. *Journal of Climate*, **17**, 4603–4619.

Burkhardt, J. P. and A. R. Lupo, 2005: The Planetary- and Synoptic-Scale Interactions in a Southeast Pacific Blocking Episode Using PV Diagnostics. *Journal of the Atmospheric Sciences*, **62**, 1901–1916.

Butler, A. H., D. W. J. Thompson, and T. Birner, 2011: Isentropic Slopes, Downgradient Eddy Fluxes, and the Extratropical Atmospheric Circulation Response to Tropical Tropospheric Heating. *Journal of the Atmospheric Sciences*, **68**, 2292–2305.

Butler, A. H., D. W. J. Thompson, and R. Heikes, 2010: The Steady-State Atmospheric Circulation Response to Climate Change–like Thermal Forcings in a Simple General Circulation Model. *Journal of Climate*, **23**, 3474–3496.

Byrne, M. P., A. G. Pendergrass, A. D. Rapp, and K. R. Wodzicki, 2018: Response of the Intertropical Convergence Zone to Climate Change: Location, Width, and Strength. *Current Climate Change Reports*, **4**, 355–370.

Byrne, N. J. and T. G. Shepherd, 2018: Seasonal Persistence of Circulation Anomalies in the Southern Hemisphere Stratosphere and Its Implications for the Troposphere. *Journal of Climate*, **31**, 3467–3483.

Byrne, N. J., T. G. Shepherd, and I. Polichtchouk, 2019: Subseasonal-to-Seasonal Predictability of the Southern Hemisphere Eddy-Driven Jet During Austral Spring and Early Summer. *Journal of Geophysical Research: Atmospheres*, **124**.

Byrne, N. J., T. G. Shepherd, T. Woollings, and R. A. Plumb, 2017: Nonstationarity in Southern Hemisphere Climate Variability Associated with the Seasonal Breakdown of the Stratospheric Polar Vortex. *Journal of Climate*, **30**, 7125–7139.

Ceppi, P. and D. L. Hartmann, 2013: On the speed of the eddy-driven jet and the width of the hadley cell in the southern hemisphere. *Journal of Climate*.

Ceppi, P., Y. T. Hwang, D. M. W. Frierson, and D. L. Hartmann, 2012: Southern Hemisphere jet latitude biases in CMIP5 models linked to shortwave cloud forcing. *Geophysical Research Letters*, **39**.

Ceppi, P., D. T. McCoy, and D. L. Hartmann, 2016: Observational evidence for a negative shortwave cloud feedback in middle to high latitudes. *Geophysical Research Letters*, **43**, 1331–1339.

Ceppi, P., G. Zappa, T. G. Shepherd, and J. M. Gregory, 2018: Fast and Slow Components of the Extratropical Atmospheric Circulation Response to CO2 Forcing. *Journal of Climate*, **31**, 1091–1105.

Chandler, R. E., 2013: Exploiting strength, discounting weakness: combining information from multiple climate simulators. *Philosophical Transactions of the Royal Society A: Mathematical, Physical and Engineering Sciences*, **371**, 20120388.

Chang, E. K., 1993: Downstream development of baroclinic waves as inferred from regression analysis. *Journal of the Atmospheric Sciences*, **50**, 2038–2053.

Chang, E. K. and I. Orlanski, 1993: On the dynamics of a storm track. *Journal of the Atmospheric Sciences*, **50**, 999–1015.

Chang, E. K. M., 1999: Characteristics of Wave Packets in the Upper Troposphere. Part II: Seasonal and Hemispheric Variations. *Journal of the Atmospheric Sciences*, **56**, 1729–1747.

Chang, E. K. M., Y. Guo, and X. Xia, 2012: CMIP5 multimodel ensemble projection of storm track change under global warming. *Journal of Geophysical Research: Atmospheres*, **117**.

Chang, E. K. M., S. Lee, and K. L. Swanson, 2002: Storm Track Dynamics. *Journal of Climate*, **15**, 2163–2183.

Charney, J. G., 1947: The dynamics of long waves in a baroclinic westerly current. *Journal of the Atmospheric Sciences*, **4**, 136–162.

Charney, J. G. and J. G. DeVore, 1979: Multiple Flow Equilibria in the Atmosphere and Blocking. *Journal of the Atmospheric Sciences*, **36**, 1205–1216.

Chavaillaz, Y., F. Codron, and M. Kageyama, 2013: Southern westerlies in LGM and future (RCP4.5) climates. *Climate of the Past*, **9**, 517–524.

Chen, G., J. Lu, and D. M. W. Frierson, 2008: Phase Speed Spectra and the Latitude of Surface Westerlies: Interannual Variability and Global Warming Trend. *Journal of Climate*, **21**, 5942–5959.

Chen, G., J. Lu, and L. Sun, 2013: Delineating the Eddy–Zonal Flow Interaction in the Atmospheric Circulation Response to Climate Forcing: Uniform SST Warming

in an Idealized Aquaplanet Model. *Journal of the Atmospheric Sciences*, **70**, 2214–2233.

Chenoli, S. N., M. Y. Ahmad Mazuki, J. Turner, and A. A. Samah, 2017: Historical and projected changes in the Southern Hemisphere Sub-tropical Jet during winter from the CMIP5 models. *Climate Dynamics*, **48**, 661–681.

Christensen, J., E. Kjellström, F. Giorgi, G. Lenderink, and M. Rummukainen, 2010: Weight assignment in regional climate models. *Climate Research*, **44**, 179–194.

Christiansen, B., 2005: Bimodality of the Planetary-Scale Atmospheric Wave Amplitude Index. *Journal of the Atmospheric Sciences*, **62**, 2528–2541.

— 2007: Atmospheric circulation regimes: Can cluster analysis provide the number? *Journal of Climate*.

Ciasto, L. M. and D. W. J. J. Thompson, 2008: Observations of large-scale ocean-atmosphere interaction in the Southern Hemisphere. *Journal of Climate*, **21**, 1244–1259.

Clem, K. R. and R. L. Fogt, 2015: South Pacific circulation changes and their connection to the tropics and regional Antarctic warming in austral spring, 1979-2012. *Journal of Geophysical Research: Atmospheres*, **120**, 2773–2792.

Clough, S. A., M. W. Shephard, E. J. Mlawer, J. S. Delamere, M. J. Iacono, K. Cady-Pereira, S. Boukabara, and P. D. Brown, 2005: Atmospheric radiative transfer modeling: A summary of the AER codes. *Journal of Quantitative Spectroscopy and Radiative Transfer*, **91**, 233–244.

Codron, F., 2007: Relations between Annular Modes and the Mean State: Southern Hemisphere Winter. *Journal of the Atmospheric Sciences*, **64**, 3328–3339.

Collins, M., R. E. Chandler, P. M. Cox, J. M. Huthnance, J. Rougier, and D. B. Stephenson, 2012: Quantifying future climate change. *Nature Climate Change*, **2**, 403–409.

Collins, M., R. Knutti, J. Arblaster, J.-L. Dufresne, T. Fichefet, P. Friedlingstein, X. Gao, W. Gutowski, T. Johns, G. Krinner, M. Shongwe, C. Tebaldi, A. Weaver, and M. Wehner, 2013: Long-term Climate Change: Projections, Commitments and Irreversibility. *2013: Long-term Climate Change: Projections, Commitments and Irreversibility. In: Climate Change 2013: The Physical Science Basis. Contribution of Working Group I to the Fifth Assessment Report of the Intergovernmental Panel on Climate Change*, T. Stocker, D. Qin, G. K. Plattner, M. Tignor, S. Allen, J. Boschung, A. Nauels, Y. Xia, V. Bex, and Midgley. P.M., eds., Cambridge University Press, chapter 12.

Colucci, S. J., D. P. Baumhefner, S. J. Colucci, and D. P. Baumhefner, 1992: Initial Weather Regimes as Predictors of Numerical 30-Day Mean Forecast Accuracy. *Journal of the Atmospheric Sciences*, **49**, 1652–1671.

Corti, S., F. Molteni, and T. N. Palmer, 1999: Signature of recent climate change in frequencies of natural atmospheric regimes. *Nature*, **398**, 799–802.

Cowan, T., P. van Rensch, A. Purich, and W. Cai, 2013: The Association of Tropical and Extratropical Climate Modes to Atmospheric Blocking across Southeastern Australia. *Journal of Climate*, **26**, 7555–7569.

Curtis, P. E., P. Ceppi, and G. Zappa, 2020: Role of the mean state for the Southern Hemispheric Jet Stream response to CO2 forcing in CMIP6 models Role of the Mean State for the Southern Hemispheric Jet Stream Response to CO 2 Forcing in CMIP6 models. *Environmental Research Letters*, **15**.

D'Andrea, F., S. Tibaldi, M. Blackburn, G. Boer, M. Déqué, M. R. Dix, B. Dugas, L. Ferranti, T. Iwasaki, A. Kitoh, V. Pope, D. Randall, E. Roeckner, D. Strauss, W. Stern, H. Van den Dool, and D. Williamson, 1998: Northern Hemisphere atmospheric blocking as simulated by 15 atmospheric general circulation models in the period 1979-1988. *Climate Dynamics*, **14**, 385–407.

Davini, P. and C. Cagnazzo, 2014: On the misinterpretation of the North Atlantic Oscillation in CMIP5 models. *Climate Dynamics*, **43**, 1497–1511.

Davini, P., C. Cagnazzo, S. Gualdi, and A. Navarra, 2012: Bidimensional Diagnostics, Variability, and Trends of Northern Hemisphere Blocking. *Journal of Climate*, **25**, 6496–6509.

Davini, P. and F. D'Andrea, 2016: Northern Hemisphere Atmospheric Blocking Representation in Global Climate Models: Twenty Years of Improvements? *Journal of Climate*, **29**, 8823–8840.

Davis, N. A. and T. Birner, 2019: Eddy Influences on the Hadley Circulation. *Journal of Advances in Modeling Earth Systems*, **11**, 1563–1581.

Dawson, A. and T. N. Palmer, 2015: Simulating weather regimes: impact of model resolution and stochastic parameterization. *Climate Dynamics*, **44**, 2177–2193.

Dawson, A., T. N. Palmer, and S. Corti, 2012: Simulating regime structures in weather and climate prediction models. *Geophysical Research Letters*, **39**, 1–6.

de Vries, H., T. Woollings, J. Anstey, R. J. Haarsma, and W. Hazeleger, 2013: Atmospheric blocking and its relation to jet changes in a future climate. *Climate Dynamics*, **41**, 2643–2654.

Dee, D. P., S. M. Uppala, A. J. Simmons, P. Berrisford, P. Poli, and S. Kobayashi, 2011: The ERA-Interim reanalysis: Configuration and performance of the data

assimilation system. *Quarterly Journal of the Royal Meteorological Society*, **137**, 553–597.

Déqué, M. and S. Somot, 2010: Weighted frequency distributions express modelling uncertainties in the ENSEMBLES regional climate experiments. *Climate Research*, **44**, 195–209.

Ding, Q., E. J. Steig, D. S. Battisti, and M. Küttel, 2011: Winter warming in West Antarctica caused by central tropical Pacific warming. *Nature Geoscience*, **4**, 398–403.

Ding, Q., E. J. Steig, D. S. Battisti, and J. M. Wallace, 2012: Influence of the Tropics on the Southern Annular Mode. *Journal of Climate*, **25**, 6330–6348.

Domeisen, D. I. V., L. Sun, and G. Chen, 2013: The role of synoptic eddies in the tropospheric response to stratospheric variability. *Geophysical Research Letters*, **40**, 4933–4937.

Dowdy, A. J., G. A. Mills, B. Timbal, and Y. Wang, 2013: Changes in the Risk of Extratropical Cyclones in Eastern Australia. *Journal of Climate*, **26**, 1403–1417.

Dritschel, D. G. and M. E. McIntyre, 2008: Multiple Jets as PV Staircases: The Phillips Effect and the Resilience of Eddy-Transport Barriers. *Journal of the Atmospheric Sciences*, **65**, 855–874.

Duchon, C. E., 1979: Lanczos Filtering in One and Two Dimensions. *Journal of Applied Meteorology*, **18**, 1016–1022.

Dunn-Sigouin, E. and S.-W. Son, 2013: Northern Hemisphere blocking frequency and duration in the CMIP5 models. *Journal of Geophysical Research: Atmospheres*, **118**, 1179–1188.

Eady, E. T., 1949: Long Waves and Cyclone Waves. *Tellus*, **1**, 33–52.

Edmon, H. J., B. J. Hoskins, and M. E. McIntyre, 1980: Eliassen-Palm Cross Sections for the Troposphere. *Journal of the Atmospheric Sciences*, **37**, 2600–2616.

Egger, J., 1978: Dynamics of Blocking Highs. *Journal of the Atmospheric Sciences*, **35**, 1788–1801.

— 1991: On the mean atmospheric circulation over Antarctica. *Geophysical & Astrophysical Fluid Dynamics*, **58**, 75–90.

Egger, J. and K. Fraedrich, 1987: Topographic Rossby waves over Antarctica. *Tellus A*, **39A**, 110–115.

Eichelberger, S. J. and D. L. Hartmann, 2007: Zonal jet structure and the leading mode of variability. *Journal of Climate*, **20**, 5149–5163.

Eyring, V., J. M. Arblaster, I. Cionni, J. Sedláček, J. Perlwitz, P. J. Young, S. Bekki, D. Bergmann, P. Cameron-Smith, W. J. Collins, G. Faluvegi, K.-D. Gottschaldt, L. W. Horowitz, D. E. Kinnison, J.-F. Lamarque, D. R. Marsh, D. Saint-Martin, D. T. Shindell, K. Sudo, S. Szopa, and S. Watanabe, 2013: Long-term ozone changes and associated climate impacts in CMIP5 simulations. *Journal of Geophysical Research: Atmospheres*, **118**, 5029–5060.

Eyring, V., S. Bony, G. A. Meehl, C. A. Senior, B. Stevens, R. J. Stouffer, and K. E. Taylor, 2016: Overview of the Coupled Model Intercomparison Project Phase 6 (CMIP6) experimental design and organization. *Geoscientific Model Development*, **9**, 1937–1958.

Eyring, V., I. Cionni, G. E. Bodeker, A. J. Charlton-Perez, D. E. Kinnison, J. F. Scinocca, D. W. Waugh, H. Akiyoshi, S. Bekki, M. P. Chipperfield, M. Dameris, S. Dhomse, S. M. Frith, H. Garny, A. Gettelman, A. Kubin, U. Langematz, E. Mancini, M. Marchand, T. Nakamura, L. D. Oman, S. Pawson, G. Pitari, D. A.

Plummer, E. Rozanov, T. G. Shepherd, K. Shibata, W. Tian, P. Braesicke, S. C. Hardiman, J. F. Lamarque, O. Morgenstern, J. A. Pyle, D. Smale, and Y. Yamashita, 2010: Multi-model assessment of stratospheric ozone return dates and ozone recovery in CCMVal-2 models. *Atmospheric Chemistry and Physics*, **10**, 9451–9472.

Farrara, J. D., M. Ghil, C. R. Mechoso, and K. C. Mo, 1989: Empirical orthogonal functions and multiple flow regimes in the Southern Hemisphere winter. *Journal of the Atmospheric Sciences*, **46**, 3219–3223.

Flato, G., J. Marotzke, B. Abiodun, B. Braconnot, S. Chou, W. Collins, P. Cox, F. Driouech, S. Emori, V. Eyring, C. Forest, P. Gleckler, E. Guilyardi, C. Jakob, V. Kattsov, C. Reason, and Rummukainen. M/, 2013: Evaluation of Climate Models. *Climate Change 2013: The Physical Science Basis. Contribution of Working Group I to the Fifth Assessment Report of the Intergovernmental Panel on Climate Change*, Cambridge University Press, chapter 9, 741–866.

Fogt, R. L. and D. H. Bromwich, 2006: Decadal Variability of the ENSO Teleconnection to the High-Latitude South Pacific Governed by Coupling with the Southern Annular Mode*. *Journal of Climate*, **19**, 979–997.

Fogt, R. L., D. H. Bromwich, and K. M. Hines, 2011: Understanding the SAM influence on the South Pacific ENSO teleconnection. *Climate Dynamics*, **36**, 1555–1576.

Folland, C. K., J. Knight, H. W. Linderholm, D. Fereday, S. Ineson, and J. W. Hurrell, 2009: The Summer North Atlantic Oscillation: Past, Present, and Future. *Journal of Climate*, **22**, 1082–1103.

Freitas, A. C. V., J. S. Frederiksen, T. J. O'Kane, and T. Ambrizzi, 2017: Simulated austral winter response of the Hadley circulation and stationary Rossby wave propagation to a warming climate. *Climate Dynamics*, **49**, 521–545.

Freitas, A. C. V. and V. B. Rao, 2014: Global changes in propagation of stationary waves in a warming scenario. *Quarterly Journal of the Royal Meteorological Society*, **140**, 364–383.

Frierson, D. M. W., I. M. Held, and P. Zurita-Gotor, 2006: A Gray-Radiation Aquaplanet Moist GCM. Part I: Static Stability and Eddy Scale. *Journal of the Atmospheric Sciences*, **63**, 2548–2566.

Garfinkel, C. I., I. White, E. P. Gerber, and M. Jucker, 2020: The impact of SST biases in the tropical east Pacific and Agulhas current region on atmospheric stationary waves in the Southern Hemisphere. *Journal of Climate*, 1–72.

Gastineau, G. and C. Frankignoul, 2015: Influence of the North Atlantic SST variability on the atmospheric circulation during the twentieth century. *Journal of Climate*, **28**, 1396–1416.

Gent, P. R., G. Danabasoglu, L. J. Donner, M. M. Holland, E. C. Hunke, S. R. Jayne, D. M. Lawrence, R. B. Neale, P. J. Rasch, M. Vertenstein, P. H. Worley, Z.-L. Yang, and M. Zhang, 2011: The Community Climate System Model Version 4. *Journal of Climate*, **24**, 4973–4991.

Gerber, E. P., M. P. Baldwin, H. Akiyoshi, J. Austin, S. Bekki, P. Braesicke, N. Butchart, M. Chipperfield, M. Dameris, S. Dhomse, S. M. Frith, R. R. Garcia, H. Garny, A. Gettelman, S. C. Hardiman, A. Karpechko, M. Marchand, O. Morgenstern, J. E. Nielsen, S. Pawson, T. Peter, D. A. Plummer, J. A. Pyle, E. Rozanov,

J. F. Scinocca, T. G. Shepherd, and D. Smale, 2010: Stratosphere-troposphere coupling and annular mode variability in chemistry-climate models. *Journal of Geophysical Research Atmospheres*, **115**, D00M06.

Gerber, E. P., C. Orbe, and L. M. Polvani, 2009: Stratospheric influence on the tropospheric circulation revealed by idealized ensemble forecasts. *Geophysical Research Letters*, **36**, L24801.

Gerber, E. P. and S. W. Son, 2014: Quantifying the summertime response of the Austral jet stream and hadley cell to stratospheric ozone and greenhouse gases. *Journal of Climate*, **27**, 5538–5559.

GFDL, 2020: 'https://www.gfdl.noaa.gov/wp-content/uploads/files/user_files/pjp/barotropic.pdf' retrieved on 01/07/2020.

Gibson, P. B., A. J. Pitman, R. Lorenz, and S. E. Perkins-Kirkpatrick, 2017: The Role of Circulation and Land Surface Conditions in Current and Future Australian Heat Waves. *Journal of Climate*, **30**, 9933–9948.

Gillett, N. P. and J. C. Fyfe, 2013: Annular mode changes in the CMIP5 simulations. *Geophysical Research Letters*, **40**, 1189–1193.

Gillett, N. P., T. D. Kell, and P. D. Jones, 2006: Regional climate impacts of the Southern Annular Mode. *Geophysical Research Letters*, **33**, L23704.

Gray, L., W. Norton, C. Pascoe, and A. Charlton, 2005: A possible influence of equatorial winds on the September 2002 Southern Hemisphere sudden warming event. *Journal of the Atmospheric Sciences*, **62**, 651–667.

Grise, K. M., S. M. Davis, I. R. Simpson, D. W. Waugh, Q. Fu, R. J. Allen, K. H. Rosenlof, C. C. Ummenhofer, K. B. Karnauskas, A. C. Maycock, X. W. Quan,

T. Birner, and P. W. Staten, 2019: Recent tropical expansion: Natural variability or forced response? *Journal of Climate*, **32**, 1551–1571.

Grise, K. M. and L. M. Polvani, 2014a: Southern Hemisphere Cloud–Dynamics Biases in CMIP5 Models and Their Implications for Climate Projections. *Journal of Climate*, **27**, 6074–6092.

— 2014b: The response of midlatitude jets to increased CO2 : Distinguishing the roles of sea surface temperature and direct radiative forcing. *Geophysical Research Letters*, **41**, 6863–6871.

Grose, M., S. Narsey, F. Delage, A. Dowdy, M. Bador, G. Boschat, C. Chung, J. Kajtar, S. Rauniyar, M. Freund, K. Lyu, H. Rashid, X. Zhang, S. Wales, C. Trenham, N. Holbrook, T. Cowan, L. Alexander, J. Arblaster, and S. Power, 2020: Insights from CMIP6 for Australia's future climate. *Earth's Future*, **8**.

Grose, M. R., J. N. Brown, S. Narsey, J. R. Brown, B. F. Murphy, C. Langlais, A. S. Gupta, A. F. Moise, and D. B. Irving, 2014: Assessment of the CMIP5 global climate model simulations of the western tropical Pacific climate system and comparison to CMIP3. *International Journal of Climatology*, **34**, 3382–3399.

Grose, M. R., M. J. Pook, P. C. McIntosh, J. S. Risbey, and N. L. Bindoff, 2012: The simulation of cutoff lows in a regional climate model: reliability and future trends. *Climate Dynamics*, **39**, 445–459.

Grose, M. R., J. S. Risbey, A. F. Moise, S. Osbrough, C. Heady, L. Wilson, and T. Erwin, 2017: Constraints on Southern Australian Rainfall Change Based on Atmospheric Circulation in CMIP5 Simulations. *Journal of Climate*, **30**, 225–242.

Grose, W. L. and B. J. Hoskins, 1979: On the Influence of Orography on Large-Scale Atmospheric Flow. *Journal of the Atmospheric Sciences*, **36**, 223–234.

Haarsma, R. J. and F. Selten, 2012: Anthropogenic changes in the Walker circulation and their impact on the extra-tropical planetary wave structure in the Northern Hemisphere. *Climate Dynamics*, **39**, 1781–1799.

Hadley, G., 1735: Concerning the cause of the general trade winds. *Philosophical Transactions of the Royal Society*, **29**, 58–62.

Hall, A. and M. Visbeck, 2002: Synchronous Variability in the Southern Hemisphere Atmosphere, Sea Ice, and Ocean Resulting from the Annular Mode. *Journal of Climate*, **15**, 3043–3057.

Hall, R. J., J. M. Jones, E. Hanna, A. A. Scaife, and R. Erdélyi, 2017: Drivers and potential predictability of summer time North Atlantic polar front jet variability. *Climate Dynamics*, **48**, 3869–3887.

Hannachi, A., 2007: Tropospheric Planetary Wave Dynamics and Mixture Modeling: Two Preferred Regimes and a Regime Shift. *Journal of the Atmospheric Sciences*, **64**, 3521–3541.

Hannachi, A., D. M. Straus, C. L. E. Franzke, S. Corti, and T. Woollings, 2017: Low-frequency nonlinearity and regime behavior in the Northern Hemisphere extratropical atmosphere. *Reviews of Geophysics*, **55**.

Hansen, A. R. and A. Sutera, 1991: Planetary-scale flow regimes in midlatitudes of the Southern Hemisphere. *Journal of the Atmospheric Sciences*, **48**, 952–964.

Hartmann, D., A. Klein Tank, M. Rusticucci, L. Alexander, S. Brönnimann, Y. Charabi, F. Dentener, E. Dlugokencky, D. Easterling, A. Kaplan, B. Soden, P. Thorne, M. Wild, and P. Zhai, 2013: Observations: Atmosphere and Surface. *Climate Change 2013: The Physical Science Basis. Contribution of Working Group I to the Fifth Assessment Report of the Intergovernmental Panel on Climate Change*,

G.-K. Stocker, T.F., D. Qin, V. B. Plattner, M. Tignor, S.K. Allen, J. Boschung, A. Nauels, Y. Xia, and P. Midgley, eds., Cambridge University Press, chapter 2, 159–254.

Hartmann, D. L., 2007: The Atmospheric General Circulation and Its Variability. *Journal of the Meteorological Society of Japan. Ser. II*, **85B**, 123–143.

Hartmann, D. L. and F. Lo, 1998: Wave-Driven Zonal Flow Vacillation in the Southern Hemisphere. *Journal of the Atmospheric Sciences*, **55**, 1303–1315.

Hausfather, Z. and G. P. Peters, 2020: Emissions – the 'business as usual' story is misleading. *Nature*, **577**, 618–620.

Held, I., 1975: Momentum Transport by Quasi-Geostrophic Eddies. *Journal of the Atmospheric Sciences*, **32**, 1494–1497.

— 2000: The general circulation of the atmosphere. *Proc. Progr. Geophys. Fluid Dyn*, I. Held, ed., Woods Hole, Woods Hole Oceanographic Institute, Woods Hole, MA, Proc. Progr. Geophys. Fluid Dyn, 1–70.

Held, I. and A. Hou, 1980: Nonlinear Axially Symmetric Circulations in a Nearly Inviscid Atmosphere. *Journal of the Atmospheric Sciences*, **37**, 515–533.

Held, I. M., 2005: The gap between simulation and understanding in climate modeling. *Bulletin of the American Meteorological Society*, **86**, 1609–1614.

Held, I. M. and I.-S. Kang, 1987: Barotropic Models of the Extratropical Response to El Niño. *Journal of the Atmospheric Sciences*, **44**, 3576–3586.

Held, I. M., R. L. Panetta, and R. T. Pierrehumbert, 1985: Stationary External Rossby Waves in Vertical Shear. *Journal of the Atmospheric Sciences*, **42**, 865–883.

Held, I. M. and B. J. Soden, 2006: Robust Responses of the Hydrological Cycle to Global Warming. *Journal of Climate*, **19**, 5686–5699.

Held, I. M. and M. J. Suarez, 1994: A Proposal for the Intercomparison of the Dynamical Cores of Atmospheric General Circulation Models. *Bulletin of the American Meteorological Society*, **75**, 1825–1830.

Held, I. M., M. Ting, and H. Wang, 2002: Northern winter stationary waves: Theory and modeling. *Journal of Climate*, **15**, 2125–2144.

Hendon, H. H., E. P. Lim, and H. Nguyen, 2014: Seasonal variations of subtropical precipitation associated with the southern annular mode. *Journal of Climate*, **27**, 3446–3460.

Hendon, H. H., D. W. J. Thompson, and M. C. Wheeler, 2007: Australian Rainfall and Surface Temperature Variations Associated with the Southern Hemisphere Annular Mode. *Journal of Climate*, **20**, 2452–2467.

Ho, E., D. V. Budescu, V. Bosetti, D. P. van Vuuren, and K. Keller, 2019: Not all carbon dioxide emission scenarios are equally likely: a subjective expert assessment. *Climatic Change*, **155**, 545–561.

Hodges, K. I., R. W. Lee, and L. Bengtsson, 2011: A Comparison of Extratropical Cyclones in Recent Reanalyses ERA-Interim, NASA MERRA, NCEP CFSR, and JRA-25. *Journal of Climate*, **24**, 4888–4906.

Hoskins, B. J. and T. Ambrizzi, 1993: Rossby Wave Propagation on a Realistic Longitudinally Varying Flow. *Journal of the Atmospheric Sciences*, **50**, 1661–1671.

Hoskins, B. J. and K. I. Hodges, 2005: A new perspective on Southern Hemisphere storm tracks. *Journal of Climate*, **18**, 4108–4129.

Hoskins, B. J. and I. N. James, 2013: *Fluid Dynamics of the Midlatitude Atmosphere*. Wiley, Chichester, 1–408 pp.

Hoskins, B. J., I. N. James, and G. H. White, 1983: The Shape, Propagation and Mean-Flow Interaction of Large-Scale Weather Systems. *Journal of the Atmospheric Sciences*, **40**, 1595–1612.

Hoskins, B. J. and D. J. Karoly, 1981: The Steady Linear Response of a Spherical Atmosphere to Thermal and Orographic Forcing. *Journal of the Atmospheric Sciences*, **38**, 1179–1196.

Hoskins, B. J. and P. J. Valdes, 1990: On the Existence of Storm-Tracks. *Journal of the Atmospheric Sciences*, **47**, 1854–1864.

Hotta, D. and H. Nakamura, 2011: On the significance of the sensible heat supply from the ocean in the maintenance of the mean baroclinicity along storm tracks. *Journal of Climate*, **24**, 3377–3401.

Hsu, C. J. and F. Zwiers, 2001: Climate change in recurrent regimes and modes of Northern Hemisphere atmospheric variability. *Journal of Geophysical Research*, **106**, 145–20.

Inatsu, M. and B. J. Hoskins, 2004: The zonal asymmetry of the Southern Hemisphere winter storm track. *Journal of Climate*, **17**, 4882–4892.

— 2006: The Seasonal and Wintertime Interannual Variability of the Split Jet and the Storm-Track Activity Minimum near New Zealand. *Journal of the Meteorological Society of Japan*, **84**, 433–445.

Irving, D. and I. Simmonds, 2016: A new method for identifying the Pacific-South American pattern and its influence on regional climate variability. *Journal of Climate*, **29**.

Itoh, H., M. Kimoto, and H. Aoki, 1999: Alternation between the single and double jet structures in the southern hemisphere troposphere part I: Chaotic wandering. *Journal of the Meteorological Society of Japan*, **79**, 399–412.

James, I. N., 1989: The Antarctic drainage flow: Implications for hemispheric flow on the Southern Hemisphere. *Antarctic Science*, **1**, 279–290.

Jin, D. and B. P. Kirtman, 2009: Why the Southern Hemisphere ENSO responses lead ENSO. *Journal of Geophysical Research Atmospheres*, **114**.

Jin, F. and B. J. Hoskins, 1995: The Direct Response to Tropical Heating in a Baroclinic Atmosphere. *Journal of the Atmospheric Sciences*, **52**, 307–319.

Joseph, R., M. Ting, and P. J. Kushner, 2004: The Global Stationary Wave Response to Climate Change in a Coupled GCM. *Journal of Climate*, **17**, 540–556.

Jucker, M. and E. P. Gerber, 2017: Untangling the Annual Cycle of the Tropical Tropopause Layer with an Idealized Moist Model. *Journal of Climate*, **30**, 7339–7358.

Juckes, M. N., I. N. James, and M. Blackburn, 1994: The influence of Antarctica on the momentum budget of the southern extratropics. *Quarterly Journal of the Royal Meteorological Society*, **120**, 1017–1044.

Justino, F., J. Marengo, F. Kucharski, F. Stordal, J. Machado, and M. Rodrigues, 2014: Influence of Antarctic ice sheet lowering on the Southern Hemisphere climate: Modeling experiments mimicking the mid-Miocene. *Climate Dynamics*, **42**, 843–858.

Justino, F., A. S. Silva, M. P. Pereira, F. Stordal, D. Lindemann, and F. Kucharski, 2015: The Large-Scale Climate in Response to the Retreat of the West Antarctic Ice Sheet. *Journal of Climate*, **28**, 637–650.

Kalnay, E., M. Kanamitsu, R. Kistler, W. Collins, D. Deaven, L. Gandin, M. Iredell, R. Jenne, and D. Joseph, 1996: The NCEP NCAR 40-Year Reanalysis Project. *Bulletin of the American Meteorological Society*, **77**, 438–472.

Kang, S. M. and J. Lu, 2012: Expansion of the Hadley Cell under Global Warming: Winter versus Summer. *Journal of Climate*, **25**, 8387–8393.

Karoly, D., 1989: Southern Hemisphere Circulation Features Associated with El Niño-Southern Oscillation Events. *Journal of Climate*, **2**, 1239–1252.

Karoly, D. J. and D. G. Vincent, 1998: *Meteorology of the Southern Hemisphere*. American Meteorological Society, 410 pp.

Kidston, J., S. M. Dean, J. A. Renwick, and G. K. Vallis, 2010: A robust increase in the eddy length scale in the simulation of future climates. *Geophysical Research Letters*, **37**.

Kidston, J. and E. P. Gerber, 2010: Intermodel variability of the poleward shift of the austral jet stream in the CMIP3 integrations linked to biases in 20th century climatology. *Geophysical Research Letters*, **37**, 1–5.

Kidston, J., J. A. Renwick, and J. McGregor, 2009: Hemispheric-scale seasonality of the southern annular mode and impacts on the climate of New Zealand. *Journal of Climate*, **22**, 4759–4770.

Kidston, J., A. A. Scaife, S. C. Hardiman, D. M. Mitchell, N. Butchart, M. P. Baldwin, and L. J. Gray, 2015: Stratospheric influence on tropospheric jet streams, storm tracks and surface weather. *Nature Geoscience*, **8**, 433–440.

Kidston, J., A. S. Taschetto, D. W. J. Thompson, and M. H. England, 2011a: The influence of Southern Hemisphere sea-ice extent on the latitude of the mid-latitude jet stream. *Geophysical Research Letters*, **38**.

Kidston, J. and G. K. Vallis, 2010: Relationship between eddy-driven jet latitude and width. *Geophysical Research Letters*, **37**.

Kidston, J., G. K. Vallis, S. M. Dean, and J. A. Renwick, 2011b: Can the increase in the eddy length scale under global warming cause the poleward shift of the jet streams? *Journal of Climate*, **24**, 3764–3780.

Kidston, J., G. K. Vallis, J. Kidston, and G. K. Vallis, 2012: The Relationship between the Speed and the Latitude of an Eddy-Driven Jet in a Stirred Barotropic Model. *Journal of the Atmospheric Sciences*, **69**, 3251–3263.

Knutti, R., R. Furrer, C. Tebaldi, J. Cermak, and G. A. Meehl, 2010: Challenges in combining projections from multiple climate models. *Journal of Climate*, **23**, 2739–2758.

Knutti, R., D. Masson, and A. Gettelman, 2013: Climate model genealogy: Generation CMIP5 and how we got there. *Geophysical Research Letters*, **40**, 1194–1199.

Knutti, R. and J. Sedláček, 2013: Robustness and uncertainties in the new CMIP5 climate model projections. *Nature Climate Change*, **3**, 369–373.

Kociuba, G. and S. B. Power, 2015: Inability of CMIP5 Models to Simulate Recent Strengthening of the Walker Circulation: Implications for Projections. *Journal of Climate*, **28**, 20–35.

Kohfeld, K. E., R. M. Graham, A. M. de Boer, L. C. Sime, E. W. Wolff, C. Le Quéré, and L. Bopp, 2013: Southern Hemisphere westerly wind changes during the Last Glacial Maximum: Paleo-data synthesis. *Quaternary Science Reviews*, **68**, 76–95.

Koo, S., A. W. Robertson, and M. Ghil, 2002: Multiple regimes and low-frequency oscillations in the Southern Hemisphere's zonal-mean flow. *Journal of Geophysical Research Atmospheres*, **107**, 1–13.

Kunz, T., K. Fraedrich, and F. Lunkeit, 2009: Synoptic scale wave breaking and its potential to drive NAO-like circulation dipoles: A simplified GCM approach. *Quarterly Journal of the Royal Meteorological Society*, **135**, 1–19.

Kuroda, Y. and K. Kodera, 1998: Interannual variability in the troposphere and stratosphere of the southern hemisphere winter. *Journal of Geophysical Research Atmospheres*, **103**, 13787–13799.

Lachlan-Cope, T. A., W. M. Connolley, and J. Turner, 2001: The role of the non-axisymmetric Antarctic orography in forcing the observed pattern of variability of the Antarctic climate. *Geophysical Research Letters*, **28**, 4111–4114.

— 2007: Effects of tropical sea surface temperature (SST) errors on the Antarctic atmospheric circulation of HadCM3. *Geophysical Research Letters*, **34**.

Le Quéré, C., C. Rödenbeck, E. T. Buitenhuis, T. J. Conway, R. Langenfelds, A. Gomez, C. Labuschagne, M. Ramonet, T. Nakazawa, N. Metzl, N. Gillett, and M. Heimann, 2007: Saturation of the Southern Ocean CO2 Sink Due to Recent Climate Change. *Science*, **316**, 1735–1738.

Lee, R. W., 2015: *Storm track biases and changes in a warming climate from an extratropical cyclone perspective using CMIP5*. Ph.D. thesis, University of Reading.

Lee, S. and S. B. Feldstein, 2013: Detecting ozone- and greenhouse gas-driven wind trends with observational data. *Science*, **339**, 563–567.

Lee, S. and H.-K. Kim, 2003: The Dynamical Relationship between Subtropical and Eddy-Driven Jets. *Journal of the Atmospheric Sciences*, **60**, 1490–1503.

Li, C. and J. J. Wettstein, 2012: Thermally driven and eddy-driven jet variability in reanalysis. *Journal of Climate*, **25**, 1587–1596.

Li, G. and S.-P. Xie, 2014: Tropical Biases in CMIP5 Multimodel Ensemble: The Excessive Equatorial Pacific Cold Tongue and Double ITCZ Problems. *Journal of Climate*, **27**, 1765–1780.

Li, X., E. P. Gerber, D. M. Holland, and C. Yoo, 2015: A Rossby Wave Bridge from the Tropical Atlantic to West Antarctica. *Journal of Climate*, **28**, 2256–2273.

Li, Y., D. W. J. Thompson, S. Bony, and T. M. Merlis, 2019: Thermodynamic Control on the Poleward Shift of the Extratropical Jet in Climate Change Simulations: The Role of Rising High Clouds and Their Radiative Effects. *Journal of Climate*, **32**, 917–934.

Lim, E., H. H. Hendon, and D. W. J. Thompson, 2018: Seasonal Evolution of Stratosphere-Troposphere Coupling in the Southern Hemisphere and Implications for the Predictability of Surface Climate. *Journal of Geophysical Research: Atmospheres*, **123**, 12,002–12,016.

Lim, E.-P., H. H. Hendon, J. M. Arblaster, F. Delage, H. Nguyen, S.-K. Min, and M. C. Wheeler, 2016: The impact of the Southern Annular Mode on future changes in Southern Hemisphere rainfall. *Geophysical Research Letters*, **43**, 7160–7167.

Lim, E. P., H. H. Hendon, and H. Rashid, 2013: Seasonal predictability of the southern annular mode due to its association with ENSO. *Journal of Climate*.

Limpasuvan, V. and D. L. Hartmann, 1999: Eddies and the annular modes of climate variability. *Geophysical Research Letters*, **26**, 3133–3136.

Lin, H., G. Brunet, and J. Derome, 2009: An observed connection between the North Atlantic oscillation and the Madden-Julian oscillation. *Journal of Climate*, **22**, 364–380.

Lorenz, D. J. and E. T. DeWeaver, 2007: Tropopause height and zonal wind response to global warming in the IPCC scenario integrations. *Journal of Geophysical Research Atmospheres*, **112**.

Lorenz, D. J. and D. L. Hartmann, 2001: Eddy–Zonal Flow Feedback in the Southern Hemisphere. *Journal of the Atmospheric Sciences*, **58**, 3312–3327.

— 2003: Eddy-zonal flow feedback in the Northern Hemisphere winter. *Journal of Climate*, **16**, 1212–1227.

Lovenduski, N. S. and N. Gruber, 2005: Impact of the Southern Annular Mode on Southern Ocean circulation and biology. *Geophysical Research Letters*, **32**.

Lovenduski, N. S., N. Gruber, S. C. Doney, and I. D. Lima, 2007: Enhanced CO2 outgassing in the Southern Ocean from a positive phase of the Southern Annular Mode. *Global Biogeochemical Cycles*, **21**.

Lu, J., G. Chen, and D. M. W. Frierson, 2010: The Position of the Midlatitude Storm Track and Eddy-Driven Westerlies in Aquaplanet AGCMs. *Journal of the Atmospheric Sciences*, **67**, 3984–4000.

Lu, J., G. Chen, and D. M. W. W. Frierson, 2008: Response of the zonal mean atmospheric circulation to El Niño versus global warming. *Journal of Climate*, **21**, 5835–5851.

Lu, J., G. A. Vecchi, and T. Reichler, 2007: Expansion of the Hadley cell under global warming. *Geophysical Research Letters*, **34**.

Luo, D., 2005: A Barotropic Envelope Rossby Soliton Model for Block–Eddy Interaction. Part I: Effect of Topography. *Journal of the Atmospheric Sciences*, **62**, 5–21.

Ma, J. and S.-P. Xie, 2013: Regional Patterns of Sea Surface Temperature Change: A Source of Uncertainty in Future Projections of Precipitation and Atmospheric Circulation. *Journal of Climate*, **26**, 2482–2501.

Ma, J., S.-P. Xie, and Y. Kosaka, 2012: Mechanisms for Tropical Tropospheric Circulation Change in Response to Global Warming. *Journal of Climate*, **25**, 2979–2994.

Madonna, E., C. Li, C. M. Grams, and T. Woollings, 2017: The link between eddy-driven jet variability and weather regimes in the North Atlantic-European sector. *Quarterly Journal of the Royal Meteorological Society*, **143**, 2960–2972.

Maher, P., E. P. Gerber, B. Medeiros, T. M. Merlis, S. Sherwood, A. Sheshadri, A. H. Sobel, G. K. Vallis, A. Voigt, and P. Zurita-Gotor, 2019: Model Hierarchies for Understanding Atmospheric Circulation. *Reviews of Geophysics*, **57**, 250–280.

Malguzzi, P. and P. Malanotte-Rizzoli, 1984: Nonlinear Stationary Rossby Waves on Nonuniform Zonal Winds and Atmospheric Blocking. Part I: The Analytical Theory. *Journal of the Atmospheric Sciences*, **41**, 2620–2628.

Manabe, S. and R. T. Wetherald, 1980: On the Distribution of Climate Change Resulting from an Increase in CO2 Content of the Atmosphere. *Journal of the Atmospheric Sciences*, **37**, 99–118.

Marshall, G. J., 2003: Trends in the Southern Annular Mode from Observations and Reanalyses. *Journal of Climate*, **16**, 4134–4143.

Marshall, G. J., D. W. J. Thompson, and M. R. Broeke, 2017: The Signature of Southern Hemisphere Atmospheric Circulation Patterns in Antarctic Precipitation. *Geophysical Research Letters*, **44**, 11,580–11,589.

Marshall, J. and R. A. Plumb, 2008: *Atmosphere, Ocean, and Climate Dynamics: An introductory text*. Elsevier, 1–345 pp.

Masato, G., B. J. Hoskins, and T. Woollings, 2013a: Wave-Breaking Characteristics of Northern Hemisphere Winter Blocking: A Two-Dimensional Approach. *Journal of Climate*, **26**, 4535–4549.

— 2013b: Winter and Summer Northern Hemisphere Blocking in CMIP5 Models. *Journal of Climate*, **26**, 7044–7059.

Masato, G., B. J. Hoskins, and T. J. Woollings, 2012: Wave-breaking characteristics of midlatitude blocking. *Quarterly Journal of the Royal Meteorological Society*, **138**, 1285–1296.

Masson, D. and R. Knutti, 2011: Climate model genealogy. *Geophysical Research Letters*, **38**.

Matsueda, M., H. Endo, and R. Mizuta, 2010: Future change in Southern Hemisphere summertime and wintertime atmospheric blockings simulated using a 20-km-mesh AGCM. *Geophysical Research Letters*, **37**.

Maycock, A. C., G. I. T. Masukwedza, P. Hitchcock, and I. R. Simpson, 2020: A regime perspective on the North Atlantic eddy-driven jet response to sudden stratospheric warmings. *Journal of Climate*, **33**, 3901–3917.

McFarlane, N. A., 1987: The Effect of Orographically Excited Gravity Wave Drag on the General Circulation of the Lower Stratosphere and Troposphere. *Journal of the Atmospheric Sciences*, **44**, 1775–1800.

McGraw, M. C. and E. A. Barnes, 2016: Seasonal sensitivity of the eddy-driven jet to tropospheric heating in an idealized AGCM. *Journal of Climate*, **29**, 5223–5240.

McIntosh, P. C. and H. H. Hendon, 2018: Understanding Rossby wave trains forced by the Indian Ocean Dipole. *Climate Dynamics*, **50**, 2783–2798.

McIntyre, M. E., 1982: How Well do we Understand the Dynamics of Stratospheric Warmings ? *Journal of the Meteorological Society of Japan*, **60**, 37–65.

McLandress, C., T. G. Shepherd, J. F. Scinocca, D. A. Plummer, M. Sigmond, A. I. Jonsson, and M. C. Reader, 2011: Separating the dynamical effects of climate change and ozone depletion. Part II: Southern Hemisphere troposphere. *Journal of Climate*, **24**, 1850–1868.

McWilliams, J. C., 1980: An application of equivalent modons to atmospheric blocking. *Dynamics of Atmospheres and Oceans*, **5**, 43–66.

Mechoso, C. R., 1980: The Atmospheric Circulation Around Antarctica: Linear Stability and Finite-Amplitude Interactions with Migrating Cyclones. *Journal of the Atmospheric Sciences*, **37**, 2209–2233.

— 1981: Topographic Influences on the General Circulation of the Southern Hemisphere: A Numerical Experiment. *Monthly Weather Review*, **109**, 2131–2139.

Meehl, G. A., 1991: A Reexamination of the Mechanism of the Semiannual Oscillation in the Southern Hemisphere. *Journal of Climate*, **4**, 911–926.

Meehl, G. A., J. W. Hurrell, and H. Van Loon, 1998: A modulation of the mechanism of the semiannual oscillation in the Southern Hemisphere. *Tellus, Series A: Dynamic Meteorology and Oceanography*.

Meinshausen, M., S. J. Smith, K. Calvin, J. S. Daniel, M. L. Kainuma, J. Lamarque, K. Matsumoto, S. A. Montzka, S. C. Raper, K. Riahi, A. Thomson, G. J. Velders, and D. P. van Vuuren, 2011: The RCP greenhouse gas concentrations and their extensions from 1765 to 2300. *Climatic Change*, **109**, 213–241.

Mendes, M. C. D., R. M. Trigo, I. F. A. A. Cavalcanti, and C. C. DaCamara, 2008: Blocking episodes in the Southern Hemisphere: Impact on the climate of adjacent continental areas. *Pure and Applied Geophysics*, **165**, 1941–1962.

Meng, Q., M. Latif, W. Park, N. S. Keenlyside, V. A. Semenov, and T. Martin, 2012: Twentieth century Walker Circulation change: Data analysis and model experiments. *Climate Dynamics*, **38**, 1757–1773.

Mindlin, J., T. G. Shepherd, C. S. Vera, M. Osman, G. Zappa, R. W. Lee, and K. I. Hodges, 2020: Storyline description of Southern Hemisphere midlatitude circulation and precipitation response to greenhouse gas forcing. *Climate Dynamics*, 1–23.

Mo, K. C., 2000: Relationships between low-frequency variability in the Southern Hemisphere and sea surface temperature anomalies. *Journal of Climate*, **13**, 3599–3610.

Mo, K. C. and M. Ghil, 1987: Statistics and dynamics of persistent anomalies. *Journal of the Atmospheric Sciences*, **44**, 877–901.

Mo, K. C., R. W. Higgins, K. C. Mo, and R. W. Higgins, 1998: The Pacific–South American Modes and Tropical Convection during the Southern Hemisphere Winter. *Monthly Weather Review*, **126**, 1581–1596.

Mo, K. C. and J. N. Paegle, 2001: The Pacific-South American modes and their downstream effects. *International Journal of Climatology*, **21**, 1211–1229.

Molteni, F., F. Kucharski, and S. Corti, 2006: On the predictability of flow-regime properties on interannual to interdecadal timescales. *Predictability of Weather and Climate*, Cambridge University Press, 365–390.

Mullen, S. L., 1987: Transient Eddy Forcing of Blocking Flows. *Journal of the Atmospheric Sciences*, **44**, 3–22.

Müller, G. V. and T. Ambrizzi, 2007: Teleconnection patterns and Rossby wave propagation associated to generalized frosts over southern South America. *Climate Dynamics*, **29**, 633–645.

Müller, G. V. and G. J. Berri, 2007: Atmospheric Circulation Associated with Persistent Generalized Frosts in Central-Southern South America. *Monthly Weather Review*, **135**, 1268–1289.

Murphy, B. F. and B. Timbal, 2008: A review of recent climate variability and climate change in southeastern Australia. *International Journal of Climatology*, **28**, 859–879.

Nakamura, H., M. Nakamura, and J. L. Anderson, 1997: The Role of High- and Low-Frequency Dynamics in Blocking Formation. *Monthly Weather Review*, **125**, 2074–2093.

Nakamura, H. and T. Sampe, 2002: Trapping of synoptic-scale disturbances into the North-Pacific subtropical jet core in midwinter. *Geophysical Research Letters*, **29**.

Nakamura, H., T. Sampe, Y. Tanimoto, and A. Shimpo, 2004: Observed associations among storm tracks, jet streams and midlatitude oceanic fronts Role of Kuroshio/Oyashio in climate View project Observed Associations Among Storm Tracks, Jet Streams and Midlatitude Oceanic Fronts. *Earth's Climate: The Ocean-Atmosphere Interaction*, C. Wang, S.-P. Xie, and J. Carton, eds., American Geophysical Union, 329–345.

Nakamura, H. and A. Shimpo, 2004: Seasonal variations in the Southern Hemisphere storm tracks and jet streams as revealed in a reanalysis dataset. *Journal of Climate*, **17**, 1828–1844.

Nakamura, N. and C. S. Y. Huang, 2018: Atmospheric blocking as a traffic jam in the jet stream. *Science*, **361**, 42–47.

Nguyen, H., H. H. Hendon, E. P. Lim, G. Boschat, E. Maloney, and B. Timbal, 2018: Variability of the extent of the Hadley circulation in the southern hemisphere: a regional perspective. *Climate Dynamics*, **50**, 129–142.

Nie, Y., Y. Zhang, X. Yang, and H. Ren, 2019: Winter and Summer Rossby Wave Sources in the CMIP5 Models. *Earth and Space Science*, **6**, 1831–1846.

Nigam, S. and E. DeWeaver, 2015: Dynamical Meteorology — Stationary Waves (Orographic and Thermally Forced). *Encyclopedia of Atmospheric Sciences*, 431–445.

Novak, L., M. H. P. Ambaum, and R. Tailleux, 2015: The Life Cycle of the North Atlantic Storm Track. *Journal of the Atmospheric Sciences*, **72**, 821–833.

Ogawa, F., H. Nakamura, K. Nishii, T. Miyasaka, and A. Kuwano-Yoshida, 2016: Importance of Midlatitude Oceanic Frontal Zones for the Annular Mode Variability: Interbasin Differences in the Southern Annular Mode Signature. *Journal of Climate*, **29**, 6179–6199.

Ogura, T. and A. Abe-Ouchi, 2001: Influence of the Antarctic Ice Sheet on southern high latitude climate during the Cenozoic: Albedo vs topography effect. *Geophysical Research Letters*, **28**, 587–590.

O'Kane, T. J., D. P. Monselesan, and J. S. Risbey, 2017: A Multiscale Reexamination of the Pacific–South American Pattern. *Monthly Weather Review*, **145**, 379–402.

O'Kane, T. J., J. S. Risbey, C. Franzke, and D. P. Monselesan, 2013: Changes in the Metastability of the Midlatitude Southern Hemisphere Circulation and the Utility of Nonstationary Cluster Analysis and Split-Flow Blocking Indices as Diagnostic Tools. *Journal of the Atmospheric Sciences*, **70**, 824–842.

O'Neill, B. C., E. Kriegler, K. L. Ebi, E. Kemp-Benedict, K. Riahi, D. S. Rothman, B. J. van Ruijven, D. P. van Vuuren, J. Birkmann, K. Kok, M. Levy, and W. Solecki, 2017: The roads ahead: Narratives for shared socioeconomic pathways describing world futures in the 21st century. *Global Environmental Change*, **42**, 169–180.

Oort, A. H. and J. J. Yienger, 1996: Observed Interannual Variability in the Hadley Circulation and Its Connection to ENSO. *Journal of Climate*, **9**, 2751–2767.

O'Reilly, C. H., S. Minobe, A. Kuwano-Yoshida, and T. Woollings, 2017: The Gulf Stream influence on wintertime North Atlantic jet variability. *Quarterly Journal of the Royal Meteorological Society*, **143**, 173–183.

Orlanski, I., 2003: Bifurcation in Eddy Life Cycles: Implications for Storm Track Variability. *Journal of the Atmospheric Sciences*, **60**, 993–1023.

O'Rourke, A. K. and G. K. Vallis, 2013: Jet Interaction and the Influence of a Minimum Phase Speed Bound on the Propagation of Eddies. *Journal of the Atmospheric Sciences*, **70**, 2614–2628.

— 2016: Meridional Rossby Wave Generation and Propagation in the Maintenance of the Wintertime Tropospheric Double Jet. *Journal of the Atmospheric Sciences*, **73**, 2179–2201.

Oueslati, B. and G. Bellon, 2015: The double ITCZ bias in CMIP5 models: interaction between SST, large-scale circulation and precipitation. *Climate Dynamics*, **44**, 585–607.

Palmer, T. N., 1999: A nonlinear dynamical perspective on climate prediction. *Journal of Climate*, **12**.

— 2001: A nonlinear dynamical perspective on model error: A proposal for non-local stochastic-dynamic parametrization in weather and climate prediction models. *Part B J. R. Meteorol. Soc*, **127**, 279–304.

Papritz, L. and T. Spengler, 2015: Analysis of the slope of isentropic surfaces and its tendencies over the North Atlantic. *Quarterly Journal of the Royal Meteorological Society*, **141**, 3226–3238.

Parish, T. R. and D. H. Bromwich, 2007: Reexamination of the Near-Surface Airflow over the Antarctic Continent and Implications on Atmospheric Circulations at High Southern Latitudes*. *Monthly Weather Review*, **135**, 1961–1973.

Parish, T. R., D. H. Bromwich, and Ren-Yow Tzeng, 1994: On the role of the Antarctic continent in forcing large-scale circulations in the high southern latitudes. *Journal of the Atmospheric Sciences*, **51**, 3566–3579.

Parker, T. J., G. J. Berry, and M. J. Reeder, 2014: The structure and evolution of heat waves in Southeastern Australia. *Journal of Climate*, **27**.

Parsons, S., J. A. Renwick, and A. J. McDonald, 2016: An Assessment of Future Southern Hemisphere Blocking Using CMIP5 Projections from Four GCMs. *Journal of Climate*, **29**, 7599–7611.

Patterson, M., T. Bracegirdle, and T. Woollings, 2019: Southern Hemisphere atmospheric blocking in CMIP5 and future changes in the Australia-New Zealand sector. *Geophysical Research Letters*, **46**, 9281–9290.

Pelly, J. L. and B. J. Hoskins, 2003: A New Perspective on Blocking. *Journal of the Atmospheric Sciences*, **60**.

Peltier, W., 2004: Global Glacial Isostasy and the surface of the Ice-Age Earth: The ICE-5G (VM2) Model and GRACE. *Annual Review of Earth and Planetary Sciences*, **32**, 111–149.

Perkins-Kirkpatrick, S. E., C. J. White, L. V. Alexander, D. Argüeso, G. Boschat, T. Cowan, J. P. Evans, M. Ekström, E. C. J. Oliver, A. Phatak, and A. Purich, 2016: Natural hazards in Australia: heatwaves. *Climatic Change*, **139**, 101–114.

Pezza, A. B., P. van Rensch, and W. Cai, 2012: Severe heat waves in Southern Australia: synoptic climatology and large scale connections. *Climate Dynamics*, **38**, 209–224.

Pfahl, S., C. Schwierz, M. Croci-Maspoli, C. M. Grams, and H. Wernli, 2015: Importance of latent heat release in ascending air streams for atmospheric blocking. *Nature Geoscience*, **8**, 610–614.

Pithan, F. and I. Polichtchouk, 2020: Effects of Topography and Realistic Drag on the Southern Hemisphere Midlatitude Jet in a Dry Model. *Journal of Advances in Modeling Earth Systems*, **12**.

Pithan, F., T. G. Shepherd, G. Zappa, and I. Sandu, 2016: Climate model biases in jet streams, blocking and storm tracks resulting from missing orographic drag. *Geophysical Research Letters*, **43**, 7231–7240.

Plesca, E., V. Grützun, and S. A. Buehler, 2018: How Robust Is the Weakening of the Pacific Walker Circulation in CMIP5 Idealized Transient Climate Simulations? *Journal of Climate*, **31**, 81–97.

Plumb, R. A., 1985: On the Three-Dimensional Propagation of Stationary Waves. *Journal of the Atmospheric Sciences*, **42**, 217–229.

Pohl, B. and N. Fauchereau, 2012: The southern annular mode seen through weather regimes. *Journal of Climate*, **25**, 3336–3354.

Polvani, L. M. and P. J. Kushner, 2002: Tropospheric response to stratospheric perturbations in a relatively simple general circulation model. *Geophysical Research Letters*, **29**, 1114.

Polvani, L. M., M. Previdi, and C. Deser, 2011: Large cancellation, due to ozone recovery, of future Southern Hemisphere atmospheric circulation trends. *Geophysical Research Letters*, **38**.

Pook, M. J., P. C. McIntosh, and G. A. Meyers, 2006: The Synoptic Decomposition of Cool-Season Rainfall in the Southeastern Australian Cropping Region. *Journal of Applied Meteorology and Climatology*, **45**, 1156–1170.

Pook, M. J., J. S. Risbey, P. C. Mcintosh, C. C. Ummenhofer, A. G. Marshall, and G. A. Meyers, 2013: The Seasonal Cycle of Blocking and Associated Physical Mechanisms in the Australian Region and Relationship with Rainfall. *Monthly Weather Review*, **141**, 4534–4553.

Potter, S. F., T. Spengler, and I. M. Held, 2013: Reflection of barotropic rossby waves in sheared flow and validity of the WKB approximation. *Journal of the Atmospheric Sciences*, **70**, 2170–2178.

Power, S. B. and G. Kociuba, 2011a: The impact of global warming on the Southern Oscillation Index. *Climate Dynamics*, **37**, 1745–1754.

— 2011b: What Caused the Observed Twentieth-Century Weakening of the Walker Circulation? *Journal of Climate*, **24**, 6501–6514.

Priestley, M. D. K., D. Ackerley, J. L. Catto, K. I. Hodges, R. E. McDonald, and R. W. Lee, 2020: An Overview of the Extratropical Storm Tracks in CMIP6 Historical Simulations. *Journal of Climate*, **33**, 6315–6343.

Quintanar, A. and C. Mechoso, 1995: Quasi-Stationary Waves in the Southern Hemisphere. Part II: Generation Mechanisms. *Journal of Climate*, **8**, 2673–2689.

Randel, W. J. and F. Wu, 1999: Cooling of the Arctic and Antarctic Polar Stratospheres due to Ozone Depletion. *Journal of Climate*, **12**, 1467–1479.

Reed, R. J., M. T. Stoelinga, and Y.-H. Kuo, 1992: A Model-aided Study of the Origin and Evolution of the Anomalously High Potential vorticity in the Inner Region of a Rapidly Deepening Marine Cyclone. *Monthly Weather Review*, **120**, 893–913.

Reinhold, B. B. and R. T. Pierrehumbert, 1982: Dynamics of Weather Regimes: Quasi-Stationary Waves and Blocking. *Monthly Weather Review*, **110**, 1105–1145.

Renwick, J. A., 2005: Persistent Positive Anomalies in the Southern Hemisphere Circulation. *Monthly Weather Review*, **133**, 977–988.

Renwick, J. A. and M. J. Revell, 1999: Blocking over the South Pacific and Rossby Wave Propagation. *Monthly Weather Review*, **127**, 2233–2247.

Rex, D. F., 1950: Blocking Action in the Middle Troposphere and its Effect upon Regional Climate. *Tellus*, **2**, 196–211.

Rhines, P. B., 1975: Waves and Turbulence on a Beta Plane. *J. Fluid Mech.*, **69**, 417–443.

— 1994: Jets. *Chaos*, **4**, 313–339.

Riahi, K., S. Rao, V. Krey, C. Cho, V. Chirkov, G. Fischer, G. Kindermann, N. Nakicenovic, and P. Rafaj, 2011: RCP 8.5-A scenario of comparatively high greenhouse gas emissions. *Climatic Change*, **109**, 33–57.

Risbey, J. S., D. P. Monselesan, T. J. O'Kane, C. R. Tozer, M. J. Pook, and P. T. Hayman, 2019: Synoptic and Large-Scale Determinants of Extreme Austral Frost Events. *Journal of Applied Meteorology and Climatology*, **58**, 1103–1124.

Risbey, J. S., T. J. O'Kane, D. P. Monselesan, C. L. E. Franzke, and I. Horenko, 2018: On the Dynamics of Austral Heat Waves. *Journal of Geophysical Research: Atmospheres*, **123**, 38–57.

Ritchie, J. and H. Dowlatabadi, 2017: Why do climate change scenarios return to coal? *Energy*, **140**, 1276–1291.

Rivière, G., 2011: A Dynamical Interpretation of the Poleward Shift of the Jet Streams in Global Warming Scenarios. *Journal of the Atmospheric Sciences*, **68**, 1253–1272.

Rivière, G. and I. Orlanski, 2007: Characteristics of the Atlantic Storm-Track Eddy Activity and Its Relation with the North Atlantic Oscillation. *Journal of the Atmospheric Sciences*, **64**, 241–266.

Robertson, A. W., Y. Kushnir, U. Lall, and J. Nakamura, 2015: Weather and Climatic Drivers of Extreme Flooding Events over the Midwest of the United States. *Extreme Events: Observations, Modeling, and Economics*, M. Chavez, M. Ghi, and J. Urrutia-Fucugauchi, eds., Wiley, chapter 9, 113–124.

Robertson, A. W. and C. R. Mechoso, 2003: Circulation regimes and low-frequency oscillations in the South Pacific sector. *Monthly Weather Review*, **131**, 1566–1576.

Rodrigues, R. and T. Woollings, 2017: Impact of Atmospheric Blocking on South America in Austral Summer. *Journal of Climate*, **30**, 1821–1837.

Roff, G., D. W. J. Thompson, and H. Hendon, 2011: Does increasing model stratospheric resolution improve extended-range forecast skill? *Geophysical Research Letters*, **38**.

Roscoe, H. K., J. D. Shanklin, and S. R. Colwell, 2005: Has the Antarctic vortex split before 2002? *Journal of the Atmospheric Sciences*, **62**, 581–588.

Rossby, C.-G., 1939: Relation between variations in the intensity of the zonal circulation of the atmosphere and the displacements of the semi-permanent centers of action. *Journal of Marine Research*, **2**, 38–55.

Salinger, M. J., J. Renwick, E. Behrens, A. B. Mullan, H. J. Diamond, P. Sirguey, R. O. Smith, M. C. T. Trought, L. Alexander, N. J. Cullen, B. B. Fitzharris, C. D. Hepburn, A. K. Parker, and P. J. Sutton, 2019: The unprecedented coupled ocean-atmosphere summer heatwave in the New Zealand region 2017/18: drivers, mechanisms and impacts. *Environmental Research Letters*, **14**.

Sallée, J. B., K. G. Speer, and S. R. Rintoul, 2010: Zonally asymmetric response of the Southern Ocean mixed-layer depth to the Southern Annular Mode. *Nature Geoscience*, **3**, 273–279.

Sampe, T., H. Nakamura, A. Goto, and W. Ohfuchi, 2010: Significance of a Midlatitude SST Frontal Zone in the Formation of a Storm Track and an Eddy-Driven Westerly Jet. *Journal of Climate*, **23**, 1793–1814.

Sardeshmukh, P. and B. Hoskins, 1988: The Generation of Global Rotational Flow by Steady Idealized Tropical Divergence. *Journal of the Atmospheric Sciences*, **45**, 1228–1250.

Scaife, A. A., D. Copsey, C. Gordon, C. Harris, T. Hinton, S. Keeley, A. O'Neill, M. Roberts, and K. Williams, 2011: Improved Atlantic winter blocking in a climate model. *Geophysical Research Letters*, **38**.

Scaife, A. A., T. Woollings, J. Knight, G. Martin, and T. Hinton, 2010: Atmospheric Blocking and Mean Biases in Climate Models. *Journal of Climate*, **23**, 6143–6152.

Schiemann, R., M.-E. Demory, L. C. Shaffrey, J. Strachan, P. L. Vidale, M. S. Mizielinski, M. J. Roberts, M. Matsueda, M. F. Wehner, and T. Jung, 2017: The Resolution Sensitivity of Northern Hemisphere Blocking in Four 25-km Atmospheric Global Circulation Models. *Journal of Climate*, **30**, 337–358.

Schneider, D. P., C. Deser, and T. Fan, 2015: Comparing the Impacts of Tropical SST Variability and Polar Stratospheric Ozone Loss on the Southern Ocean Westerly Winds*. *Journal of Climate*, **28**, 9350–9372.

Schneider, D. P., Y. Okumura, and C. Deser, 2012: Observed Antarctic interannual climate variability and tropical linkages. *Journal of Climate*, **25**, 4048–4065.

Schneider, E. K., 1977: Axially Symmetric Steady-State Models of the Basic State for Instability and Climate Studies. Part II. Nonlinear Calculations. *Journal of the Atmospheric Sciences*, **34**, 280–296.

Schneider, T., 2006: The General Circulation of the Atmosphere. *Annual Review of Earth and Planetary Sciences*, **34**, 655–688.

Schneider, T. and S. Bordoni, 2008: Eddy-Mediated Regime Transitions in the Seasonal Cycle of a Hadley Circulation and Implications for Monsoon Dynamics. *Journal of the Atmospheric Sciences*, **65**, 915–934.

Schwendike, J., P. Govekar, M. J. Reeder, R. Wardle, G. J. Berry, and C. Jakob, 2014: Local partitioning of the overturning circulation in the tropics and the connection to the Hadley and Walker circulations. *Journal of Geophysical Research*.

Schwerdtfeger, W. and F. Prohash, 1956: The semi-annual pressure oscillation, its cause and effects. *J Atmos Sci*, **13**, 217–218.

Seager, R., M. Cane, N. Henderson, D. E. Lee, R. Abernathey, and H. Zhang, 2019: Strengthening tropical Pacific zonal sea surface temperature gradient consistent with rising greenhouse gases. *Nature Climate Change*, **9**, 517–522.

Seager, R., N. Harnik, W. A. Robinson, Y. Kushnir, M. Ting, H. P. Huang, and J. Velez, 2005: Mechanisms of ENSO-forcing of hemispherically symmetric precipitation variability. *Quarterly Journal of the Royal Meteorological Society*, **131**, 1501–1527.

Selten, F. M., G. W. Branstator, H. A. Dijkstra, and M. Kliphuis, 2004: Tropical origins for recent and future Northern Hemisphere climate change. *Geophysical Research Letters*, **31**.

Sen Gupta, A. and M. H. England, 2006: Coupled Ocean–Atmosphere–Ice Response to Variations in the Southern Annular Mode. *Journal of Climate*, **19**, 4457–4486.

Seviour, W. J., S. C. Hardiman, L. J. Gray, N. Butchart, C. Maclachlan, and A. A. Scaife, 2014: Skillful seasonal prediction of the southern annular mode and Antarctic Ozone. *Journal of Climate*, **27**, 7462–7474.

Shaw, T. A., 2019: Mechanisms of Future Predicted Changes in the Zonal Mean Mid-Latitude Circulation. *Current Climate Change Reports*, **5**, 345–357.

Shaw, T. A. and A. Voigt, 2016: Understanding the Links between Subtropical and Extratropical Circulation Responses to Climate Change Using Aquaplanet Model Simulations. *Journal of Climate*, **29**, 6637–6657.

Shepherd, T. G., 2014: Atmospheric circulation as a source of uncertainty in climate change projections. *Nature Geoscience*, **7**, 703–708.

Shutts, G. J., 1983: The propagation of eddies in diffluent jetstreams: Eddy vorticity forcing of 'blocking' flow fields. *Quarterly Journal of the Royal Meteorological Society*, **109**, 737–761.

Sillmann, J., M. Croci-Maspoli, M. Kallache, and R. W. Katz, 2011: Extreme Cold Winter Temperatures in Europe under the Influence of North Atlantic Atmospheric Blocking. *Journal of Climate*, **24**, 5899–5913.

Simmonds, I. and R. Law, 1995: Associations between Antarctic katabatic flow and the upper level winter vortex. *International Journal of Climatology*, **15**, 403–421.

Simpkins, G. R., S. McGregor, A. S. Taschetto, L. M. Ciasto, and M. H. England, 2014: Tropical Connections to Climatic Change in the Extratropical Southern Hemisphere: The Role of Atlantic SST Trends. *Journal of Climate*, **27**, 4923–4936.

Simpson, I. R., M. Blackburn, and J. D. Haigh, 2009: The Role of Eddies in Driving the Tropospheric Response to Stratospheric Heating Perturbations. *Journal of the Atmospheric Sciences*, **66**, 1347–1365.

Simpson, I. R. and L. M. Polvani, 2016: Revisiting the relationship between jet position, forced response, and annular mode variability in the southern midlatitudes. *Geophysical Research Letters*, **43**, 2896–2903.

Simpson, I. R., R. Seager, M. Ting, and T. A. Shaw, 2016: Causes of change in Northern Hemisphere winter meridional winds and regional hydroclimate. *Nature Climate Change*, **6**, 65–70.

Simpson, I. R., T. Shaw, and R. Seager, 2014: A diagnosis of the seasonally and longitudinally varying mid-latitude circulation response to global warming. *Journal of the Atmospheric Sciences*, **71**, 2489–2515.

Sinclair, M. R., 1996: A Climatology of Anticyclones and Blocking for the Southern Hemisphere. *Monthly Weather Review*, **124**, 245–264.

Singh, H. K. A., C. M. Bitz, and D. M. W. Frierson, 2016: The Global Climate Response to Lowering Surface Orography of Antarctica and the Importance of Atmosphere–Ocean Coupling. *Journal of Climate*, **29**, 4137–4153.

Solomon, S., D. J. Ivy, D. Kinnison, M. J. Mills, R. R. Neely, and A. Schmidt, 2016: Emergence of healing in the Antarctic ozone layer. *Science*, **353**, 269–274.

Son, S.-W., E. P. Gerber, J. Perlwitz, L. M. Polvani, N. P. Gillett, K.-H. Seo, V. Eyring, T. G. Shepherd, D. Waugh, H. Akiyoshi, J. Austin, A. Baumgaertner, S. Bekki, P. Braesicke, C. Brühl, N. Butchart, M. P. Chipperfield, D. Cugnet, M. Dameris, S. Dhomse, S. Frith, H. Garny, R. Garcia, S. C. Hardiman, P. Jöckel, J. F. Lamarque, E. Mancini, M. Marchand, M. Michou, T. Nakamura, O. Morgenstern, G. Pitari, D. A. Plummer, J. Pyle, E. Rozanov, J. F. Scinocca, K. Shibata, D. Smale, H. Teyssèdre, W. Tian, and Y. Yamashita, 2010: Impact of stratospheric ozone on Southern Hemisphere circulation change: A multimodel assessment. *Journal of Geophysical Research*, **115**.

Son, S.-W. and S. Lee, 2005: The Response of Westerly Jets to Thermal Driving in a Primitive Equation Model. *Journal of the Atmospheric Sciences*, **62**, 3741–3757.

Son, S. W., L. M. Polvani, W. Waugh, H. Akiyoshi, R. Garcia, D. Kinnison, S. Pawson, E. Rozanov, T. G. Shepherd, and K. Shibata, 2008: The impact of stratospheric ozone recovery on the Southern Hemisphere westerly jet. *Science*, **320**, 1486–1489.

Son, S.-W., A. Purich, H. H. Hendon, B.-M. Kim, and L. M. Polvani, 2013: Improved seasonal forecast using ozone hole variability? *Geophysical Research Letters*, **40**, 6231–6235.

Son, S.-W., M. Ting, and L. M. Polvani, 2009: The Effect of Topography on Storm-Track Intensity in a Relatively Simple General Circulation Model. *Journal of the Atmospheric Sciences*, **66**, 393–411.

Spensberger, C., M. J. Reeder, T. Spengler, and M. Patterson, 2019: The connection between the Southern Annular Mode and a feature-based perspective on Southern Hemisphere mid-latitude winter variability. *Journal of Climate*, **33**, 115–129.

Spensberger, C. and T. Spengler, 2020: Feature-based Jet Variability in the Upper Troposphere. *Journal of Climate*.

Steinfeld, D. and S. Pfahl, 2019: The role of latent heating in atmospheric blocking dynamics: a global climatology. *Climate Dynamics*, **53**, 6159–6180.

Stephenson, D. B., A. Hannachi, and A. O'Neill, 2004: On the existence of multiple climate regimes. *Quarterly Journal of the Royal Meteorological Society*, **130**, 583–605.

Stephenson, D. B. and I. M. Held, 1993: GCM Response of Northern Winter Stationary Waves and Storm Tracks to Increasing Amounts of Carbon Dioxide. *Journal of Climate*, **6**, 1859–1870.

Stocker, T. F., D. Qin, G.-K. Plattner, M. M. B. Tignor, S. K. Allen, J. Boschung, A. Nauels, Y. Xia, V. Bex, and P. M. Midgley, 2013: *Climate Change 2013 The Physical Science Basis Working Group I Contribution to the Fifth Assessment Report of the Intergovernmental Panel on Climate Change Edited by*. Cambridge University Press, Cambridge.

Strong, C. and R. E. Davis, 2008: Variability in the position and strength of winter jet stream cores related to northern hemisphere teleconnections. *Journal of Climate*, **21**, 584–592.

Sura, P. and A. Hannachi, 2015: Perspectives of non-gaussianity in atmospheric synoptic and low-frequency variability. *Journal of Climate*, **28**, 5091–5112.

Sura, P., M. Newman, C. Penland, and P. Sardeshmukh, 2005: Multiplicative Noise and Non-Gaussianity: A Paradigm for Atmospheric Regimes? *Journal of the Atmospheric Sciences*, **62**, 1391–1409.

Sutton, R. T., B. Dong, and J. M. Gregory, 2007: Land/sea warming ratio in response to climate change: IPCC AR4 model results and comparison with observations. *Geophysical Research Letters*, **34**.

Swart, N. C. and J. C. Fyfe, 2012: Observed and simulated changes in the Southern Hemisphere surface westerly wind-stress. *Geophysical Research Letters*, **39**.

Swart, N. C., J. C. Fyfe, N. Gillett, and G. J. Marshall, 2015: Comparing Trends in the Southern Annular Mode and Surface Westerly Jet. *Journal of Climate*, **28**, 8840–8859.

Takaya, K. and H. Nakamura, 2001: A Formulation of a Phase-Independent Wave-Activity Flux for Stationary and Migratory Quasigeostrophic Eddies on a Zonally Varying Basic Flow. *Journal of the Atmospheric Sciences*, **58**, 608–627.

Tandon, N. F., E. P. Gerber, A. H. Sobel, and L. M. Polvani, 2013: Understanding hadley cell expansion versus contraction: Insights from simplified models and implications for recent observations. *Journal of Climate*, **26**, 4304–4321.

Taylor, K. E., R. J. Stouffer, and G. A. Meehl, 2012: An Overview of CMIP5 and the Experiment Design. *Bulletin of the American Meteorological Society*, **93**, 485–498.

Taylor, K. E., D. Williamson, and F. Zwiers, 2000: The sea surface temperature and sea-ice concentration boundary conditions for AMIP II simulations. Technical report.

Tennant, W., 2004: Considerations when using pre-1979 NCEP/NCAR reanalyses in the southern hemisphere. *Geophysical Research Letters*, **31**.

Thompson, D. W. and E. A. Barnes, 2014: Periodic variability in the large-scale Southern Hemisphere atmospheric circulation. *Science*, **343**, 641–645.

Thompson, D. W. and J. M. Wallace, 2001: Regional climate impacts of the Northern Hemisphere annular mode. *Science*, **293**, 85–9.

Thompson, D. W. J., S. Solomon, E. T. Buitenhuis, T. J. Conway, R. Langenfelds, A. Gomez, C. Labuschagne, M. Ramonet, T. Nakazawa, N. Metzl, N. Gillett, and M. Heimann, 2002: Interpretation of recent Southern Hemisphere climate change. *Science*, **296**, 895–899.

Thompson, D. W. J., S. Solomon, P. J. Kushner, M. H. England, K. M. Grise, and D. J. Karoly, 2011: Signatures of the Antarctic ozone hole in Southern Hemisphere surface climate change. *Nature Geoscience*, **4**, 741–749.

Thompson, D. W. J. and J. M. Wallace, 2000: Annular Modes in the Extratropical Circulation. Part I: Month-to-Month Variability*. *Journal of the Atmospheric Sciences*, **13**, 1000–1016.

Thompson, D. W. J. and J. D. Woodworth, 2014: Barotropic and Baroclinic Annular Variability in the Southern Hemisphere. *Journal of the Atmospheric Sciences*, **71**, 1480–1493.

Thomson, S. I. and G. K. Vallis, 2018: Atmospheric Response to SST Anomalies. Part I: Background-State Dependence, Teleconnections, and Local Effects in Winter. *Journal of the Atmospheric Sciences*, **75**, 4107–4124.

Tibaldi, S. and F. Molteni, 1990: On the operational predictability of blocking. *Tellus A*, **42**, 343–365.

Tibaldi, S., E. Tosi, A. Navarra, and L. Pedulli, 1994: Northern and Southern Hemisphere Seasonal Variability of Blocking Frequency and Predictability. *Monthly Weather Review*, **122**, 1971–2003.

Tilly, D. E., A. R. Lupo, C. J. Melick, and P. S. Market, 2008: Calculated Height Tendencies in Two Southern Hemisphere Blocking and Cyclone Events: The Contribution of Diabatic Heating to Block Intensification. *Monthly Weather Review*, **136**, 3568–3578.

Tozer, C. R., J. S. Risbey, T. J. O'Kane, D. P. Monselesan, and M. J. Pook, 2018: The Relationship between Wave Trains in the Southern Hemisphere Storm Track and Rainfall Extremes over Tasmania. *Monthly Weather Review*, **146**, 4201–4230.

Trenberth, K. E., 1991: Storm Tracks in the Southern Hemisphere. *Journal of the Atmospheric Sciences*, **48**, 2159–2178.

Trenberth, K. E. and J. M. Caron, 2001: Estimates of Meridional Atmosphere and Ocean Heat Transports. *Journal of Climate*, **14**, 3433–3443.

Trenberth, K. E. and J. T. Fasullo, 2012: Climate extremes and climate change: The Russian heat wave and other climate extremes of 2010. *Journal of Geophysical Research Atmospheres*, **117**.

Trenberth, K. F. and K. C. Mo, 1985: Blocking in the Southern Hemisphere. *Monthly Weather Review*, **113**, 3–21.

Tripathi, O. P., M. Baldwin, A. Charlton-Perez, M. Charron, S. D. Eckermann, E. Gerber, R. G. Harrison, D. R. Jackson, B. M. Kim, Y. Kuroda, A. Lang, S. Mahmood, R. Mizuta, G. Roff, M. Sigmond, and S. W. Son, 2015: The predictability of the extratropical stratosphere on monthly time-scales and its impact on the skill of tropospheric forecasts. *Quarterly Journal of the Royal Meteorological Society*, **141**, 987–1003.

Tung, K. K. and R. S. Lindzen, 1979: A Theory of Stationary Long Waves. Part I: A Simple Theory of Blocking. *Monthly Weather Review*, **107**, 714–734.

Turner, J., T. Phillips, J. S. Hosking, G. J. Marshall, and A. Orr, 2013: The amundsen sea low. *International Journal of Climatology*, **33**, 1818–1829.

Uppala, S. M., P. W. Kållberg, and A. J. Simmons, 2005: The ERA-40 re-analysis. *Quarterly Journal of the Royal Meteorological Society*, **131**, 2961–3012.

Vallis, G. K., 2017: *Atmospheric and oceanic fluid dynamics: Fundamentals and large-scale circulation, second edition*. Cambridge University Press, 1–946 pp.

Vallis, G. K., G. Colyer, R. Geen, E. Gerber, M. Jucker, P. Maher, A. Paterson, M. Pietschnig, J. Penn, and S. I. Thomson, 2018: Isca, v1.0: a framework for the global modelling of the atmospheres of Earth and other planets at varying levels of complexity. *Geoscientific Model Development*, **11**, 843–859.

Vallis, G. K., E. P. Gerber, P. J. Kushner, and B. A. Cash, 2004: A Mechanism and Simple Dynamical Model of the North Atlantic Oscillation and Annular Modes. *Journal of the Atmospheric Sciences*, **61**, 264–280.

Vallis, G. K., P. Zurita-Gotor, C. Cairns, and J. Kidston, 2015: Response of the large-scale structure of the atmosphere to global warming. *Quarterly Journal of the Royal Meteorological Society*, **141**, 1479–1501.

van Loon, H., 1967: The half-yearly oscillations in middle and high Southern latitudes and the coreless winter. *J Atmos Sci*, **24**, 472–486.

van Loon, H., J. J. Taljaard, T. Sasamori, J. London, D. V. Hoyt, K. Labitzke, and C. W. Newton, 1972: *Meteorology of the Southern Hemisphere*. American Meteorological Society.

van Niekerk, A., J. F. Scinocca, and T. G. Shepherd, 2017: The Modulation of Stationary Waves, and Their Response to Climate Change, by Parameterized Orographic Drag. *Journal of the Atmospheric Sciences*, **74**, 2557–2574.

Vecchi, G. A. and B. J. Soden, 2007: Global Warming and the Weakening of the Tropical Circulation. *Journal of Climate*, **20**, 4316–4340.

Vecchi, G. A., B. J. Soden, A. T. Wittenberg, I. M. Held, A. Leetmaa, and M. J. Harrison, 2006: Weakening of tropical Pacific atmospheric circulation due to anthropogenic forcing. *Nature*, **441**, 73–76.

Voigt, A. and T. A. Shaw, 2015: Circulation response to warming shaped by radiative changes of clouds and water vapour. *Nature Geoscience*, **8**, 102–106.

— 2016: Impact of Regional Atmospheric Cloud Radiative Changes on Shifts of the Extratropical Jet Stream in Response to Global Warming. *Journal of Climate*, **29**, 8399–8421.

Walker, C. C. and T. Schneider, 2006: Eddy Influences on Hadley Circulations: Simulations with an Idealized GCM. *Journal of the Atmospheric Sciences*, **63**, 3333–3350.

Walker, N. D., 1990: Links between South African summer rainfall and temperature variability of the Agulhas and Benguela Current systems. *Journal of Geophysical Research*, **95**, 3297.

Wallace, J. M. and D. S. Gutzler, 1981: Teleconnections in the Geopotential Height Field during the Northern Hemisphere Winter. *Monthly Weather Review*, **109**, 784–812.

Walsh, K. J., I. Simmonds, and M. Collier, 2000: Sigma-coordinate calculation of topographically forced baroclinicity around Antarctica. *Dynamics of Atmospheres and Oceans*, **33**, 1–29.

Wang, C., 2002: Atmospheric Circulation Cells Associated with the El Niño–Southern Oscillation. *Journal of Climate*, **15**, 399–419.

Wang, H. and M. Ting, 1999: Seasonal Cycle of the Climatological Stationary Waves in the NCEP–NCAR Reanalysis. *Journal of the Atmospheric Sciences*, **56**, 3892–3919.

Waugh, D. W., A. Banerjee, J. C. Fyfe, and L. M. Polvani, 2020: Contrasting recent trends in Southern Hemisphere Westerlies across different ocean basins. *Geophysical Research Letters*.

Waugh, D. W., C. I. Garfinkel, and L. M. Polvani, 2015: Drivers of the Recent Tropical Expansion in the Southern Hemisphere: Changing SSTs or Ozone Depletion? *Journal of Climate*, **28**, 6581–6586.

Waugh, D. W., W. J. Randel, S. Pawson, P. A. Newman, and E. R. Nash, 1999: Persistence of the lower stratospheric polar vortices. *Journal of Geophysical Research: Atmospheres*, **104**, 27191–27201.

WCRP, 2008: 'https://pcmdi.llnl.gov/mips/cmip5/', retrieved on 04/03/2020.

Wilcox, L. J., A. J. Charlton-Perez, and L. J. Gray, 2012: Trends in Austral jet position in ensembles of high- and low-top CMIP5 models. *Journal of Geophysical Research Atmospheres*, **117**, 1–10.

Williams, A. P., E. R. Cook, J. E. Smerdon, B. I. Cook, J. T. Abatzoglou, K. Bolles, S. H. Baek, A. M. Badger, and B. Livneh, 2020: Large contribution from an-

thropogenic warming to an emerging North American megadrought. *Science*, **368**, 314–318.

Williams, L. N., S. Lee, and S.-W. Son, 2007: Dynamics of the Southern Hemisphere Spiral Jet. *Journal of the Atmospheric Sciences*, **64**, 548–563.

Wills, R. C., R. H. White, and X. J. Levine, 2019: Northern Hemisphere Stationary Waves in a Changing Climate. *Current Climate Change Reports*, **5**, 372–389.

Wirth, V., 2020: Waveguidability of idealized midlatitude jets and the limitations of ray tracing theory. *Weather and Climate Dynamics*, **1**, 111–125.

Woollings, T., 2010: Dynamical influences on European climate: an uncertain future. *Philosophical transactions. Series A, Mathematical, physical, and engineering sciences*, **368**, 3733–3756.

Woollings, T., E. Barnes, B. Hoskins, Y.-O. Kwon, R. W. Lee, C. Li, E. Madonna, M. McGraw, T. Parker, R. Rodrigues, C. Spensberger, and K. Williams, 2017: Daily to decadal modulation of jet variability. *Journal of Climate*, **31**, 1297–1314.

Woollings, T., D. Barriopedro, J. Methven, S.-W. Son, O. Martius, B. Harvey, J. Sillmann, A. R. Lupo, and S. Seneviratne, 2018: Blocking and its Response to Climate Change. *Current Climate Change Reports*, 1–14.

Woollings, T., C. Czuchnicki, and C. Franzke, 2014: Twentieth century North Atlantic jet variability. *Quarterly Journal of the Royal Meteorological Society*, **140**, 783–791.

Woollings, T., A. Hannachi, and B. Hoskins, 2010a: Variability of the North Atlantic eddy-driven jet stream. *Quarterly Journal of the Royal Meteorological Society*, **136**, 856–868.

Woollings, T., A. Hannachi, B. Hoskins, and A. Turner, 2010b: A regime view of the North Atlantic oscillation and its response to anthropogenic forcing. *Journal of Climate*, **23**, 1291–1307.

Woollings, T., B. Hoskins, M. Blackburn, and P. Berrisford, 2008: A New Rossby Wave–Breaking Interpretation of the North Atlantic Oscillation. *Journal of the Atmospheric Sciences*, **65**, 609–626.

Woollings, T., L. Papritz, C. Mbengue, and T. Spengler, 2016: Diabatic heating and jet stream shifts: A case study of the 2010 negative North Atlantic Oscillation winter. *Geophysical Research Letters*, **43**, 9994–10002.

Woollings, T., J. G. Pinto, and J. A. Santos, 2011: Dynamical Evolution of North Atlantic Ridges and Poleward Jet Stream Displacements. *Journal of the Atmospheric Sciences*, **68**, 954–963.

Wu, Y., R. Seager, T. A. Shaw, M. Ting, and N. Naik, 2013: Atmospheric Circulation Response to an Instantaneous Doubling of Carbon Dioxide. Part II: Atmospheric Transient Adjustment and Its Dynamics. *Journal of Climate*, **26**, 918–935.

Wu, Y., R. Seager, M. Ting, N. Naik, and T. A. Shaw, 2012: Atmospheric Circulation Response to an Instantaneous Doubling of Carbon Dioxide. Part I: Model Experiments and Transient Thermal Response in the Troposphere*. *Journal of Climate*, **25**, 2862–2879.

Xie, S., 2020: Ocean Warming Pattern Effect On Global And Regional Climate Change. *AGU Advances*, **1**.

Xie, S. P., T. Miyama, Y. Wang, H. Xu, S. P. de Szoeke, R. J. O. Small, K. J. Richards, T. Mochizuki, and T. Awaji, 2007: A regional ocean-atmosphere model for eastern Pacific climate: Toward reducing tropical biases. *Journal of Climate*, **20**, 1504–1522.

Yamazaki, A. and H. Itoh, 2013: Vortex–Vortex Interactions for the Maintenance of Blocking. Part I: The Selective Absorption Mechanism and a Case Study. *Journal of the Atmospheric Sciences*, **70**, 725–742.

Yang, X. and E. K. M. Chang, 2006: Variability of the Southern Hemisphere Winter Split Flow—A Case of Two-Way Reinforcement between Mean Flow and Eddy Anomalies. *Journal of the Atmospheric Sciences*, **63**, 634–649.

Yiu, S. and A. C. Maycock, 2019: On the seasonality of the El Niño teleconnection to the Amundsen Sea region. *Journal of Climate*, **32**, 4829–4845.

Yoden, S., M. Shiotani, and I. Hirota, 1987: Multiple planetary flow regimes in the Southern Hemisphere. *Journal of the Meteorological Society of Japan*, **65**, 571–580.

Zappa, G., G. Masato, L. Shaffrey, T. Woollings, and K. Hodges, 2014: Linking Northern Hemisphere blocking and storm track biases in the CMIP5 climate models. *Geophysical Research Letters*, **41**, 135–139.

Zappa, G. and T. G. Shepherd, 2017: Storylines of atmospheric circulation change for European regional climate impact assessment. *Journal of Climate*, **30**, 6561–6577.